

Electronic Thesis and Dissertation Repository

---

12-10-2013 12:00 AM

## Experimental Modeling of Wind Farm Topography and Canopy

Dan S. Parvu, *The University of Western Ontario*

Supervisor: Horia Hangan, *The University of Western Ontario*

Joint Supervisor: Yves Gagnon, *The University of Western Ontario*

A thesis submitted in partial fulfillment of the requirements for the Master of Engineering Science degree in Civil and Environmental Engineering

© Dan S. Parvu 2013

Follow this and additional works at: <https://ir.lib.uwo.ca/etd>



Part of the [Other Civil and Environmental Engineering Commons](#)

---

### Recommended Citation

Parvu, Dan S., "Experimental Modeling of Wind Farm Topography and Canopy" (2013). *Electronic Thesis and Dissertation Repository*. 1852.

<https://ir.lib.uwo.ca/etd/1852>

This Dissertation/Thesis is brought to you for free and open access by Scholarship@Western. It has been accepted for inclusion in Electronic Thesis and Dissertation Repository by an authorized administrator of Scholarship@Western. For more information, please contact [wlsadmin@uwo.ca](mailto:wlsadmin@uwo.ca).

EXPERIMENTAL MODELING OF WIND FARM TOPOGRAPHY AND CANOPY

(Thesis format: Monograph)

by

Dan-Stefan Parvu

Department of Civil and Environmental Engineering

A thesis submitted in partial fulfillment  
of the requirements for the degree of  
Master of Engineering Science

The School of Graduate and Postdoctoral Studies  
The University of Western Ontario  
London, Ontario, Canada

© Dan-Stefan Parvu 2013

## **Abstract**

As an important renewable energy source for electricity generation, wind energy must rely on efficient and accurate wind resource assessment for the siting and the design of wind farms. Traditionally relying on numerical modeling, current wind farms built in Canada, notably, experience an under-performance in terms of power generation. This work studies an alternative approach to wind farm modeling through experimental wind tunnel testing.

A reliable wind resource and the local topographic features are the principal factors that determine the eligibility of a potential site for a wind farm. The wind turbines within a wind farm have to be located in the site based on wind resource data [1]. Among other effects, we suspect that the forest canopy and the surrounding topography have an influence on the under-performance of wind farms. The objective of this exploratory research is to determine the usefulness of wind tunnel studies for wind farm design and siting. Towards this goal an attempt has been made at developing methodologies for topography and forest canopy physical modeling. The models developed are validated by comparing data from the wind tunnel experiments with production data at an existing wind farm and with computational models. The Eastern Kings wind farm (PEI, Canada), is used as a test-case for the models.

A Leaf Area Index (LAI) – porosity canopy model was developed based on remote sensed data and the findings are in agreement with previous studies. The LAI – porosity canopy model was tested in the wind tunnel and the results showed an encouraging match with full scale measurements.

### **KEYWORDS:**

Wind farm siting, WAsP, topographic modeling, LAI-porosity canopy model, wind tunnel experiment.

## **Acknowledgments**

I would like to express my gratitude to Professors Dr. Horia Hangan and Dr. Yves Gagnon for their supervision and patience throughout this project. Their knowledge and contribution was paramount to the improvement and completion of this research. I would also like to thank the examining Professors – Dr. Craig Miller, Dr. Timothy Newson and Dr. Kamran Siddiqui – for their insightful comments and their help with the revisions of this thesis.

I am also grateful to Mr. Vasile Ionescu and Dr. Ashkan Rasouli for the help they provided for the completion of the topographic experimental model and the faculty and technical staff of the Boundary Layer Wind Tunnel Laboratory for their help throughout the course of the experimental part of this work.

I would also like to thank my friends Maryam and Djordje for their useful insights, comments and discussions on the subject of my thesis, as well as great support over the course of my studies.

Finally, I would like to express my affectionate gratitude to my parents and brother for their much appreciated support, patience and advice. Last but not least, I would like to thank Veronica for her love and patience throughout the completion of my thesis.

# Table of Contents

Abstract.....	ii
Acknowledgments.....	iii
List of Appendices .....	vi
List of Symbols and Abbreviations.....	vii
Abbreviations.....	viii
List of Tables .....	ix
List of Figures.....	x
Chapter 1.....	1
1. Introduction.....	1
1.1 Overview.....	1
1.2 Predicting Wind Farm Performance .....	3
1.2.1 Numerical Modeling.....	3
1.2.2 Wind Tunnel Modeling.....	5
1.3 Scope of the Work .....	11
1.4 Outline.....	12
Chapter 2.....	13
2. Case Study and Full Scale Data .....	13
2.1 Case Study – Prince Edward Island Wind Farm.....	13
2.1.1 Location .....	13
2.1.2 Wind Farm Description.....	13
2.2 Full Scale Data.....	15
2.2.1 Data Processing.....	15
2.2.2 Data Analysis .....	20
2.3 Stationary Data Segments.....	25
2.4 Final Comparison Sets.....	29
2.4.1 Atmospheric Stability .....	30
2.4.2 Time Series Equivalence.....	31
2.5 Wind Resource Assessment Using WAsP.....	32
Chapter 3.....	36
3. Experimental Setup.....	36
3.1 Wind Tunnel .....	36

3.2	Boundary Layer .....	37
3.3	Topographic Model.....	39
3.3.1	Geospatial Data.....	39
3.3.2	CAD Model.....	39
3.3.3	Finished Physical Model.....	42
3.4	Forest Canopy Model.....	43
3.5	Case Study Experimental Setup.....	44
3.5.1	Model .....	44
3.5.2	Instrumentation .....	45
3.5.3	Wind Tunnel Tests.....	48
3.6	Similarity analysis.....	50
Chapter 4	.....	53
4.	Preliminary Canopy Modeling.....	53
4.1	Preliminary Results.....	53
4.1.1	Topographic Model Results.....	53
4.1.2	Preliminary Forest Canopy Model Results.....	65
4.2	Discussion of Preliminary Results.....	74
Chapter 5	.....	76
5.	Improved Canopy Modeling .....	76
5.1	Proposed Approach.....	76
5.2	LAI Relationship to Wind Tunnel Modeling.....	79
5.3	Final Case Study Modeling Results.....	83
5.4	Comparison between Wind Tunnel Tests.....	83
5.5	Results and Discussion of the Improved Canopy Model.....	94
Chapter 6	.....	102
6.	Conclusion and Future Work .....	102
6.1	Conclusion .....	102
6.2	Future Work.....	104
7.	References.....	105
	CURRICULUM VITAE.....	145

## **List of Appendices**

Appendix A: Vertical Wind Profile Logarithmic Fit.....	71
Appendix B: Time Series Equivalence.....	72
Appendix C: Comparison Results.....	74
Appendix D: Experimental Model And Placement In The Wind Tunnel .....	88

## List of Symbols and Abbreviations

$a_i$	averaging intervals in full scale	[-]
$d_{total}$	vertical wind profile shift distance	[m]
$Fr$	Froude number	[-]
$h$	height	[m]
$k$	von Kármán constant	[-]
$l$	length	[m]
$L_{wt/fs}$	length scale for wind tunnel / full scale	[m]
$r$	wind tunnel model radius	[m]
$R^2$	correlation coefficient	[-]
$Re$	Reynolds number	[-]
$Ro$	Rossby number	[-]
$T_{wt/fs}$	time scale for wind tunnel / full scale	[s]
$u(z)$	wind speed at height $z$ above ground	[m/s]
$u^*$	friction velocity	[m/s]
$U_0$	free stream velocity	[m/s]
$V_{wt/fs}$	velocity scale for wind tunnel / full scale	[m/s]
$w$	width	[m]
$z_0$	roughness length	[m]
$\Delta$	difference	[-]
$\alpha$	power law coefficient	[-]
$\varepsilon$	porosity	[-]
$\theta$	wind tunnel model rotation angle	[°]
$\rho$	density	[kg/m <sup>3</sup> ]



## Abbreviations

<i>AVHRR</i>	Advanced Very-High Resolution Radiometer
<i>CAD</i>	Computer Aided Design
<i>CAM</i>	Computer Aided Manufacturing
<i>CF</i>	Capacity Factor
<i>CFD</i>	Computational Fluid Dynamics
<i>CNC</i>	Computer Numerically Controlled
<i>DIU</i>	Data-acquisition Interface Unit
<i>GIS</i>	Geographic Information System
<i>GLOBCARBON</i>	Global Land Products for Carbon Model Assimilation
<i>IDW</i>	Inverse Distance Weighting
<i>LAI</i>	Leaf Area Index
<i>LAD</i>	Leaf Area Density
<i>LDV</i>	Laser Doppler Velocimetry
<i>LES</i>	Large Eddy Simulation
<i>L-system</i>	Lindenmayer system
<i>Met tower</i>	Meteorological Tower
<i>MODIS</i>	Moderate Resolution Imaging Spectroradiometer
<i>NASA</i>	National Aeronautics and Space Administration
<i>NOAA</i>	National Oceanic and Atmospheric Administration
<i>PEI</i>	Prince Edward Island
<i>PIV</i>	Particle Image Velocimetry
<i>PPI</i>	Pores Per Inch
<i>USB</i>	Universal Serial Bus
<i>USGS</i>	United States Geological Survey
<i>WAsP</i>	Wind Atlas Analysis and Application Program

## List of Tables

Table 2.1: Sample range test criteria.....	16
Table 2.2: Sample relational test criteria. ....	17
Table 2.3: Sample validation criteria. ....	17
Table 2.4: Wake effect sectors for the wind turbines. ....	18
Table 2.5: Time series summary for all wind turbines. ....	18
Table 2.6: Time series statistics for wind turbines. ....	19
Table 2.7: Turbine vs. met tower correlation statistics; (letters in parenthesis refer to sub-figures from Figure 2.9). ....	23
Table 2.8: Data segment validation criteria. ....	26
Table 2.9: Number of valid data segments identified per month at the 80 m height of the met tower. ....	28
Table 2.10: Valid data segments identified per month at the 80 m height of the met tower and at the wind turbines (80 m height). ....	28
Table 2.11: Valid data segments identified per month at the 80 m height of the met tower and at the wind turbines (height of 80 m) with wind speed over 10 m/s. ....	29
Table 2.12: Final valid data segments set identified per month at the 80 m height of the met tower and at the wind turbines (height of 80 m) with wind speed over 10 m/s. ....	30
Table 3.1: Flow conditions for the topographic model. ....	37
Table 3.2: Land type and power law coefficient of various land types as per Bañuelos et al. [56]. ....	38
Table 3.3: Wind tunnel experiment runs.....	50
Table 5.1: Topographic model height at respective locations. ....	97
Table 5.2: Variables used for vertical wind profile calculation, 202.5° direction. ....	99
Table 5.3: Variables used for vertical wind profile calculation, 157.5° direction. ....	99
Table 5.4: Vertical wind profile shift; 202.5° direction. ....	100
Table 5.5: Vertical wind profile shift; 157.5° direction. ....	100
Table A.1: Upstream profile log law fit. ....	113
Table C.1: Comparison data sets divided per month and wind direction. ....	116

## List of Figures

Figure 1.1: Performance of ecoERP Projects – Wind. Source: [4].....	2
Figure 2.1: Wind farm location and surrounding topography. Source: [46]. .....	14
Figure 2.2: Eastern Kings wind farm on PEI’s East Point, showing seven of the ten wind turbines. Source: <a href="http://www.windsorstar.com">http://www.windsorstar.com</a> .....	14
Figure 2.3: Full scale data processing.....	15
Figure 2.4: 80 m wind frequency rose. ....	19
Figure 2.5: Aerial view with wind rose and predominant wind directions. Source: <a href="https://maps.google.com">maps.google.com</a> , 46.453352,-62.058361. ....	19
Figure 2.6: Monthly wind speed profile shown at three heights at the met tower.....	20
Figure 2.7: Monthly temperature statistics measured at met tower. ....	21
Figure 2.8: Average monthly wind speeds at the met tower compared to the measurements done at the wind turbines. ....	22
Figure 2.9: Wind speed correlations between the data measured at the met tower and the data from the wind turbines at 80 m height. ....	24
Figure 2.10: Energy spectrum of the wind speed at 100 m above the ground. Source: [52]..	25
Figure 2.11: Example of Matlab segment identification and validation. Figure (a) shows the evaluated trend of the segment, and figure (b) shows the wind direction variation within the set limits. ....	27
Figure 2.12: Influence of stability on the vertical wind speed profile and comparison with the average vertical wind profiles measured at the met tower for directions 157.5°, 202.5° and 315°. Adapted from Sucevic and Djurusic [55]. ....	31
Figure 2.13: WASP wind atlas methodology. Source: [58]. ....	34
Figure 2.14: (a) PEI wind atlas for East Point at 80 m height. Source: [64]; (b) resource grid at 80 m, generated for the Eastern Kings wind farm using WASP. ....	35
Figure 3.1: Boundary Layer Wind Tunnel Laboratory - Tunnel II, Western University; showing the low speed section. Source: <a href="http://www.blwtl.uwo.ca">http://www.blwtl.uwo.ca</a> .....	37
Figure 3.2: Streamwise velocity profile upstream of the model from hot-wire measurements; Adapted from Rasouli [16]. ....	38
Figure 3.3: Modeling procedure. The algorithm was used to build the topographic model... ..	39
Figure 3.4: PEI East Point Contour Map. Source: PEI Energy Corporation. ....	40
Figure 3.5: IDW surface interpolation technique. ....	41
Figure 3.6: Kriging surface interpolation technique. ....	41
Figure 3.7: Surface interpolated using kriging. ....	41
Figure 3.8: Surface interpolated using IDW. ....	41


Figure 3.9: Finished CAD model showing (a) met tower and turbine locations; (b) extent of the physical model (circled).....	42
Figure 3.10: Model placement in the wind tunnel with forest canopy and Cobra probes. ....	44
Figure 3.11: (a) Model extent drawn on CAD model; (b) Cobra probe. ....	45
Figure 3.12: Series 100 Cobra probe main features. Source: [71].....	46
Figure 3.13: Schematic of an example Data-acquisition Interface Unit with integrated data acquisition. Source: [71]. ....	47
Figure 3.14: Model orientation in wind tunnel for the selected wind directions; $U_0$ is the free stream velocity; $\Delta$ shows the met tower location and  represent wind turbine locations..	49
Figure 3.15: Model rotation procedure; linear dimensions in meters. ....	49
Figure 3.16: Reynolds dependency tests; (a) topographic model only; (b) 48% porosity canopy model; (c). 90% porosity canopy model. ....	52
Figure 4.1: Example of full scale data segments extracted for January 2008, direction: 315°	56
Figure 4.2: Wind tunnel results and comparison with full scale data. “No forest” case, direction: 315°, January 2008.....	57
Figure 4.3: Wind tunnel results and comparison with full scale data. “No forest” case, direction: 315°, March 2008.....	58
Figure 4.4: Wind tunnel results and comparison with full scale data. “No forest” case, direction: 315°, September 2008.....	59
Figure 4.5: Wind tunnel results and comparison with full scale data. “No forest” case, direction: 315°, October 2008. ....	60
Figure 4.6: Wind tunnel results and comparison with full scale data. “No forest” case, direction: 315°, December 2008.....	61
Figure 4.7: Summary plot of the comparison between the wind tunnel test and full scale data. “No forest” case, direction: 315°, yearly data.....	62
Figure 4.8: Summary plot of the comparison between the wind tunnel test and full scale data. “No forest” case, direction: 202.5°, yearly data.....	63
Figure 4.9: Summary plot of the comparison between the wind tunnel test and full scale data. “No forest” case, direction: 157.5°, yearly data.....	64
Figure 4.10: Wind tunnel results and comparison with full scale data. “90% canopy model” case, direction: 315°, January 2008.....	66
Figure 4.11: Wind tunnel results and comparison with full scale data. “90% canopy model” case, direction: 315°, March 2008.....	67
Figure 4.12: Wind tunnel results and comparison with full scale data. “90% canopy model” case, direction: 315°, September 2008.....	68
Figure 4.13: Wind tunnel results and comparison with full scale data. “90% canopy model” case, direction: 315°, October 2008. ....	69

Figure 4.14: Wind tunnel results and comparison with full scale data. “90% canopy model” case, direction: 315°, December 2008.....	70
Figure 4.15: Summary plot of the comparison between the wind tunnel test and full scale data. “90% canopy model” case, direction: 315°, yearly data. ....	71
Figure 4.16: Summary plot of the comparison between the wind tunnel test and full scale data. “90% canopy model” case, direction: 202.5°, yearly data. ....	72
Figure 4.17: Summary plot of the comparison between the wind tunnel test and full scale data. “90% canopy model” case, direction: 157.5°, yearly data. ....	73
Figure 4.18: Location of wind turbines 1, 5 and 6 with relation to forest edges. ....	75
Figure 5.1: (a) Contour map with met tower and turbine locations; (b) LAI from MODIS data.....	78
Figure 5.2: (a) black and white image – 5 mm slice of blue filter material (b) binary image for processing.....	80
Figure 5.3: 2nd degree polynomial and data extrapolation for LAD.....	81
Figure 5.4: Completed wind tunnel experimental model, with attached 48% porosity forest canopy model and its placement in the wind tunnel. ....	82
Figure 5.5: Wind tunnel results and comparison with full scale data. “48% canopy model” case, direction: 315°, January 2008.....	85
Figure 5.6: Wind tunnel results and comparison with full scale data. “48% canopy model” case, direction: 315°, March 2008.....	86
Figure 5.7: Wind tunnel results and comparison with full scale data. “48% canopy model” case, direction: 315°, September 2008.....	87
Figure 5.8: Wind tunnel results and comparison with full scale data. “48% canopy model” case, direction: 315°, October 2008. ....	88
Figure 5.9: Wind tunnel results and comparison with full scale data. “48% canopy model” case, direction: 315°, December 2008.....	89
Figure 5.10: Summary plot of the comparison between the wind tunnel test and full scale data. “48% canopy model” case, direction: 315°, yearly data. ....	90
Figure 5.11: Summary plot of the comparison between the wind tunnel test and full scale data. “48% canopy model” case, direction: 202.5°, yearly data. ....	91
Figure 5.12: Summary plot of the comparison between the wind tunnel test and full scale data. “48% canopy model” case, direction: 157.5°, yearly data. ....	92
Figure 5.13: Comparison between the three wind tunnel test setups.....	93
Figure 5.14: Terrain contours, wind turbine locations, modeled area and measured fetches. Measured distance for the incoming flow for: (a) direction 315°: 3.12km; (b) direction 202.5°: 8.86km; (c) direction 157.5°: 4.48km.....	95
Figure 5.15: Satellite imagery and wind directions; for the 157.5° and 202.5° directions the flow encounters large patches of forest. ....	95

Figure 5.16: Modifications of the vertical wind profile by forest canopy; Adapted from Tajchman [82].	96
Figure 5.17: Upstream and downstream vertical wind profiles; $z_1$ and $z_2$ are the heights relative to the wind tunnel floor, at which the same wind speed, $u(z_1) = u(z_2)$ , occurs for both the upstream and downstream profiles.	98
Figure 5.18: Comparison between upstream and downstream vertical wind profiles; Met tower data for 202.5° direction.	99
Figure 5.19: Structure of the internal boundary layer downwind of a roughness change; Adapted from Wiernga [83].	101
Figure D.1: Topographic model placement in the wind tunnel showing installed ramps and Cobra probes.	143
Figure D.2: Experimental model with blue filter material forest canopy installed.	143
Figure D.3: Experimental model with installed ramps, pink fiber glass forest canopy model and Cobra probes.	144

# Chapter 1

## 1. Introduction

### 1.1 Overview

Despite the growing concerns regarding climate change, fossil fuels are still extensively used in world economies. Researchers are actively working on reducing the need to use these non-renewable resources, with an objective of decreasing their harmful environmental effects. To this extent, wind power is one of the more attractive options available. In the past two decades, the wind power industry has seen a large growth and the demand for clean energy is greater every year.

According to the Global Wind Energy Council (GWEC) [2], between 1996 and 2012, a total of 282,587 MW of wind energy capacity was installed worldwide, while 24 countries had more than 1,000 MW of installed wind capacity. In 2011 alone, Canada installed 1,267 MW of wind energy capacity, thus surpassing for the first time the 1 GW milestone in one year [2].

Wind energy drives jobs and local benefits at prices that are competitive with other sources of electricity [3]. Based on the wind facts aggregated by CanWEA [3], Canada is now ranked 9<sup>th</sup> in terms of wind energy producers, having a total installed capacity of 6,500 MW. With the addition of 936 MW, wind energy grew by nearly 20 per cent in 2012. Canada is expected to reach 12,000 MW of total wind energy installed capacity by 2016 and remains on track to meet CanWEA's WindVision target of supplying 20 per cent of Canada's electricity from wind energy by 2025.

Since wind power capacity is a rapidly growing industry, efforts need to be made in order to better understand and design wind farms. Important factors need to be analyzed, such as the topography around the actual wind turbines as well as any other obstacles. Canada has a predominantly flat terrain, while 53.8 per cent of its total surface is covered by forests. As wind energy is developing, in Canada and abroad, a growing number of wind farms are deployed in forested areas. There are instances of wind farms being placed near, or within

forests or clear cuts. This raises the problem of how such forests, or their edges, influence the aerodynamics and the performance of the wind turbines. In Canada, numerical models for the design of wind farms predict a production of energy higher than the actual production. Royer [4] shows, in a study by Natural Resources Canada (NRCan), that the wind farms in Canada are actually under-performing; and from the analysis of 36 projects, it was found that their cumulative performance is 91 per cent of the expected capacity factor (CF). The capacity factor is the ratio between the total amount of energy the plant produced during a period of time and the amount of energy the plant would have produced at full capacity, where the “Cum CF” line is the average cumulative capacity factor. Figure 1.1 shows that the cumulative CF is always below the expected CF, and there are significant differences from one year to another. The largest differences have been observed for the 2010 fiscal year, where the deficit was 15 per cent, and over the whole period, approximately 8 per cent.

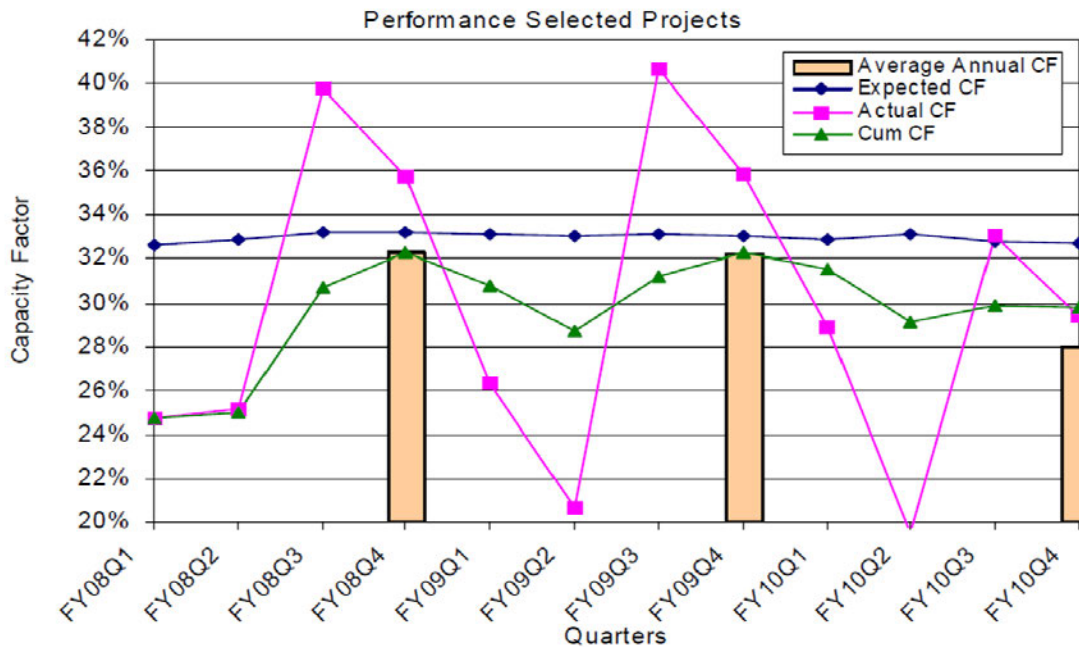


Figure 1.1: Performance of ecoERP Projects – Wind<sup>1</sup>. Source: [4].

<sup>1</sup>The ecoENERGY for Renewable Power program was launched in April 2007 to encourage the generation of electricity from renewable energy sources such as wind, low-impact hydro, biomass, photovoltaic and geothermal energy.



## 1.2 Predicting Wind Farm Performance

A reliable wind resource and the local topographic features are the principal factors that determine the eligibility of a potential site for a wind farm. The wind turbines within a wind farm have to be located in the site based on wind resource data. Each wind turbine rotor is continuously orientated to face the incoming wind direction in order to maximize the potential available energy. In order to avoid turbulence, wind turbines have to be spaced out from each other. The industry standards for spacing of wind turbines generally range from 1.5 to 5 times the rotor diameters apart (about 123 to 450 m) [1].

In order to ensure that the operation of wind farms installed at sites with different characteristics will be reliable and cost effective, the development and validation of software and tools is essential. Numerical models have been developed and employed in the design of wind farms. There are two types of numerical models currently in use: linear and non-linear. Up until recently, the wind energy industry has relied on linear models such as WAsP (the Wind Atlas Analysis and Application Program), which is a linearised, small-perturbation method [5]. A newer approach to wind resource assessment has been the use of commercial non-linear software packages. Such packages are represented by Meteodyn WT, which is an engineering method flow-modelling package intended for use in the wind power industry for complex terrain [6].

### 1.2.1 Numerical Modeling

Wind turbines and wind farms are being deployed in areas of increasing topographic complexity. Since traditional numerical models have been found to over predict power output, the exclusive use of mathematical models needs to be revised.

Walmsley and Taylor [7] describe the Askervein Hill Project, which was used to verify models of flow and turbulence over a low hill. While wind tunnel experiments, that represented the topography and flow conditions in detail, had good results and agreement with the measured data, the numerical models had varied degrees of success. Linear numerical models (Salmon et al. [8], Mason and King [9], Walmsley et al. [10] and Beljaars et al. [11]) performed very well for the windward side of the hill as well as the crest, but tended to underestimate the speed-up ratio for the leeward side. Nonlinear models (Raithby et

al. [12], Beljaars et al. [11], Lalas et al. [13] and Zeman and Jensen [14]) tended to perform better overall, yet they had a high computational cost.

Palma et al. [15] showed that there are a number of methods that can be used in order to positively affect wind resource assessment, since the conventional analysis is not sufficient. Field anemometer measurements are a first indication of complex wind patterns and nonlinear Computational Fluid Dynamics (CFD) flow models agree better than the simple linear models with field measurements.

Rasouli [16] designed a Reynolds Averaged Navier-Stokes (RANS) CFD simulation of the complex topographic features surrounding Hong Kong. The results from the CFD study were validated with Particle Image Velocimetry (PIV) measurements performed during a wind tunnel experiment in which a model with the same topographic features was used. The velocity profiles and speed-up ratios obtained numerically were compared to the ones obtained in the wind tunnel experiment and were found to be in agreement.

Clarenc et al. [17] attempt a validation of the commercially available ‘engineering method’ flow-modeling package “Meteodyn WT”, which includes a full Navier-Stokes equation solver. The paper presents three test sites, for which field data was available, located in France. The results obtained from the software package are compared to measured data with limited success. The discrepancies between measured data and simulation data are attributed by the authors to the existence of forested areas upwind of the met tower used on site. The authors acknowledge that further investigation is necessary in order to properly determine the role of roughness length. Manning et al. [6] study the ability of “Meteodyn WT” and “WAsP” to produce simulations comparable to full scale measurements in the case of steep hills. The “Meteodyn WT” results present a significant improvement over the results obtained using “WAsP” concerning the agreement with full scale measurements upstream of a hill crest.

## 1.2.2 Wind Tunnel Modeling

### **Topographic modeling**

Topographic models used in wind tunnel experiments have always represented a challenge in terms of geometrical scaling as well as accurately replicating their effects on the flow. Several studies have analyzed the flow over generic, simpler topographic models. Topographic modeling proves to be a main challenge in wind tunnel experimentation. Methods and materials for building experimental models were shown to have great influence on the results obtained in wind tunnel.

Ngo and Letchford [18] measured three-component velocity profiles and turbulence parameters for different generic ridge, escarpment and cliff models using a 4-hole conical pressure probe. They used seven wooden models at a scale of 1:1000 which represented 50 m high topographic features. While their results matched with data from other studies, their experimental model was over-predicting speed-ups when compared to the major wind load codes. Lubitz and White [19] used a single hot-wire probe to measure wind speed-up factors over generic hill models in different wind directions and compared them with their field measurements. They manufactured three different hill models from polystyrene foam. Their experimental setup was predicting wind conditions with a smaller degree of accuracy. Ishihara et al. [20] measured velocity profiles over a three-dimensional hill model using hot wires and three-dimensional laser Doppler velocimetry (LDV). The model hill was machined from wood but its maximum slope was only 32 degrees. Ayotte and Hughes [21] constructed two sets of isolated two-dimensional hills from high density foam. The hill height was kept constant and the length of the hill varied to achieve the required slope. Their experiment yielded good results and when compared to those of referenced scientific literature, it was found that they had good agreement. Simpson et al. [22] used three-orthogonal velocity-component LDV system to measure flow properties in a vertical plane behind an axisymmetric hill. The model was mounted in the center of the test section. It was machined from wood and coated with a clear sealer. They compared the two different tests performed and pointed out that they are consistent with each other, as well as with other experimental results from cited works. Ruel et al. [23] ran wind tunnel simulations of erosion on hills using 1:2500 scale models, each containing a test hill and its surroundings. The models were made

from polystyrene plates, 2 mm thick, which were cut along contour lines. Attaching the plates to each other produced rough, terraced scale models. They obtained results for a multitude of different tests which correlated well with each other.

A few experiments were performed using complex topographies. In this case, the Askervein Hill Project still represents a benchmark for experimental models.

Teunissen et al. [24] conducted a wind tunnel study of the Askervein Hill Project. Their findings have shown that a wind tunnel model provides an excellent means of simulating a boundary layer flow over a low hill. Their model was manufactured by cutting out contours using a pantograph machine and the result was then smoothed by sanding. One of their main findings was that turbulence changes did not depend significantly on surface roughness, yet it played a large role in affecting the flow on the leeward side of the hill, where separation occurred. When using a smooth surfaced model, an over estimation of flow speeds could be seen. All the different tests they ran, using three different length scales in two different facilities showed good consistency between each other. For the smaller scales it was harder to setup measurements close to the model surface. Chock and Cochran [25] performed velocity measurements using hot-wire probes over a complete topographic model of Hawaii and Guam regions. Each model was built to a linear scale of 1:6000. The elevation contours for model construction were developed using a commercial program using ten meter elevation data obtained from the United States Geological Survey (USGS). Rasouli [16] performed Particle Image Velocimetry (PIV) measurements on a complex topographic model in several horizontal and vertical planes. The results from PIV were compared to hot wire measurements which showed a good agreement. Moreover, the author reproduced the experiment numerically, using a Reynolds Averaged Navier-Stokes (RANS) CFD model. The velocity profiles and speed-up ratios obtained numerically were compared to the ones obtained in the wind tunnel experiment and were found to be in agreement. The model was done at a scale of 1:3000, and represented the surrounding terrain of Hong Kong.

The general consensus on this matter is that the topographic models for wind tunnel experiments are usually made by machining either from wood or foam. Different treatments are applied to the model's surface in order to obtain diverse roughness characteristics. Model scales, in typical Boundary Layer Wind Tunnels range from 1:1000 to 1:6000, and are

usually dictated by the size of the experimental chamber of the wind tunnel in use. The works cited show that a wind tunnel experiment is an important tool that can be used in analyzing flows over different types of terrains.

### **Forest canopy modeling**

Forest canopy modeling poses another challenge to experimenters. The models themselves have to be an accurate representation of a dynamic environment which interacts with the flow. Since it would not be practical to model the complex structural and geometric details of a whole forest, equivalent simplified models are sought after.

Raupach et al. [26] studied the phenomenon that takes place at the top of a forest canopy. Their findings emphasize a mixing-layer plane between the flow in the canopy and the flow above it. The authors predicted that the behavior of the turbulent length scales of the dominant eddies responsible for vertical transfer near the top of the canopy is controlled by the shear length scale and tested their assumptions and predictions on full scale and wind tunnel data.

Neff and Meroney [27] used a carpet with three different bristle heights to study the effect of forests on the flow over bidimensional hills. The results were found to be in agreement with field data as well as similar experiments. Brunet et al. [28] made a realistic representation of flexibility and natural frequency as well as mixing plane analogies, but their model represented a wheat crop and not trees. Meroney [29] designed a wind tunnel study of several species of trees in order to simulate the meteorological characteristics of typical forests and studied their drag characteristics as well as wind flow in and above the canopy, but without taking into account any aeroelastic effects. The forest designed for the experiment was composed of model trees which had equivalent wake and drag characteristics to real trees.

Gromke and Ruck [30] presented results of force and flow field measurements of individually produced small-scale model trees. Different permeabilities were realized by varying the tree crown forming material (wood wool, sisal fiber or porous foam) and its packing density or pore volume. The purpose of their study was to evaluate how much the drag and wake characteristics of model trees could be influenced by modifying crown porosity and by changing the chosen material.

Finnigan and Mulhearn [31] modeled waving crops in the wind tunnel. The material chosen for the model stalks was cylindrical, monofilament nylon fishing line. This complex modeling procedure was employed in order to obtain a model crop which could replicate the aeroelastic properties of live crops. An attempt to model the overall aerodynamic force was done in this report, since it would have been impossible to correctly replicate the geometry of the individual plants as well as the Reynolds number of the flow around them. The overall aerodynamic force was modified by varying the drag coefficient and aerodynamic width of the wheat plant.

Stacey et al. [32] performed wind tunnel studies using 1:75 scale plastic trees. Sets of idealized branch elements were fitted over the model trees and were molded in low density polyethylene. This was an attempt to produce an aeroelastic tree model; dynamic similarity was assessed by ensuring that the models had the correct overall shape and aerodynamic drag. The model trees were examined from an aeroelastic point of view, and their aerodynamic features were simplified by reducing the model to a lumped system which causes drag as it obstructs the air flow.

Wind tunnel models of forest canopies based on drag and wake characteristics seem to be suitable when individual tree modeling is possible. In order to represent a large forested area, another approach needs to be examined and employed. A relatively accessible method is to attempt to match the model's physical properties to those of the full scale subject. A common parameter that is widely used to describe forests is Leaf Area Index (LAI). LAI represents the total one-sided leaf area per unit ground surface area (Chen and Black [33]).

Kobayashi and Hiyama [34] measured flow characteristics above the canopy of a forest. Measurements were taken using an instrument tower at two different heights. Omnidirectional sonic anemometers were used to obtain three-dimensional wind velocities and sonic temperatures. The canopy LAI was measured and was found to range from 1 to 2.3.

Pietri et al. [35] conducted a comprehensive wind tunnel experiment in which the aim was to study the parameters that govern the transition from the mixing layer, concept that was first introduced by Brunet et al. [28] and developed by Raupach et al. [26], observed at the top of a forest canopy, to the boundary layer. Pietri et al. characterize a forests density based on the

significant parameter, i.e. the LAI. The authors limit their study to moderately dense and sparse forest canopies which are homogeneously distributed in an aligned and staggered configuration. The canopy model developed for their work was created using artificial coniferous tree models, which were designed to have metal stems and trunks and fine foam to represent the needles. Most of their measurements were made in the center of a forest patch, while some other profiles were measured at different locations, using Laser Doppler Velocimetry (LDV) which allowed for one and two velocity components to be resolved. Their results were in agreement with literature data for full scale forest studies as well as other wind tunnel experiments, and it was found that they were significantly different for the two studied ground arrangements. An important observation was that, by changing the arrangement of the model trees, the global porosity of the canopy was modified. Another observation that was emphasized was the insensitivity of Reynolds stresses to the modification of the ground arrangement. This work focused on a single type of tree, coniferous in this case, with a single LAI value, which were examined in two placement configurations. Other canopy configurations would involve different tree models, with other geometries, ground placements and LAIs.

Rodrigo et al. [36] used Particle Image Velocimetry (PIV) for a generic representation of forest cuts in a wind tunnel simulating the atmospheric boundary layer. They used simple foam models to simulate homogeneous forest canopies of fixed height. This model was validated by matching the foam characteristics with the LAI. The vegetation parameters found using this approach match those of similar studies, but the findings only apply to bidimensional flows.

Aubrun and Leitl [37] used a layout of rings made of metallic mesh to simulate the forest around the Juelich Research Centre, from which they had field measurements at various locations; the metallic mesh was made out of steel wires. The increase in the canopy density was simulated by bending twice the uppermost third of the ring. Instead of attempting to achieve a model forest with similar parameters to full scale, such as geometry, drag coefficient or LAI, an effort was made to replicate the aerodynamic properties of the site. Using this approach they managed to reproduce wind profiles similar to those found within and over a dense forest canopy.

Warland [38] examined the turbulent flow in thinned forests, using uniformly spaced model trees. The model trees consisted of plastic strips with an interwound steel wire trunk, and similarity was assessed using the LAI parameter. The findings of this study sustain that the turbulence regimes are strongly influenced by the density of the forest. Marshall [39] uses 1:75 scale wind tunnel experiments to investigate the wind flow over and through three different forest models, in an attempt to improve a numerical Large Eddy Simulation (LES) model.

Novak et al. [40] investigated the effects of thinning in forested areas by measuring wind speed and turbulence statistics in model forests of various densities. The model trees were cylindrically symmetric, and the upper part had a mildly conical shape; an attempt to match the vertical leaf area distribution of the model trees with full scale trees was made, using and analyzing horizontal video projections of several trees. Several tree densities and leaf area indices were studied in their wind tunnel experiments, and wind speeds were measured in and above the model forest. The measurements obtained from the wind tunnel experiment were in good agreement with the field measurements.

Zhu et al. [41] compared turbulence measurements performed in the field and in a wind tunnel model for a crop canopy. The model canopy was manufactured from wooden sticks, therefore the model did not account for any aeroelastic features. The model's similarity with full scale was based on another vegetation index, which is similar to the LAI parameter: the Projected Frontal Area Index (PFAI), which also affected the density of the setup.

Yue et al. [42] managed to create an LES simulation of the wind tunnel experiment of Zhu et al. [41]. The results obtained from the numerical study were in good agreement with the PIV and hotwire measurements performed in the wind tunnel experiment.

Several approaches to forest canopy modeling have been reviewed and a consensus could not be identified between authors. Each experimenter designed a different forest canopy model and tried validating it by either comparison with full scale data or numerical models. While there have been several attempts at recreating a forest for wind tunnel testing from different perspectives such as geometric and dynamic similarity, a common methodology has not been established in the scientific community. Each of the cited authors had a different way of designing the forest and canopy model. In most cases, the results were validated by



comparing the final model to vegetation indices, such as leaf area index, and/or wind velocities measured on site.

### **1.3 Scope of the Work**

Through the study performed by Royer [4] for NRCan an under performance of wind farms, in terms of energy production, was identified. It is assumed that the deficit is due to the use of linear numerical models in the industry. As is the case with WAsP (Wind Atlas Analysis and Application Program), which at this time is the industry standard for wind resource assessment and siting of wind farms, numerical models are susceptible to prediction errors due to topography – either too mild or too harsh – or due to inadequate forest modeling techniques [43, 44].

The scientific literature review has shown that numerical modeling based on simple linear mathematical models has weaknesses in regards to obtaining a wind resource assessment over the area of a projected wind farm. The aim of this work is to develop methodologies on how topographic terrain and forest canopies could be modeled for wind tunnel studies of wind farms, to determine the potential use of wind tunnel experiments for wind resource assessment, and to provide detailed experimental measurements for the development and benchmarking of more robust and more accurate linear and non-linear numerical models for wind farm design.

In this work, a methodology for creating the topographic experimental model is presented, while a different approach to the assessment and implementation of Leaf Area Index (LAI) in wind tunnel experimentation is introduced, using satellite remote sensed data.

The topographic and canopy models developed are evaluated by comparing data from the wind tunnel experiments with production data available from an existing wind farm.

## 1.4 Outline

This work will focus on the potential use of wind tunnel experiments for wind resource assessment, with the help of available data from an existing wind farm. The proposed method consists of running an experimental wind tunnel model of the existing wind farm in an attempt to match the wind tunnel measurements to full scale data. This experimental model is composed of a topographic model and a forest canopy model. Observations are made on the topographic and forest canopy modeling procedure. The novelty of this approach lies in the attempt to model a forest canopy based on a potential relationship between remote sensed parameters (such as Leaf Area Index) and full scale forest canopy parameters.

Chapter 2 of this thesis presents the case study which is used as a basis for the design of a wind tunnel experiment. The PEI wind farm case study provided the necessary topographic and wind speed and topographic data. The topographic and roughness data were used to create a computer aided design (CAD) model, which was then sent to a computer numerically controlled (CNC) milling machine in order to create a physical representation of the terrain surrounding the wind farm (discussed in Section 3.3).

The full scale wind speed data was analyzed and validated using the rules outlined in the Wind Resource Assessment Handbook [45] which was then used as a base for comparison with the wind tunnel experiment. Full scale wind speed data segments are identified and presented in Section 3.6 and are then compared to the results from the wind tunnel experiment and preliminary results are presented in Chapter 4.

Chapter 5 presents the proposed method to acquire and use remote sensed parameters in order to design a forest canopy model for use in the wind tunnel and the potential relationship between full scale forest parameters and material properties is discussed. The findings in Chapter 0 point towards a redesign of the canopy model for the wind tunnel experiment. A new forest canopy model was tested in the wind tunnel, yet the results have shown that the model for the canopy is not conclusive at this time and therefore future work is necessary. Wind tunnel test results are discussed for the proposed forest canopy model, followed by a conclusion and discussion on future work in Chapter 6.

## Chapter 2

### 2. Case Study and Full Scale Data

For the purpose of this work, an existing wind farm, composed of ten utility-scale wind turbines, has been used as case study. This site was chosen based on wind data availability, which was obtained from the site's owners. The site itself provided some challenging problems that are analyzed in this work, which ranged from terrain issues, i.e. little variation in topographic features, to more complex problems, such as the influence of the forest canopy on the wind flow.

#### 2.1 Case Study – Prince Edward Island Wind Farm

##### 2.1.1 Location

The subject of the case study is a 30 MW wind farm (composed of ten 3 MW Vestas V90 wind turbines) situated on the eastern end of Prince Edward Island (PEI) on the eastern coast of Canada. The Eastern Kings wind farm is owned and operated by the PEI Energy Corporation [45].

The wind farm is located approximately 1.7 km away from the northern coast of the island, situated in the Gulf of Saint Lawrence, and is close to two main roads. It is surrounded by forested areas as well as agricultural fields. The closest lake, North Lake, is 1.74 km away, and the closest settlement is at a distance of 1.65 km. The wind farm is situated on a ridge in the East-West direction, as shown in Figure 2.1. This figure also shows the meteorological tower (referred to herein as “met tower”) and wind turbine locations.

##### 2.1.2 Wind Farm Description

The wind turbines used are version 5 of the V-90, and they make up the first V-90 wind farm in North America. The rotor diameter is 90 m, with a hub height of 80 m – equivalent to a 26 storey building. Their nacelles weigh approximately 90 tons, and each blade weighs 6.7 tons [45]. The wind farm consists of ten wind turbines (Figure 2.2 shows seven of the ten turbines) with a capacity of three megawatts each – for a total capacity of 30 megawatts. The

Annual Energy Production is 90-95 million kilowatt hours [45]. In Eastern Canada, the average house uses about 8,000 kilowatt hours of electricity annually [45], therefore the wind farm produces enough electricity to power about 12,000 homes. The Eastern Kings wind farm supplies about 7.5 per cent of PEI's electricity and it displaces 70,000 tons of greenhouse gases per year. That is the equivalent of taking about 15,000 cars off the road [45].

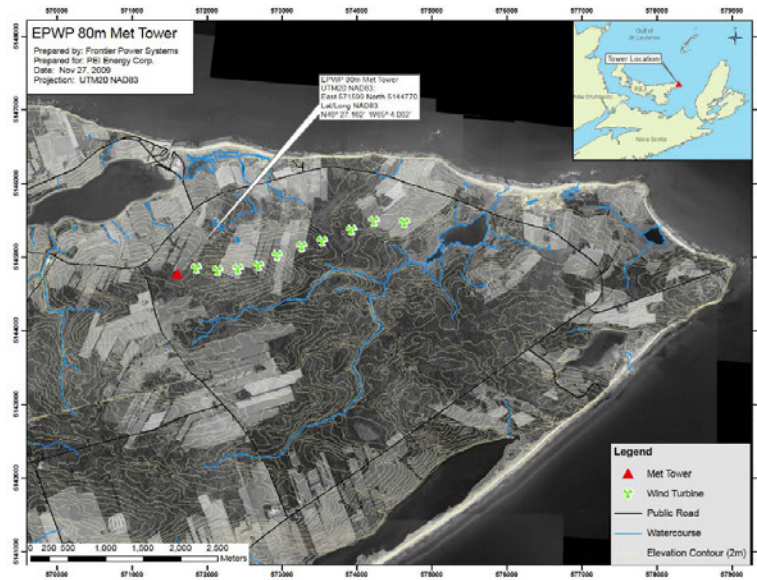


Figure 2.1: Wind farm location and surrounding topography.

Source: [46].



Figure 2.2: Eastern Kings wind farm on PEI's East Point, showing seven of the ten wind turbines. Source: <http://www.windsorstar.com>.

## 2.2 Full Scale Data

The data were in digital format, and were composed of wind parameters (speed, direction), temperature and power production time series for all of the wind turbines and the met tower. These measurements were taken at hub height in the case of the wind turbines, and at three different heights on the met tower (30 m, 50 m and 80 m high). Other information supplied were geospatial data in the form of a topographic contour map, as well as a roughness map and mast location.

Several NRG #40C standard anemometers, as well as FT702LT sonic anemometers were used on the met tower. The same type of sonic anemometer is used on each of the wind turbines. Standard anemometers sample data at a rate of 1Hz [47], while the sonic ones have a sampling rate of 5Hz [48]. The signals from the measurement equipment are then sent to the data logger. This Symphonie data logger is also manufactured by NRG Systems, and it logs ten minute averages for the anemometer data [49].

Figure 2.3 shows the sequence applied to the wind data from the wind farm. The data was retrieved, validated and then used as a base for comparison with the wind tunnel experiments.

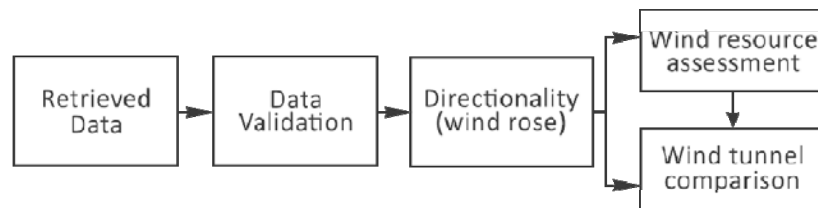


Figure 2.3: Full scale data processing.

### 2.2.1 Data Processing

Wind data was retrieved for each of the wind turbines and the met tower. Covering a period of one year, its period of collection was from January 1<sup>st</sup>, 2008, 00:00 to December 31<sup>st</sup>, 2008, 24:00.

Data files were received in the form of Excel spreadsheets containing multiple columns and were then processed using a dedicated wind analysis software, Windographer [50], capable of generating wind frequency roses, wind speed and temperature statistics.

Data validation was carried out using the rules outlined in the Wind Resource Assessment Handbook [51]. This involved a series of procedures called “flagging”. The bad and suspicious data segments were identified and excluded from the analysis (these segments included tower shading and icing phenomena). Validation routines are designed to screen each measured parameter for suspect values before they are incorporated into the archived database and used for site analysis, as per the Wind Resource Assessment Handbook [51].

There are two main categories of checks: general system checks and parameter checks. The general system checks evaluate the completeness of data sets and are applied to the data records and time sequence, to make sure that time steps are not skipped and that there are no gaps in the data. The measured parameter checks consist of range checks, relational and trend checks. Range tests are the simplest and most common, in which the data are compared to allowable upper and lower limits, as shown in Table 2.1.

Table 2.1: Sample range test criteria.

Sample parameter	Validation criteria
<b>Wind speed: horizontal</b>	
Average	Offset < Avg. < 25 m/s
Standard deviation	0 < Std. Dev. < 3 m/s
Maximum gust	Offset < Max. < 30 m/s
<b>Wind direction</b>	
Average	$0^{\circ} < \text{Avg.} < 360^{\circ}$
Standard deviation	$3^{\circ} < \text{Std. Dev.} < 75^{\circ}$
Maximum gust	$0^{\circ} < \text{Max.} < 360^{\circ}$

Source: [51].

Relational tests are based on expected physical relationships between various parameters. Table 2.2 shows examples of relational test criteria. The left column of the table shows the conditions that are applied, while the column on the right shows the validation criteria. For example, in the case of horizontal wind speed, the maximum gust cannot have a value that is larger than 2.5 times its average value. The rest of the conditions refer to the relationship between measurements at two different heights. For example, the condition that needs to be fulfilled in the case of the wind direction parameters is that the difference between the average wind direction measured at 40 m height and the one measured at 25 m height should be less than or equal to  $20^{\circ}$ .

Table 2.2: Sample relational test criteria.

Sample parameter	Validation criteria
<b>Wind speed: horizontal</b>	
Max gust vs. average	Max gust $\leq 2.5 * \text{Avg.}$
40 m/25 m Average $\Delta$	$\leq 2.0 \text{ m/s}$
40 m/25 m Daily max $\Delta$	$\leq 5 \text{ m/s}$
40 m/10 m Average $\Delta$	$\leq 4 \text{ m/s}$
40 m/10 m Daily max $\Delta$	$\leq 7.5 \text{ m/s}$
<b>Wind direction</b>	
40 m/25 m Average $\Delta$	$\leq 20^{\circ}$

Source: [51];  $\Delta$  symbolizes difference.

Trend tests are based on the rate of change in a value over time. An example of a trend that indicates a potential problem would be a change in air temperature greater than  $5^{\circ}\text{C}$  in one hour. This abrupt change in temperature over such a short interval normally implies a hardware fault in the measurement device. Missing data points are replaced by the system with a different value that has no physical relevance (which acts as a code for debugging). A common designation for data rejection is assigning a -900 series validation code. All these error codes are shown in Table 2.3. In this case, the values were -999, indicative of missing data / no value possible.

The directionality sectors that could be influenced by wake effects from the other towers have also been removed from the main time series. For the met tower, the possible wake directionality sector was from  $67.5^{\circ}$  to  $90^{\circ}$ , while Table 2.4 shows what sectors were considered in the case of the wind turbines.

Table 2.3: Sample validation criteria.

Code	Rejection criteria
-990	Unknown event
-991	Icing or wet snow event
-992	Static voltage discharge
-993	Wind shading from tower
-995	Wind vane deadband
-996	Operator error
-997	Equipment malfunction
-998	Equipment service
-999	Missing data (no value possible)

Source: [51].

Table 2.4: Wake effect sectors for the wind turbines.

Turbine 1		Turbine 2		Turbine 3	
East	67.5° – 112.5°	East	67.5° – 112.5°	East	67.5° – 112.5°
West	247.5° – 270°	West	247.5° – 292.5°	West	292.5° – 247.5°
Turbine 4		Turbine 5		Turbine 6	
East	45° – 67.5°	East	67.5° – 90°	East	67.5° – 90°
West	247.5° - 270°	West	225° – 247.5°	West	247.5° – 270°

Icing was another factor that was considered. In order to identify and remove data that were affected by icing, another rule was defined: if the temperature sensor reported a value below 0° C and the wind direction sensor did not show any variation for a length of time longer than one hour, the data segment was flagged. After all these procedures were done, the data recovery rate was calculated using Eq. (2.1). This is the ratio of valid data records collected versus the total possible number of recordings over the reporting period.

$$\text{Data recovery rate} = \frac{\text{Data records collected}}{\text{Data records possible}} (100) \quad (2.1)$$

The majority of missing data are due to invalid entries in the time series and the summary is presented in Table 2.5. The statistics for each turbine separately, after the flagging rules have been applied are shown in Table 2.6.

Table 2.5: Time series summary for all wind turbines.

	Turbine 1	Turbine 2	Turbine 3	Turbine 4	Turbine 5	Turbine 6
Possible records	52,704	52,704	52,704	52,704	52,704	52,704
Valid records	40,505	38,421	38,173	41,197	43,448	42,648
Missing records	12,199	14,283	14,531	11,507	9,256	10,056
Data recovery rate (%)	76.85	72.9	72.43	78.17	82.44	80.92



Table 2.6: Time series statistics for wind turbines.

Flag Rule	N° time steps identified					
	Turbine 1	Turbine 2	Turbine 3	Turbine 4	Turbine 5	Turbine 6
Average wind direction max	105	243	102	0	440	144
Average wind direction min	0	0	0	0	0	0
Average wind speed max	20	36	34	17	24	23
Average wind speed min	0	0	0	0	0	0
Average wind speed std max	630	766	712	575	655	686
Average wind speed std min	0	0	0	0	0	0
Invalid data	15,195	16,333	19,210	14,167	20,582	16,950
Max gust vs. average	513	399	347	349	388	446
Temperature average trend	78	78	78	72	558	2,202
Wake effect east	3,890	2,991	2,946	2,255	1,364	1,472
Wake effect west	3,674	6,686	6,702	3,105	2,916	2,948
Wind dir gust max	105	243	102	0	440	144
Wind dir gust min	0	0	0	0	0	0
Wind speed average trend	2,298	2,742	3,006	3,180	3,354	3,954

The full scale wind data allowed for the creation of a wind frequency rose, which shows how wind speed and direction are distributed at the considered location. Three main wind directions were chosen for analysis in full scale as well as the wind tunnel experiments (Figure 2.4). Figure 2.5 shows the three chosen wind directions (which were 315°, 157.5° and 202.5° from North). The wind rose is centered on the met tower, as this was the location where the data used to generate it was collected.

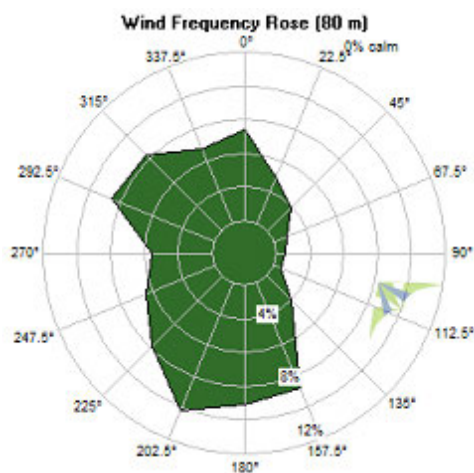


Figure 2.4: 80 m wind frequency rose.



Figure 2.5: Aerial view with wind rose and predominant wind directions.

Source: maps.google.com, 46.453352,-62.058361.

It is important to note that for the  $315^\circ$  direction, most of the terrain is covered by agricultural fields and there is a smoother roughness transition for the incoming flow. For the  $157.5^\circ$  direction, the terrain is mostly forested which is similar for the  $202.5^\circ$  direction, but the distance to the coast in this direction is longer. These wind direction/terrain correlations will be later used to interpret and discuss some of the data and comparison with the wind tunnel results.

## 2.2.2 Data Analysis

The processed data set was further analyzed and statistical analysis was performed. Figure 2.6 shows the average monthly wind speed measured at the met tower, where the wind speed data has been averaged over the interval of a month for each of the three measurement heights: 30 m, 50 m and 80 m. Each data point represents the average monthly wind speed value at each of the considered heights. Lower wind speeds have been observed during the warmer spring and summer months, while higher wind speeds have been observed during the colder months. This is a typical seasonal variability observed for Atlantic Canada.

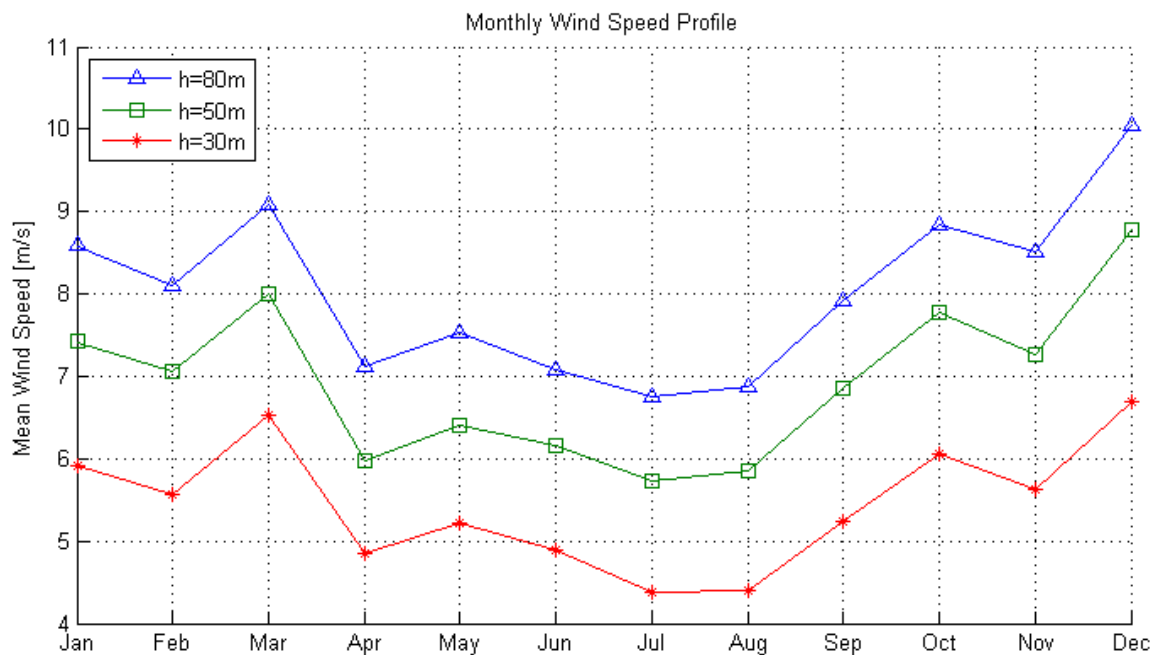


Figure 2.6: Monthly wind speed profile shown at three heights at the met tower.

## Temperature statistics

Figure 2.7 shows the temperature variation for the period considered, and is presented in monthly averages. The graph shows the daily maximum and minimum temperatures, represented by the red solid bar, as well as the monthly maximum and minimum temperatures represented by the thinner capped bars. The first three months of the year show approximately the same maximum temperature, with a small increase in the minimum temperature. Afterwards, the atmosphere tends to warm up steadily heading towards the hottest month, July. As the year enters its last third, a steady decrease in temperature can be observed, heading towards the minimum temperatures, which are usually recorded in January. A higher variability in temperature values can be observed for the colder months, while for the warmer months there is less variability. Considering that the temperature falls below  $0^{\circ}\text{C}$  in the months of January, February, March, April, May, November and December, icing was an issue. This effect was removed from the data set prior to analysis, and was presented in the previous section (Section 2.2.1).

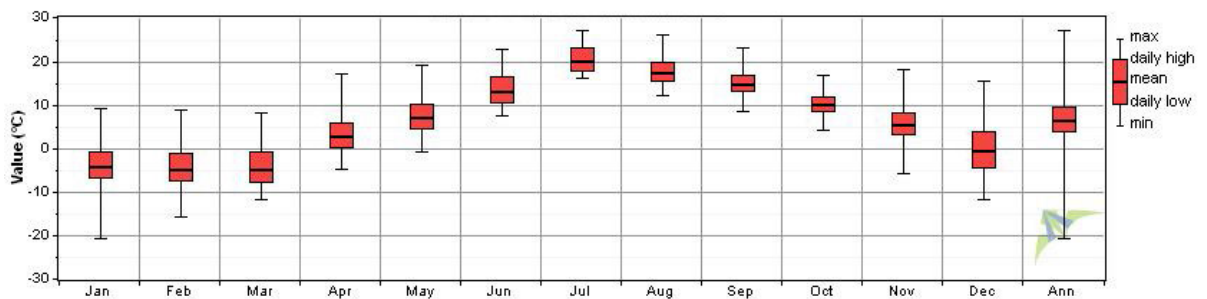


Figure 2.7: Monthly temperature statistics measured at met tower.

## Correlation comparison

Met tower measurements are crucial for wind resource assessment, and are the standard for wind farm siting. That being said, the met tower represents a single point of measurements at a given site, and relying on a single measurement point can lead to significantly different wind conditions as you move away from the met tower, despite still being within the wind farm.

Figure 2.8 shows a comparison between the average monthly wind speeds measured at the met tower and the average monthly wind speeds measured at each of the studied wind turbines, at a height of 80 m. This figure shows that significant differences are indeed observed for the average wind speeds, where the largest differences for individual turbines can be up to 12% of the average wind speed at the met tower. Although the differences are significant, the overall trend of the data for the individual wind turbines is similar to the data measured at the met tower.

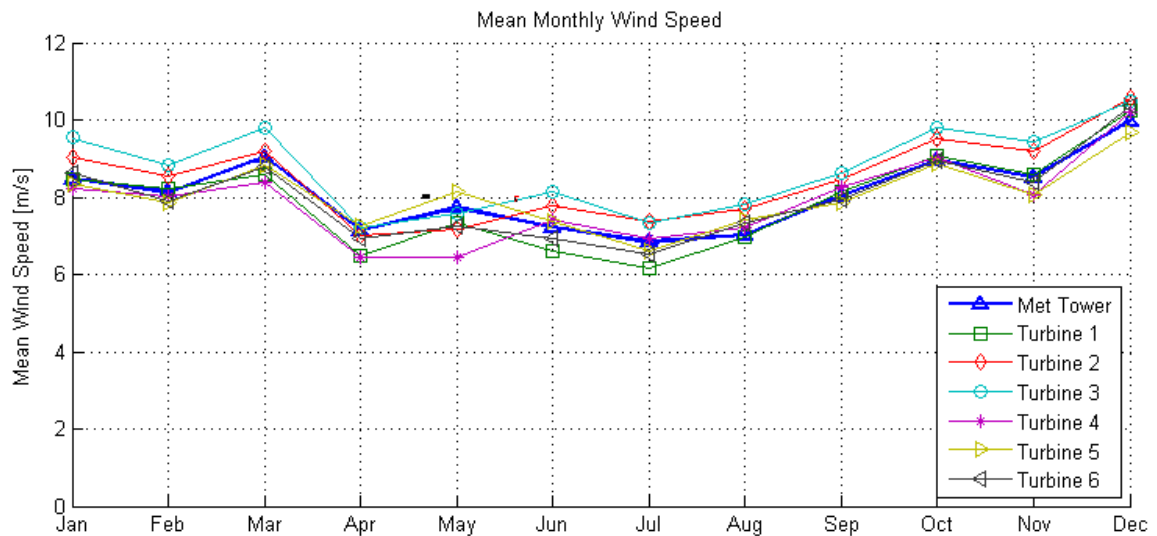


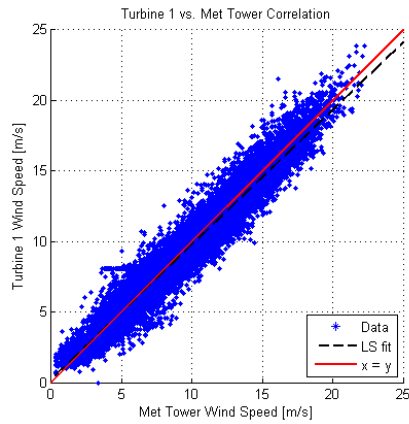
Figure 2.8: Average monthly wind speeds at the met tower compared to the measurements done at the wind turbines.

This section presents the sample by sample correlation of the data from each of the turbines to the data obtained at the met tower. Table 2.7 shows data statistics for Figure 2.9, which presents the wind speed scatter plots. Figure 2.9 essentially shows how well the met tower measurements compare to the measurements taken at each of the wind turbines, using a least

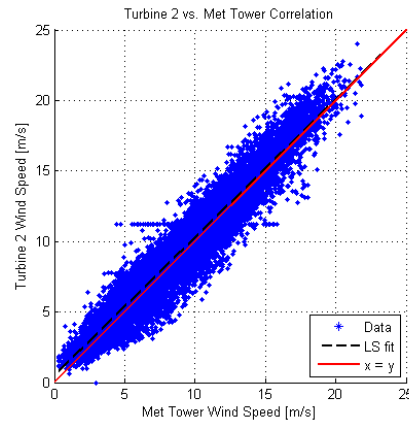
squares fit. At a height of 80 m (wind turbine hub height), the anemometers from the wind turbines measured a slightly lower wind speed than the met tower, as per the linear least square fits presented in the figures. The correlation was very good over the analyzed samples with an average correlation coefficient  $R^2$  of over 0.9, where  $R^2$  is the coefficient of determination and indicates how well data points fit a curve.

Table 2.7: Turbine vs. met tower correlation statistics;  
(letters in parenthesis refer to sub-figures from Figure 2.9).

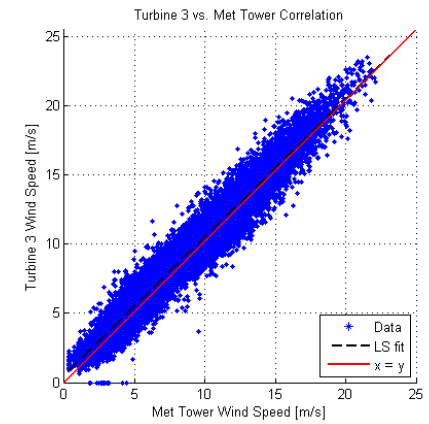
Location	$R^2$	Number of samples
(a) Turbine 1	0.947	35,988
(b) Turbine 2	0.940	34,149
(c) Turbine 3	0.952	34,034
(d) Turbine 4	0.914	35,729
(e) Turbine 5	0.911	38,032
(f) Turbine 6	0.870	37,149



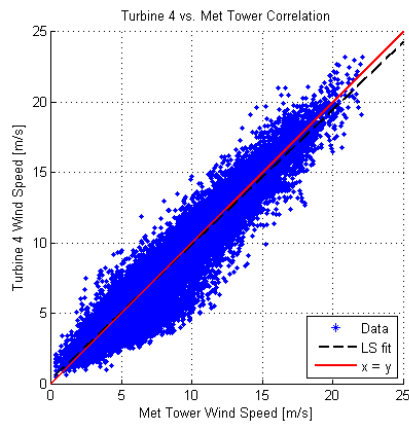
(a)  $R^2 = 0.947$ ; Samples: 35,988



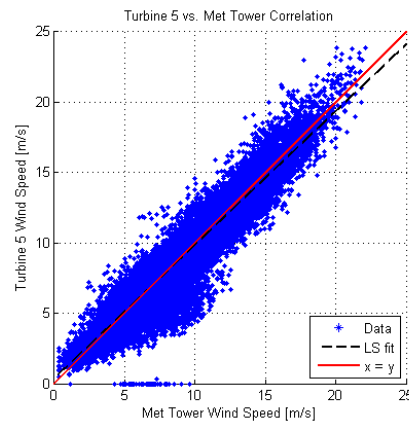
(b)  $R^2 = 0.940$ ; Samples: 34,149



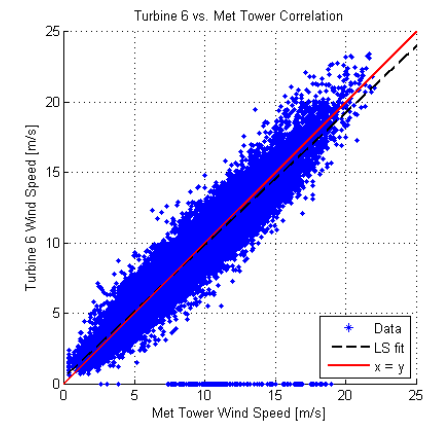
(c)  $R^2 = 0.952$ ; Samples: 34,034



(d)  $R^2 = 0.914$ ; Samples: 35,729



(e)  $R^2 = 0.911$ ; Samples: 38,032



(f)  $R^2 = 0.870$ ; Samples: 37,149

Figure 2.9: Wind speed correlations between the data measured at the met tower and the data from the wind turbines at 80 m height.

## 2.3 Stationary Data Segments

Data segments that represented, as best as possible, stationary data were identified in the full scale data set. The segments were identified by searching in the full scale data set, available from the met tower, values of wind direction and wind speed that were within a certain range. The intervals were chosen to be 100 minute long, as this time duration contains enough measurement sample points. This length of time also corresponds to the spectral gap present in the wind energy spectrum graph presented in Figure 2.10.

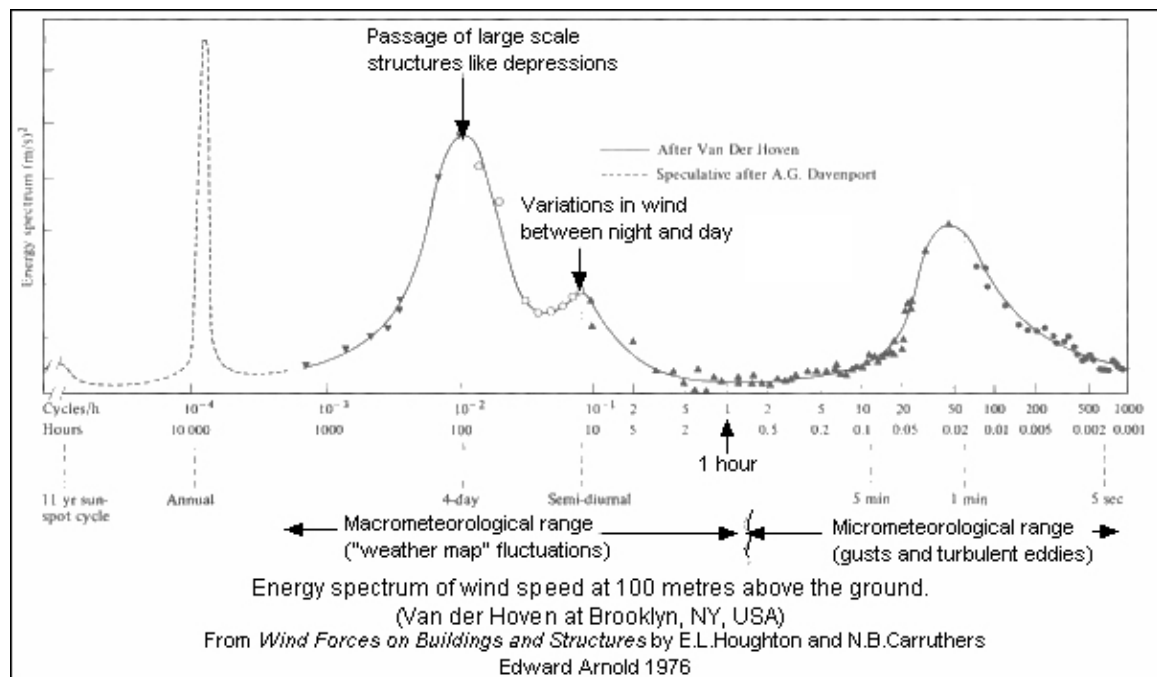


Figure 2.10: Energy spectrum of the wind speed at 100 m above the ground. Source: [52].

In order to identify valid segments in the full scale data series, a suite of Matlab<sup>2</sup> programs were written. The programs were used to minimize factors such as direction and standard deviation of wind speed segments, as presented in Table 2.8. This validation was required to ensure that the selected segments were indeed stationary.

<sup>2</sup>MATLAB® is a high-level language and interactive environment for numerical computation, visualization, and programming (<http://www.mathworks.com/products/matlab/>).

Table 2.8: Data segment validation criteria.

Validation criteria	Condition
Length	100 minutes
Polynomial slope (trend)	Within range: (-2, 2) m/s <sup>2</sup>
Standard deviation	< 2 m/s
Direction variation	Within 30° sector

The first step was to extract data segments of sufficient length (100 min = 1h 40min, equal to ten intervals, each ten minutes long) from the met tower time series. In order to assess if a selected segment represented stationary data, the wind speed and wind direction it represented were plotted and the resulting data was analyzed. Figure 2.11 shows an example of a selected data segment, graphs (a) and (b) show the wind speed and direction plots with the different constraints applied, i.e. data trend and direction variation, respectively, in order to validate the selection. Figure 2.11a shows a linear regression fitted to the wind speed data segment in order to evaluate the trend of the selected data. The slope of the resulting curve is constrained to a range of (-2, 2) m/s<sup>2</sup>, where a value closer to zero is preferred as it shows the wind speed was not increasing or decreasing. In this case, the slope had a value of approximately -0.8 m/s<sup>2</sup> thus it passed the validation criterion.

Another constraint is the standard deviation of data. This shows how much variation exists from the average value and lower standard deviation values show that analyzed data points are close to the average value. In the case presented in Figure 2.11a, the standard deviation value was 0.67 m/s.

The wind direction sensor is always mobile; therefore the measurements from this sensor cannot have a constant value. In order to determine the wind direction for a given segment of data a directionality sector of 30° was used. Figure 2.11b shows wind direction variations as well as the acceptable range (i.e. 157° ± 15°). The extracted segment meets this criterion as well. Once a data segment from the met tower time series was accepted and deemed valid, another program identifies the equivalent segments for each of the wind turbine time series and stores it. A third program was written to plot the data sequentially, and save the figures automatically.



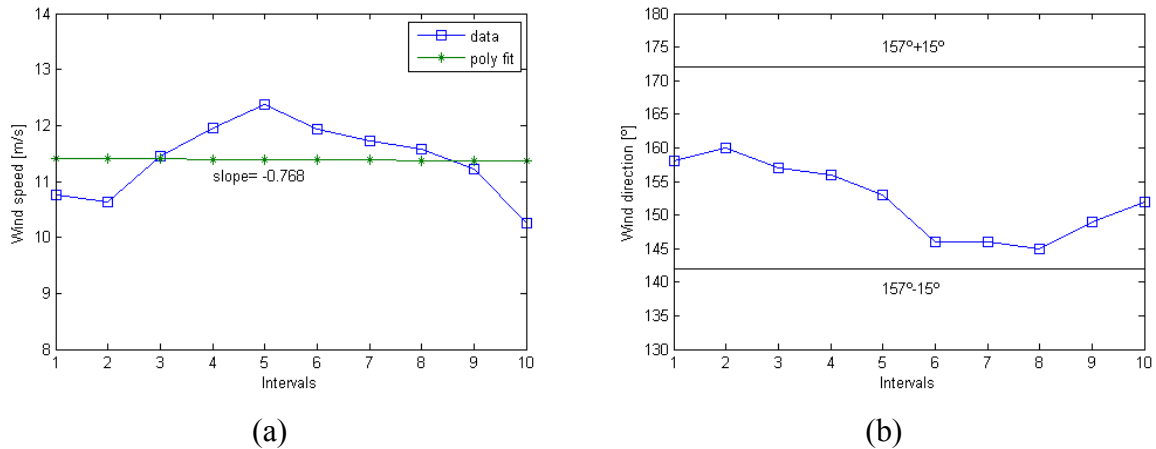


Figure 2.11: Example of Matlab segment identification and validation. Figure (a) shows the evaluated trend of the segment, and figure (b) shows the wind direction variation within the set limits.

This approach to the selection of data is similar to the one presented by Levitan and Mehta [53] for the Texas Tech field experiments. Essentially, if a data segment for the met tower was accepted, the corresponding data for the wind turbines were selected as well.

The Matlab program succeeded in identifying several 100 minute time segments for which all of the criteria stated were satisfied, as presented in Table 2.9. This table shows the number of valid data segments found from the data recorded at the met tower at 80 m height. Table 2.10 shows the remaining number of extracted valid segments, where both data at the met tower and data at the wind turbines were available.

Table 2.9: Number of valid data segments identified per month at the 80 m height of the met tower.

month \ direction [°]	315	157.5	202.5
January	14	6	10
February	14	5	5
March	28	14	14
April	5	5	4
May	12	7	26
June	15	20	13
July	7	46	30
August	16	15	16
September	25	8	58
October	27	27	17
November	2	21	6
December	34	5	35

Table 2.10: Valid data segments identified per month at the 80 m height of the met tower and at the wind turbines (80 m height).

month \ direction [°]	315	157.5	202.5
January	14 (-)	5 (-)	10 (-)
February	12 (-2)*	4 (-1)	5 (-)
March	24 (-4)	12 (-2)	9 (-5)
April	5 (-)	5 (-)	2 (-2)
May	3 (-9)	3 (-4)	0 (-26)
June	0 (-15)	0 (-20)	0 (-13)
July	0 (-7)	15 (-31)	3 (-27)
August	14 (-2)	12 (-3)	16 (-)
September	24 (-1)	7 (-1)	47 (-11)
October	26 (-1)	18 (-11)	14 (-3)
November	0 (-2)	17 (-4)	5 (-1)
December	31 (-3)	3 (-2)	30 (-5)

\*the numbers in parentheses show how many segments have been discarded relative to the previous case, the dash (-) symbol signals no change (measurements available at the met tower), shown in Table 2.9.

## 2.4 Final Comparison Sets

A comparison is carried out between the full scale data segments (segments were extracted from the full scale data set, as stated in Section 2.3) and the wind tunnel experiment runs. A further filtration of the extracted segments is done based on atmospheric stability. Since the atmospheric stability cannot be measured directly, time segments which did not show the characteristics of near neutrally stable regimes – the ones that had an average wind speed below 10 m/s - were discarded.

The remaining number of monthly valid segments is presented in Table 2.11 and the final comparison set of segments (a complete set is considered to have valid segments for each direction in each month) is presented in Table 2.12.

Table 2.11: Valid data segments identified per month at the 80 m height of the met tower and at the wind turbines (height of 80 m) with wind speed over 10 m/s.

month	315	157.5	202.5
direction [°]			
January	3 (-11)*	5 (-)	5 (-5)
February	1 (-11)	2 (-2)	0 (-5)
March	6 (-18)	1 (-11)	5 (-4)
April	0 (-5)	1 (-4)	0 (-2)
May	0 (-3)	3 (-4)	0 (-)
June	0 (-)	0 (-)	0 (-)
July	0 (-)	5 (-10)	0 (-3)
August	0 (-14)	0 (-12)	5 (-11)
September	2 (-22)	3 (-4)	4 (-43)
October	2 (-24)	18 (-)	3 (-11)
November	0 (-)	10 (-7)	0 (-5)
December	15 (-16)	2 (-1)	26 (-4)

\*the numbers in parentheses show how many segments have been discarded relative to the previous case, the dash (-) symbol signals no change (measurements available at met tower and all wind turbines), shown in Table 2.10.

Table 2.12: Final valid data segments set identified per month at the 80 m height of the met tower and at the wind turbines (height of 80 m) with wind speed over 10 m/s.

month	315	157.5	202.5
direction [°]			
January	3	5	5
March	6	1	5
September	2	3	4
October	2	18	3
December	15	2	26

### 2.4.1 Atmospheric Stability

Atmospheric stability depends on the vertical motions of air. If these motions are suppressed or enhanced, the stability of the homogeneous boundary layer is affected. Over a period of an entire day, stratification is caused by the heating and cooling of the surface. The boundary layer can be divided into three regimes, depending on the main source of turbulence [54], [55], [56]:

- Convective or unstable: during daytime, convectively driven turbulence is generated from the heating of the surface. Essentially, the air is warmed from the bottom and rises.
- Stable: during night time, the cooling of the surface tends to suppress turbulence. The air density is increased near the surface and the vertical motion of air is damped.
- Neutral: occurs when overcast and strong winds are present near the surface. The heat flux is close to zero in this state and the vertical motions are neither enhanced nor damped.

The stable regime is characterized by the accentuated increase in wind speed with height when compared to the neutral state. In the unstable regime the vertical motions of the air prevent a strong increase of wind speed with height. This influence of wind shear on the regimes of the boundary layer can be observed in Figure 2.12. The comparison between the measured wind profile and the stable wind speed profile in Figure 2.12 shows that the

selected full scale data segments are representative of a stable regime. The 157.5°, 202.5° and 315° curves on the graph represent the vertical wind speed profile, measured at the met tower, averaged over the selected full scale data segments for the five selected months for each of the main wind directions. The height used for non-dimensionalizing was 200 m.

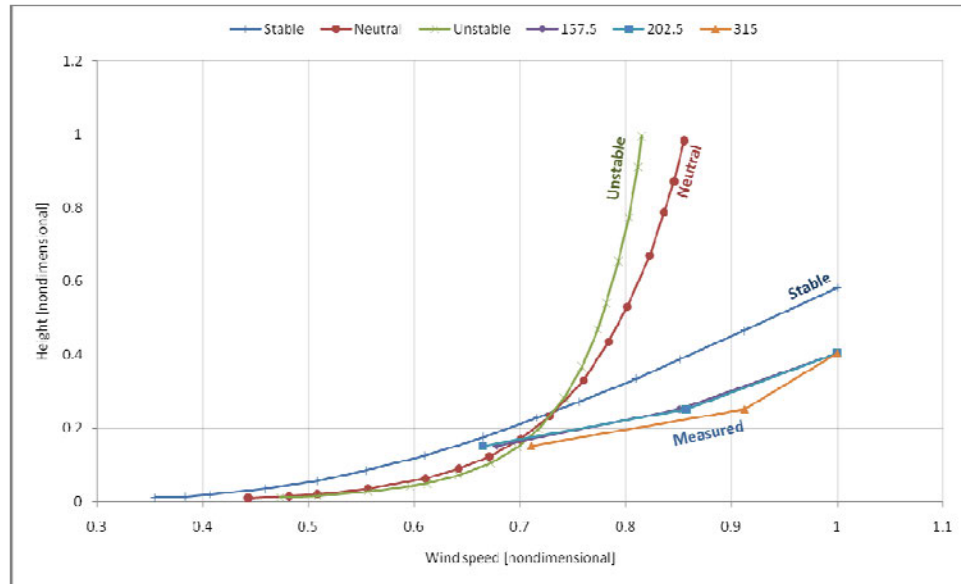


Figure 2.12: Influence of stability on the vertical wind speed profile and comparison with the average vertical wind profiles measured at the met tower for directions 157.5°, 202.5° and 315°.

Adapted from Sucevic and Djuricic [55].

## 2.4.2 Time Series Equivalence

The length of the wind tunnel experiment time series needed to be matched to the stationary full scale data segments identified previously, in Section 2.3, a series of Matlab programs were written in order to determine time series segments. Using Eq. (2.2) and Eq. (2.3), as well as the ones in Appendix B (the full calculation is presented in this appendix) and with a sampling rate of 312.5 Hz, it was determined that a sampling time of 20 seconds (6272 samples from each Cobra probe) are equivalent to 100 minutes in full scale.

$$\frac{L_{wt}}{L_{fs}} = \frac{1}{500} \quad (2.2)$$

$$\frac{V_{wt} \cdot T_{wt}}{L_{wt}} = \frac{V_{fs} \cdot T_{fs}}{L_{fs}} \quad (2.3)$$

where  $V$ ,  $T$  and  $L$  stand for velocity, time and length scales, respectively, while the indices  $wt$  and  $fs$  stand for “wind tunnel” and “full scale”, respectively.

The design of the wind tunnel experiment was detailed in this chapter. Full scale topographic data was used to generate an experimental model to which a preliminary forest canopy model was added. A similarity analysis was performed and Reynolds number independency was shown. Stationary data segments were identified in the full scale wind speed data set which was used as a basis for comparison with the wind tunnel experimental results. The next chapter presents the preliminary results of the wind tunnel tests.

## 2.5 Wind Resource Assessment Using WAsP

As an initial assessment of the site, the data were analyzed using Wind Atlas Analysis and Application Program (WAsP). WAsP generates statistics for wind climates, such as raw wind data analysis, wind atlas data generation, wind climate estimation, estimation of wind power potential and calculation of wind farm production, based on the extrapolation of vertical and horizontal data [57]. Mortensen et al. [58] explain that WAsP contains several models which are used to characterize wind flow over diverse terrains. Figure 2.13 illustrates the use of these models on measured wind data to calculate a regional wind climatology or wind atlas, where a wind atlas encompasses the wind speed and wind direction data for a specific site. The figure presents two arrows, one pointing upward, and the second pointing downward. The upward pointing arrow emphasizes the use of meteorological models in the calculation of regional wind climatology from the observed wind data; this is the analysis part of the program. The downward pointing arrow represents the application of the wind atlas data, where the wind climate at a specific site is calculated from the regional climatology. Essentially, the raw data are processed and meteorological models are employed to generate regional wind climatologies. Frank and Rathmann [59] discuss the reverse process, where wind atlas data are applied in order to compute the wind climate in a defined region.

The contour map, roughness map and wind data are input to WAsP, which was used as per the schematic shown in Figure 2.13. A linear orographic model is used in WAsP. By using a polar representation and the assumption of linear motion equations, the model is capable of creating a high resolution terrain area around the site studied. The model then calculates the potential flow perturbation induced by the terrain, which is modified afterwards to include the effects of surface friction in the inner-layer close to the surface. The model is restricted to neutrally-stable flows over smooth topographic features with attached flows [57], [60]. In the work of Frank et al. [59], as well as Troen [61], measured field data from the benchmark experiments of Askervein [62] and Blasheval [63] hills are well matched with the WAsP predictions for plain isolated hills. Walmsley and Taylor [7] have shown that wind tunnel experiments of the Askervein and Blasheval hills produced good results and were in good agreement with the measured data, while the numerical models for the same hills had varied degrees of success. Bowen and Mortensen [5] explain that the WAsP analysis and application procedures associate the wind data at the initial location with those at the investigated site. WAsP defines wind direction sectors based on roughness and topographic features at both sites and proceeds to generate a relative speed-up factor between both sites which does not depend on climatic conditions [60].

### **WAsP and the Eastern Kings Wind Farm**

An analysis has been done on the Eastern Kings wind farm using the measured wind speeds and terrain data. An observed wind climate is generated, using WAsP, from the available wind data and a digital elevation map is created using terrain data. The met tower and each of the wind turbines are placed on the digital elevation map using their respective location coordinates. The observed wind climate, mast locations for the met tower and wind turbines and terrain and roughness data are used to make the calculation of a wind resource grid possible.

A wind resource grid represents the way WAsP outputs the predicted wind resource over an area, and is usually presented at the same altitude as the turbine hub height.

The wind data measured at the Eastern Kings wind farm was used to generate a wind resource grid over an area in the vicinity of the wind farm; this was essentially achieved by removing the orographic influence from the observed wind speeds and predicting values for the other locations in a grid.

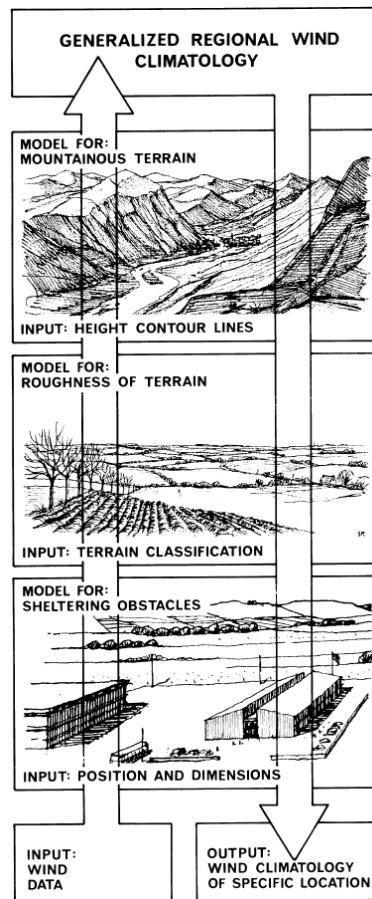


Figure 2.13: WASP wind atlas methodology.

Source: [58].

Figure 2.14 shows a comparison between the PEI wind atlas [64], and the wind resource map generated from WASP using the wind measurements at the Eastern Kings wind farm. A wind atlas is a collection of data that contains the wind speed and wind direction in a region and it is employed when pre-selecting wind farm sites.

The PEI wind atlas was created using the Canadian Wind Energy Atlas as input meteorological data. The PEI wind atlas was computed for three different heights: 30 m, 50



m and 80 m, with a resolution of 200 m, as shown in Figure 2.14a [64]. The slight differences between the two wind resource maps are due to the fact that the PEI wind atlas (Figure 2.14a) mapped a far larger area - the entire surface of PEI - at a lower resolution than the resource grid that was generated using WAsP for the eastern tip of PEI (Figure 2.14b). Even so, the resulting wind resource grid is similar to the PEI wind atlas for the area surrounding the Eastern Kings Wind Farm.

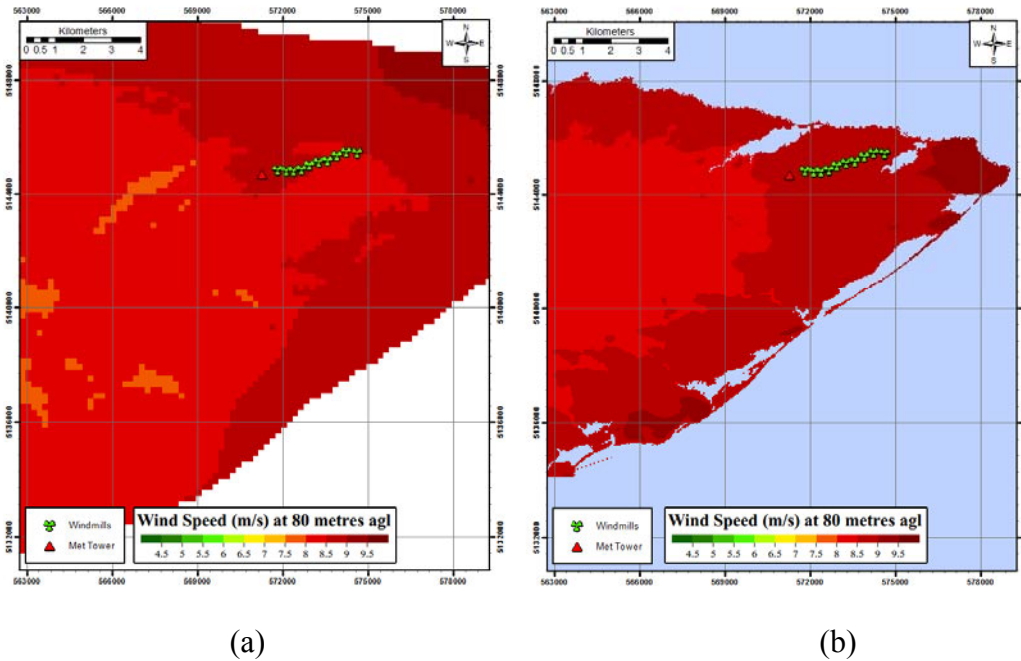


Figure 2.14: (a) PEI wind atlas for East Point at 80 m height. Source: [64];  
 (b) resource grid at 80 m, generated for the Eastern Kings wind farm using WAsP.

For this case study there was only one complete year of available data. The intent was to use the WAsP model to predict wind speeds at a location far enough from the wind farm to act as a reference inflow speed for the comparison with a wind tunnel experiment. The way WAsP works has made this approach irrelevant, as the predictions generated are yearly means. A wind tunnel experiment would require shorter wind speed data segments. The WAsP analysis was still useful as a means of data validation by comparing the WAsP output – the wind resource grid – to an existing study – the PEI wind atlas.

## Chapter 3

### 3. Experimental Setup

A wind tunnel experiment was designed in order to determine the usefulness of wind tunnel studies for wind resource assessment applied to wind energy. The case study presented in the previous section provides the basis for the wind tunnel experiment. The full scale topographic data for the case study was employed to create a wind tunnel topographic model and a forest canopy model while the full scale wind data was used for results comparison. In this section, the wind tunnel facility is described, as well as the experimental setup, the instrumentation and details about the topographic and forest canopy models. Appendix D contains photographs of the experimental setup.

#### 3.1 Wind Tunnel

The wind tunnel testing has been conducted in Tunnel II of the Boundary Layer Wind Tunnel Laboratory, Western University in London, Ontario, Canada. This is a closed circuit wind tunnel, with a low speed and a high speed test sections. The low speed test section is used for aeroelastic studies of long span bridges, dispersion of pollutants studies, and rain and snow studies as well as topographic studies. Underneath the low speed section's movable floor panels, a wave tank can be used to study the interaction of wind and wave with offshore structures and ships. The high speed test section has two study areas: the upstream section is used to study section models of bridges and towers while the downstream section is used to study the aeroelastic behavior and pressures on buildings and other structures [65].

For this work, the experiments were performed in the low speed section of the wind tunnel. This section is 4 by 5 m, thus wide enough to accommodate the topographic model, with a 52 m length, and it can provide wind speeds of up to 10 m/s (36 km/h). The free stream velocity was measured at the centerline by using a Pitot tube at the center of the wind tunnel's cross section. The model was placed 25 m downstream of the slow speed test section's inlet. The slow speed test section is indicated by the arrow seen in Figure 3.1.

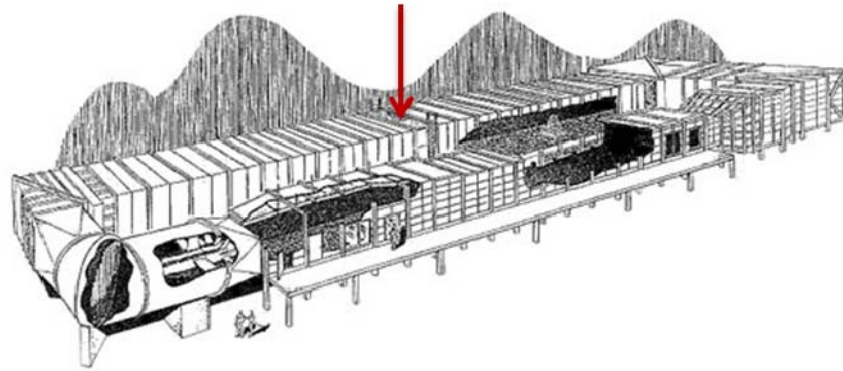


Figure 3.1: Boundary Layer Wind Tunnel Laboratory - Tunnel II, Western University; showing the low speed section. Source: <http://www.blwtl.uwo.ca>.

## 3.2 Boundary Layer

Flow conditions are presented in Table 3.1. The Reynolds number calculated is based on the scaled hub height and the three examined wind tunnel free stream velocities, and had a value ranging from  $5 \cdot 10^4$  to  $7.35 \cdot 10^4$ . The wind speed profile was available from hot-wire measurements in the wind tunnel, based on the work of Rasouli [16], and are shown in Figure 3.2. An Excel spreadsheet was created in order to calculate the wind profile parameters and to identify what terrain it fits best. The logarithmic wind profile law and the power law were used to determine the wind profile parameters. The fitting data are presented in Appendix A.

Table 3.1: Flow conditions for the topographic model.

	Free stream velocity
Test 1	4.57 m/s
Test 2	5.67 m/s
Test 3	6.71 m/s
Velocity profile	<i>Figure 3.2</i>

The power law coefficient ( $\alpha$ ) obtained from using the power law for the wind tunnel vertical wind profile upstream of the test section resulted in a value of approximately 0.1. This value was compared to other values found in the scientific literature (presented in Table 3.2) and indicates that this profile is consistent with the one found over large bodies of water.

Each of the experiment's runs consisted of three tests, with increasing wind speeds: 4.57 m/s, 5.67 m/s and 6.71 m/s. The results from these tests are discussed in the similarity analysis presented in Section 3.5.3.

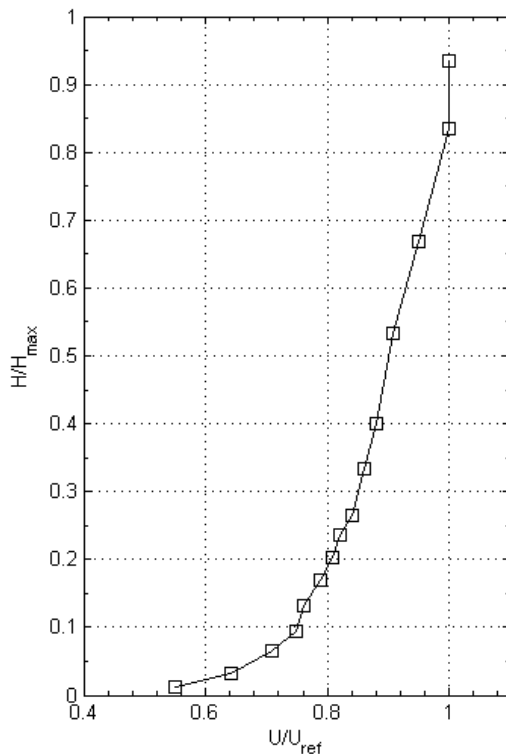


Figure 3.2: Streamwise velocity profile upstream of the model from hot-wire measurements; Adapted from Rasouli [16].

Table 3.2: Land type and power law coefficient of various land types as per Bañuelos et al. [66].

Land type	$\alpha$
Lakes, ocean and smooth hard ground	0.1
Grasslands (ground level)	0.15
Tall crops, hedges and shrubs	0.20
Heavily forested land	0.25
Small town with some trees and shrubs	0.30
City areas with high rise buildings	0.40

### 3.3 Topographic Model

The geospatial data available for the PEI wind farm are in the form of a detailed contour map and a roughness map. These digital files contain the various terrain features measured on site as well as the various obstacles that are present. In order to create a physical model of the terrain at the Eastern Kings wind farm, the geospatial data was converted into a format that could be read by the CNC machine's CAM (Computer Aided Manufacturing) software. An algorithm was designed to generate a CAD/CAM model for the PEI site, as shown in Figure 3.3. In this case, the topography is represented using large high resolution raster files, which could not be used as input for CAM.

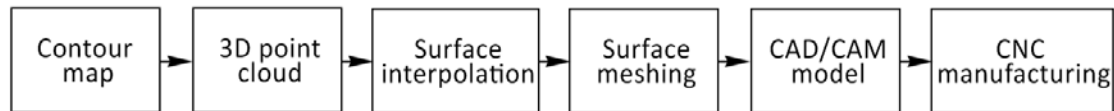


Figure 3.3: Modeling procedure. The algorithm was used to build the topographic model.

#### 3.3.1 Geospatial Data

The geospatial data were in the form of a digital contour map, shown in Figure 3.4, which is a visual representation of elevation for PEI's East Point. Each line represents a different height, with a total of 4810 different contours. This representation ranges from sea-level to a maximum height of 62 m. The contour map has a very good resolution, as the equidistance of the contours is 2 m.

#### 3.3.2 CAD Model

In order to convert from two-dimensional line data to a three dimensional representation of the model, some extra steps were needed. The contours were converted to a point cloud. Interpolation methods were used to create a shell of the terrain. This shell was then exported to meshing software which created triangular faces on the surface. The triangular mesh was read by the CAD software, imported and processed. A "solid" model was created by

extruding this surface by a set amount. After this final step, the CAD model was ready to be sent to a CNC machine.

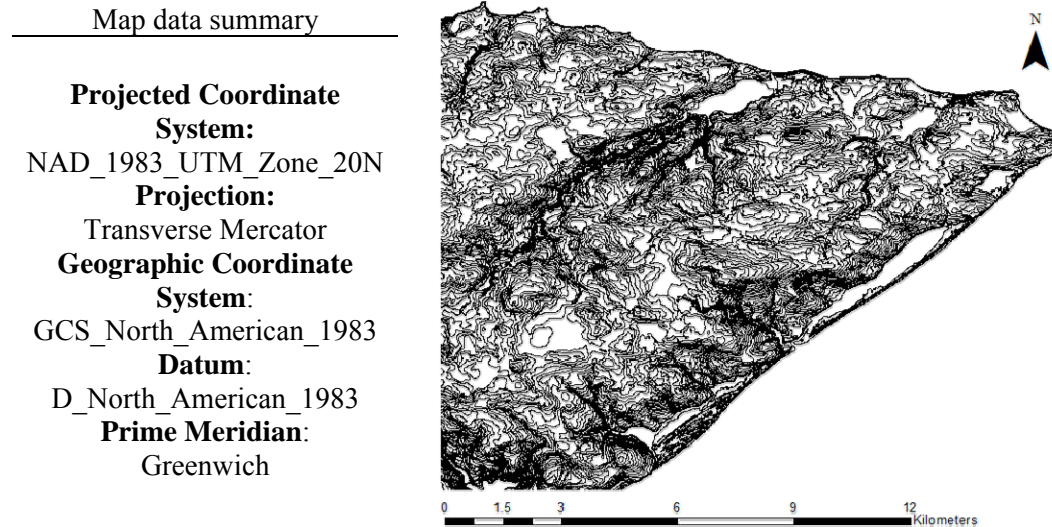


Figure 3.4: PEI East Point Contour Map. Source: PEI Energy Corporation.

### Surface Interpolation

ArcMap<sup>3</sup> (Geographic Information System software [67]) was used, which provides a tool that iterates through all the input features and converts all the vertices (points which describe the intersection of various shapes) that make up the feature's geometry to point features. After this conversion, the points needed to be made into a surface. This was accomplished through interpolation. There are several ways to interpolate a surface through points; the best options in this case were IDW (Inverse Distance Weighting) and kriging. IDW is an exact interpolator, where the maximum and minimum values in the interpolated surface can only occur at sample points as shown in Figure 3.5, while kriging relies on the autocorrelation among measured points, as presented in Figure 3.6. IDW is referred to as a deterministic

---

<sup>3</sup> ArcMap is the main component of ESRI's ArcGIS suite of geospatial processing programs, and is used primarily to view, edit, create, and analyze geospatial data. ArcMap allows the user to explore data within a data set, symbolize features accordingly, and creates maps.

interpolation method - it is directly based on the surrounding measured values that determine the smoothness of the resulting surface. Even though kriging is more accurate than IDW, it is not that efficient when it comes to large datasets. When considering which interpolation method to use, computing resources must be taken into account. Both methods yielded similar results, but in the case of kriging, due to localized interpolation errors, small holes were present in the surface as shown in Figure 3.7. Therefore, IDW was selected as the preferred way of interpolating the topographic surface of the wind farm, as presented in Figure 3.8.



Figure 3.5: IDW surface interpolation technique.

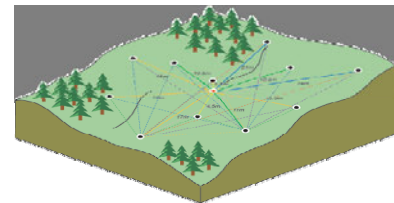


Figure 3.6: Kriging surface interpolation technique.

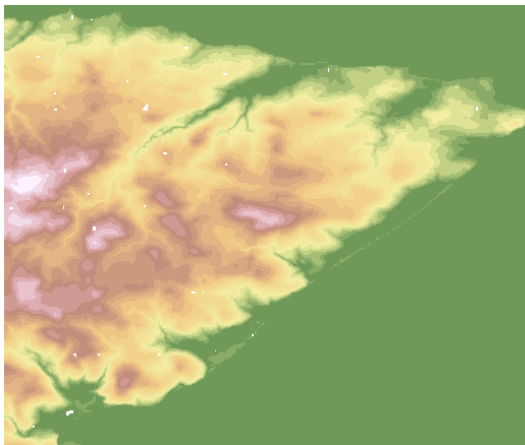


Figure 3.7: Surface interpolated using kriging.

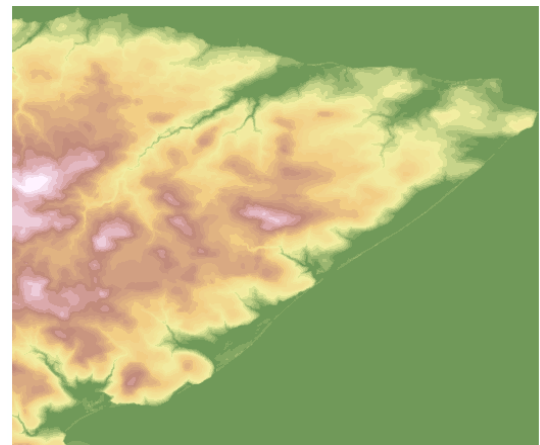


Figure 3.8: Surface interpolated using IDW.

### Model scale

Analyzing the contour map, it was found that the variations in height were not large enough to show any significant topographic features for a preliminary scale of 1:2000. The maximum height found at the studied site was 39 m above sea level; therefore the model was rescaled at 1:500. The change to a larger scale provided more resolution but led to lesser area to be

modeled, as the model for the whole site would not fit inside the wind tunnel. The final model had a diameter of five meters in the wind tunnel, and covered an equivalent full scale area of  $4.906 \text{ km}^2$ . A consequence of changing the scale was that not all of the wind turbines could be included in the experiment. Only six of the ten turbines could be modeled experimentally (as seen in Figure 3.9b).

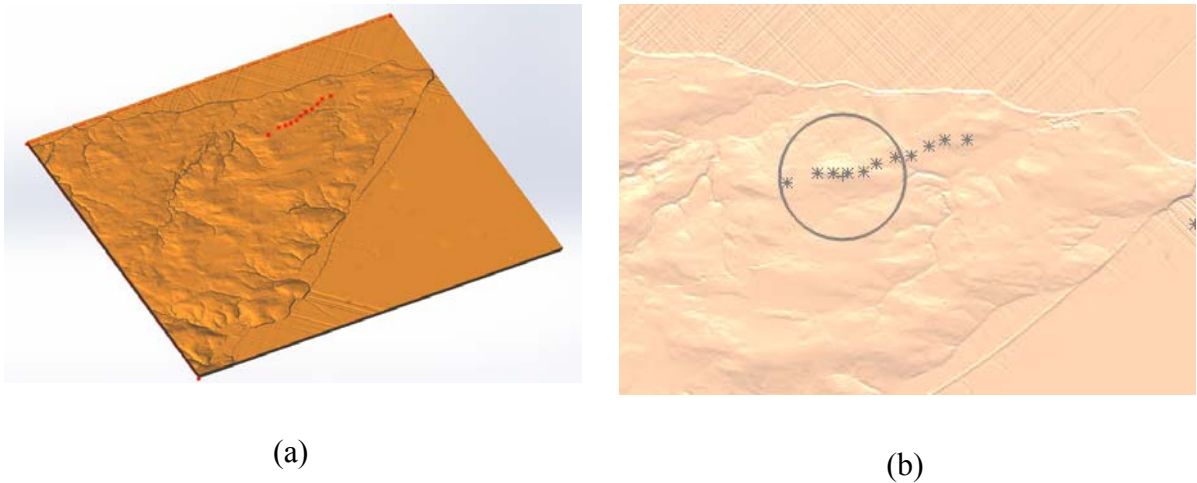


Figure 3.9: Finished CAD model showing (a) met tower and turbine locations; (b) extent of the physical model (circled).

### 3.3.3 Finished Physical Model

After the surface has been created by means of interpolation and triangular meshing, it was imported into CAD software (SolidWorks<sup>4</sup>). The surface was then thickened in order to create a geometry that can be read by a CNC milling machine. The file was sent for milling at the CNC facilities of Bradken (London, ON). The topographic model was delivered in two halves that make up the round area delimited in Figure 3.9b by the gray circle, it has a 5 m diameter and an average thickness of 13 cm; the model covers an area of  $19.64 \text{ m}^2$ .

---

<sup>4</sup>SolidWorks is a 3D mechanical CAD (computer-aided design) program that is being developed by Dassault Systèmes SolidWorks Corp.



### 3.4 Forest Canopy Model

As stated in the Introduction, Section 1.2.2, the scientific literature does not provide an established way in which to model a forest canopy. It is basically a trial-and-error approach, by matching the results obtained to various site characteristics, such as velocity measurements or remote sensed parameters. This implies that modeling a forest canopy is a site-specific operation and further advancements were needed in order to develop a methodology to create a valid forest canopy model.

Given the lack of information on how to model a forest canopy, we chose as a starting point one available material, thus the first attempt at creating a forest canopy model was the use of 90% porous foam. The reasoning behind this choice was that a full scale forest canopy is essentially a porous obstacle for the incoming flow. The tree trunks were not taken into consideration and the whole forest was modeled as being uniformly porous.

A second attempt at modeling the forest canopy is presented in Chapter 5. Remote sensed satellite data are obtained and analyzed and a material for the forest canopy model is chosen based on the equivalence between the remote sensed parameter and the foam material's porosity. In this second case, 48% porosity foam was used to represent the forest canopy.

The Environmental Impact Statement Documents [68] of the Eastern Kings wind farm, in the vegetation section, allows for the identification of the tree species present on the surrounding site. A mix of deciduous and conifer trees make up the forest surrounding the site. At a scale of 1:500, and with an average full scale tree height of 20 m, the model canopy had to be 4 cm tall. The model forest covered an area of roughly  $12 \text{ m}^2$  out of the total area of the model, which was  $19.64 \text{ m}^2$ . The patches of forested terrain were identified using satellite imaging maps, as well as the roughness maps provided by the site's owners.

## 3.5 Case Study Experimental Setup

### 3.5.1 Model

The experimental model was placed in the slow speed section of Tunnel II at the Boundary Layer Wind Tunnel Laboratory at Western University, Canada. The model was placed mid length, i.e. 25 m away from the inlet (additional details of the experimental model and placement in the wind tunnel can be found in Appendix D).

A section of the wind tunnel's floor was lowered by 10.9 cm, because of the model's thickness. This allowed for the floor to line up with most of the top part of the model. Foam boards were used to create a smooth ramp between the tunnel floor and parts of the model that were higher because of the differences in topographic elevation.

The model canopy was fastened to the model using double sided tape. In Figure 3.10 one of the two materials used to model the forest canopy can be seen. The first material used for modeling the forest canopy was 90% porous. Based on the analysis presented in Chapter 5, a 48% porous fiber glass insulation was chosen for the second round of tests.

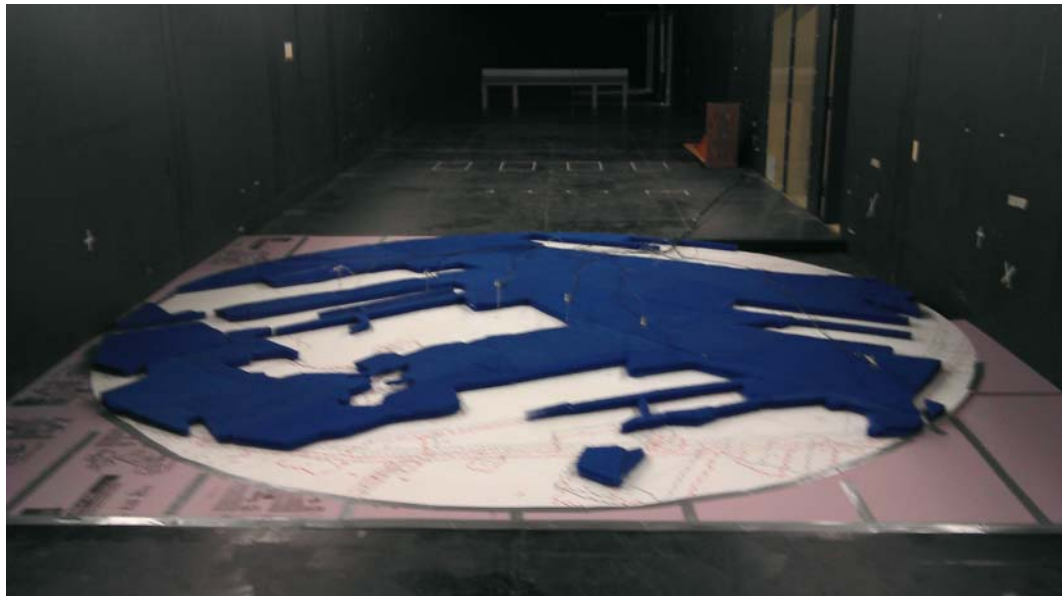


Figure 3.10: Model placement in the wind tunnel with forest canopy and Cobra probes.

### 3.5.2 Instrumentation

The instrumentation used in the wind tunnel experiment consisted of wind velocity probes (Cobra probe). The probes were placed on the model at specific locations that correspond to the full scale placement of the wind turbines and the met tower, at a height over the topographic model representative of turbine hub height in full scale. For each of the three studied wind directions the probes were rotated so that they would face the incoming flow, to attempt to minimize their wake effects. The circle in Figure 3.11a shows the model extent, with the met tower on the left and six wind turbines. Figure 3.11b shows a Cobra probe setup for measurements and surrounded by the canopy model (here the material for the first canopy tests, which has a porosity of 90%, is shown).

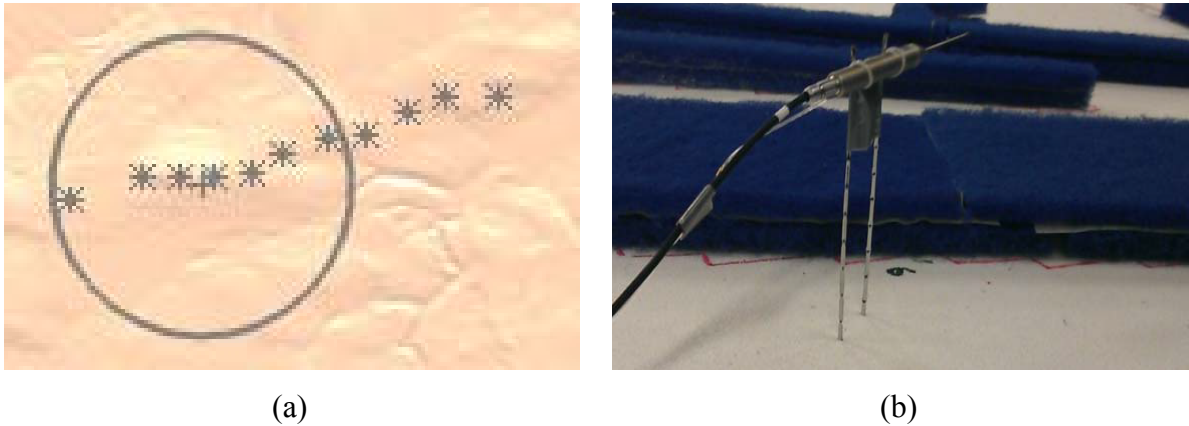


Figure 3.11: (a) Model extent drawn on CAD model; (b) Cobra probe.

The Cobra probe is a multi-hole pressure probe that provides dynamic, 3-component velocity and local static pressure measurements in real-time [71]. It is capable of a linear frequency-response from 0 Hz to more than 2 kHz and is available in various ranges for use between 2 m/s and 100 m/s [71]. Figure 3.12 shows a diagram of the Series 100 Cobra probe indicating its main features, extracted from the manual provided by the manufacturer [71].

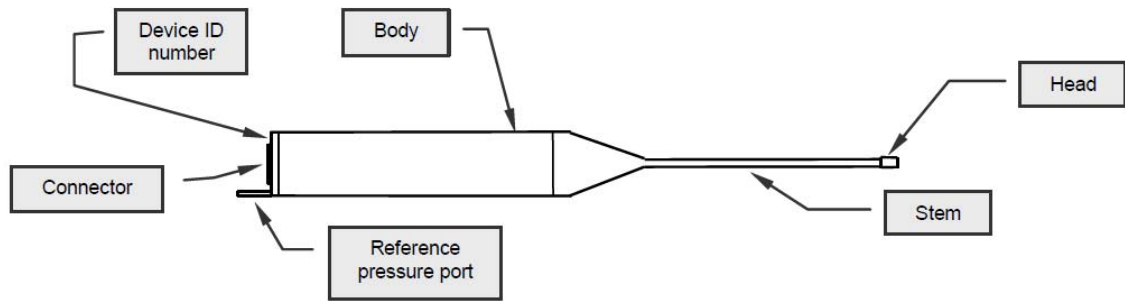


Figure 3.12: Series 100 Cobra probe main features.

Source: [71].

The reference pressure port (shown in Figure 3.12) provides the common reference pressure for the transducers. Therefore, pressures measured by the probe, including local static pressure, are relative to the pressure applied at the reference port.

The probes are then connected to an interface unit with integrated data acquisition. This type of interface unit contains an internal data acquisition system and is known as a Data-acquisition Interface Unit (DIU). Analogue signals from the probes or other sensors are converted to digital signals before being sent to a computer via a USB cable. Power is supplied to the DIU and probe via the USB cable (plugged into a powered USB hub). Figure 3.13 shows an example of this type of interface unit and the typical connections required for operation [71].

In terms of experimental accuracy, the Cobra probes measure velocities with an accuracy of  $\pm 0.5$  m/s, as stated in the Cobra probe guide [71]. In full scale, the anemometers used on the met tower have an accuracy of  $\pm 0.45$  m/s (extracted from the NRG #40C technical sheet [47]), while the sonic anemometers installed on the wind turbines are accurate within  $\pm 0.5$  m/s (from the FT702LT technical sheet [48]).

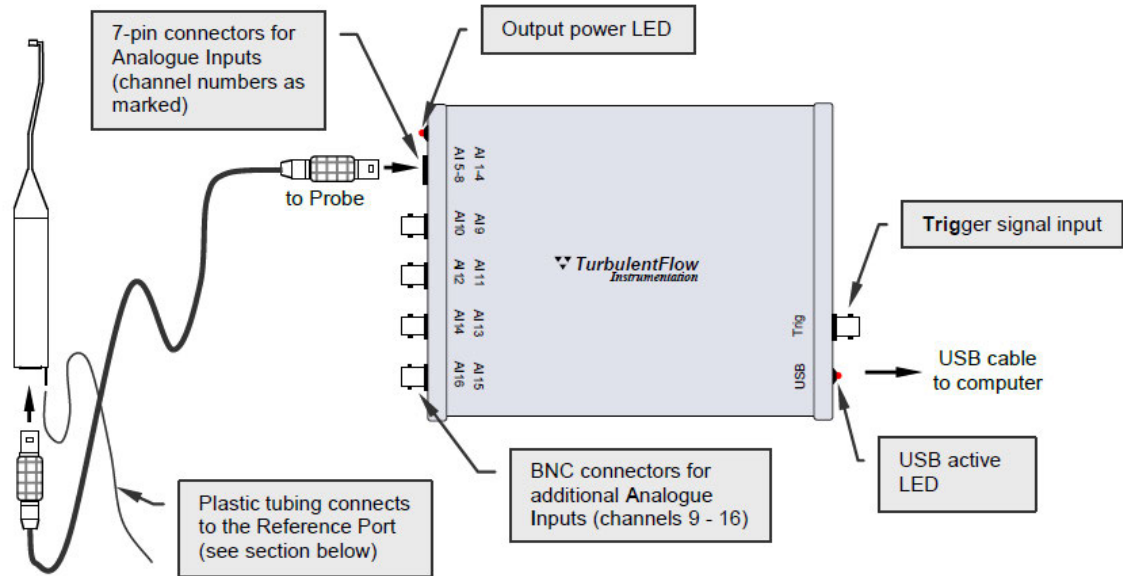


Figure 3.13: Schematic of an example Data-acquisition Interface Unit with integrated data acquisition. Source: [71].

The probe has three types of calibration: static; frequency response; and head calibrations. The only calibration required by the user is a periodic ‘static calibration’ check, as the probes are supplied calibrated and ready to use [71]. Static calibration determines the voltage-to-pressure scaling factors of the pressure transducers. Frequency response and head calibrations should not change unless the probe is physically damaged or ports become blocked [71].

### 3.5.3 Wind Tunnel Tests

Three main wind directions were chosen for the experimental tests. These were selected based on the wind frequency rose, which was generated from the analysis of full scale data and was shown in Section 2.2.1, Figure 2.4. The three wind directions chosen were 315°, 202.5° and 157.5° from North.

Figure 3.14 shows the model orientation in the wind tunnel for the three different wind directions selected. On the model, the North direction is marked as well as the wind turbine locations.

Since the wind tunnel can only create flow in one direction, the model had to be rotated manually for each of the tests. This involved removing the ramps, re-setting the Cobra probes and taping the ramps back to the model and the wind tunnel floor.

The method used to rotate the model to an exact orientation was to calculate the chord for each of the desired angles. Using Eq. (3.1) and starting from the known location of North, three chord values were obtained; the points for all the selected directions were marked on the model prior to the actual rotation.

$$\text{chord}(\theta) = 2 \cdot r \cdot \sin\left(\frac{\theta}{2}\right) \quad (3.1)$$

where  $r$  is the radius of the model (2.5 m) and  $\theta$  is the angle by which the model is rotated.

Figure 3.15 shows the rotation procedure. The first direction is 315° from North, which means rotation of the model by 45° trigonometrically (the point at the end of the red arrow was aligned with the wind tunnel mid line). The next two rotations, i.e. 202.5° and 157.5°, were done in the same way, depicted in Figure 3.15 by the green and blue arrows, respectively.

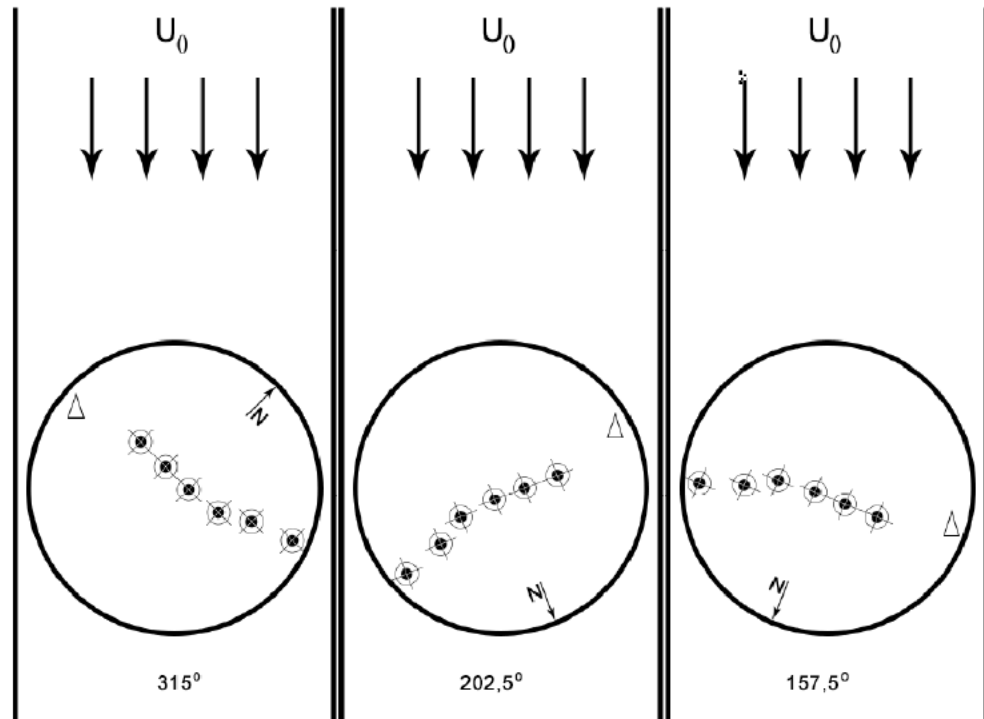


Figure 3.14: Model orientation in wind tunnel for the selected wind directions;  $U_0$  is the free stream velocity;  $\Delta$  shows the met tower location and  $\odot$  represent wind turbine locations.

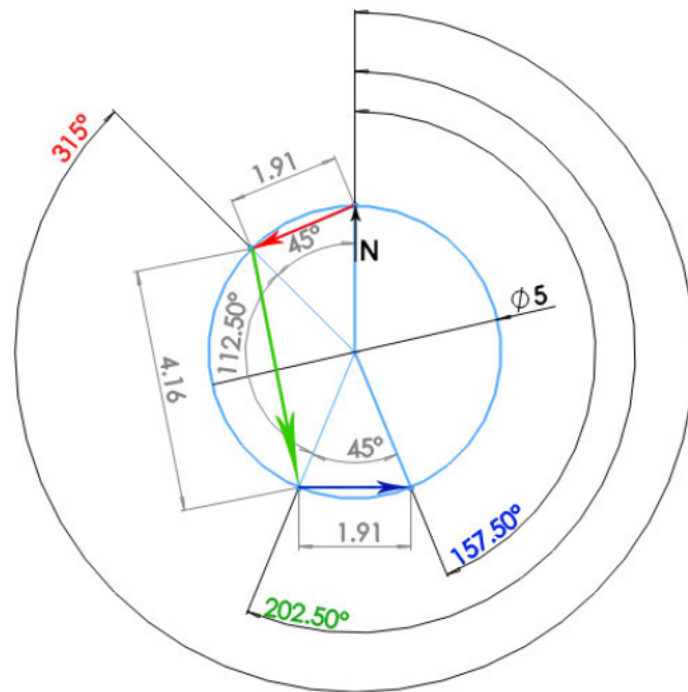


Figure 3.15: Model rotation procedure; linear dimensions in meters.

### 3.6 Similarity analysis

In order for the wind tunnel tests to be valid, three similarity laws need to be addressed: the geometric, the kinematic and dynamic similarities. There are three main scaling ratios involved: the time, length and kinematic scales. Since the length scale is known from the geometry of the model, and the time scale is discussed in Section 2.4.2, the one remaining is the kinematic similarity. The Reynolds (Re), Rossby (Ro) and Froude (Fr) numbers must be equivalent for both cases. The calculated Reynolds number for the scaled wind turbine hub height was from  $5 \cdot 10^4$  to  $7.35 \cdot 10^4$ . Castillo et al. [69] discuss that for Reynolds numbers between 2000 and 160000, the main boundary layer parameters remain independent of the local Reynolds number. Another step taken in order to determine Reynolds dependency was to run the wind tunnel model, for each of the selected wind directions, with three increasing wind speeds. The nine main runs are shown in Table 3.3. For each of the runs presented in the table, the wind tunnel was used three times, with different wind speeds. The three wind speeds were 4.57 m/s, 5.67 m/s and 6.71 m/s.

Figure 3.16 shows the plots for the Reynolds number dependency tests. Each of the plots present the three curves, one for each of the wind speeds used, and another mean curve, which shows the average of the previous three. The order is kept the same as presented in Table 3.3. All of the plots show little variation of the non-dimensional wind speed from one test to another, therefore Reynolds number independence can be observed.

Table 3.3: Wind tunnel experiment runs.

Test number	Model	Wind direction
1	Topographic model only – no forest canopy	315°
2	Topographic model and 48% porous (blue foam filter) material for forest canopy	202.5°
3	Topographic model and 90% porous (fiber glass filter) material for forest canopy	157.5°



The Rossby ( $Ro$ ) number expresses the Coriolis force effects on the systems. Sadeh et al. [70] stated that if the full scale site has a horizontal length of less than 150 km, the Rossby number can be eliminated from the similarity requirement. Also, since the temperature throughout the experiments has been constant, the Froude number requirement may be neglected.

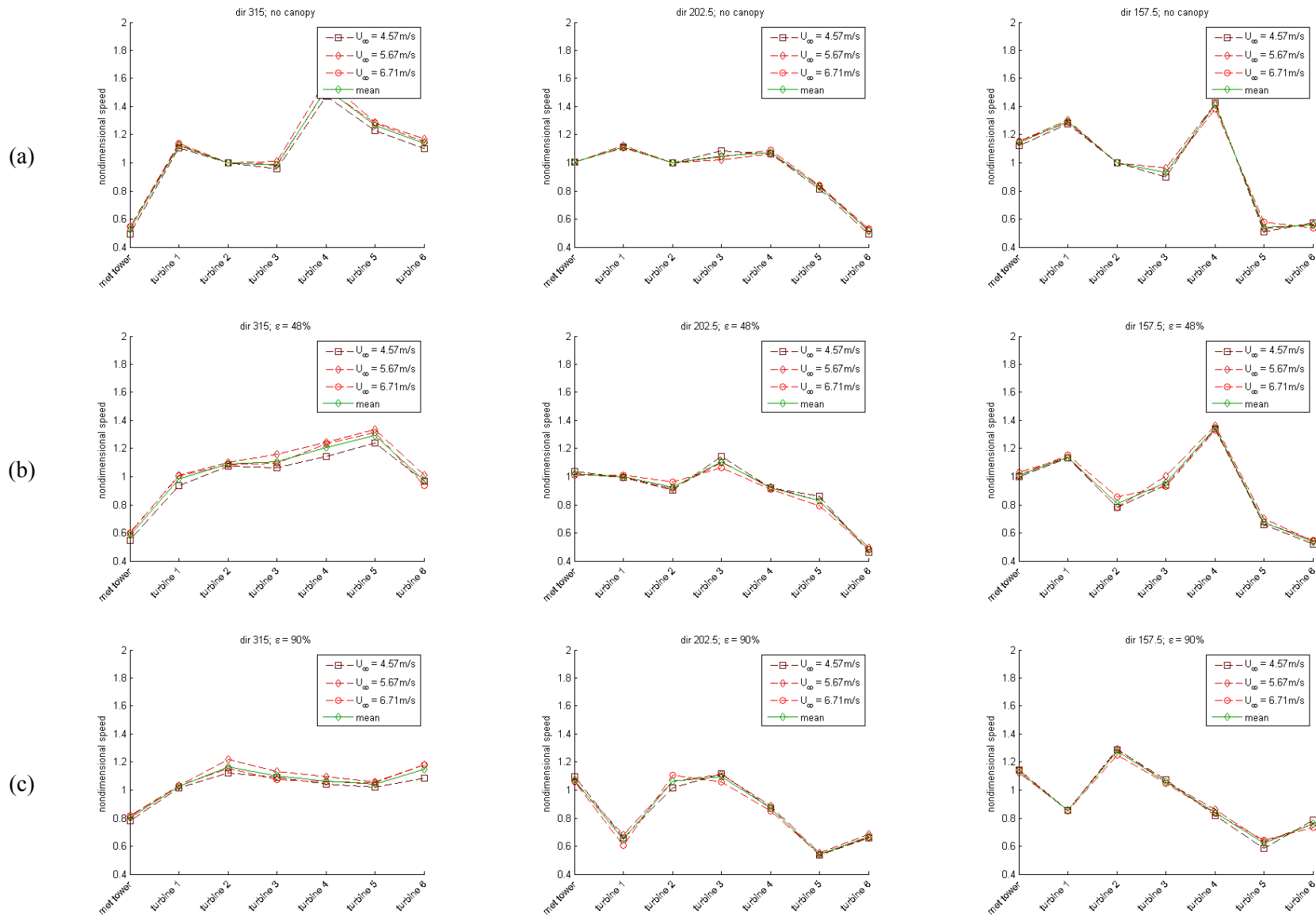


Figure 3.16: Reynolds dependency tests; (a) topographic model only; (b) 48% porosity canopy model; (c). 90% porosity canopy model.

## Chapter 4

### 4. Preliminary Canopy Modeling

#### 4.1 Preliminary Results

For the month of January 2008, three valid data segments were identified, as per Table 2.12. These three segments each consist of ten averaging intervals, which on their own represent data averaged over ten minutes (this is the data available from the data logger mounted on the met tower).

Therefore, a single extracted full scale segment is 100 minute long, as per Eq. (4.1):

$$10 \cdot a_i \cdot 10 \cdot \text{min} = 100\text{min} \quad (4.1)$$

where  $a_i$  stands for averaging interval.

Figure 4.1 shows how the full scale data was plotted and prepared for comparison with the wind tunnel experiments.

Figure 4.1a, shows an example of how the full scale data was plotted. The data presented in this plot correspond to the 315° direction, and was extracted for January 3<sup>rd</sup>, 2008, in the time interval between 3:50 am to 5:30 am (one hour and 40 minutes, or 100 minutes). Each curve in Figure 4.1a represents a 10 minute averaging interval of wind speed data. The 11<sup>th</sup> thicker curve, labeled *interval mean* on the plot, represents the average wind speed over the 100 minutes.

##### 4.1.1 Topographic Model Results

During the design phase of the CAD model, it was apparent that the topography would be shallow. This triggered a change in model scale, as discussed in Section 3.3.2. The largest height difference on the topography is 41 m, which is close to the forest canopy height (21 m). The topographic model and placement in the wind tunnel are presented in Figure D.1, in

Appendix D. A set of wind tunnel experiments was setup in order to determine to what extent the topography affects the flow. The findings of these experiments are presented in this section.

The preliminary wind tunnel experiment was done with the bare topographic model, referred from here on as the “no forest” case. The selected 100 minute full scale velocity data segments, which were divided into 10 minute averaging intervals, were plotted and their average was extracted.

Figure 4.2a shows the comparison between the wind tunnel results and full scale data averaged over the three identified segments for only the topographic model. The *Full scale* curve in this figure is the average of the three identified full scale data segments represented as curves which are labeled *interval curve* in Figure 4.1a, b and c. The error bars for the *Full scale* curve represent the variation of the three segments. The *Wind tunnel* curve shows the measured wind velocity in the wind tunnel experiment ran with the no forest topographic model. In this case, the error bars represent the variation of the wind tunnel results from the three runs which had increasing wind velocity (also used in determining the Reynolds number independence in Section 3.5.3).

The values recorded at wind turbine 2 were used for non-dimensionalizing – this turbine was selected based on the setup of the model in the wind tunnel, where turbine 2 was closest to the model center for all the investigated directions.

Figure 4.2b shows the comparison between the vertical wind speed profile used in the wind tunnel and the one measured at the met tower (which only has 3 measurement points at 80 m, 50 m and 30 m). The full scale wind profile is averaged over the three identified full scale data segments available for the month of January 2008. The horizontal error bars show the maximum variability of the measured profile for the month of January in the 315° direction. The two vertical wind profiles were non-dimensionalized using the maximum height at which measurements were available at the met tower, i.e. 80 m. The wind tunnel profile was measured up to the middle of the test section, which in full scale would be equivalent to 233.5 m. The upper limit of the graph was set at  $0.35 * 233.5 \text{ m} \cong 80 \text{ m}$ .

Full scale data was plotted in the same manner in order to achieve a comparison between the full scale data and the wind tunnel experiment results for the remaining months as described in Table 2.12 (March, September, October and December), and the result sets are presented in Figure 4.3, Figure 4.4, Figure 4.5 and Figure 4.6, respectively.

Figure 4.7 shows the summary plot for the wind tunnel to full scale data comparison, for direction  $315^\circ$ . In this figure all of the previous *Full scale* curves were centralized and compared to the *Wind tunnel* curve, for the direction in cause. Figure 4.8 and Figure 4.9 show the centralized results for the “No forest” case in the  $202.5^\circ$  and  $157.5^\circ$  directions, respectively. For the purpose of this work, the results for the first month have been presented, as well as the summary plots. The complete set of results, i.e. plots for each month and wind direction, is presented in Appendix C. Discussion of these preliminary results will follow in Section 4.2.

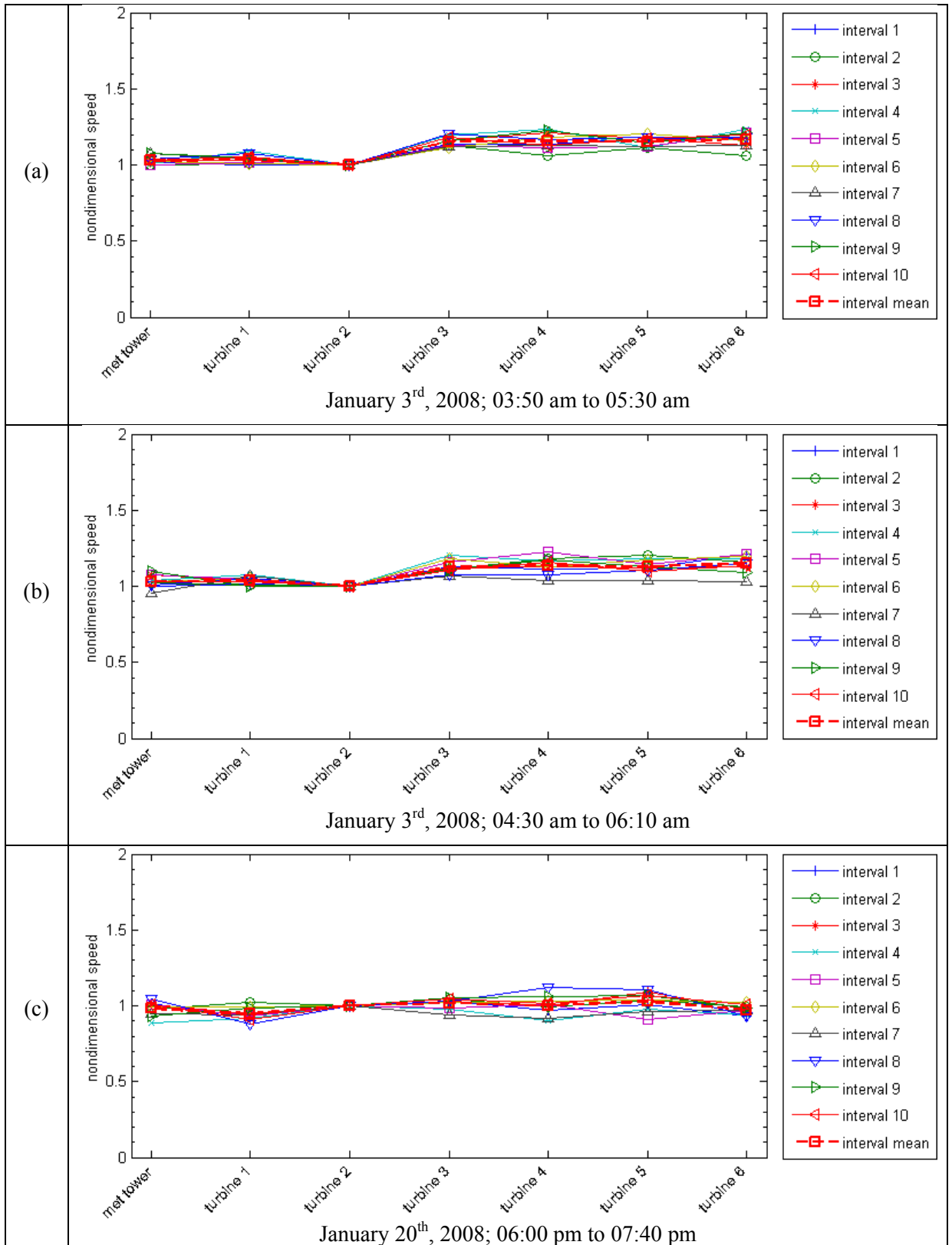
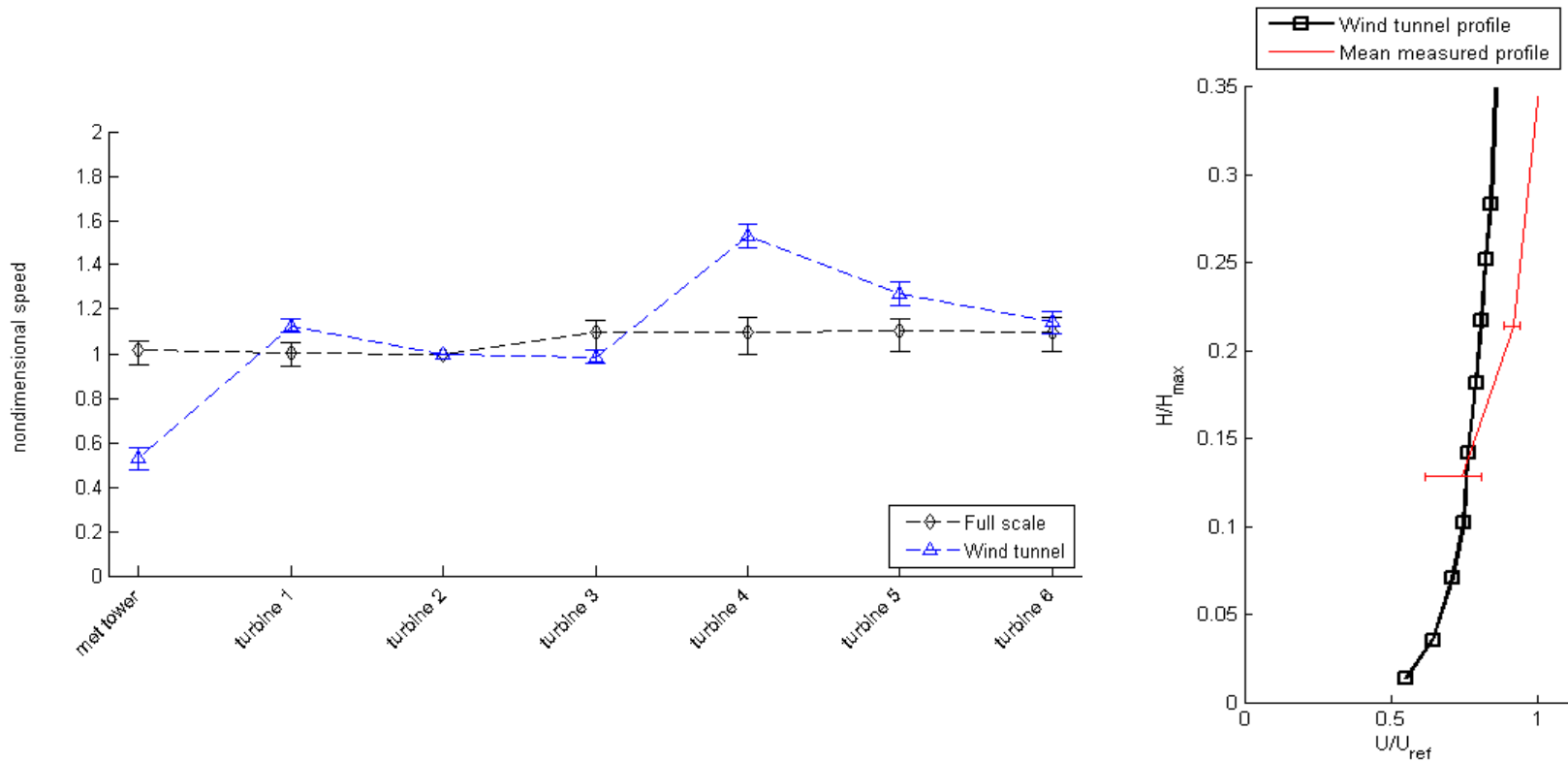


Figure 4.1: Example of full scale data segments extracted for January 2008, direction: 315°

- Wind tunnel result set description:
- Direction 315°;
  - “No forest” case;
  - Full scale data for January 2008;

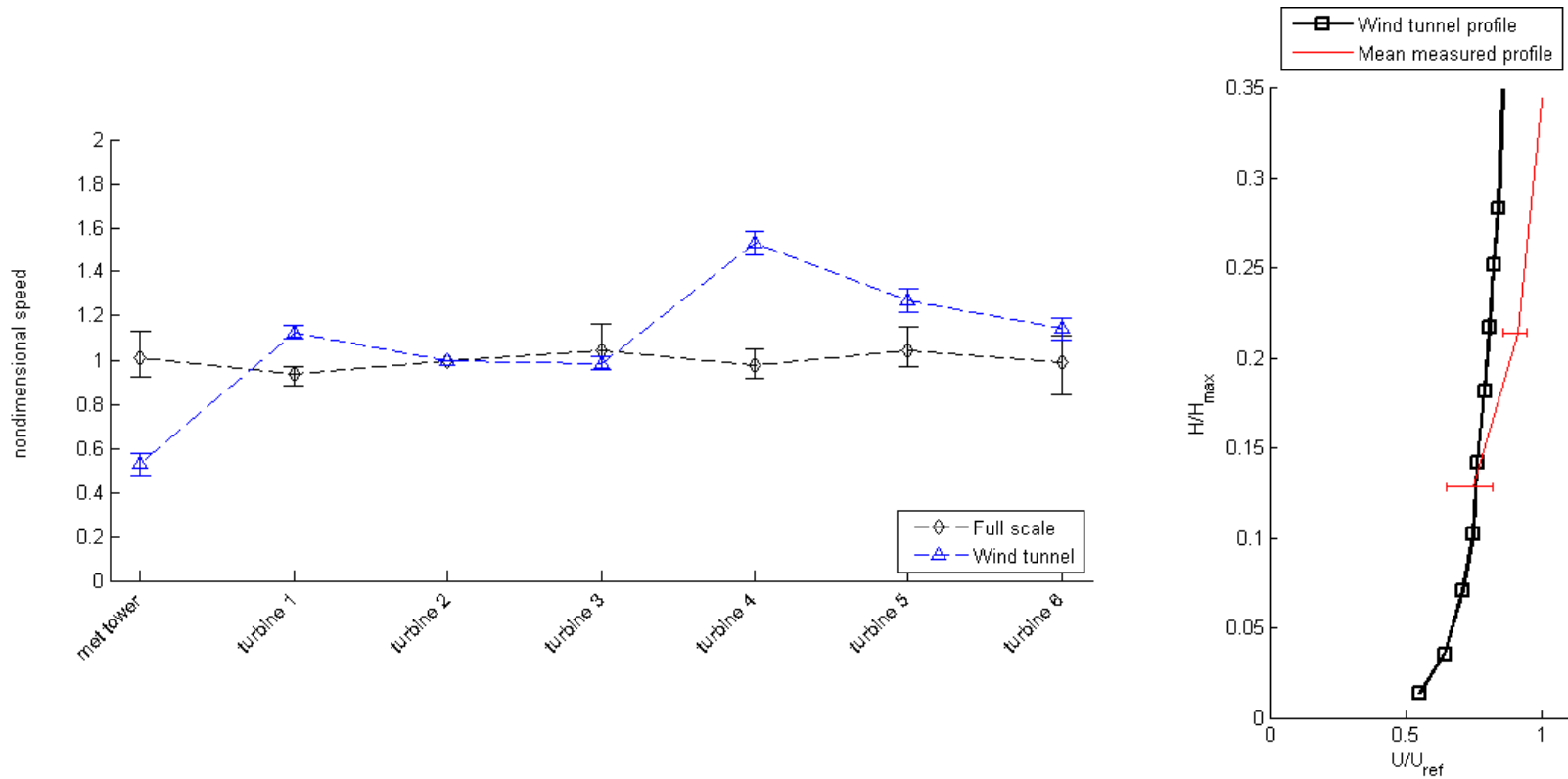


(a) Comparison between wind tunnel data (topographic model only) and full scale data for the 315° direction. Full scale data was extracted for the month of January.

(b) Comparison between wind tunnel inlet profile and vertical profile measured at the met tower. Full scale data was extracted for the month of January.

Figure 4.2: Wind tunnel results and comparison with full scale data. “No forest” case, direction: 315°, January 2008.

- Wind tunnel result set description:
- Direction 315°;
  - “No forest” case;
  - Full scale data for March 2008;



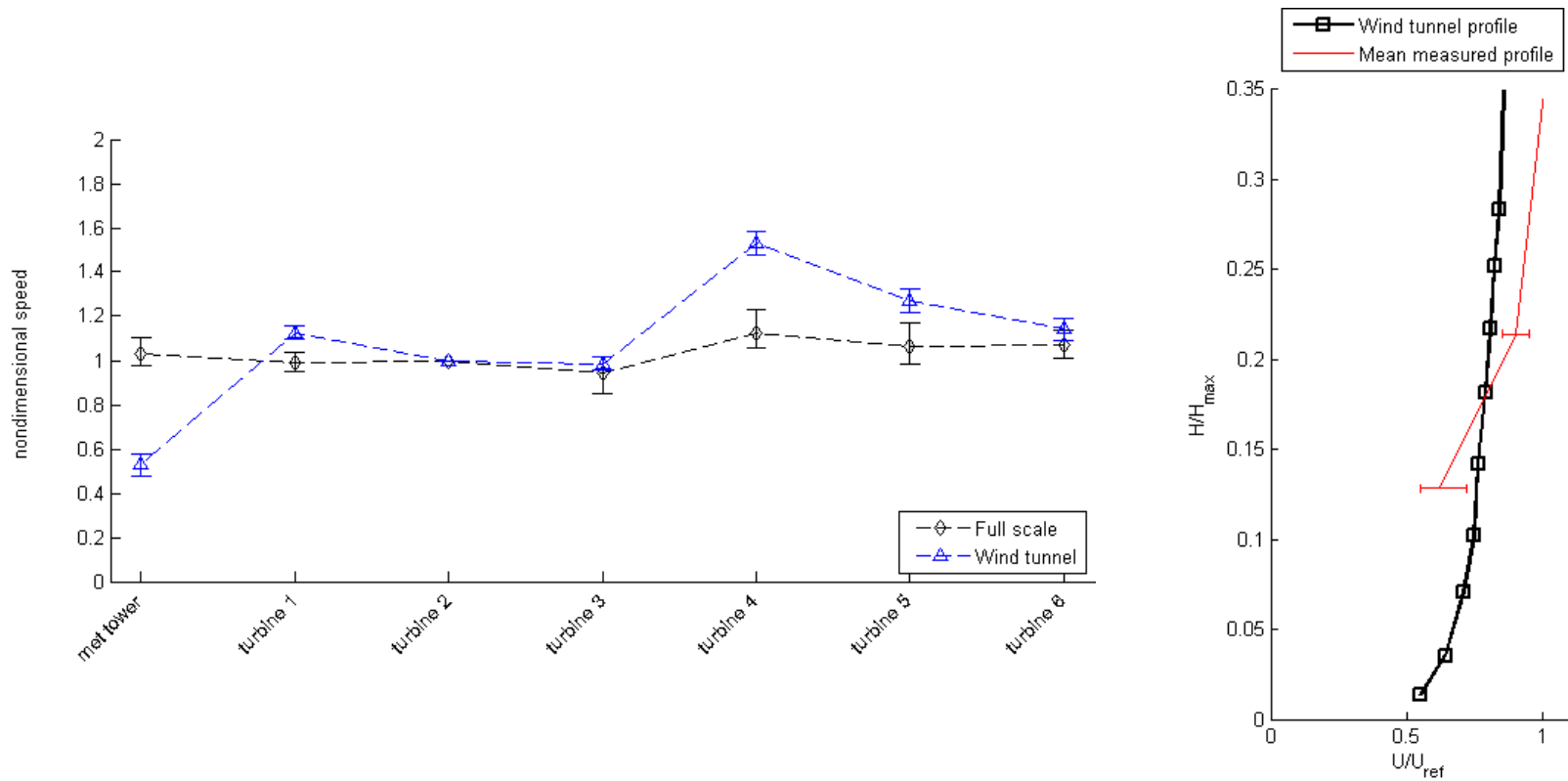
(a) Comparison between wind tunnel data (topographic model only) and full scale data for the 315° direction. Full scale data was extracted for the month of March.

(b) Comparison between wind tunnel inlet profile and vertical profile measured at the met tower. Full scale data was extracted for the month of March.

Figure 4.3: Wind tunnel results and comparison with full scale data. “No forest” case, direction: 315°, March 2008.



- Wind tunnel result set description:
- Direction 315°;
  - “No forest” case;
  - Full scale data for September 2008;

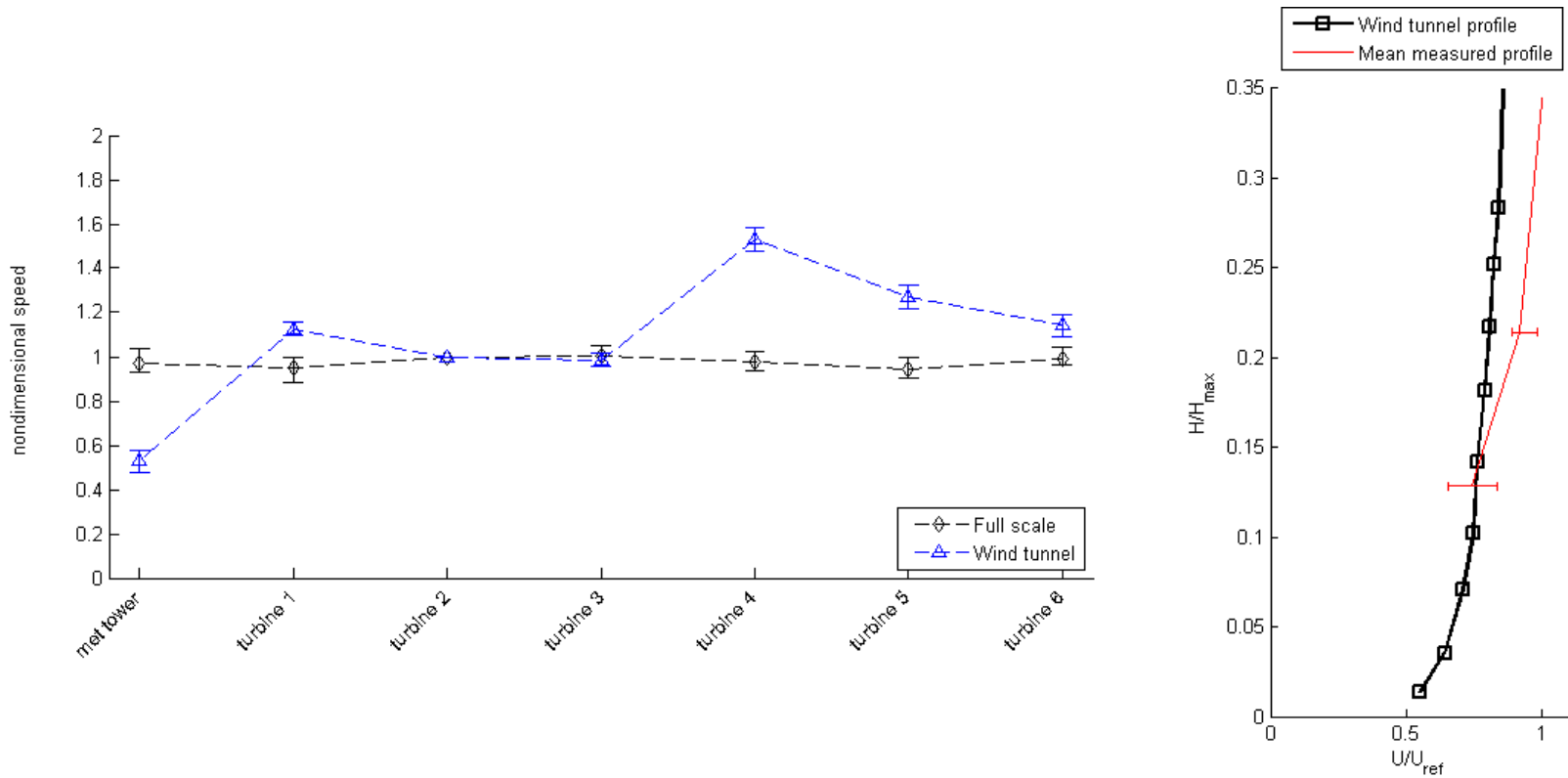


(a) Comparison between wind tunnel data (topographic model only) and full scale data for the 315° direction. Full scale data was extracted for the month of September.

(b) Comparison between wind tunnel inlet profile and vertical profile measured at the met tower. Full scale data was extracted for the month of September.

Figure 4.4: Wind tunnel results and comparison with full scale data. “No forest” case, direction: 315°, September 2008.

- Wind tunnel result set description:
- Direction 315°;
  - “No forest” case;
  - Full scale data for October 2008;

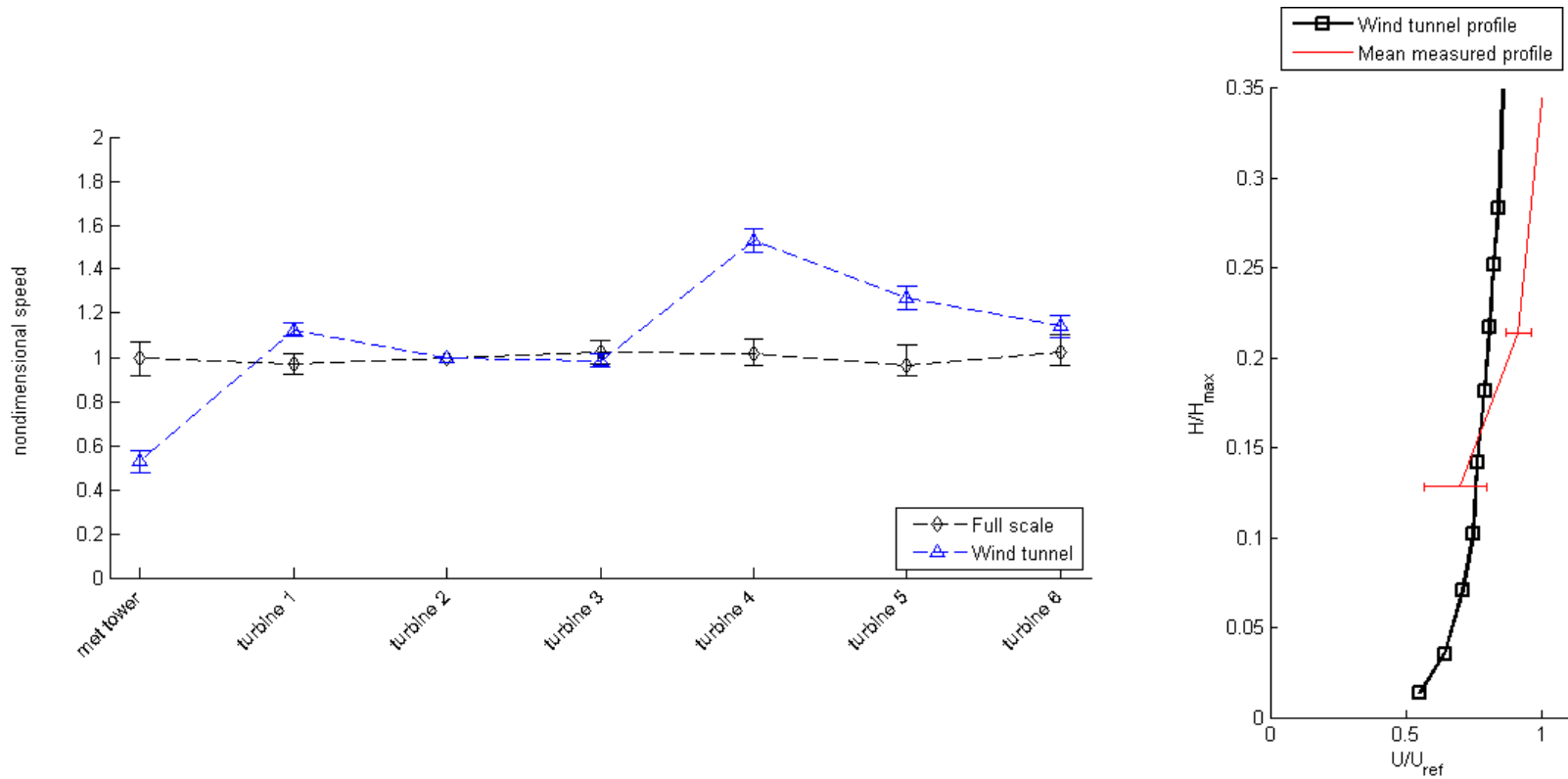


(a) Comparison between wind tunnel data (topographic model only) and full scale data for the 315° direction. Full scale data was extracted for the month of October.

(b) Comparison between wind tunnel inlet profile and vertical profile measured at the met tower. Full scale data was extracted for the month of October.

Figure 4.5: Wind tunnel results and comparison with full scale data. “No forest” case, direction: 315°, October 2008.

- Wind tunnel result set description:
- Direction 315°;
  - “No forest” case;
  - Full scale data for December 2008;

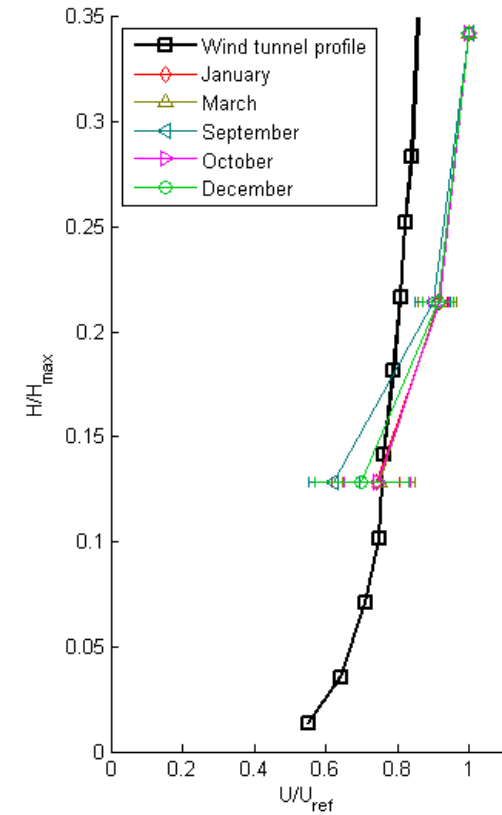
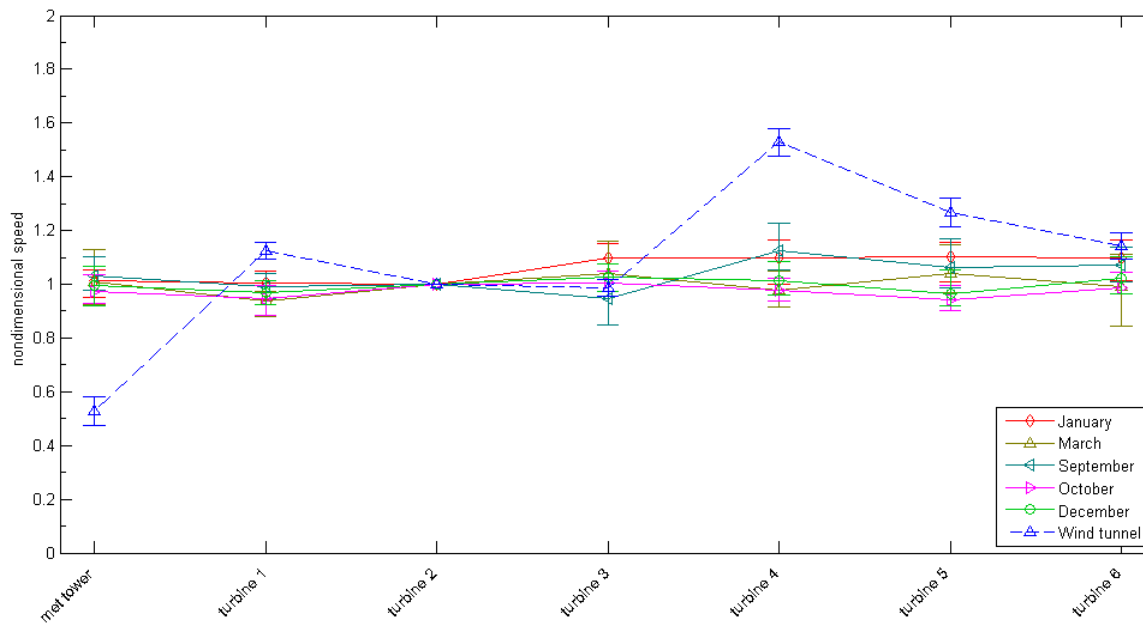


(a) Comparison between wind tunnel data (topographic model only) and full scale data for the 315° direction. Full scale data was extracted for the month of December.

(b) Comparison between wind tunnel inlet profile and vertical profile measured at the met tower. Full scale data was extracted for the month of December.

Figure 4.6: Wind tunnel results and comparison with full scale data. “No forest” case, direction: 315°, December 2008.

- Result set description:
- Direction 315°;
  - “No forest” case;
  - Yearly full scale data;

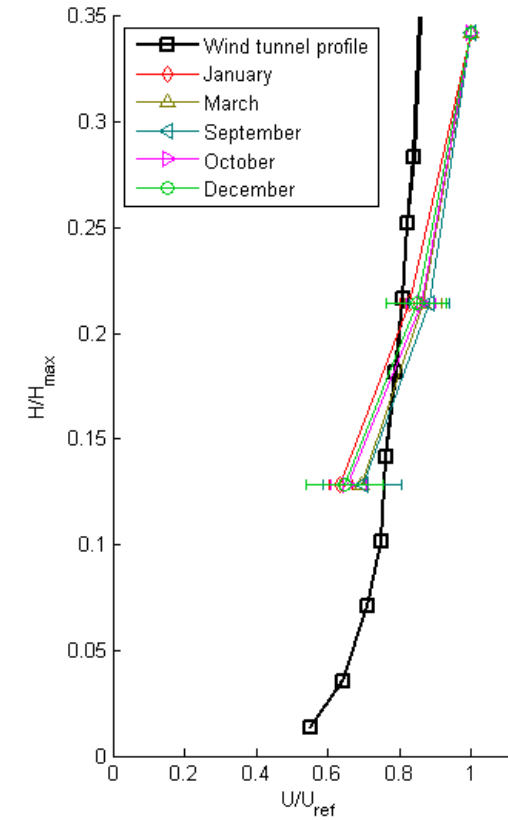
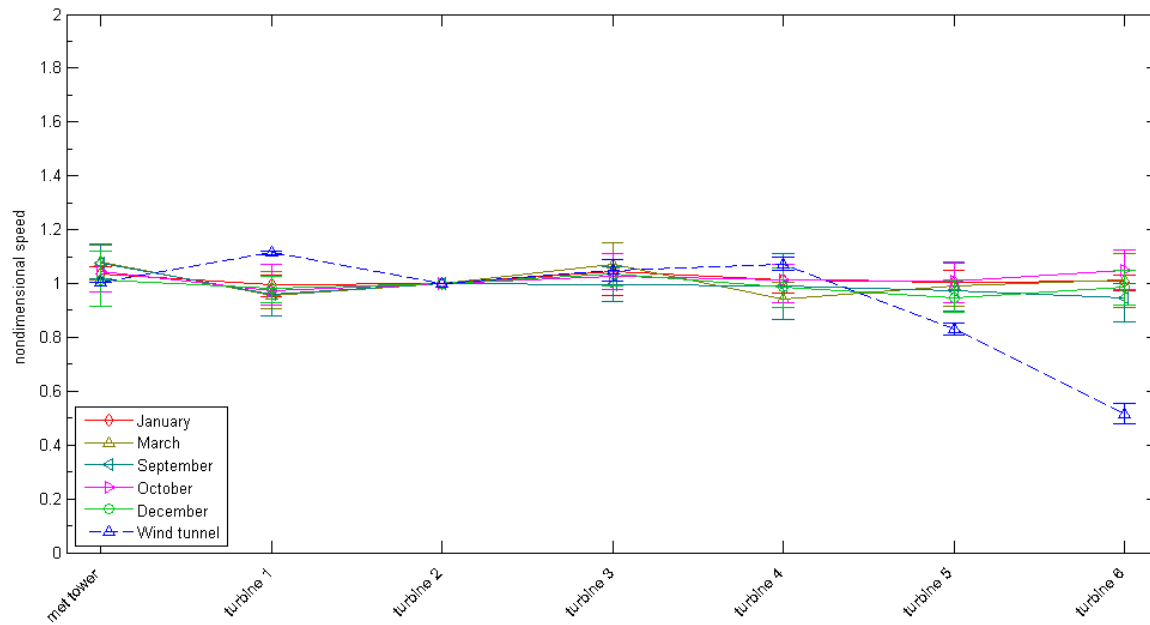


Comparison between wind tunnel data (topographic model only) and full scale data for the 315° direction. Full scale data was plotted for each of the months which had valid segments.

Comparison between wind tunnel inlet profile and vertical profile measured at the met tower.

Figure 4.7: Summary plot of the comparison between the wind tunnel test and full scale data. “No forest” case, direction: 315°, yearly data.

- Result set description:
- Direction 202.5°;
  - “No forest” case;
  - Yearly full scale data;

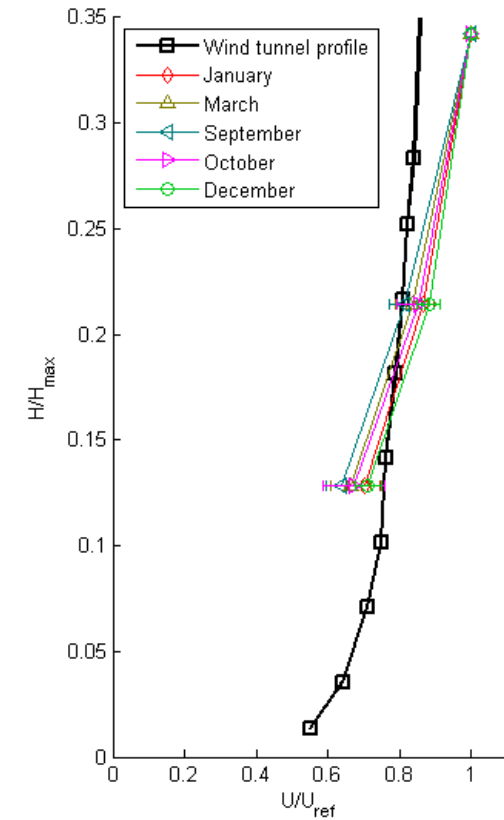
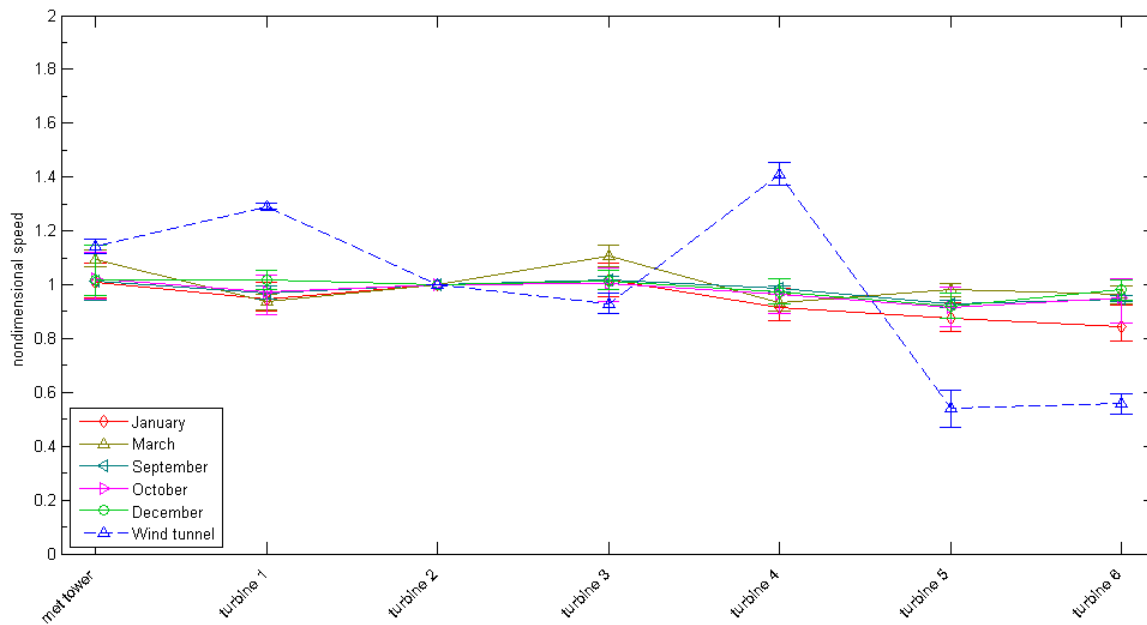


Comparison between wind tunnel data (topographic model only) and full scale data for the 202.5° direction. Full scale data was plotted for each of the months which had valid segments.

Comparison between wind tunnel inlet profile and vertical profile measured at the met tower.

Figure 4.8: Summary plot of the comparison between the wind tunnel test and full scale data. “No forest” case, direction: 202.5°, yearly data

- Result set description:
- Direction 157.5°;
  - “No forest” case;
  - Yearly full scale data;



Comparison between wind tunnel data (topographic model only) and full sale data for the 157.5° direction. Full scale data was plotted for each of the months which had valid segments.

Comparison between wind tunnel inlet profile and vertical profile measured at the met tower.

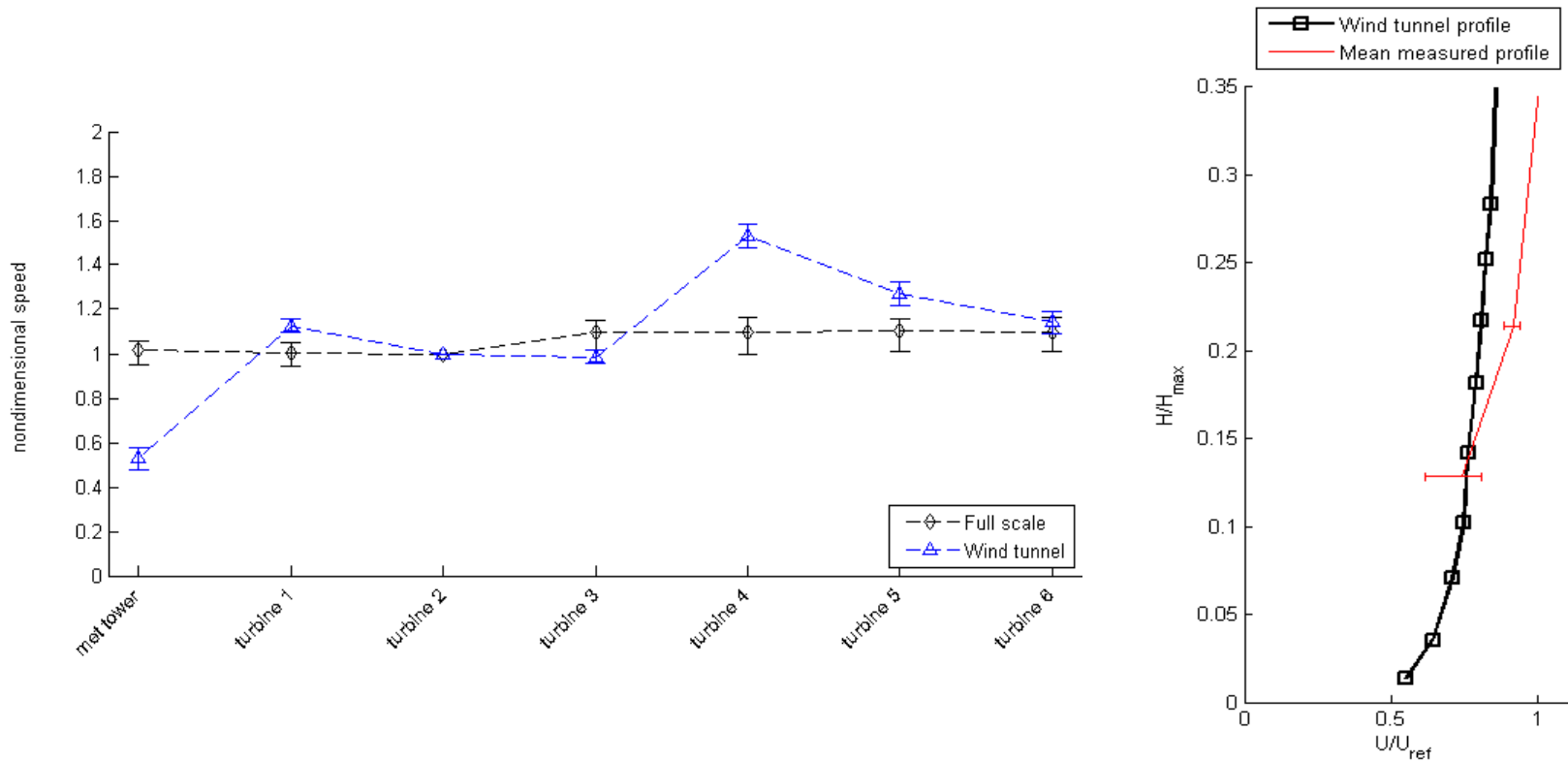
Figure 4.9: Summary plot of the comparison between the wind tunnel test and full scale data. “No forest” case, direction: 157.5°, yearly data.

#### 4.1.2 Preliminary Forest Canopy Model Results

A preliminary forest canopy model attempt was made. The initial attempt was to model each tree individually, by making tree stands and adding porous material to reproduce the tree crowns. The forested area on the model is approximately 12 m<sup>2</sup>, and covering it would have meant approximately 30,000 individual trees. This approach was deemed not achievable in the allotted time, therefore the solution adopted was to cover the model in porous foam material, which would allow air to flow through it. A readily available material was used, and this was furnace filter with a foam porosity of 90%. The foam was fastened on top of the topographic model and its properties were presented in Section 3.4. This test case is noted “90% canopy model”. The preliminary forest canopy model and its placement on the topographic model and in the wind tunnel is presented in Figure D.2, in Appendix D.

Figure 4.10a shows the comparison between the wind tunnel results for the “90% canopy model” and full scale data averaged over the three identified segments, in the same manner as the “No forest” case. Figure 4.10b shows the comparison between the wind speed profile used in the wind tunnel and the one measured at the met tower. Figure 4.11, Figure 4.12, Figure 4.13 and Figure 4.14 present the comparison between the wind tunnel experiment and full scale data in the 315° direction, for the months of March, September, October and December, respectively. Figure 4.15, Figure 4.16 and Figure 4.17 show the summary plots for the wind tunnel to full scale data comparison, for directions 315°, 202.5° and 157.5°, respectively. In these figures all of the previous *Full scale* curves were centralized and compared to the *Wind tunnel* curve. A discussion of these preliminary results is provided in Section 4.2.

- Wind tunnel result set description:
- Direction 315°;
  - “90% canopy model” case;
  - Full scale data for January 2008;



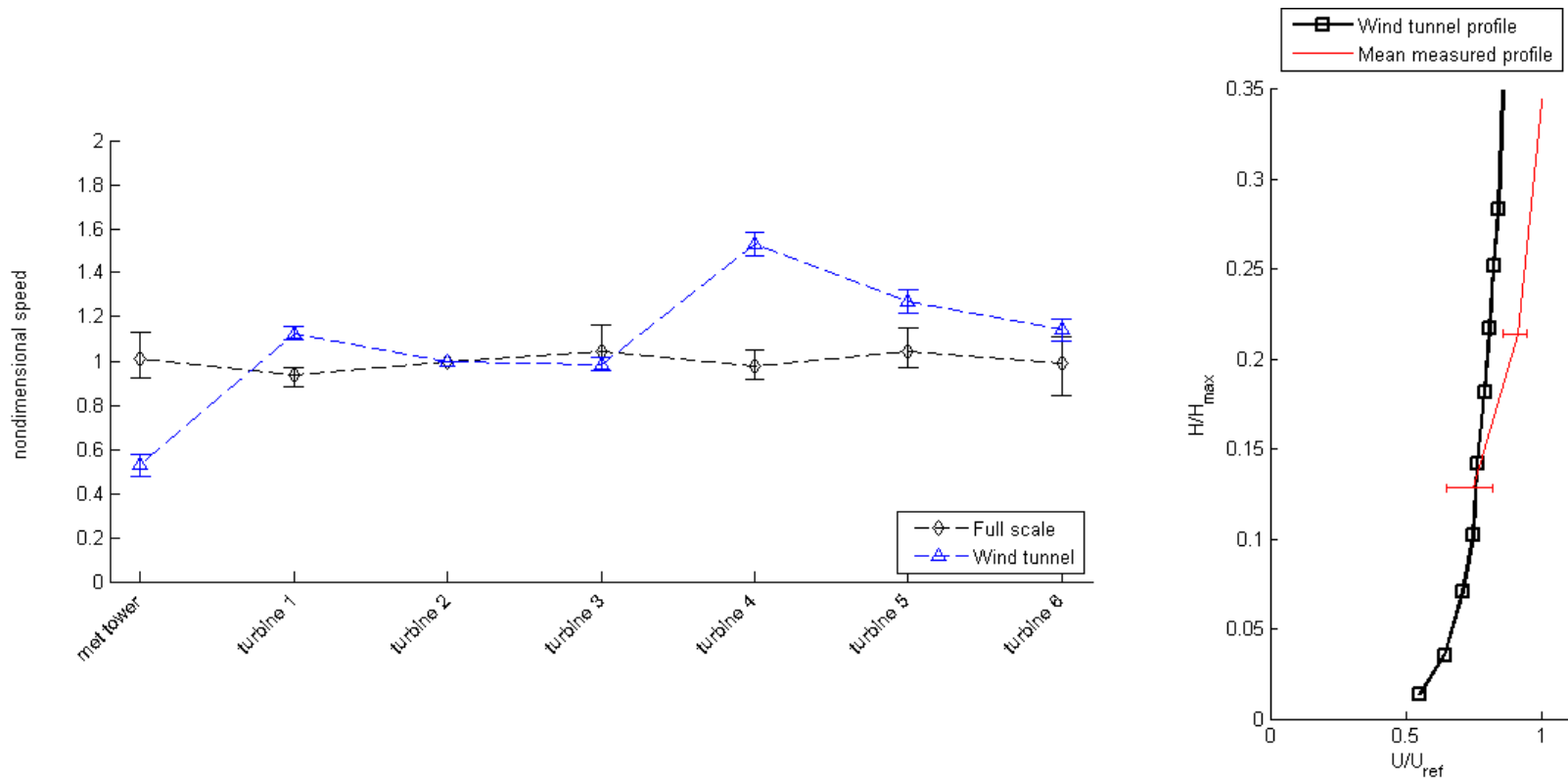
(a) Comparison between wind tunnel data (90% canopy model) and full scale data for the 315° direction. Full scale data was extracted for the month of January.

(b) Comparison between wind tunnel inlet profile and vertical profile measured at the met tower. Full scale data was extracted for the month of January.

Figure 4.10: Wind tunnel results and comparison with full scale data. “90% canopy model” case, direction: 315°, January 2008



- Wind tunnel result set description:
- Direction 315°;
  - “90% canopy model” case;
  - Full scale data for March 2008;

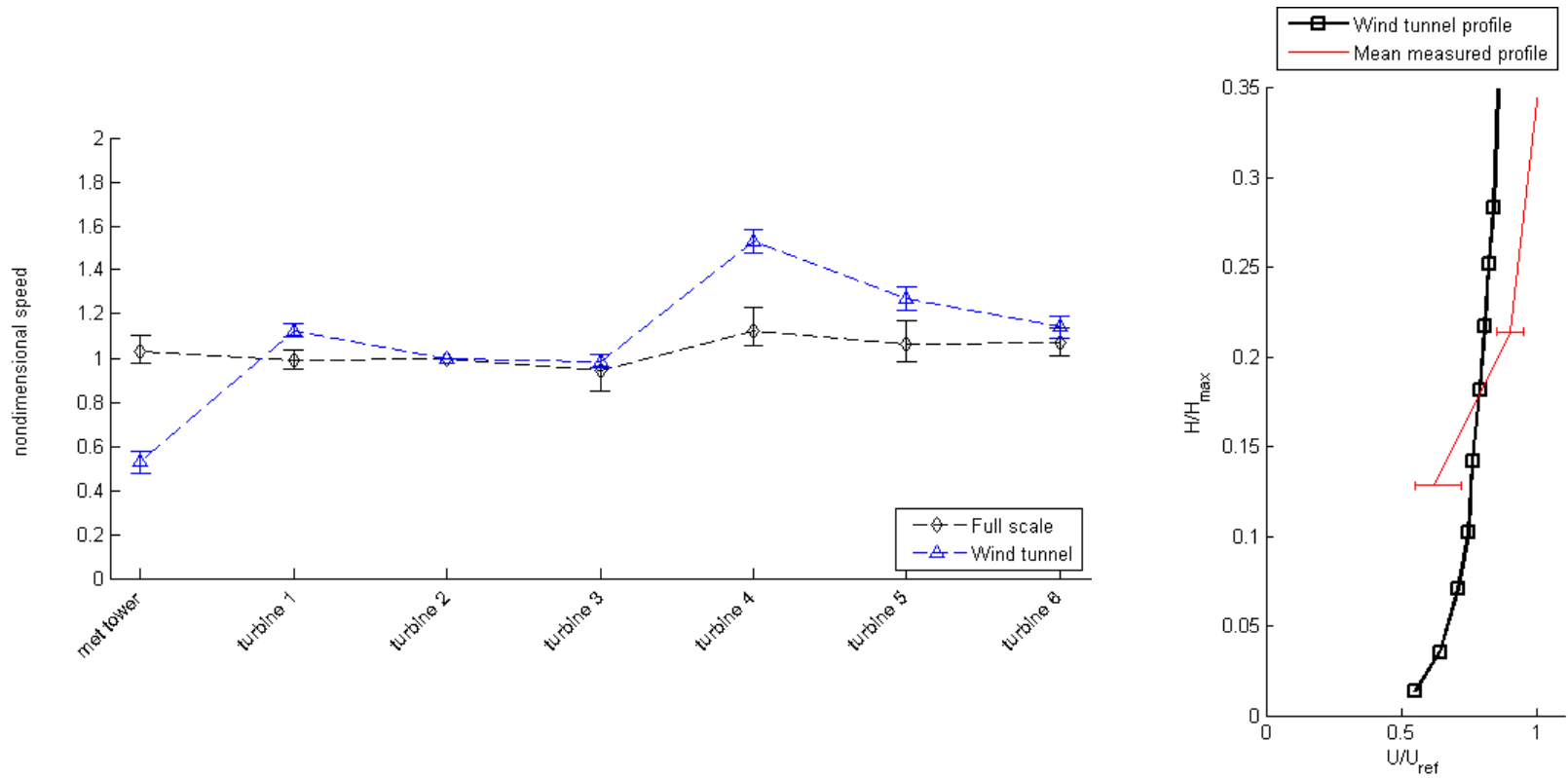


(a) Comparison between wind tunnel data (90% canopy model) and full scale data for the 315° direction. Full scale data was extracted for the month of March.

(b) Comparison between wind tunnel inlet profile and vertical profile measured at the met tower. Full scale data was extracted for the month of March.

Figure 4.11: Wind tunnel results and comparison with full scale data. “90% canopy model” case, direction: 315°, March 2008.

- Wind tunnel result set description:
- Direction 315°;
  - “90% canopy model” case;
  - Full scale data for September 2008;

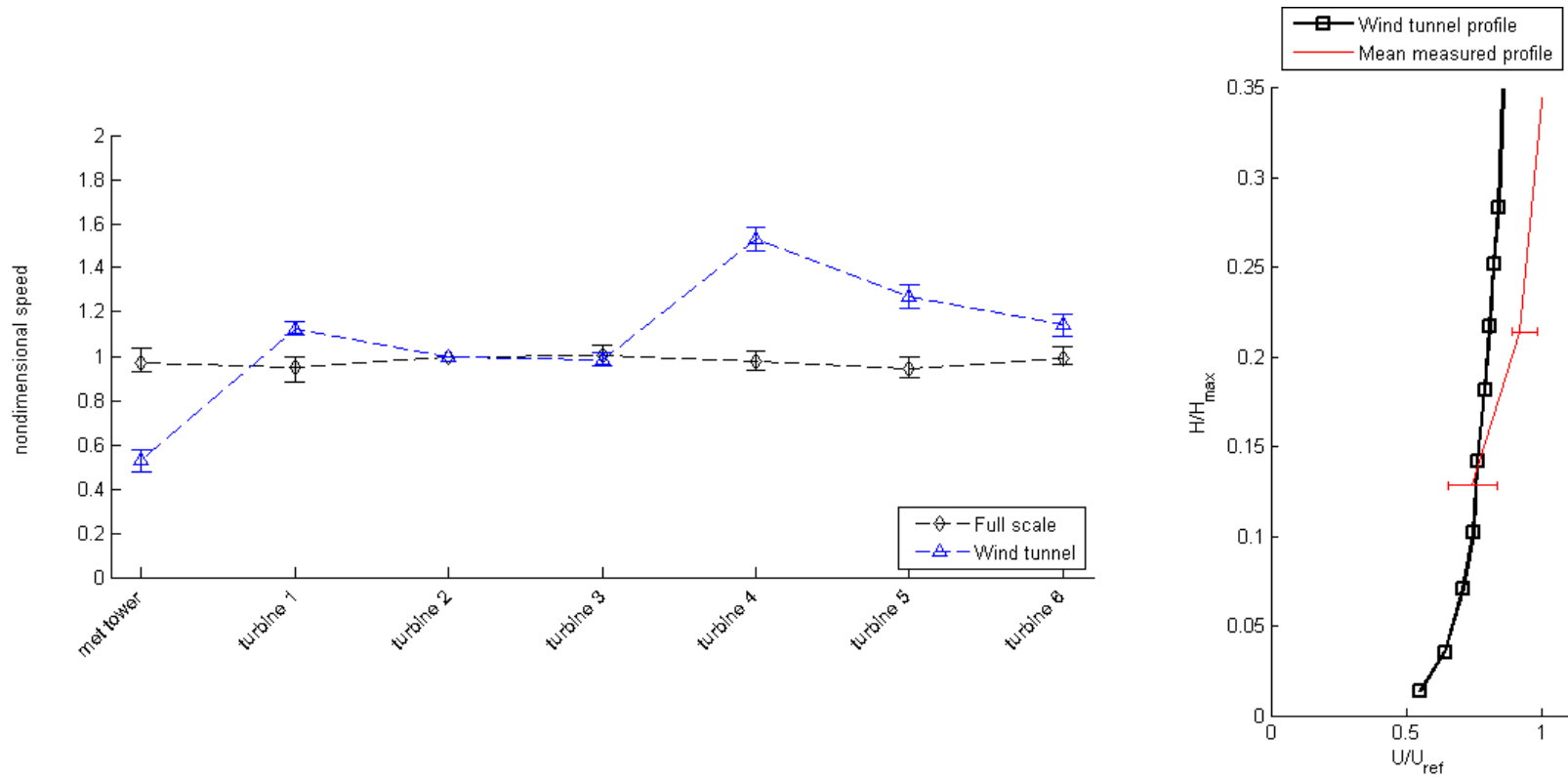


(a) Comparison between wind tunnel data (90% canopy model) and full scale data for the 315° direction. Full scale data was extracted for the month of September.

(b) Comparison between wind tunnel inlet profile and vertical profile measured at the met tower. Full scale data was extracted for the month of September.

Figure 4.12: Wind tunnel results and comparison with full scale data. “90% canopy model” case, direction: 315°, September 2008.

- Wind tunnel result set description:
- Direction 315°;
  - “90% canopy model” case;
  - Full scale data for October 2008;

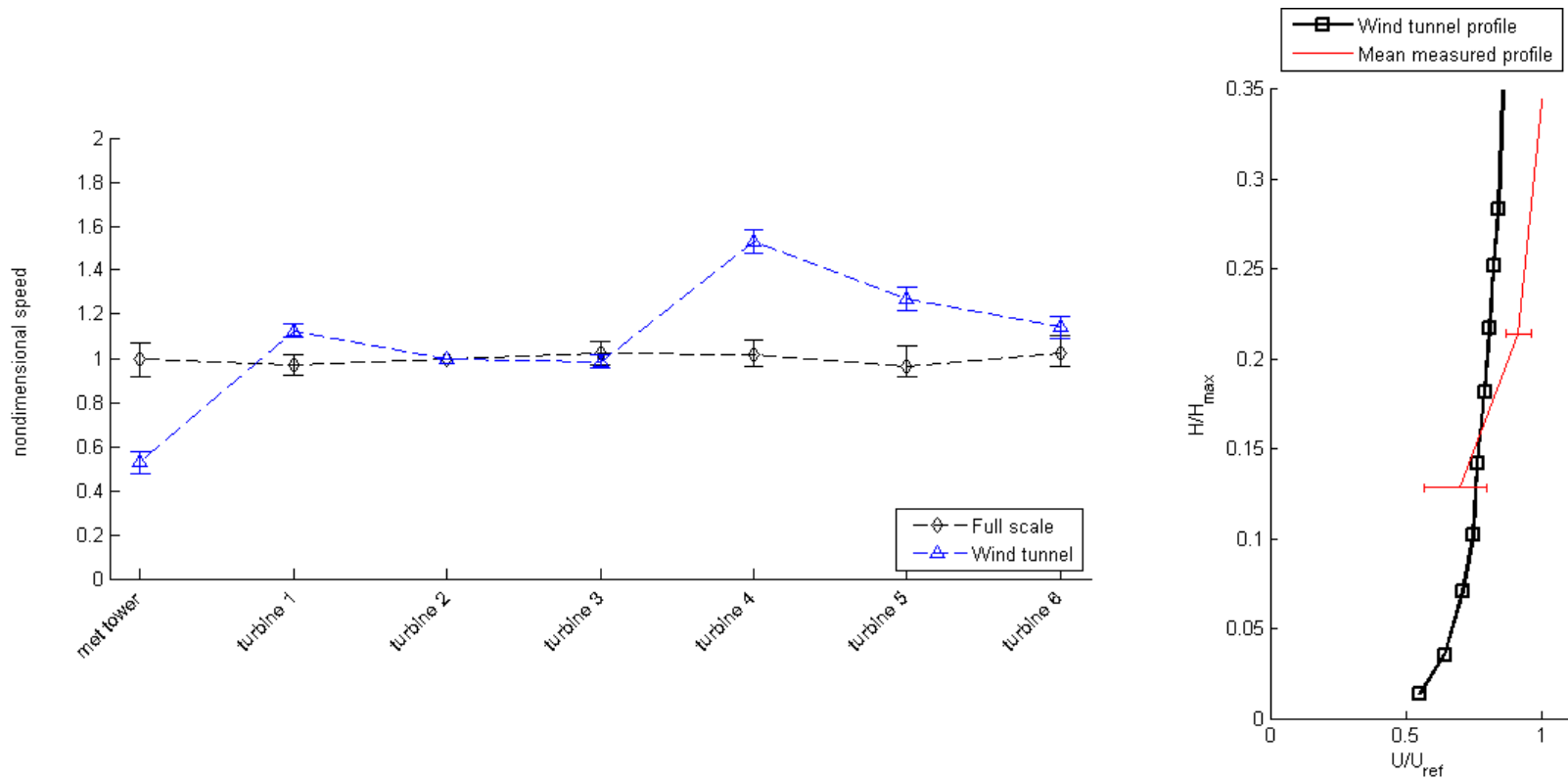


(a) Comparison between wind tunnel data (90% canopy model) and full scale data for the 315° direction. Full scale data was extracted for the month of October.

(b) Comparison between wind tunnel inlet profile and vertical profile measured at the met tower. Full scale data was extracted for the month of October.

Figure 4.13: Wind tunnel results and comparison with full scale data. “90% canopy model” case, direction: 315°, October 2008.

- Wind tunnel result set description:
- Direction 315°;
  - “90% canopy model” case;
  - Full scale data for December 2008;

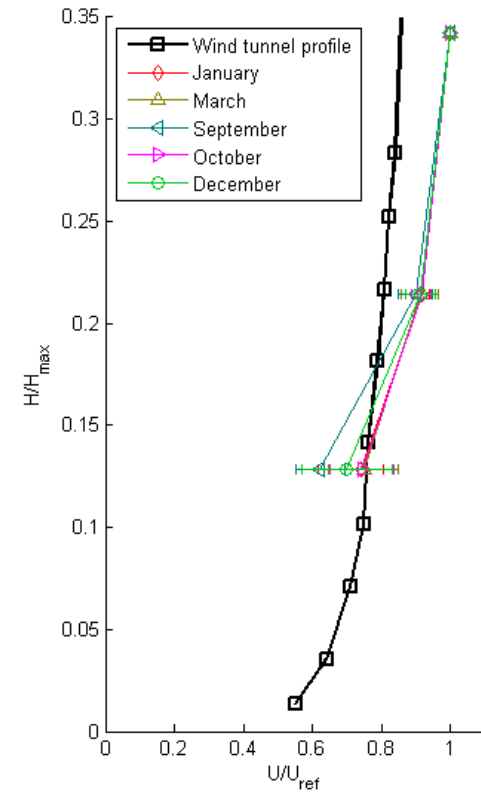
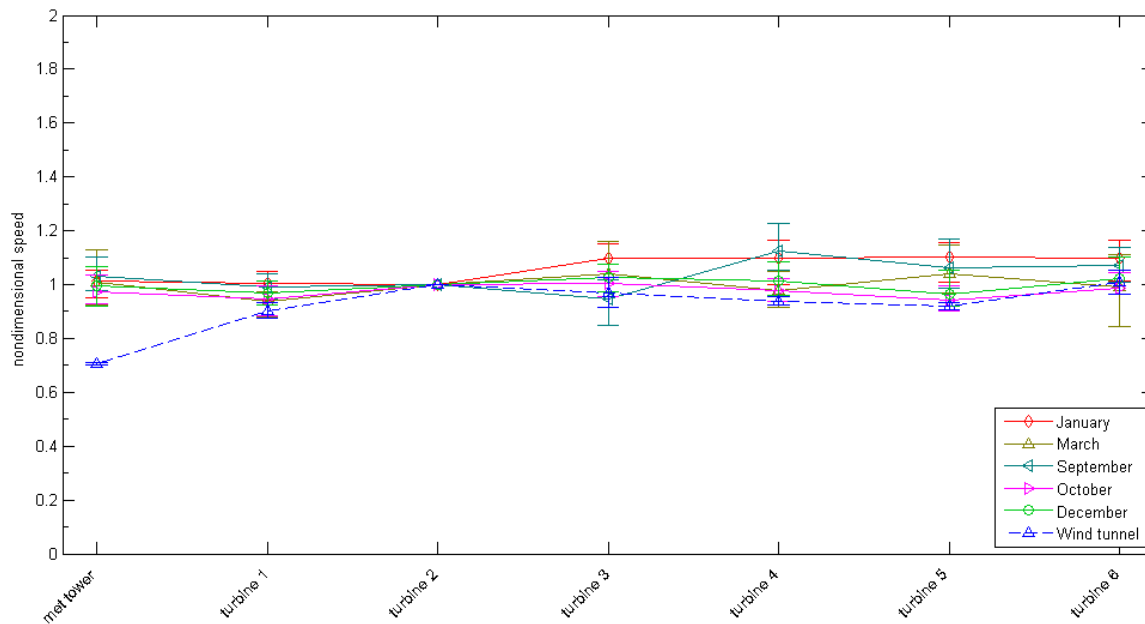


(a) Comparison between wind tunnel data (90% canopy model) and full scale data for the 315° direction. Full scale data was extracted for the month of December.

(b) Comparison between wind tunnel inlet profile and vertical profile measured at the met tower. Full scale data was extracted for the month of December.

Figure 4.14: Wind tunnel results and comparison with full scale data. “90% canopy model” case, direction: 315°, December 2008.

- Result set description:
- Direction 315°;
  - “90% canopy model” case;
  - Yearly full scale data;

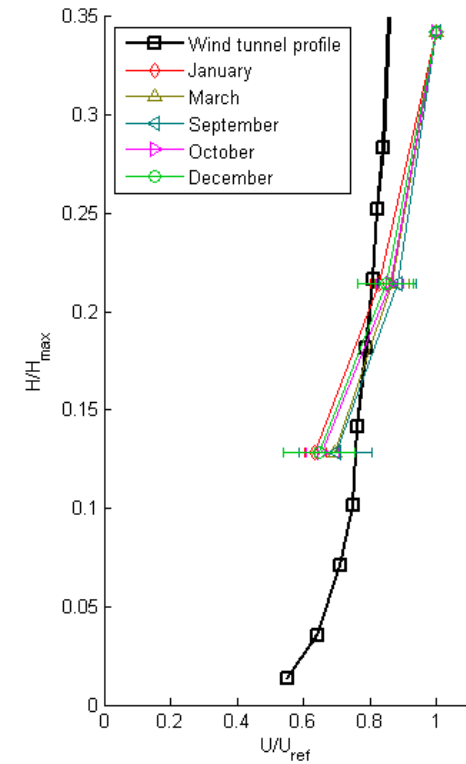
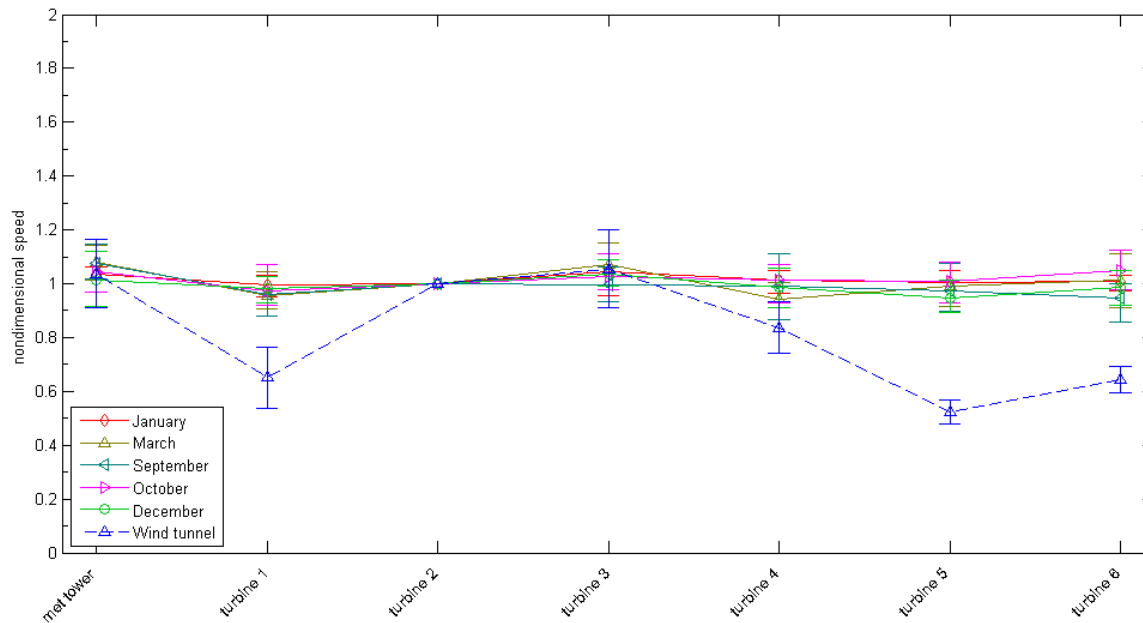


Comparison between wind tunnel data (90% canopy model) and full scale data for the 315° direction. Full scale data was plotted for each of the months which had valid segments.

Comparison between wind tunnel inlet profile and vertical profile measured at the met tower.

Figure 4.15: Summary plot of the comparison between the wind tunnel test and full scale data. “90% canopy model” case, direction: 315°, yearly data.

- Result set description:
- Direction 202.5°;
  - “90% canopy model” case;
  - Yearly full scale data;



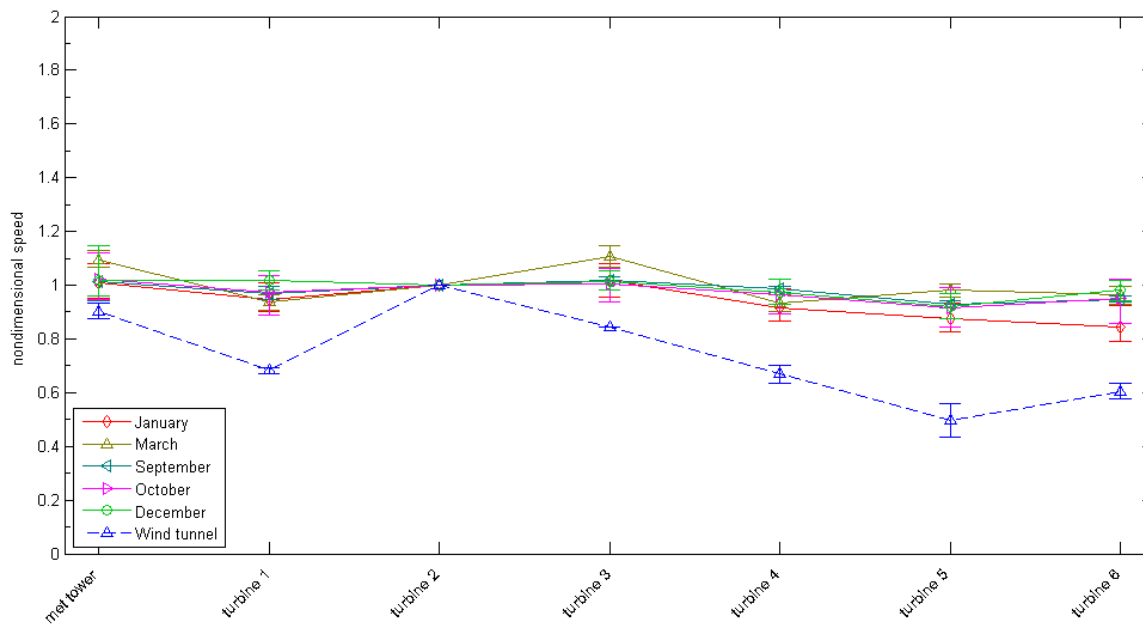
Comparison between wind tunnel data (90% canopy model) and full scale data for the 202.5° direction. Full scale data was plotted for each of the months which had valid segments.

Comparison between wind tunnel inlet profile and vertical profile measured at the met tower.

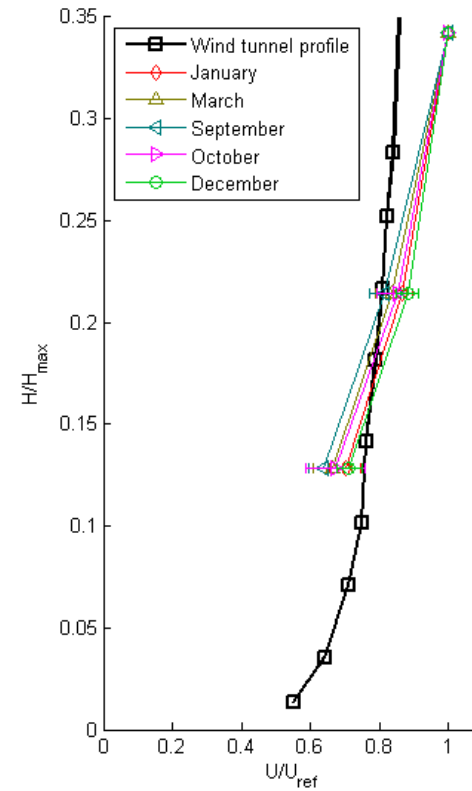
Figure 4.16: Summary plot of the comparison between the wind tunnel test and full scale data.

“90% canopy model” case, direction: 202.5°, yearly data.

- Result set description:
- Direction 157.5°;
  - “90% canopy model” case;
  - Yearly full scale data;



Comparison between wind tunnel data (90% canopy model) and full scale data for the 157.5° direction. Full scale data was plotted for each of the months which had valid segments.



Comparison between wind tunnel inlet profile and vertical profile measured at the met tower.

Figure 4.17: Summary plot of the comparison between the wind tunnel test and full scale data.

“90% canopy model” case, direction: 157.5°, yearly data.

## 4.2 Discussion of Preliminary Results

The preliminary testing of the no forest topographic model was done in order to have a control set of results. Since only the topographic model was used, the results from the wind tunnel experiment do not match well with the full scale data. This is seen in the results plots (Figure 4.2 to Figure 4.9), where the *Wind tunnel* curve does not follow the same trend as the full scale data curve, which seems to occur due to the missing forest canopy model.

For preliminary testing, the blue filter foam material was used to model the forest canopy for the “90% canopy model” test case. The summarized wind tunnel results for directions 315°, 202.5° and 157.5°, presented in Figure 4.15, Figure 4.16 and Figure 4.17, respectively, do not match well with full scale data, but an improvement is observed over the “No forest” case. The largest discrepancies occur consistently over the last two directions examined (157.5° and 202.5°) for turbines 1, 5 and 6 (their location is shown in Figure 4.18).

By looking at the aerial imagery data in Figure 4.18, we can speculate that the discrepancies also occur because of the wind turbines’ proximity to the forest edges. Since wind speed is under predicted in the wind tunnel tests, this could be attributed to a recirculation zone behind the larger forest patches. This led us to believe that the forest has a much more important effect on the flow, so the canopy model had to be redesigned.

Another possible important issue was the incoming wind speed profile. Upstream roughness was not taken into account as it was assumed that the model would be large enough to allow the flow to develop, and an over-water profile was used. The boundary layer recovery after a change in roughness is investigated and discussed in Section 5.5.

These results have shown that the wind tunnel modeling for the preliminary forest canopy model matched full scale data best in the case of the 315° direction. At this point it was concluded that the preliminary canopy model used did not perform as adequately for the other two directions investigated (157.5° and 202.5°), and a new forest canopy model had to be developed.





Figure 4.18: Location of wind turbines 1, 5 and 6 with relation to forest edges.

The forest canopy modeling approach had yet another effect on the results. Because the model forest now had sharper edges than would be normally found in full scale forests, the flow from the forest edge and over the forest was affected.

A difference in results can be seen for the wind turbines that are closest to the forest's edges. Based on these preliminary findings, it was concluded that the forest canopy had a significant influence on the flow and a more detailed analysis had to be performed in order to achieve good results. A potential relationship between full scale forest parameters and material properties is discussed in Chapter 5. The resulting forest canopy model is tested and the wind tunnel experiment results are discussed in Section 5.5.

## Chapter 5

### 5. Improved Canopy Modeling

The main challenge for modeling canopy in wind tunnel setting relates to the small scale of testing. Usually scales of 1/1000 or more are used, which impacts both the ability to reproduce a range of scales of motion as well as the measurement resolution.

Previous studies have researched different possibilities to model forests, with mixed results. There is no general consensus in the scientific literature on how a forest should be modeled for a wind tunnel experiment. From literature and from an aerodynamic point of view, the two most important factors for a model forest are the leaf area index (LAI) and the drag coefficient. Considering past approaches, it is clear that a forest model needs to be chosen carefully. Herein we propose an approach to achieve this.

#### 5.1 Proposed Approach

A relationship between wind tunnel parameters, in this case porosity, and a forest parameter that can be measured – Leaf Area Index (LAI) – was developed. LAI is a common parameter used to describe forests and it can be measured indirectly by using remote sensed data in the form of satellite sensed electromagnetic energy. In this work, satellite data from the NASA/MODIS mission was used to obtain LAI estimates.

##### Leaf Area Index

Leaf Area Index (LAI) references can be found in the work of several authors, while Rodrigo et al. [36] contribute to its definition. Leaf Area Index can be defined as the upper green leaf area per unit ground area in broad leaf canopies or the projected needle leaf area per unit ground area in needle canopies. This index is directly related with the energy and mass exchange between the trees and the atmosphere [36].

##### Measuring LAI

There are different ways which allow the measurement of LAI. A review of these methods is presented by Jonckheere et al. [72]. Direct measurement is time consuming and laborious.

Also, the procedures required for direct measurement can involve destructive sampling, which is undesirable in protected areas. A direct assessment of LAI can be performed in several ways: the destructive sampling of the harvested green leaves from a designated plot; the model tree method, which consists of sampling an amount of representative tree species; or, in autumn, by traps that collect fallen leaves in deciduous forests. These traps are boxes that are open on one side which have a preset size. Their lateral sides prevent the transition of leaves during windy periods.

Light interception in canopies is another way of measuring LAI. Fassnacht et al. [73], Stenberg et al. [74] and Küßner and Mosandl [75] wrote papers on indirect LAI estimation. Devices such as LAI-2000 Plant Canopy Analyzer (LI-COR, Lincoln, NE, USA) and DEMON (CSIRO, Centre for Environmental Mechanics, Canberra, Australia) are helpful in avoiding destructive sampling. The drawback is that these instruments tend to underestimate the LAI, when compared to direct estimates.

Another approach was attempted by Hagiwara et al. [76] using an airborne laser scanner. They studied an isolated forest in Kyoto City, Japan that contained mixed tree species, mainly deciduous. The laser scans were done from a helicopter at a height of 400 m. While this seems to be a good approach, in the sense that it is non-destructive, it has its uncertainties. The authors only tested this method in winter, when the leaf coverage is fairly low. A summer campaign would have been more valuable, since the full forest canopy is of greater interest.

Leaf area can be estimated indirectly as well, by observing and measuring another variable. These methods are faster, they can be automated, and they enable the inspection of larger plots of land. Hemispherical canopy photography is a technique presented by Jonckheere et al. [72] for studying plant canopies via photographs acquired through a hemispherical (fisheye) lens from beneath the canopy (oriented towards zenith) or placed above the canopy looking downward. Again, the disadvantage with this method is that it will underestimate the LAI for dense forest canopies, as it does not take into account leaves that lie on each other.

Finally, another approach is to use satellite remote sensing data. This eliminates the need for on-site LAI measurements, which also are incapable of providing LAI estimation over large areas. There are several missions that are ongoing and can provide remote sensing LAI

estimates, such as NASA MODIS (Moderate Resolution Imaging Spectroradiometer), NASA/NOAA AVHRR (Advanced Very-High Resolution Radiometer) or ESA GLOBCARBON (Global Land Products for Carbon Model Assimilation).

### MODIS Satellite Data

MODIS data has been chosen for the analysis work done in this paper. It was selected because of several benefic properties over the other similar products: fairly high spatial resolution (1000 m) and is easily obtainable by download through the NASA/MODIS<sup>5</sup> website service.

Once the data are obtained and downloaded locally, it has to undergo processing in order to be usable. These steps are described in detail by Huang [77]; the procedure involves processing of the data using GIS software (ArcMap). The results are LAI distribution maps over the selected terrain (as shown in Figure 5.1).

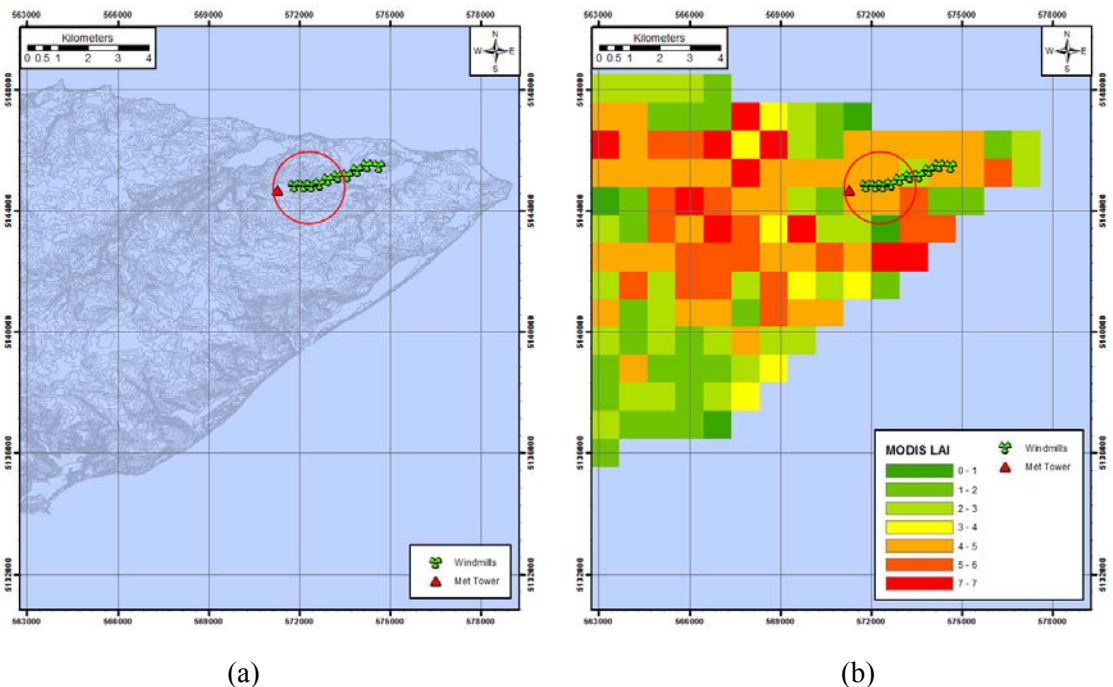


Figure 5.1: (a) Contour map with met tower and turbine locations;  
(b) LAI from MODIS data.

<sup>5</sup>Source: [https://lpdaac.usgs.gov/get\\_data/](https://lpdaac.usgs.gov/get_data/)

Analyzing Figure 5.1, one disadvantage can be identified. The spatial resolution is somewhat low to enable a precise LAI value estimation. Therefore, an average value for the model area was extracted from this data. Again, using ArcMap, the average value for LAI within the model boundary had a value of 3.9.

## 5.2 LAI Relationship to Wind Tunnel Modeling

Rodrigo et al. [36] discuss the relationship between LAI and physical properties of different foams. They measured the porosity of two types of foam with different porosity by means of binary image processing. Taking 5 mm thick sheets of material, the porosity was calculated as the ratio between the polyester material and total area. Their values for normalized LAI (which is noted as LAD and is actually LAI multiplied by forest height) are between 1.7 and 2.2. Similar values are found in the work of Le Dantec et al. [78]. They measured LAI variations in a large mixed deciduous-coniferous forest close to Paris, France and obtained values for LAI that range between 0.5 and 8.

Zhang and Scurlock [79] have done field measurements for 17 forest types in China, in 29 provinces. Their LAI values range from 0.17 (in tugai forests) to 41.78 (in evergreen broadleaf forests).

By adopting the same concept as Rodrigo et al. [36], the filter material initially (the 90% porosity material) used to create the forest canopy is analyzed. This filter has a known porosity value of 90%, which was measured by volumetric ratio, and also calculated analytically. The calculation was done for a 13 by 13 cm sample using Eqs. (5.1) to (5.5):

$$l = 13\text{cm}; w = 13\text{cm}; h = 2\text{cm}; \text{weight} = 48\text{g} \quad (5.1)$$

$$\text{volume, } V = l \cdot w \cdot h = 338 \text{ cm}^3 \quad (5.2)$$

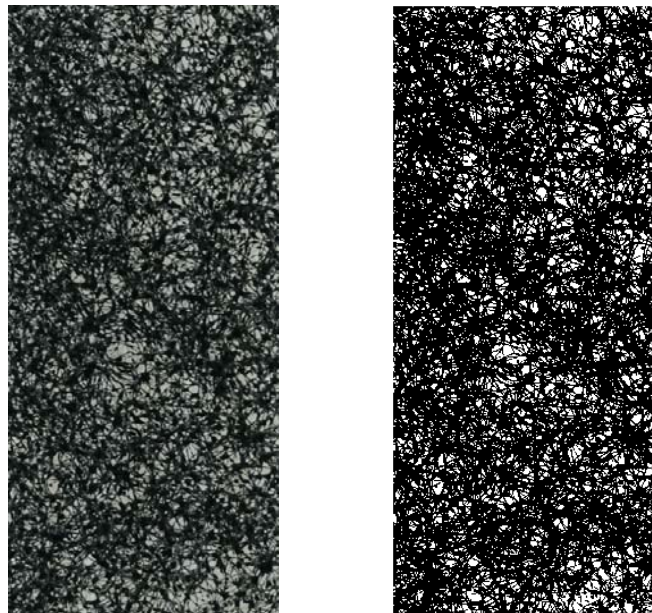
$$\text{sample density, } \rho_s = \frac{\text{weight}}{\text{volume}} = 142.012 \text{ kg/m}^3 \quad (5.3)$$

$$\text{material density (polyester), } \rho_f = 1400 \text{ kg/m}^3 \quad (5.4)$$

$$\text{sample porosity, } \varepsilon_s = 1 - \frac{\rho_s}{\rho_f} = 0.899 \quad (5.5)$$

A Matlab program was written to process the image data and compute LAI values. The obtained LAD value for the blue filter material was 2.4.

Using data from Rodrigo et al. [36] and the data obtained from the blue filter analysis (Figure 5.2), a relationship could be established between LAI and porosity. A second degree polynomial has been fitted to the three data points – a tentative fit. This allowed for extrapolation in order to get a LAD value as close as possible to the one obtained from MODIS data (Figure 5.3). The green data points in Figure 5.3 represent data available previously – the first two data points represent data adapted from [36] while the third represents the 90% porosity material used previously; the grey horizontal bars represent extrapolated data and the blue triangle represents the LAD value equivalent to a 48.4% porosity.



(a)

(b)

Figure 5.2: (a) black and white image – 5 mm slice of blue filter material  
(b) binary image for processing.

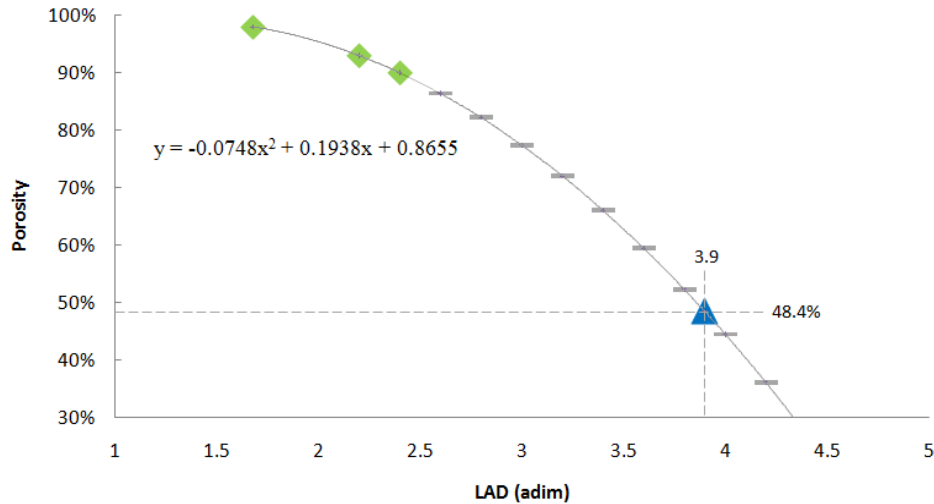


Figure 5.3: 2nd degree polynomial and data extrapolation for LAD.

The LAI value obtained from satellite data for the PEI site is approximately 3.9. Assuming the value is the same throughout the forest height, LAD becomes equivalent to LAI. Using this assumption and the extrapolated data, it was found that the filter material initially used to represent the forest canopy was too porous (it had the equivalent of a LAD value of 2.4). In order to properly describe the forest canopy, another material needed to be used. For the LAD value of 3.9, the new material was to be 48.4% porous (blue triangular symbol in Figure 5.3).

Obtaining such a material proved to be an issue. Many filter manufacturers do not provide any information on porosity, and it is not possible to directly estimate this property using readily available material information.

An easily available material is fiber glass insulation. Since this is a fibrous material, its porosity can be calculated as the ratio of sample density and material density. For a 13 cm square sample, with a 3.8 cm thickness, porosity was calculated with the following procedure; it was found that this material's porosity matches closely to the extrapolated porosity value from Figure 5.3.

$$l = 13\text{cm}; w = 13\text{cm}; h = 3.8\text{cm}; \text{weight} = 7\text{g} \quad (5.6)$$

$$\text{volume, } V = l \cdot w \cdot h = 642.2 \text{ cm}^3 \quad (5.7)$$

$$\text{sample density, } \rho_s = \frac{\text{weight}}{\text{volume}} = 10.9 \text{ kg/m}^3 \quad (5.8)$$

$$\text{material density, } \rho_f = 21 \text{ kg/m}^3 \quad (5.9)$$

$$\text{sample porosity, } \varepsilon_s = 1 - \frac{\rho_s}{\rho_f} = 0.485 \quad (5.10)$$

### Re-designed porosity based forest canopy model

After the forest canopy model was re-designed based on the findings above, a second suite of experiments was done. The forest canopy was made using a 48% porosity material. Figure 5.4 shows the completed model and its placement in the wind tunnel (the model is presented from another view in Figure D.3, Appendix D). Foam boards were used to create a smooth transition between the tunnel's floor and the topographic model. In order to keep the same base of comparison, the experimental parameters remained the same as for the preliminary tests. Thus, the vertical wind velocity profile and the model's position in the tunnel were maintained. The results are presented in the next section (Section 5.3), in the same format as the preliminary results.



Figure 5.4: Completed wind tunnel experimental model, with attached 48% porosity forest canopy model and its placement in the wind tunnel.



### 5.3 Final Case Study Modeling Results

In this chapter the final results are presented using the same format as the preliminary results in Section 4.1. The final wind tunnel experiment was performed using the topographic model with the 48% forest canopy model fastened to it, referred from here on as the “48% canopy model” case.

Figure 5.5a shows the comparison between the wind tunnel results for the “48% canopy model” and full scale data averaged over the three identified segments, in the same manner as the preliminary results. Figure 5.5b shows the comparison between the wind speed profile used in the wind tunnel and the one measured at the met tower. Figures 5.6 to 5.9 present the comparison between the wind tunnel experiment and full scale data in the 315° direction for the months of March, September, October and December, respectively.

Figures 5.10 to 5.12 show the summary plots for the comparison of the wind tunnel and full scale measurements for directions 315°, 202.5° and 157.5°, respectively. In these figures all of the previous *Full scale* curves were centralized and compared to the *Wind tunnel* curve. The complete set of results, which contains the intermediary results plots, is available in Appendix C.

Figure 5.12 shows the comparison between the wind tunnel data and full scale for the 157.5° direction. The large differences that were observed in this figure are assumed to be caused by the abrupt change in roughness when the flow transitions from water to land which also underlines the discrepancies between the inlet profile used in the wind tunnel experiment and the full scale profile. The boundary layer recovery distance and how this distance affects the flow in the case of direction 157.5° is discussed in detail in Section 5.5.

### 5.4 Comparison between Wind Tunnel Tests

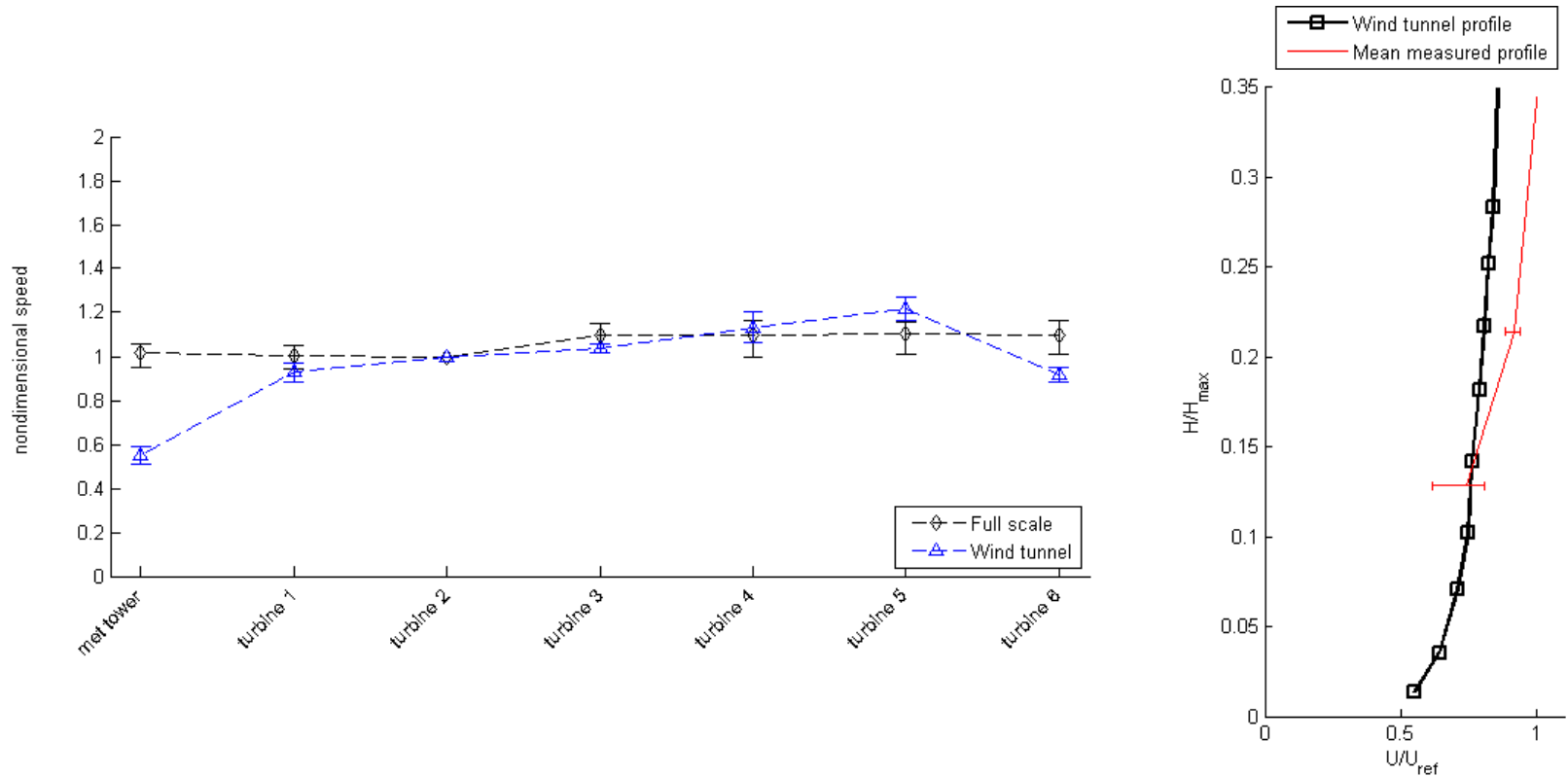
Three test cases were available for comparison; two using different materials for the forest canopy models and one case without a forest canopy model. The results are presented in Figure 5.13, and are divided into three graphs. Each graph represents one of the selected main wind directions: 315°, 202.5° and 157.5°, respectively.

Figure 5.13 shows that, even though the topography is shallow, it has an influence on the flow. This fact sets aside the concerns about the topography, but also emphasizes the importance of an adequate forest canopy model. By analyzing Figure 5.13a, for the 315° direction, the preliminary “90% canopy model” results ( $\varepsilon = 90\%$  curve) are visibly different from the bare topography results (*no forest* curve); the “48% canopy model” results ( $\varepsilon = 48\%$  curve) follow approximately the same trend as the initial “90% canopy model” case. For this wind direction the forest upstream of the measurement location is non-homogeneous as it is dispersed into a large number of smaller forested patches. For this flow direction the boundary layer also does not recover over the available fetch, so the boundary layer is not in an “equilibrium” state and the flow most probably is transitioning. Unsteady transitional flows of this kind are usually highly dependent on the Reynolds number(s) involved. It is therefore probable that the small Reynolds number of the model compared to the full scale is an important factor for the discrepancies noticed between the wind tunnel modes (both porosity cases) and full scale. The analysis performed in this section will focus on the 202.5° and 157.5° directions, where the forest upstream is less fragmented.

In the case the 202.5° and 157.5° directions it is assumed that the material used for the 48% canopy model acts as a bluff body. This conclusion is drawn from Figure 5.13, where graphs (b) and (c) show that this case ( $\varepsilon = 48\%$  curve) is offset from the trend of the “no forest” case (*no forest* curve). This implies an upward shift of the velocity profile by a distance noted in Section 5.5 as  $d_{\text{total}}$ .

Section 5.5 analyzes the results presented in Figures 5.5 to 5.13 by exploring the effects caused by an abrupt roughness transition on the incoming flow. Boundary layer recovery distances are calculated and then compared to the measured distances from the coast to the investigated site for each of the considered wind directions.

- Wind tunnel result set description:
- Direction 315°;
  - “48% canopy model” case;
  - Full scale data for January 2008;

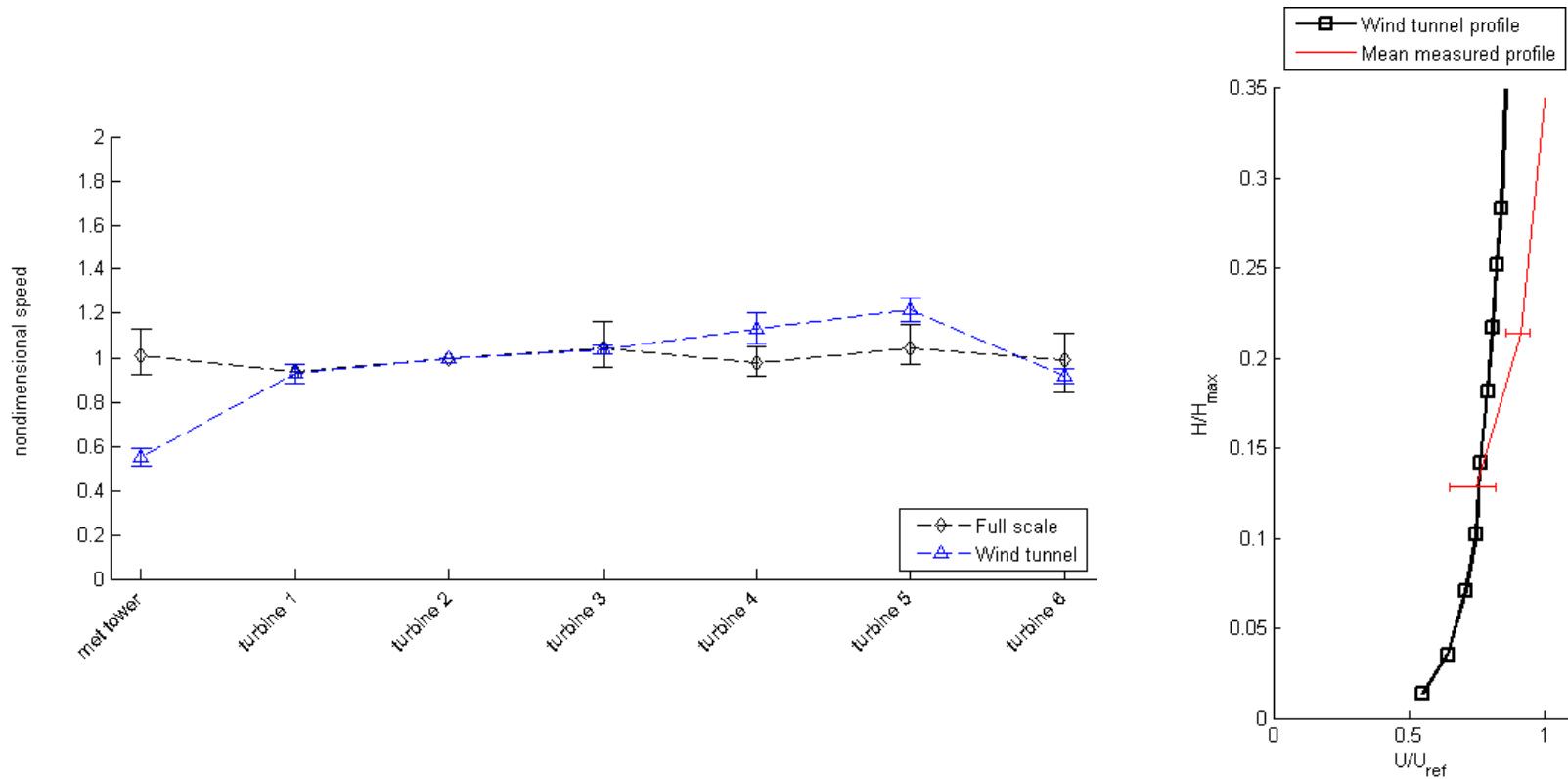


(a) Comparison between wind tunnel data (topographic model with canopy model) and full scale data for the 315° direction. Full scale data was extracted for the month of January.

(b) Comparison between wind tunnel inlet profile and vertical profile measured at the met tower. Full scale data was extracted for the month of January.

Figure 5.5: Wind tunnel results and comparison with full scale data. “48% canopy model” case, direction: 315°, January 2008.

- Wind tunnel result set description:
- Direction 315°;
  - “48% canopy model” case;
  - Full scale data for March 2008;

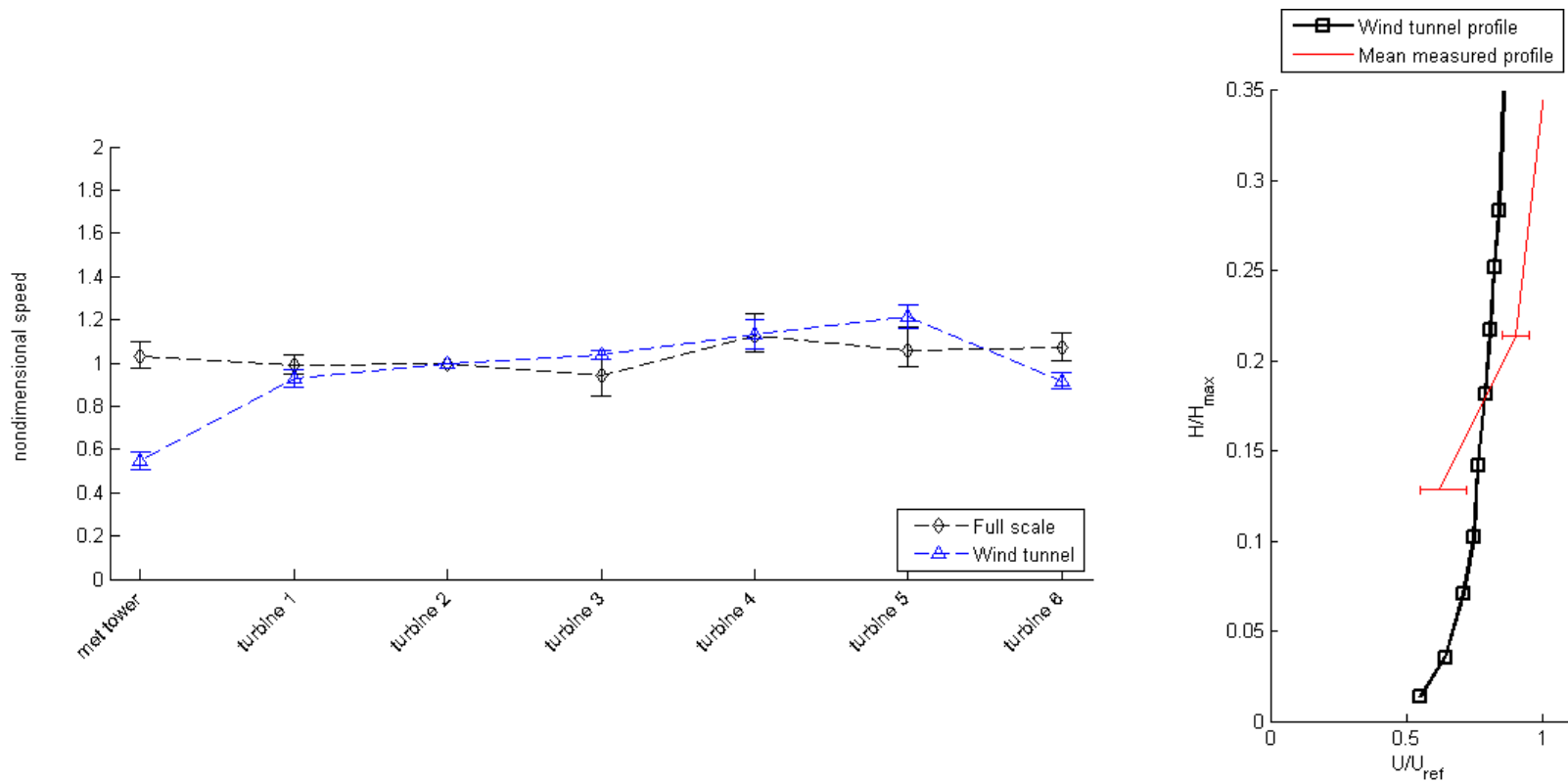


(a) Comparison between wind tunnel data (topographic model with canopy model) and full scale data for the 315° direction. Full scale data was extracted for the month of March.

(b) Comparison between wind tunnel inlet profile and vertical profile measured at the met tower. Full scale data was extracted for the month of March.

Figure 5.6: Wind tunnel results and comparison with full scale data. “48% canopy model” case, direction: 315°, March 2008.

- Wind tunnel result set description:
- Direction 315°;
  - “48% canopy model” case;
  - Full scale data for September 2008;

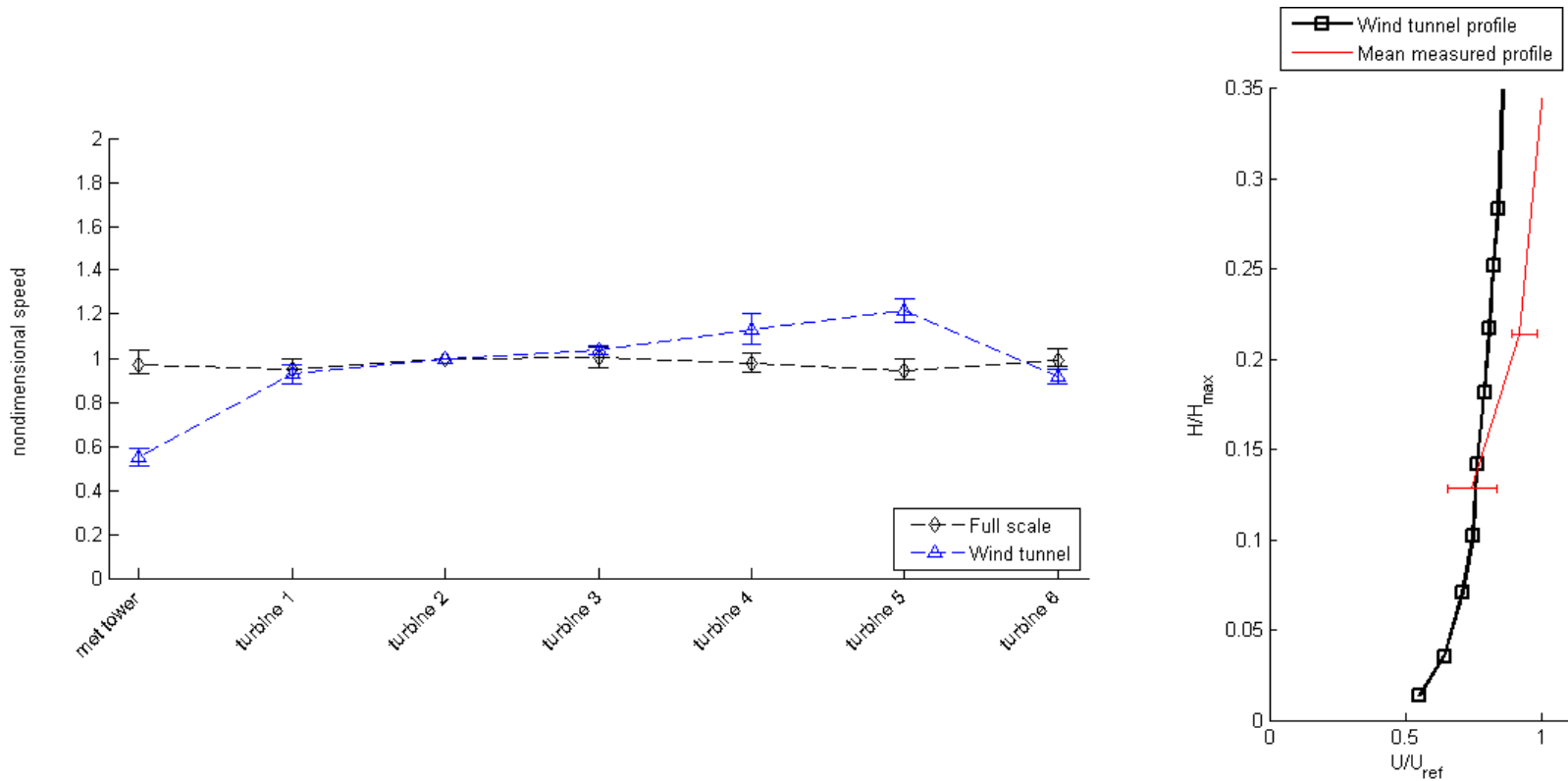


(a) Comparison between wind tunnel data (topographic model with canopy model) and full scale data for the 315° direction. Full scale data was extracted for the month of September.

(b) Comparison between wind tunnel inlet profile and vertical profile measured at the met tower. Full scale data was extracted for the month of September.

Figure 5.7: Wind tunnel results and comparison with full scale data. “48% canopy model” case, direction: 315°, September 2008.

- Wind tunnel result set description:
- Direction 315°;
  - “48% canopy model” case;
  - Full scale data for October 2008;

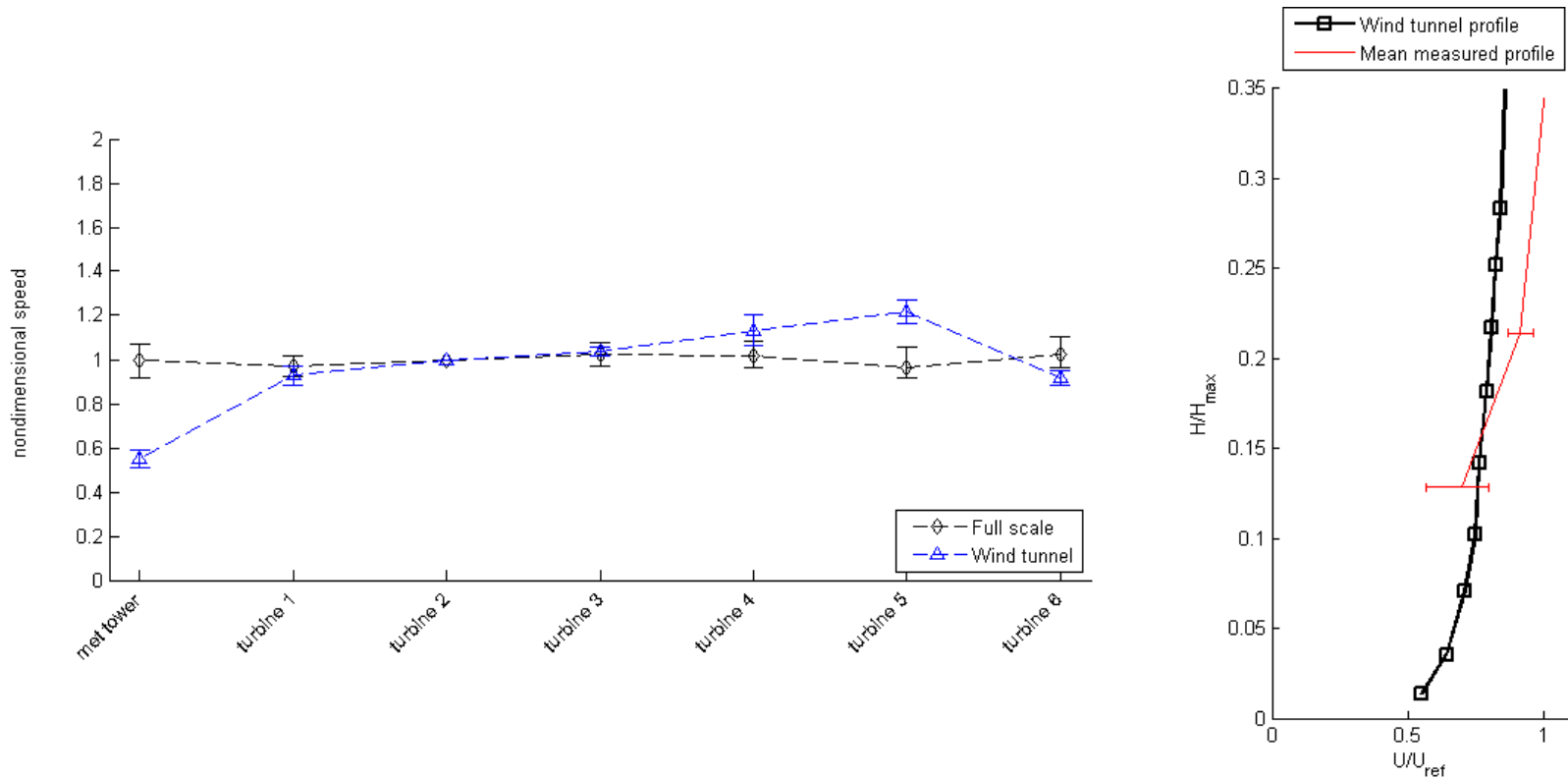


(a) Comparison between wind tunnel data (topographic model with canopy model) and full scale data for the 315° direction. Full scale data was extracted for the month of October.

(b) Comparison between wind tunnel inlet profile and vertical profile measured at the met tower. Full scale data was extracted for the month of October.

Figure 5.8: Wind tunnel results and comparison with full scale data. “48% canopy model” case, direction: 315°, October 2008.

- Wind tunnel result set description:
- Direction 315°;
  - “48% canopy model” case;
  - Full scale data for December 2008;

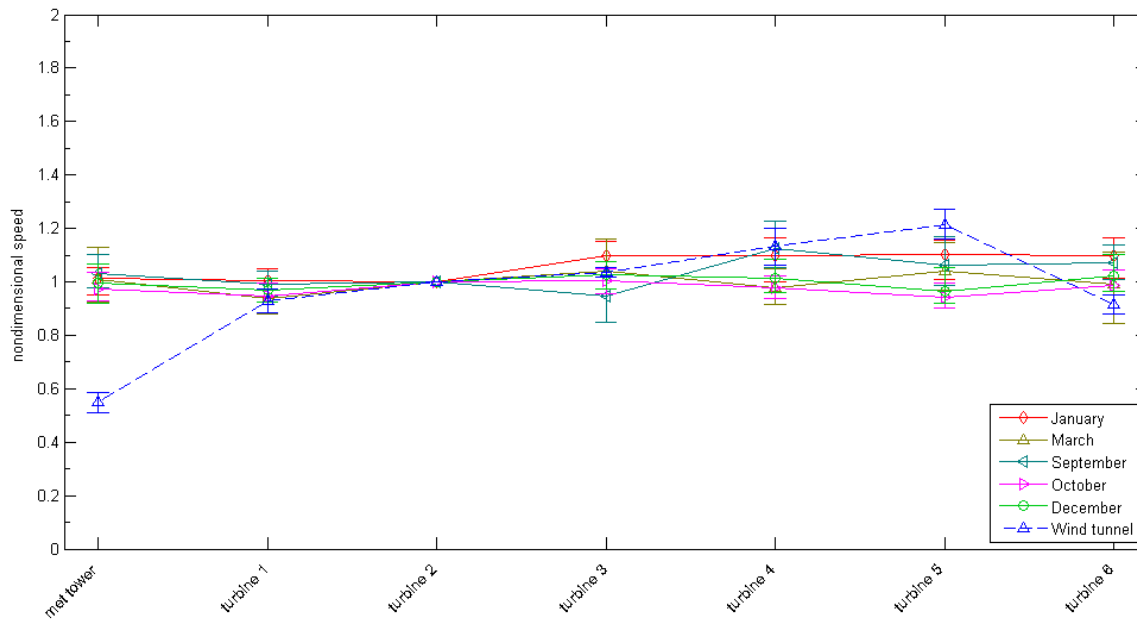


(a) Comparison between wind tunnel data (topographic model with canopy model) and full scale data for the 315° direction. Full scale data was extracted for the month of December.

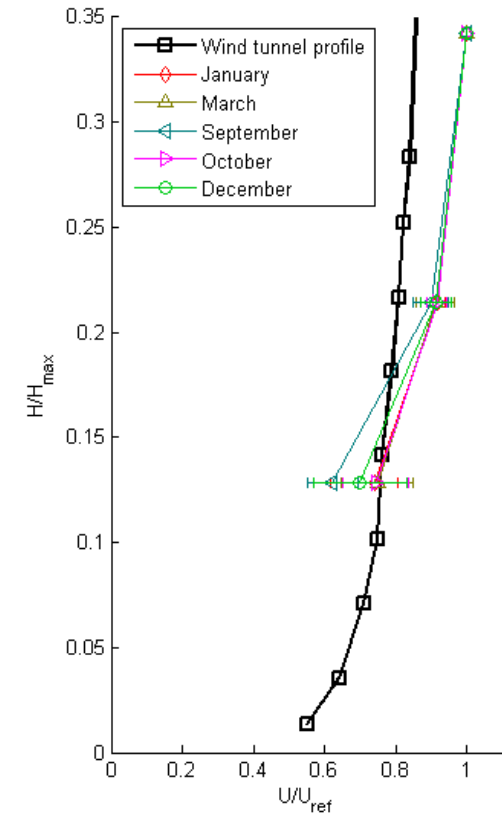
(b) Comparison between wind tunnel inlet profile and vertical profile measured at the met tower. Full scale data was extracted for the month of December.

Figure 5.9: Wind tunnel results and comparison with full scale data. “48% canopy model” case, direction: 315°, December 2008.

- Result set description:
- Direction 315°;
  - “48% canopy model” case;
  - Yearly full scale data;



Comparison between wind tunnel data (topographic model and canopy model) and full scale data for the 315° direction. Full scale data was plotted for each of the months which had valid segments.

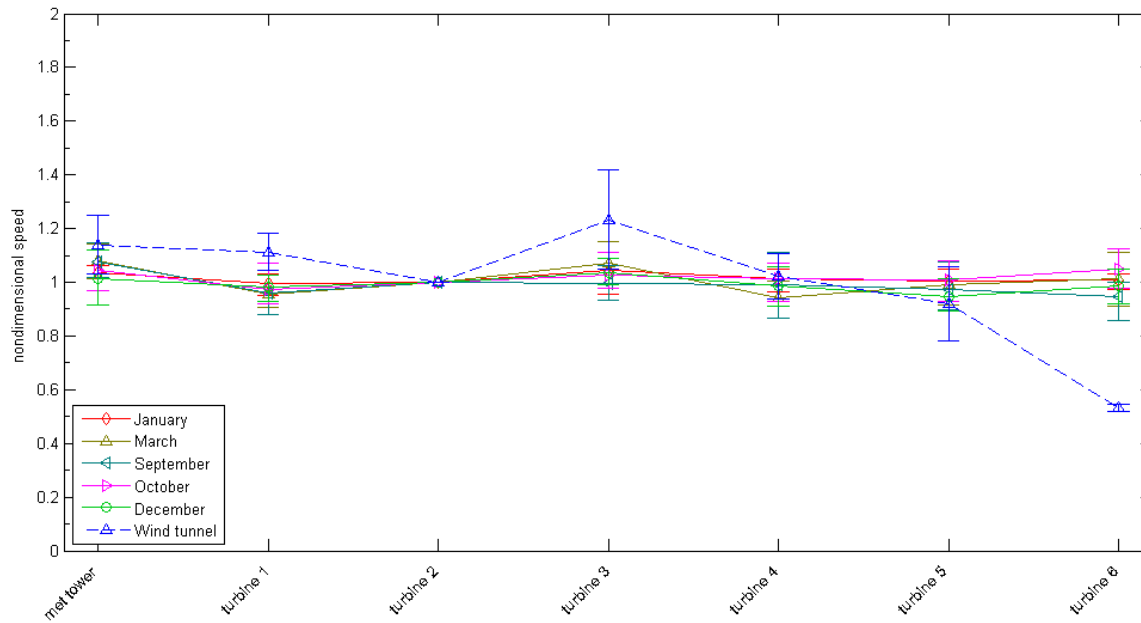


Comparison between wind tunnel inlet profile and vertical profile measured at the met tower.

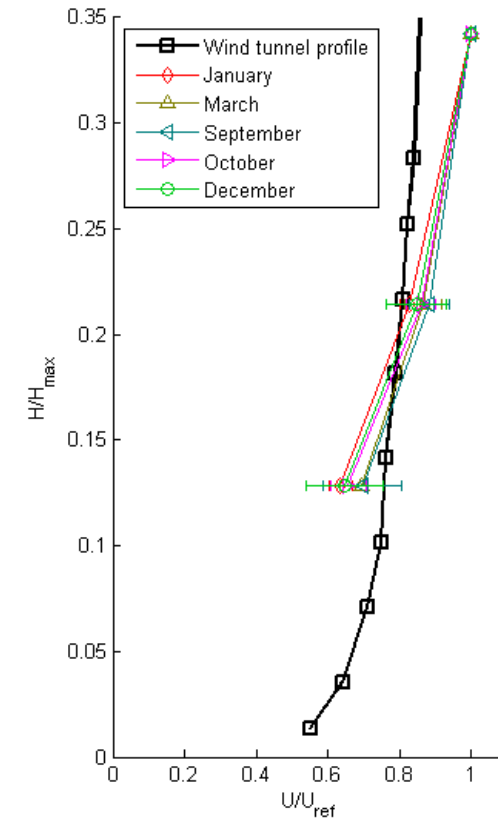
Figure 5.10: Summary plot of the comparison between the wind tunnel test and full scale data. “48% canopy model” case, direction: 315°, yearly data.



- Result set description:
- Direction 202.5°;
  - “48% canopy model” case;
  - Yearly full scale data;



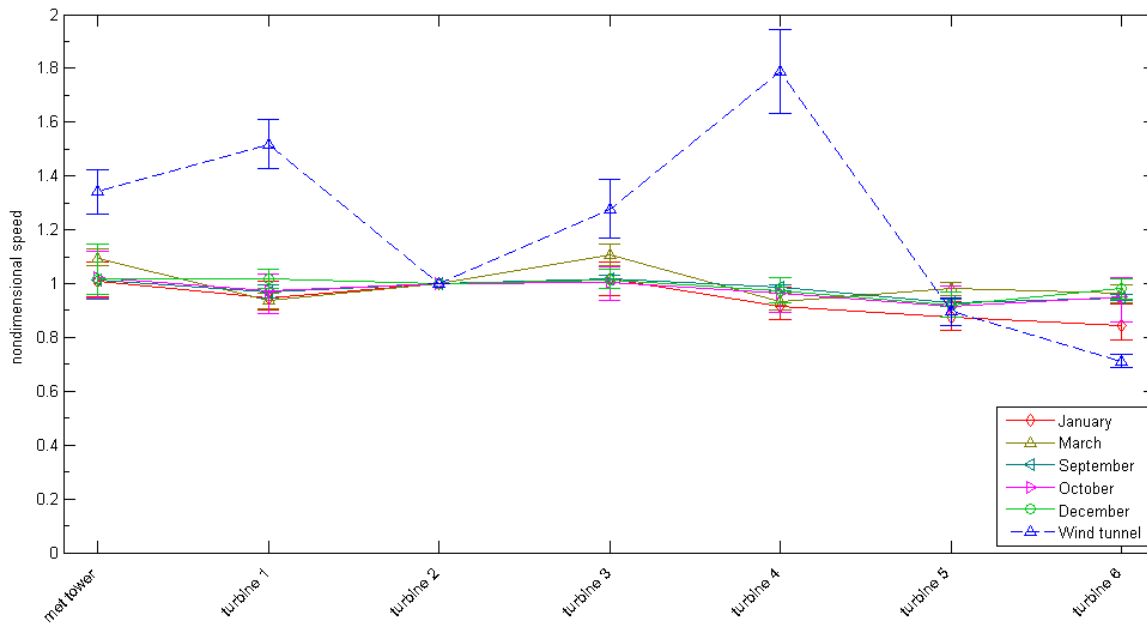
Comparison between wind tunnel data (topographic model with canopy model) and full scale data for the 202.5° direction. Full scale data was plotted for each of the months which had valid segments.



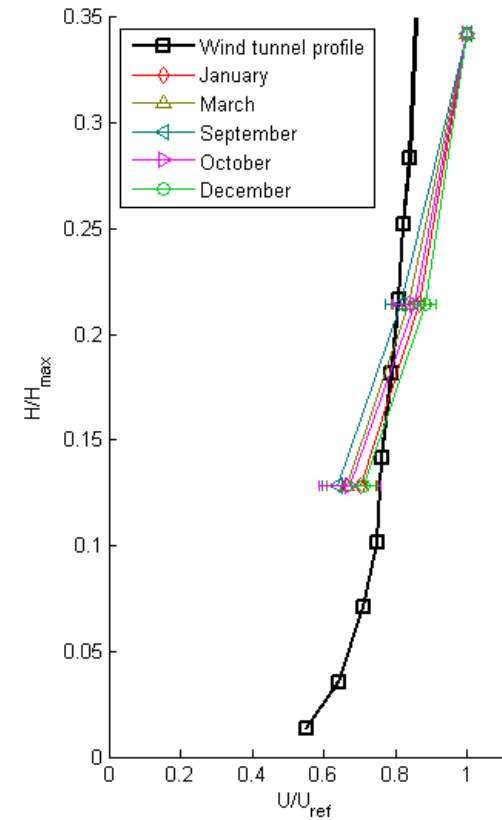
Comparison between wind tunnel inlet profile and vertical profile measured at the met tower.

Figure 5.11: Summary plot of the comparison between the wind tunnel test and full scale data. “48% canopy model” case, direction: 202.5°, yearly data.

- Result set description:
- Direction 157.5°;
  - “48% canopy model” case;
  - Yearly full scale data;



Comparison between wind tunnel data (topographic model with canopy model) and full scale data for the 157.5° direction. Full scale data was plotted for each of the months which had valid segments.



Comparison between wind tunnel inlet profile and vertical profile measured at the met tower.

Figure 5.12: Summary plot of the comparison between the wind tunnel test and full scale data. “48% canopy model” case, direction: 157.5°, yearly data.

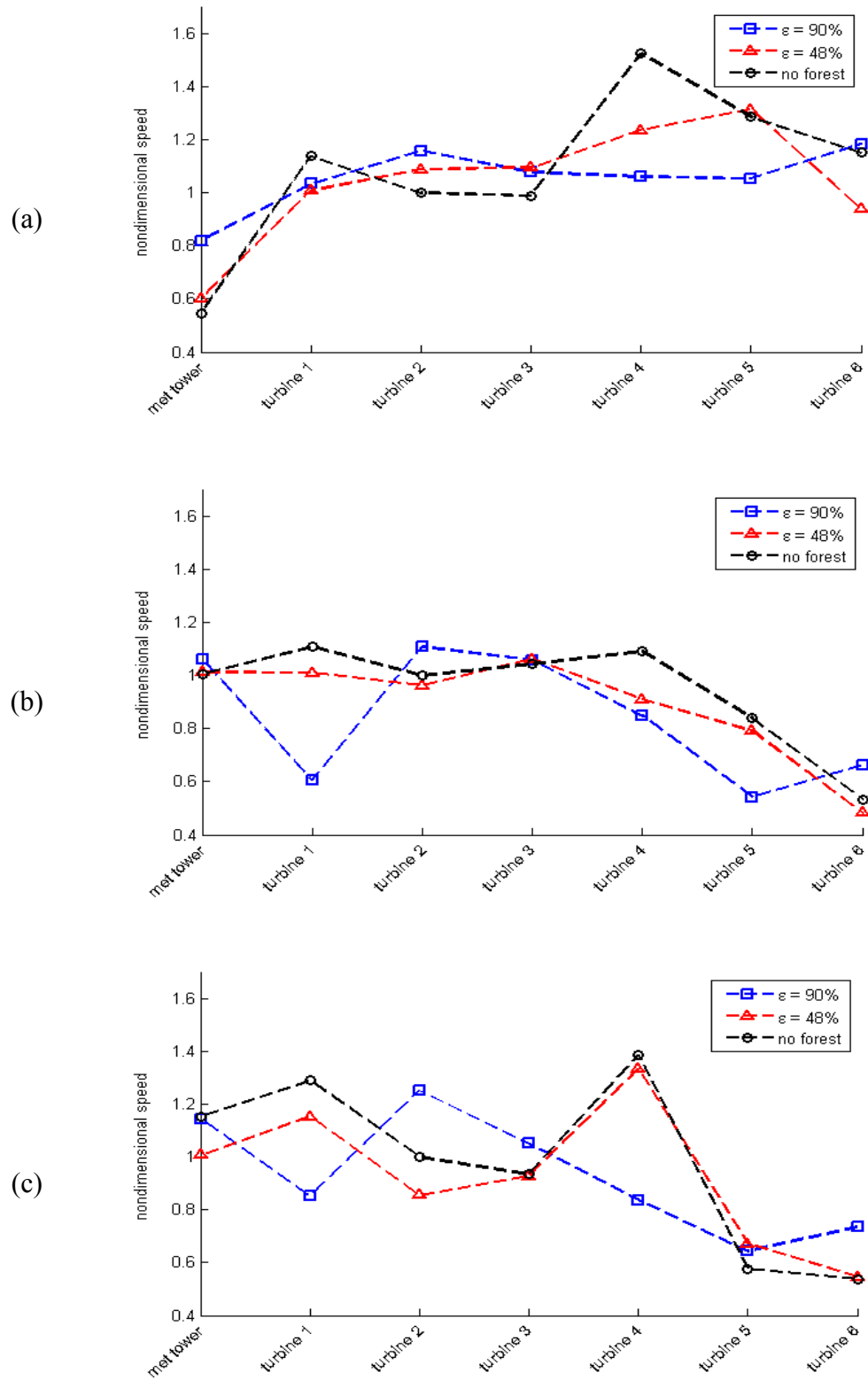


Figure 5.13: Comparison between the three wind tunnel test setups.

## 5.5 Results and Discussion of the Improved Canopy Model

### Effects of Roughness Transition

The incoming flow has to overcome an abrupt change in roughness when it transitions from water to land. The boundary layer recovery distance to the new roughness for a forest wind profile was calculated using Elliot's formula in Eq. (5.11) for the height of the internal boundary layer [80].

$$\frac{\delta}{z_{0D}} = \left(0.75 - 0.03 \cdot \ln \frac{z_{0D}}{z_{0U}}\right) \left(\frac{x}{z_{0D}}\right)^{0.8} \quad (5.11)$$

Where  $z_{0U}$  and  $z_{0D}$  represent roughness lengths for upwind and downwind,  $\delta$  is the boundary layer height and  $x$  is the distance from a change in roughness (recovery distance). The recovery distance was found to be approximately 4.1 km. This distance was then compared to the measured distances from the coast to the investigated site for all the directions and presented in Figure 5.14. For the 315° direction, the incoming profile transitions from water to agricultural fields. This is a slight roughness transition, and the profile is not changing very much. Also, the distance from the coast to the site is small. In the 202.5° direction the incoming profile has a long enough fetch which is larger than the boundary layer recovery distance from water to forest, so it had time to recover. In the case of the 157.5° direction, the distance between the coast and the site corresponds almost exactly to the transition distance. The wind profile starts over water but it does not have enough time to adjust to the forest roughness. It is still in a transitional state and therefore, as explained before, the wind tunnel tests at low Reynolds number cannot accurately reproduce the flow behavior. This would be a possible explanation as to why the results do not match and a potential solution would be to run the canopy experiments at larger scales, and therefore higher Reynolds numbers, which was not possible in the present boundary layer wind tunnel.

With the help of satellite imagery in Figure 5.15 it is observable that, for the 157.5° and 202.5° directions, the flow encounters large patches of forest. By looking at the wind tunnel tests comparison in Figure 5.13, a trend is identified for the 157.5 and 202.5° directions: the 48% porosity case has a similar trend to that of the no forest case, and is offset.

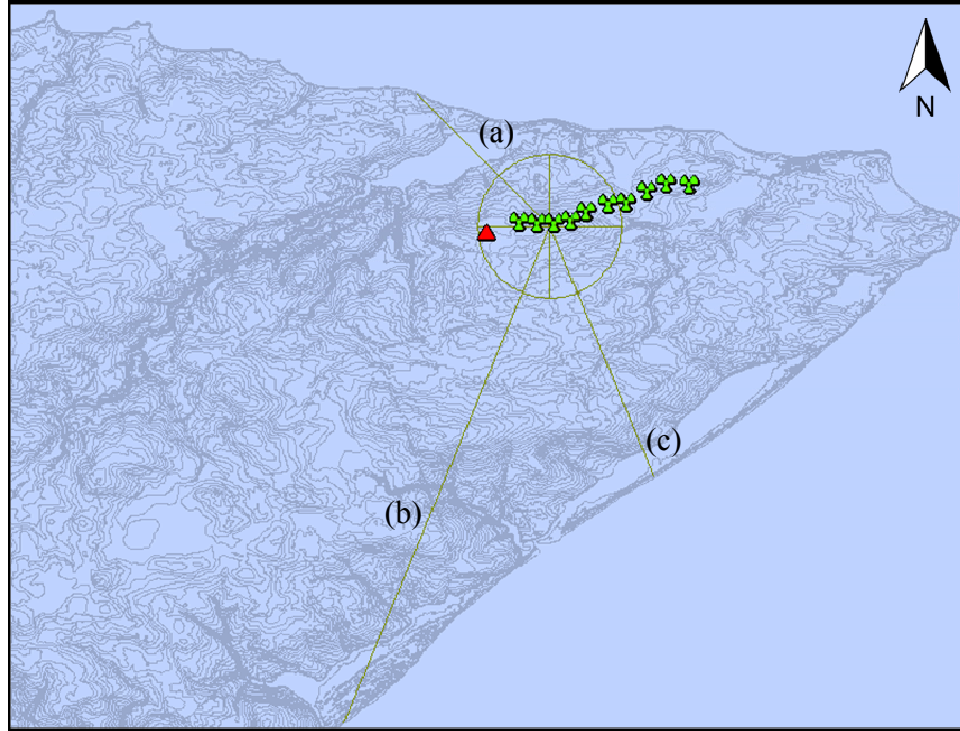


Figure 5.14: Terrain contours, wind turbine locations, modeled area and measured fetches.

Measured distance for the incoming flow for:

(a) direction  $315^\circ$ : 3.12km; (b) direction  $202.5^\circ$ : 8.86km; (c) direction  $157.5^\circ$ : 4.48km.



Figure 5.15: Satellite imagery and wind directions; for the  $157.5^\circ$  and  $202.5^\circ$  directions the flow encounters large patches of forest.

Lo [81] explains that the air flow within the forest canopy plays a significant role in the development of the boundary layer over canopies, as this is where momentum exchanges take place and that the transfer mechanisms and turbulence characteristics within and immediately above the canopy are significantly different from those of the atmospheric boundary layer over an open field. The idealized flow field over the boundary layer is characterized by parameters such as  $z_0$  (roughness length) and  $d$  (zero plane displacement height), when modeling boundary layer flows over forest canopies, as shown in Figure 5.16.

The velocity profile upward shift distance,  $d_{total}$ , was determined as follows in order to verify the previous assumption that the fiber glass material acts as a bluff body. A wind profile above the forest can be described by the logarithmic law in Eq. (5.12):

$$u(z) = \frac{u_*}{k} \ln\left(\frac{z}{z_0}\right) \quad (5.12)$$

where  $u(z)$  is the wind speed at height  $z$  above ground,  $u_*$  is the friction velocity,  $k$  is the von Kármán constant with a typical value of 0.4, and  $z_0$  is the roughness length.

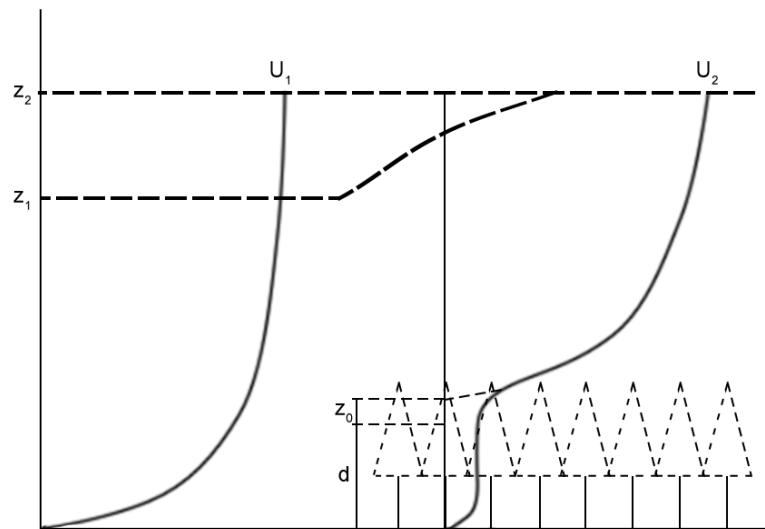


Figure 5.16: Modifications of the vertical wind profile by forest canopy;  
Adapted from Tajchman [82].

The upstream profile is presented in Section 3.2, Figure 3.2 and was obtained from hot-wire measurements. The roughness length and friction velocity have been determined using the log law (presented in Appendix A), and are as follows:  $z_0 = 3.43\text{e-}5$  m and  $u^* = 0.306$  m/s.

Two locations were considered, i.e. the met tower and the first wind turbine, since these measurement points were directly above the forest canopy and at a considerable distance downstream from the forest edge. Using the velocity measurements from the Cobra probes and the free stream velocity, a wind profile was generated at the measurement locations (met tower and turbine 1), as shown in Figure 5.17. In this figure, point *A* represents the measurement location and  $U_0$  is the free stream velocity. The two known velocities,  $u(z_1)$  and  $u(z_2)$ , were matched and the vertical distance between where they occur on their respective vertical profiles,  $d_{total}$ , was determined, as shown in Figure 5.18.

The Cobra probes were placed 0.16 m above the topographic model, which corresponds to the scaled wind turbine hub height (the full scale wind turbine hub height is 80 m; using a scale of 1:500,  $80 \text{ m}/500 = 0.16$  m) and is noted as  $h_{turbine}$  in Figure 5.17. Considering the thickness of the topographic model (noted as  $h_{topography}$ ), the total height at which the Cobra probes were placed relative to the tunnel floor is different for the two locations considered. The thickness of the forest canopy model was 0.04 m and the elevation at the considered locations was measured with the help of the CAD model and presented in Table 5.1:

Table 5.1: Topographic model height at respective locations.

Location	$h_{topography}$ [m]
Met tower	0.033
Turbine 1	0.039

For this comparison to be meaningful, the measured wind speeds at the locations of the met tower and wind turbine 1 were matched to wind speeds from the upstream profile, and the height at which they occur was measured.

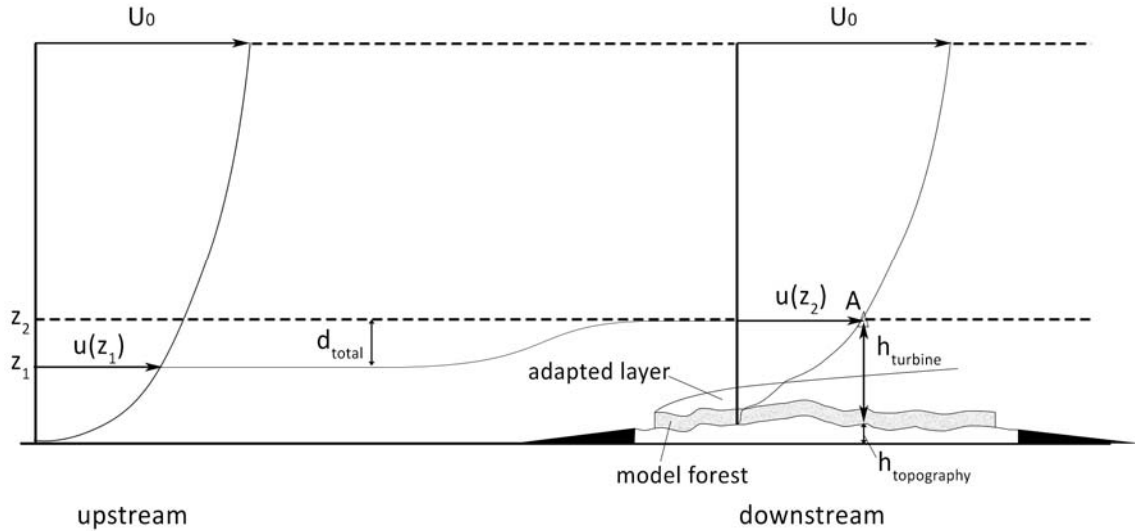


Figure 5.17: Upstream and downstream vertical wind profiles;  $z_1$  and  $z_2$  are the heights relative to the wind tunnel floor, at which the same wind speed,  $u(z_1) = u(z_2)$ , occurs for both the upstream and downstream profiles.

The input data needed to generate the downstream vertical wind profile were  $U_0$ , the free stream velocity measured at mid-height in the wind tunnel,  $z_0$  - roughness length,  $u(z_2)$  - the speed measured at turbine height and the von Kármán constant,  $k$ . Using these data (presented in Tables 5.2 and 5.3) and Eq. (5.13), the friction velocity ( $u_*$ ) was computed and then the wind profile was generated.

$$u_* = \frac{u(z) \cdot k}{\ln\left(\frac{z}{z_0}\right)} \quad (5.13)$$

Figure 5.18 shows a comparison between the wind profile obtained using the log law and the profile measured upstream for the met tower location. By examining the two profiles in Figure 5.18, the distance,  $d_{total}$ , by which the downstream profile is shifted upward, was determined and the results are presented in Tables 5.4 and 5.5 for the two wind directions,  $202.5^\circ$  and  $157.5^\circ$ , respectively.



Table 5.2: Variables used for vertical wind profile calculation, 202.5° direction.

Variable	Met tower	Turbine 1
$U_0$ [m/s]	6.71	6.71
$z_0$ [m]	0.0014	0.0014
$u(z_2)$ [m/s]	4.84	4.83
$z_2$ [m]	0.193	0.194

Table 5.3: Variables used for vertical wind profile calculation, 157.5° direction.

Variable	Met tower	Turbine 1
$U_0$ [m/s]	6.71	6.71
$z_0$ [m]	0.0014	0.0014
$u(z_2)$ [m/s]	4.22	4.84
$z_2$ [m]	0.193	0.194

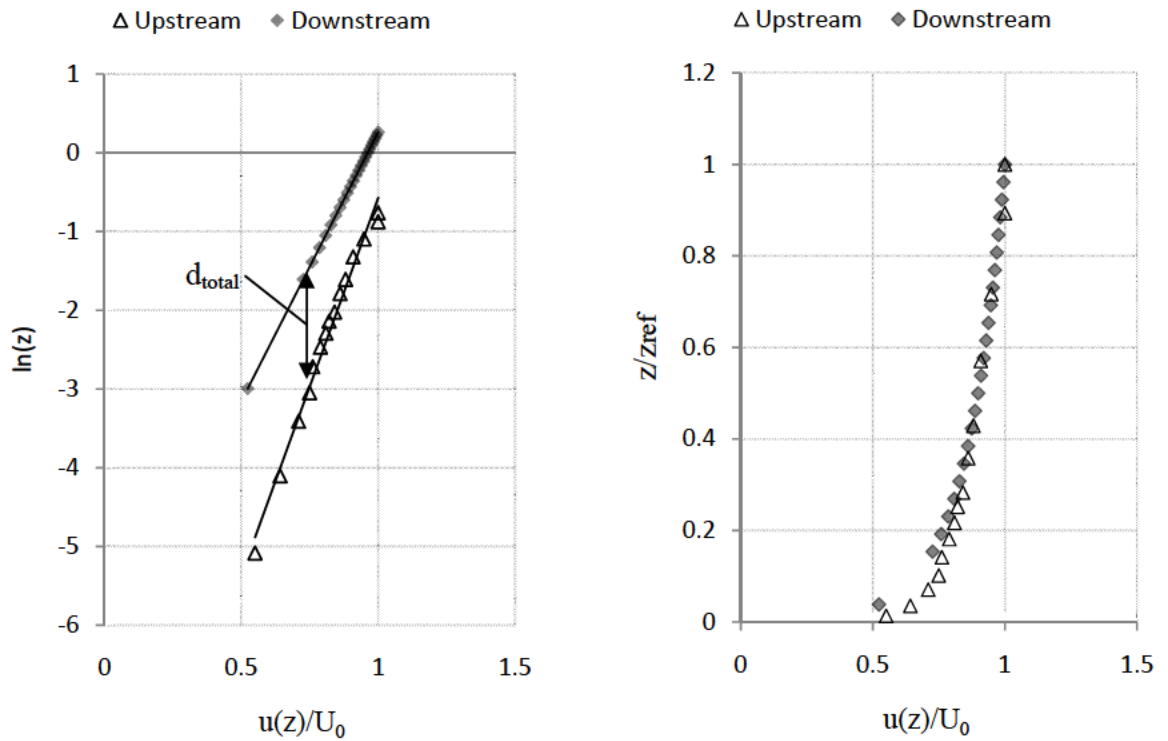
Figure 5.18: Comparison between upstream and downstream vertical wind profiles;  
Met tower data for 202.5° direction.

Table 5.4: Vertical wind profile shift; 202.5° direction.

Location	Upstream		Downstream		$d_{total}$ ( $z_2 - z_1$ ) [m]
	$u(z_1)/U_0$	$z_1$ [m]	$u(z_2)/U_0$	$z_2$ [m]	
Met tower	0.721	0.039	0.721	0.193	0.154
Turbine 1	0.721	0.039	0.720	0.194	0.155

Table 5.5: Vertical wind profile shift; 157.5° direction.

Location	Upstream		Downstream		$d_{total}$ ( $z_2 - z_1$ ) [m]
	$u(z_1)/U_0$	$z_1$ [m]	$u(z_2)/U_0$	$z_2$ [m]	
Met tower	0.628	0.016	0.629	0.193	0.177
Turbine 1	0.721	0.039	0.722	0.194	0.155

The values obtained in Tables 5.4 and 5.5 for the wind profile shift were larger than the height of the modeled forest canopy (which was 0.04 m high). A first conclusion is that the model canopy does not, in fact, perform as a simple bluff body.

Wiernga [83] reviewed the effects of upwind changes in terrain roughness. His study showed that the wind profile will only be related to the local terrain roughness within an internal boundary layer of limited thickness, while the wind structure at higher levels will still be determined by the roughness at greater upwind distances.

Figure 5.19 shows the structure of a boundary layer after an upstream change in roughness. The “adapted layer” refers to the new equilibrium layer that develops downstream of the change in terrain roughness.

The distances determined and presented in Table 5.4 and Table 5.5 ( $d_{total}$ ) are assumed to be the combined thicknesses of the forest canopy and the adapted layer. Forest canopy thickness does not account for the wind profile shift observed; therefore, the remainder of that distance is attributed to the thickness of the adapted layer, as presented in Figure 5.17 and Figure 5.19.

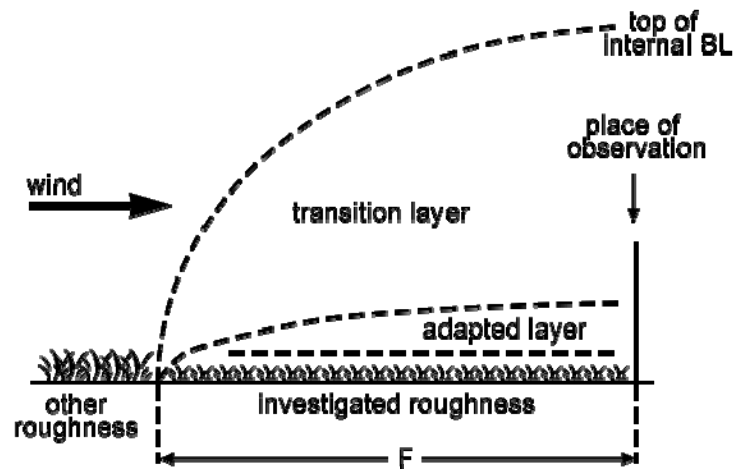


Figure 5.19: Structure of the internal boundary layer downwind of a roughness change;

Adapted from Wiernga [83].

Analyzing the results, it was found that the effect that the 48% porous forest canopy model had on the flow was not desirable. While these results matched well for the 315° direction, there were significant discrepancies for the other two directions analyzed.

By examining the vertical shift of the wind profile from the upstream station to the downstream station, it was concluded that for two of the analyzed directions (202.5° and 157.5°, where the forest canopy upstream of the measurement points was almost homogeneous) the 48% porosity fiber glass material behaves as an obstacle addition to the “no forest” case. It did not behave as a simple bluff body, but as a bluff body with added roughness elements on its upper surface. This might be an alternate possibility for experimental modelers to explore as they might be able to represent low porosity forest canopies as a roughness model on top of topography.

A new forest model was developed, based on the porosity parameter which was derived from remote sensed data. The findings in Chapter 5 point towards a redesign of the canopy model for the wind tunnel experiment. A new forest canopy model was tested in the wind tunnel, yet the results have shown that the model for the canopy is not conclusive at this time and therefore future work is necessary. A potential relationship between high density forest canopies and topography was investigated, which would enable the improvement of existing models as well as the development of simple numerical models.

## Chapter 6

### 6. Conclusion and Future Work

#### 6.1 Conclusion

In Canada, numerical models for the design of wind farms predict a production of energy higher than the actual energy production. The study by Natural Resources Canada (NRCan) shows that the wind farms in Canada are actually under-performing; from the analysis of 36 projects it was found that their cumulative performance was 91% of the expected capacity factor [4]. Two of the main difficulties related to the modeling of wind farms seem to be tied to the effects of topography and canopy. The present work explores an alternative way of addressing these issues in wind farm modeling through the experimental modeling of topography and forest canopy.

The work is based on a case study of the PEI (Prince Edward Island) Eastern Kings wind farm. A series of wind tunnel experiments were designed to reproduce the wind environment at the site. A multitude of factors have been taken into account when designing the wind tunnel experiment.

Full scale data was analyzed and quality control checks were performed using specific procedures outlined in this work. Analyzing large data sets and ensuring a qualitative, while at the same time, quantitative analysis posed a first challenge. The full scale data was used for a preliminary site assessment using the industry standard software, WAsP (Wind Atlas Analysis and Application Program). The wind atlas produced by the model was in good accordance with previous studies, such as the one undertaken by Gasset et al. [64]. WAsP generates average yearly estimates of wind velocity while the main interest for comparison with the wind tunnel tests was aimed at a shorter time span and a more detailed analysis.

The first step in the study was to generate an adequate topographic model for wind tunnel experiments. The topographic model was generated by the conversion between GIS (Geographic Information System) and CAD (Computer Aided Design) / CAM (Computer Aided Machining) data. Starting from 2D height contours and concluding with a 3D model

that was easily interpreted by a CNC (Computer Numerically Controlled) milling machine, a comprehensive step by step approach was introduced to successfully build a wind tunnel model. During the experimental testing, even though the scale of the model (1:1500) and the size restrictions of the wind tunnel test section did not allow for a more prominent topography to be represented, it was shown that the model performed well. The bare topographic model was used as basis of comparison for the forest canopy models.

The second step was to determine the way canopy should be modeled for the wind tunnel experiments. A common methodology has not been established in the scientific community on how to model a forest with a dense canopy. A preliminary series of wind tunnel experiments were performed using the generated topography model with a preliminary model of forest canopy. These tests yielded the first set of results which formed the basis for improving forest canopy modeling.

In order to improve the canopy model, a relationship between remote sensed vegetation parameters (such as Leaf Area Index and geometric features) and model properties was derived. The site was investigated using satellite data available online and, using previous studies, a porosity model was developed. A method was derived to enable the simulation of large forest canopies with different densities. The application of this new method yielded a different porosity to be used for the canopy modeling.

The third step was to re-run the wind tunnel experiments with the newly designed canopy porosity. It was found that the new fiber glass canopy model behaves as a bluff body with added roughness elements on its upper surface. The results have shown that the model for the canopy is still not conclusive at this time, yet a potential relationship between high density forest canopies and porosity has been investigated, which if proven correct would enable the creation of simple numerical models as well as improvement of the existing models. Further investigation is needed on detailing the relation between the simple geometric scaling (porosity based) proposed herein and the kinematic and dynamic scaling.

While there are several problems that still need to be addressed, the presented approach to modeling topography and forest canopies forms a good base for further wind tunnel experimental studies. These models can also be used for further investigations in order to benchmark numerical studies, both linear and non-linear.

## 6.2 Future Work

In terms of future work, a main step would be to investigate forest canopy models of different porosities from a momentum deficit point of view as opposed to a geometric scale point of view. This could be done as a parametric wind tunnel study for different porosities for a uniform forest patch, where we won't look at just matching the geometry of the block of forest with a real forest but also at matching measurements upwind and downwind of it. Full scale data for such an experiment would be needed in order to make a comparison.

There is still room for improvement on the LAI (Leaf Area Index) relationship to wind tunnel modeling. While the theoretical basis seems to be straightforward, the physical modeling technique would benefit from further improvement. Specifically, another material could be used to model the forest canopy, while keeping the same base parameters. While the fiber glass insulation material had the needed porosity, it was not easily modeled into the required shapes and also presented problems when attaching it to the topographic model.

Another issue that needs to be addressed is the size of the wind tunnel's experimental chamber. The size restriction dictated the scale of 1:500 in the Boundary Layer Wind Tunnel Laboratory at Western. With the commissioning of the new, large scale WindEEE Dome at Western University, it will be possible to enlarge the model scale by a factor of approximately 5.

## 7. References

- [1] "Land Use Planning for Wind Energy Systems in Manitoba", report prepared by EDS Consulting, Winnipeg, MB, October 9, 2009.
- [2] GWEC. "Global Wind Report Annual Market Update 2012" (PDF). [Online]. 2013 (5/8/2013), Available:  
[http://www.gwec.net/wp-content/uploads/2012/06/Annual\\_report\\_2012\\_LowRes.pdf](http://www.gwec.net/wp-content/uploads/2012/06/Annual_report_2012_LowRes.pdf).
- [3] CanWEA. "Wind facts". [Online]. 2013(5/12/2013), Available:  
[http://www.canwea.ca/wind-energy/windfacts\\_e.php](http://www.canwea.ca/wind-energy/windfacts_e.php).
- [4] J. Royer, "Status of the ecoENERGY for Renewable Power Program", in CanWEA 2010, 26th Annual Conference and Exhibition, Montreal, Quebec, 2010, .
- [5] A. Bowen and N. Mortensen, "Exploring The Limits of WASP the Wind Atlas Analysis And Application Program" in EWEC, Göteborg, 1996, .
- [6] J. Manning, P. Hancock and R. Whiting, "A Study of The Ability of Meteodyn WT to Replicate Measurements around Steep Hills using Wind Tunnel Data from the 'RUSHIL' Experiment". *Wind Eng* 34(5), pp. 477-499. 2010.
- [7] J. L. Walmsley and P. A. Taylor, "Boundary-Layer Flow over Topography: Impacts of The Askervein Study". *Bound. -Layer Meteorol.* 78(3-4), pp. 291-320. 1996.
- [8] J. Salmon, H. Teunissen, R. Mickle and P. Taylor, "The Kettles Hill Project: Field Observations, Wind-Tunnel Simulations and Numerical Model Predictions for Flow over a Low Hill". *Bound. -Layer Meteorol.* 43(4), pp. 309-343. 1988.
- [9] P. Mason and J. King, "Measurements and Predictions of Flow and Turbulence over an Isolated Hill of Moderate Slope". *Q. J. R. Meteorol. Soc.* 111(468), pp. 617-640. 1985.
- [10] J. L. Walmsley, I. Troen, D. P. Lalas and P. J. Mason, "Surface-Layer Flow in Complex Terrain: Comparison of Models and Full-Scale Observations". *Bound. -Layer Meteorol.* 52(3), pp. 259-281. 1990.

- [11] A. Beljaars, J. Walmsley and P. Taylor, "A Mixed Spectral Finite-Difference Model for Neutrally Stratified Boundary-Layer Flow over Roughness Changes and Topography". *Bound. -Layer Meteorol.* 38(3), pp. 273-303. 1987.
- [12] G. Raithby, G. Stubble and P. Taylor, "The Askervein Hill Project: A Finite Control Volume Prediction of Three-Dimensional Flows over The Hill". *Bound. -Layer Meteorol.* 39(3), pp. 247-267. 1987.
- [13] D. Lalas, T. Panagiotidis and D. Tryfonopoulos, "A Hybrid Micrositing Model for Wind Flow Simulations over Complex Topographies". Presented at Proc., 5th European Wind Energy Assoc. Conf. 1994, .
- [14] O. Zeman and N. O. Jensen, "Modification of Turbulence Characteristics in Flow over Hills". *Q. J. R. Meteorol. Soc.* 113(475), pp. 55-80. 1987.
- [15] J. Palma, F. Castro, L. Ribeiro, A. Rodrigues and A. Pinto, "Linear and Nonlinear Models in Wind Resource Assessment and Wind Turbine Micro-Siting in Complex Terrain". *J. Wind Eng. Ind. Aerodyn.* 96(12), pp. 2308-2326. 2008.
- [16] A. Rasouli, "Experimental and Numerical Modeling of Wind Flow over Complex Topography". 2010.
- [17] T. Clarenc, N. Girard, D. Delaunay and A. Chantelot, "Wind Farm Production Assessment in Complex Terrain: New Validations of Meteodyn WT". Presented at European Wind Energy Conference. 2007.
- [18] T. T. Ngo and C. W. Letchford, "Experimental Study of Topographic Effects on Gust Wind Speed". *J. Wind Eng. Ind. Aerodyn.* 97(9), pp. 426-438. 2009.
- [19] W. D. Lubitz and B. R. White. "Wind-Tunnel and Field Investigation of the Effect of Local Wind Direction on Speed-Up over Hills". *J. Wind Eng. Ind. Aerodyn.* 95(8), pp. 639-661. 2007.
- [20] T. Ishihara, K. Hibi and S. Oikawa, "A Wind Tunnel Study of Turbulent Flow over a Three-Dimensional Steep Hill". *J. Wind Eng. Ind. Aerodyn.* 83(1), pp. 95-107. 1999.



- [21] K. W. Ayotte and D. E. Hughes, "Observations of Boundary-Layer Wind-Tunnel Flow over Isolated Ridges of Varying Steepness and Roughness". *Bound. -Layer Meteorol.* 112(3), pp. 525-556. 2004.
- [22] R. L. Simpson, C. Long and G. Byun, "Study of Vortical Separation from an Axisymmetric Hill". *Int J Heat Fluid Flow* 23(5), pp. 582-591. 2002.
- [23] J. Ruel, D. Pin, L. Spacek, K. Cooper and R. Benoit, "The Estimation of Wind Exposure for Windthrow Hazard Rating: Comparison Between Strongblow, MC2, Topex and a Wind Tunnel Study". *Forestry* 70(3), pp. 253-266. 1997.
- [24] H. Teunissen, M. Shokr, A. Bowen, C. Wood and D. Green, "The Askervein Hill Project: Wind-Tunnel Simulations at Three Length Scales". *Bound. -Layer Meteorol.* 40(1-2), pp. 1-29. 1987.
- [25] G. Y. Chock and L. Cochran, "Modeling of Topographic Wind Speed Effects in Hawaii". *J. Wind Eng. Ind. Aerodyn.* 93(8), pp. 623-638. 2005.
- [26] M. Raupach, J. Finnigan and Y. Brunei, "Coherent Eddies and Turbulence in Vegetation Canopies: The Mixing-Layer Analogy". *Bound. -Layer Meteorol.* 78(3-4), pp. 351-382. 1996.
- [27] D. E. Neff and R. N. Meroney, "Wind-Tunnel Modeling of Hill and Vegetation Influence on Wind Power Availability". *J. Wind Eng. Ind. Aerodyn.* 74pp. 335-343. 1998.
- [28] Y. Brunet, J. Finnigan and M. Raupach, "A Wind Tunnel Study of Air Flow in Waving Wheat: Single-Point Velocity Statistics". *Bound. -Layer Meteorol.* 70(1-2), pp. 95-132. 1994.
- [29] R. Meroney, "Characteristics of Wind and Turbulence in and Above Model Forests". *J. Appl. Meteorol.* 7(5), pp. 780-788. 1968.
- [30] C. Gromke and B. Ruck, "Aerodynamic Modelling of Trees for Small-Scale Wind Tunnel Studies". *Forestry* 81(3), pp. 243-258. 2008.
- [31] J. Finnigan and P. Mulhearn, "Modelling Waving Crops in a Wind Tunnel". *Bound. -Layer Meteorol.* 14(2), pp. 253-277. 1978.
- [32] G. Stacey, R. Belcher, C. Wood and B. Gardiner, "Wind Flows and Forces in a Model Spruce Forest". *Bound. -Layer Meteorol.* 69(3), pp. 311-334. 1994.

- [33] J. M. Chen and T. Black, "Defining Leaf Area Index for Non-Flat Leaves". *Plant, Cell & Environment* 15(4), pp. 421-429. 1992.
- [34] N. Kobayashi and T. Hiyama, "Stability Dependence of Canopy Flows over a Flat Larch Forest". *Bound. -Layer Meteorol.* 139(1), pp. 97-120. 2011.
- [35] L. Pietri, A. Petroff, M. Amielh and F. Anselmet, "Turbulence Characteristics within Sparse and Dense Canopies". *Environmental Fluid Mechanics* 9(3), pp. 297-320. 2009.
- [36] J. Sanz Rodrigo, J. Van Beeck and G. Dezsö-Weidinger, "Wind Tunnel Simulation of the Wind Conditions Inside Bidimensional Forest Clear-Cuts. Application to Wind Turbine Siting". *J. Wind Eng. Ind. Aerodyn.* 95(7), pp. 609-634. 2007.
- [37] S. Aubrun and B. Leidl, "Development of an Improved Physical Modelling Of a Forest Area in a Wind Tunnel". *Atmos. Environ.* 38(18), pp. 2797-2801. 2004.
- [38] J. S. Warland, "Turbulent Air Flow in Forest Stands: A Wind Tunnel Study". *Boundary-Layer Meteorology* 1996.
- [39] B. J. Marshall, "Wind Flow Structures and Wind Forces in Forests". University of Oxford, vol. Diss., 1998.
- [40] M. D. Novak, J. S. Warland, A. L. Orchansky, R. Ketler and S. Green, "Wind Tunnel and Field Measurements of Turbulent Flow in Forests. Part I: Uniformly Thinned Stands". *Bound. -Layer Meteorol.* 95(3), pp. 457-495. 2000.
- [41] W. Zhu, R. van Hout, L. Luznik, H. Kang, J. Katz and C. Meneveau, "A Comparison of PIV Measurements of Canopy Turbulence Performed in the Field and in a Wind Tunnel Model". *Exp. Fluids* 41(2), pp. 309-318. 2006.
- [42] W. Yue, C. Meneveau, M. B. Parlange, W. Zhu, H. S. Kang and J. Katz, "Turbulent Kinetic Energy Budgets in a Model Canopy: Comparisons Between LES and Wind-Tunnel Experiments". *Environmental Fluid Mechanics* 8(1), pp. 73-95. 2008.
- [43] N. G. Mortensen, "Planning and Development of Wind Farms: Wind". 2012.
- [44] Ebba Dellwik, Lars Landberg and N. O. Jensen, "WAsP in the Forest". *Wind Energy* 9pp. 211-218. 2005.

- [45] Prince Edward Island. Department of finance, energy and municipal affairs. [Online]. 2013(5/8/2013), Available: [http://www.gov.pe.ca/photos/original/eef\\_windfarmfax.pdf](http://www.gov.pe.ca/photos/original/eef_windfarmfax.pdf).
- [46] Frontier Power Systems, "Site 9644 - EPWP 80m Met Tower Install Report; prepared for PEI Energy Corporation" 2009.
- [47] NRG Systems. - NRG #40C anemometer, calibrated, with boot. [Online]. 2013(5/8/2013), Available: <http://www.nrgsystems.com/sitecore/content/products/1900.aspx>.
- [48] Ultrasonic wind sensors. – Turbine control – FT702LT-V22 anemometer. [Online]. 2013(5/8/2013), Available: <http://www.fttech.co.uk/ft702-lt-v22-wind-sensor/>.
- [49] NRG Systems. - NRG SymphoniePLUS3®Logger with (1) SD card and accessories. [Online]. 2013(5/8/2013), Available: <http://www.nrgsystems.com/sitecore/content/Products/5504.aspx?pf=Symphonie>.
- [50] Windographer. | Wind resource analysis | wind resource assessment software | wind SoDAR | wind LiDAR. [Online]. 2013(5/8/2013), Available: <https://www.windographer.com/>.
- [51] B. Bailey, S. McDonald, D. Bernadett, M. Markus and K. Elsholtz, "Wind Resource Assessment Handbook". AWS Scientific, Inc., Prepared for: National Renewable Energy Laboratory Sub Co Ntract Number TAT-5-15-283-01 1997.
- [52] E. L. Houghton and N. Carruthers, "Wind Forces on Buildings and Structures: An Introduction" 1976.
- [53] M. L. Levitan and K. C. Mehta, "Texas Tech Field Experiments for Wind Loads Part 1: Building and Pressure Measuring System". J. Wind Eng. Ind. Aerodyn. 43(1), pp. 1565-1576. 1992.
- [54] A. Peña, "Sensing the Wind Profile". Risø-PhD-45 (EN) ISBN pp. 978-987. 2009.
- [55] N. Sucevic and Z. Djuriscic, "Influence of Atmospheric Stability Variation on Uncertainties of Wind Farm Production Estimation". EWEA, 2012.
- [56] J. W. Deardorff, "Numerical Investigation of Neutral and Unstable Planetary Boundary Layers". J. Atmos. Sci. 29(1), pp. 91-115. 1972.

- [57] N. G. Mortensen, D. N. Heathfield, L. Myllerup, L. Landberg and O. Rathmann, "Getting Started with WAsP 9", Risø National Laboratory, Technical University of Denmark, Roskilde, Denmark, June, 2007.
- [58] N. G. Mortensen, D. N. Heathfield, O. Rathmann and M. Nielsen, "Wind Atlas Analysis and Application Program: WAsP 10 Help Facility". 2012.
- [59] H. P. Frank, O. Rathmann, N. G. Mortensen and L. Landberg, "The Numerical Wind Atlas - The KAMM/Wasp Method". 2001.
- [60] A. J. Bowen and N. G. Mortensen, "WAsP Prediction Errors due to Site Orography", Risø National Laboratory, Technical University of Denmark, Roskilde, Denmark, December, 2004.
- [61] I. Troen, "A High Resolution Spectral Model for Flow in Complex Terrain". 1990.
- [62] P. Taylor and H. Teunissen, "The Askervein Hill Project: Overview and Background Data". Bound. -Layer Meteorol. 39(1-2), pp. 15-39. 1987.
- [63] P. Mason and J. King, "Measurements and Predictions of Flow and Turbulence over an Isolated Hill of Moderate Slope". Q. J. R. Meteorol. Soc. 111(468), pp. 617-640. 1985.
- [64] N. Gasset, Y. Gagnon and G. J. Poitras, "Prince Edward Island Wind Atlas". 2005.
- [65] Alan G. Davenport Wind Engineering Group, "BLWTL - BLWTL 2," vol. 2013.
- [66] F. Bañuelos-Ruedas, C. Á. Camacho and S. Rios-Marcuello, "Methodologies used in the Extrapolation of Wind Speed Data at Different Heights and its Impact in the Wind Energy Resource Assessment in a Region". 2011.
- [67] ESRI (Environmental Systems Resource Institute), "ArcMap Release 10," vol. Redlands, CA: Environmental Systems Research Institute. 2011.
- [68] K. MacDonald, "Environmental Assessment of the 30MW East Point Wind Plant". [Online]. 2012(March), Available:  
[http://www.gov.pe.ca/photos/original/eef\\_epwf\\_jn1506.pdf](http://www.gov.pe.ca/photos/original/eef_epwf_jn1506.pdf).

- [69] L. Castillo, J. Seo, D. Walker, J. Johansson, H. Hangan, "Turbulent Boundary Layers at Very High Reynolds Number and its Relation to the Initial Condition", in 31st AIAA Fluid Dynamics Conference, 2001, pp. 2001-2913.
- [70] W. Sadeh, J. Cermak and T. Kawatani, "Flow over High Roughness Elements". *Bound.-Layer Meteorol.* 1(3), pp. 321-344. 1971.
- [71] Getting Started Series 100 Cobra Probe, "User's Guide, Turbulent Flow Instrumentation Pty. Ltd." 2011.
- [72] I. Jonckheere, S. Fleck, K. Nackaerts, B. Muys, P. Coppin, M. Weiss and F. Baret, "Review of Methods for In Situ Leaf Area Index Determination: Part I. Theories, Sensors and Hemispherical Photography". *Agric. for. Meteorol.* 121(1), pp. 19-35. 2004.
- [73] K. S. Fassnacht, S. T. Gower, J. M. Norman and R. E. McMurtric, "A Comparison of Optical and Direct Methods for Estimating Foliage Surface Area Index in Forests". *Agric. for. Meteorol.* 71(1), pp. 183-207. 1994.
- [74] P. Stenberg, S. Linder, H. Smolander and J. Flower-Ellis, "Performance of the LAI-2000 Plant Canopy Analyzer in Estimating Leaf Area Index of Some Scots Pine Stands". *Tree Physiol.* 14(7-8-9), pp. 981-995. 1994.
- [75] R. Kùßner and R. Mosandl, "Comparison of Direct and Indirect Estimation of Leaf Area Index in Mature Norway Spruce Stands of Eastern Germany". *Canadian Journal of Forest Research* 30(3), pp. 440-447. 2000.
- [76] A. Hagiwara, J. Imanishi, H. Hashimoto and Y. Morimoto, "Estimating Leaf Area Index in Mixed Forest Using an Airborne Laser Scanner", *International Archives of Photogrammetry, Remote Sensing and Spatial Information Sciences*, pp. 299-300, 2004.
- [77] L. Huang, "The Impact of Drought on Leaf Area Index (LAI) over Texas".
- [78] V. Le Dantec, E. Dufrêne and B. Saugier, "Interannual and Spatial Variation in Maximum Leaf Area Index of Temperate Deciduous Stands". *For. Ecol. Manage.* 134(1), pp. 71-81. 2000.
- [79] J. Ni, X. Zhang and J. M. Scurlock, "Synthesis and Analysis of Biomass and Net Primary Productivity in Chinese Forests". *Ann. for. Sci.* 58(4), pp. 351-384. 2001.

- [80] W. P. Elliott, "The Growth of the Atmospheric Internal Boundary Layer". Transactions, American Geophysical Union 39pp. 1048-1054. 1958.
- [81] A. K. Lo, "On the Determination of Zero-Plane Displacement and Roughness Length for Flow over Forest Canopies", Boundary-Layer Meteorology, vol. 51.3, pp. 255-268., (1990).
- [82] S. J. Tajchman, "Comments on Measuring Turbulent Exchange Within and Above Forest Canopy", Bulletin of the American Meteorological Society, vol. 62, pp. 1550-1550, 1981.
- [83] J. Wiernga, "Representative Roughness Parameters for Homogeneous Terrain". Bound. - Layer Meteorol. 63(4), pp. 323-363. 1993.

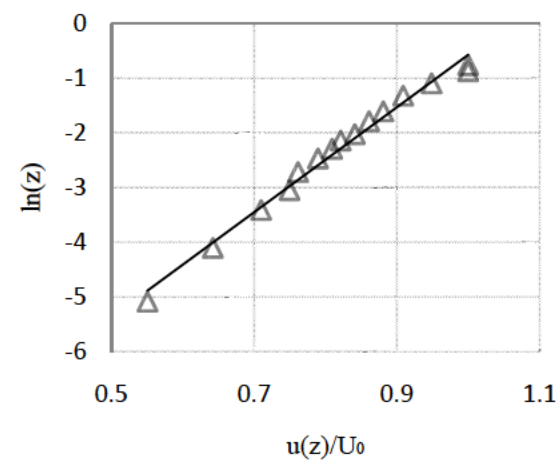
### Appendix A: Vertical wind profile logarithmic fit

An Excel spreadsheet has been done, and is shown in Table A.1, and used to calculate the wind profile parameters in order to identify what terrain it fits best. A common method is the logarithmic wind profile law.

$$U_0 = 7.44 \text{ m/s}$$

Table A.1: Upstream profile log law fit.

z [m]	u(z)/U <sub>0</sub>	u(z) [m/s]	ln(z)				
0	0	0	0				
0.006198	0.550442	4.095288	-5.08347				
0.016529	0.642035	4.77674	-4.10264				
0.033058	0.709735	5.280428	-3.40949				
0.047521	0.749558	5.576712	-3.04659				
0.066116	0.761504	5.66559	-2.71635				
0.084711	0.789381	5.872995	-2.46851				
0.10124	0.809292	6.021132	-2.29026				
0.117769	0.821239	6.110018	-2.13903				
0.132231	0.84115	6.258156	-2.0232				
0.167355	0.861062	6.406301	-1.78764				
0.200413	0.880973	6.554439	-1.60738				
0.266529	0.90885	6.761844	-1.32227				
0.334711	0.948673	7.058127	-1.09449				
0.417355	1	7.44	-0.87382				
0.466942	1	7.44	-0.76155				
ln(z) <sub>0</sub> =	-10.281		n=	0.24		z <sub>ref</sub> =	0.5
z <sub>0</sub> =	3.42E-05	m	u*= m/s	0.305	m/s	α=	0.1043



The values of interest are  $z_0$ ,  $u^*$  and  $\alpha$ . Using this fit it can be stated that the measured profile is equivalent to a water profile.

## Appendix B: Time series equivalence

The geometric scaling is 1:500, thus

$$\frac{L_{wt}}{L_{fs}} = \frac{1}{500} \quad (\text{B.1})$$

and

$$\frac{V_{wt} \cdot T_{wt}}{L_{wt}} = \frac{V_{fs} \cdot T_{fs}}{L_{fs}} \quad (\text{B.2})$$

If we use Eq. B.1 and replace in Eq. B.2:

$$\frac{V_{wt} \cdot T_{wt}}{L_{wt}} = \frac{V_{fs} \cdot T_{fs}}{L_{wt} \cdot 500} \quad (\text{B.3})$$

thus:

$$\frac{T_{fs}}{T_{wt}} = \frac{V_{wt} \cdot 500}{V_{fs}} \quad (\text{B.4})$$

Taking into account the sampling frequency for each instrument, we have:

$$f_{fs} = 1\text{Hz}; f_{wt} = 312.5\text{Hz} \quad (\text{B.5})$$

Thus, the relationship between instrument frequencies will be:

$$f_{fs} = \frac{f_{wt}}{500 \cdot \frac{V_{wt}}{V_{fs}}} \quad (\text{B.6})$$

and

$$\frac{V_{wt}}{V_{fs}} = \frac{312.5\text{Hz}}{500 \cdot 1\text{Hz}} = 0.625 \quad (\text{B.7})$$



Returning to Eq. (B.4)

$$\frac{T_{fs}}{T_{wt}} = \frac{V_{wt} \cdot 500}{V_{fs}} = 0.625 \cdot 500; T_{fs} = 312.5 \cdot T_{wt} \quad (\text{B.8})$$

Therefore, the equivalent length of time in full scale for 20 s in the wind tunnel will be:

$$T_{fs} = 312.5 \cdot 20 = 6250s \quad (\text{B.9})$$

this equals to 1.73 hours, or 1 hour and 44 minutes.

## Appendix C: Comparison results

In this appendix the rest of the wind tunnel comparison graphs are presented. They are divided by the direction examined. Table C.1 sums up the sets analyzed. The figures presented in this section show the averaged results over the considered sets, as well as centralized plots used to present the data variation over the whole year of available data.

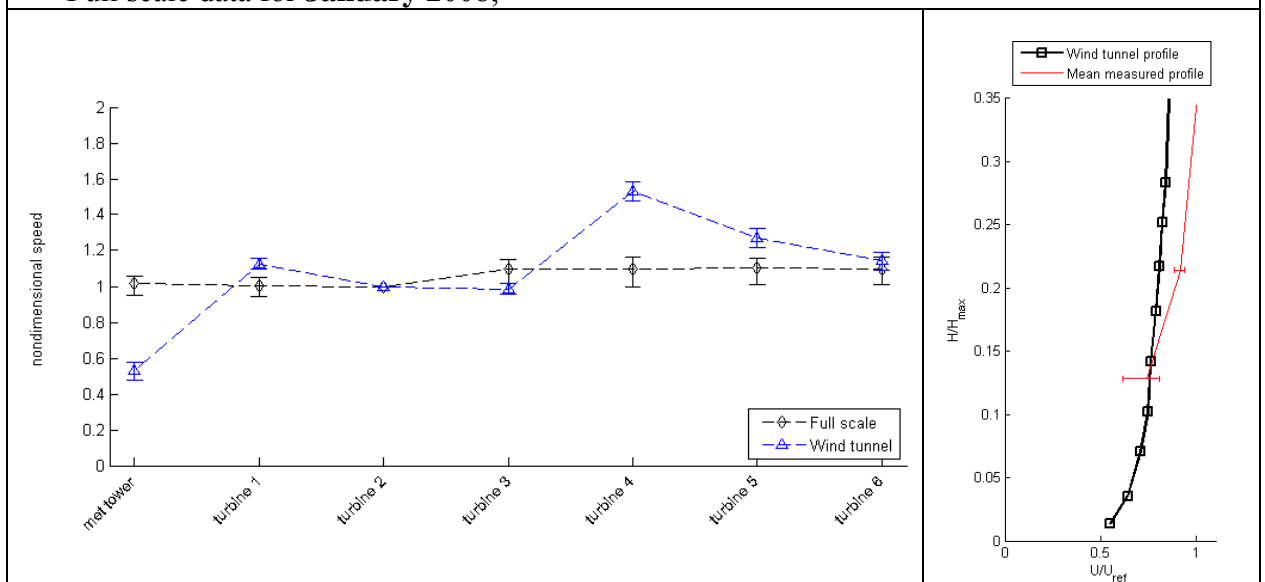
Table C.1: Comparison data sets divided per month and wind direction.

month	direction [°]		
	315	157.5	202.5
January	3	5	5
March	6	1	5
September	2	3	4
October	2	18	3
December	15	2	26

### 1. “No forest” test case

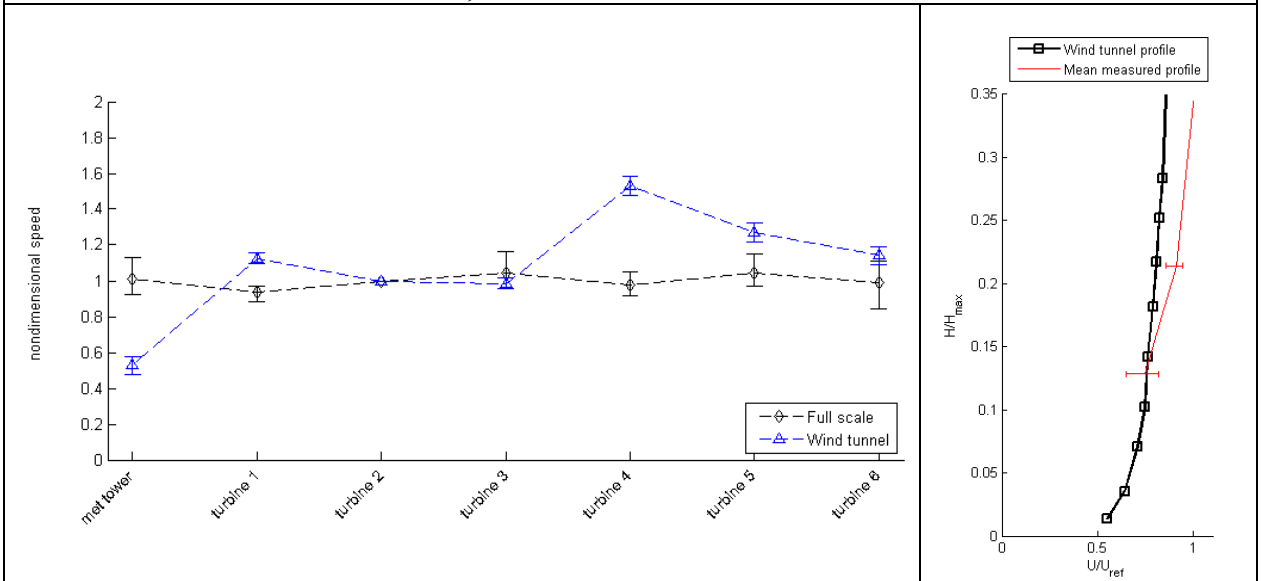
Wind tunnel result set description:

- Direction **315°**;
- “No forest” case;
- Full scale data for **January 2008**;



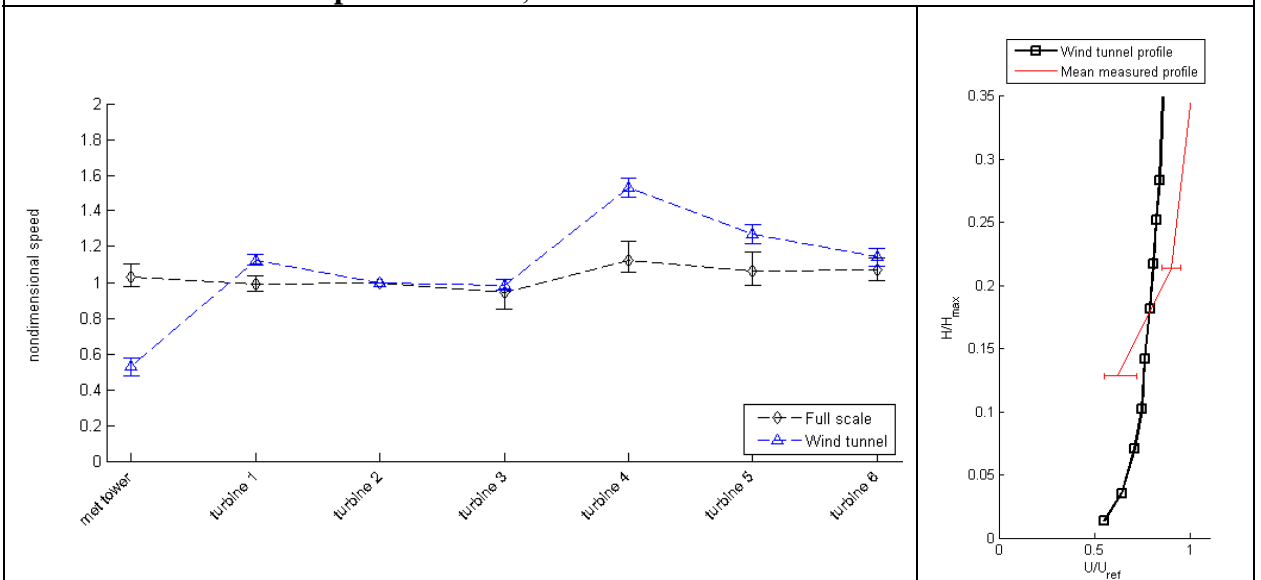
Wind tunnel result set description:

- Direction **315°**;
- “No forest” case;
- Full scale data for **March 2008**;



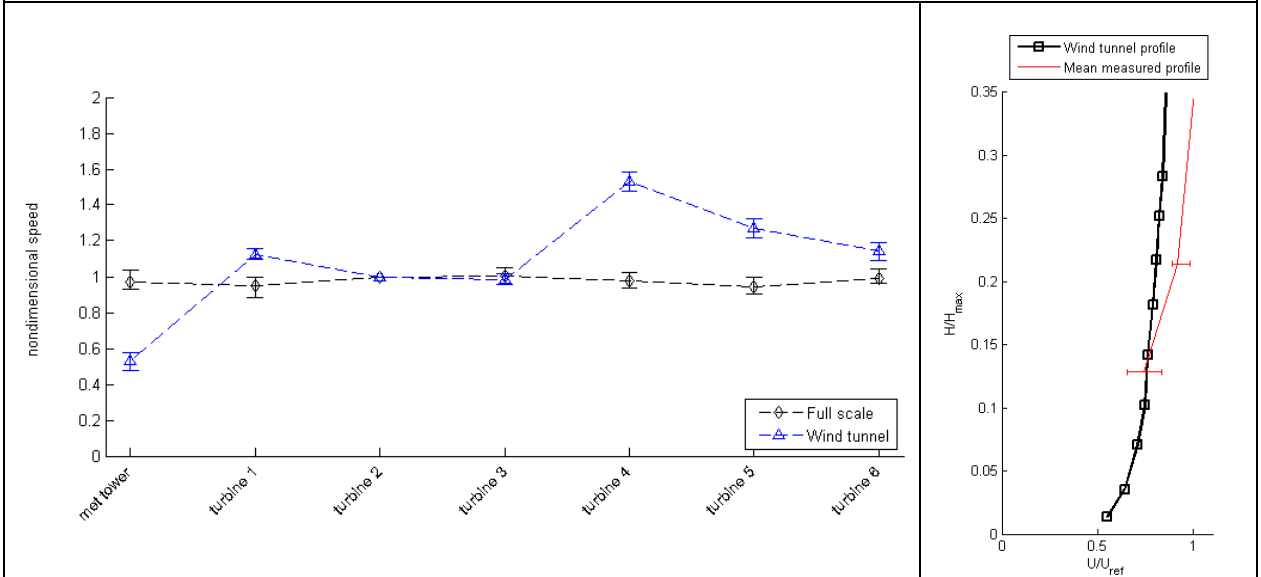
Wind tunnel result set description:

- Direction **315°**;
- “No forest” case;
- Full scale data for **September 2008**;



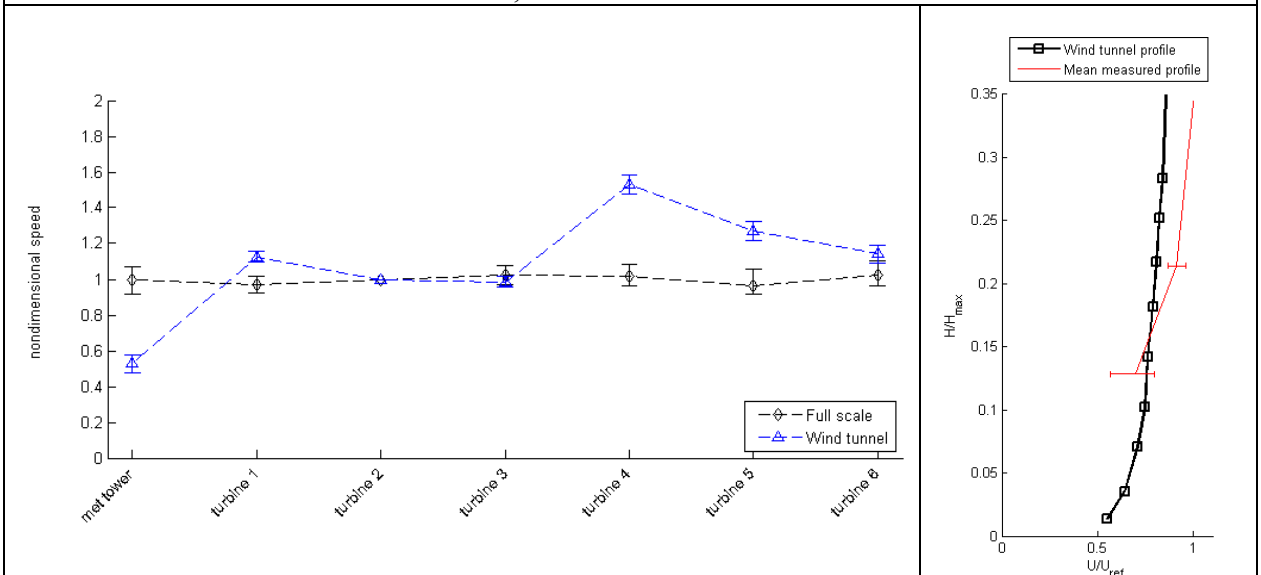
Wind tunnel result set description:

- Direction **315°**;
- “No forest” case;
- Full scale data for **October 2008**;



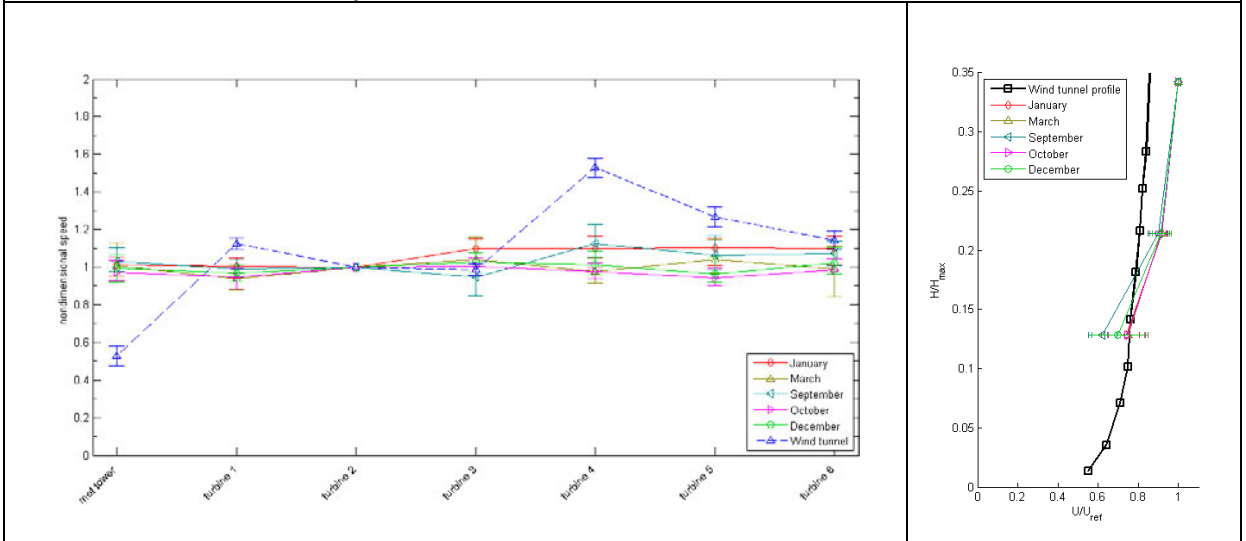
Wind tunnel result set description:

- Direction **315°**;
- “No forest” case;
- Full scale data for **December 2008**;



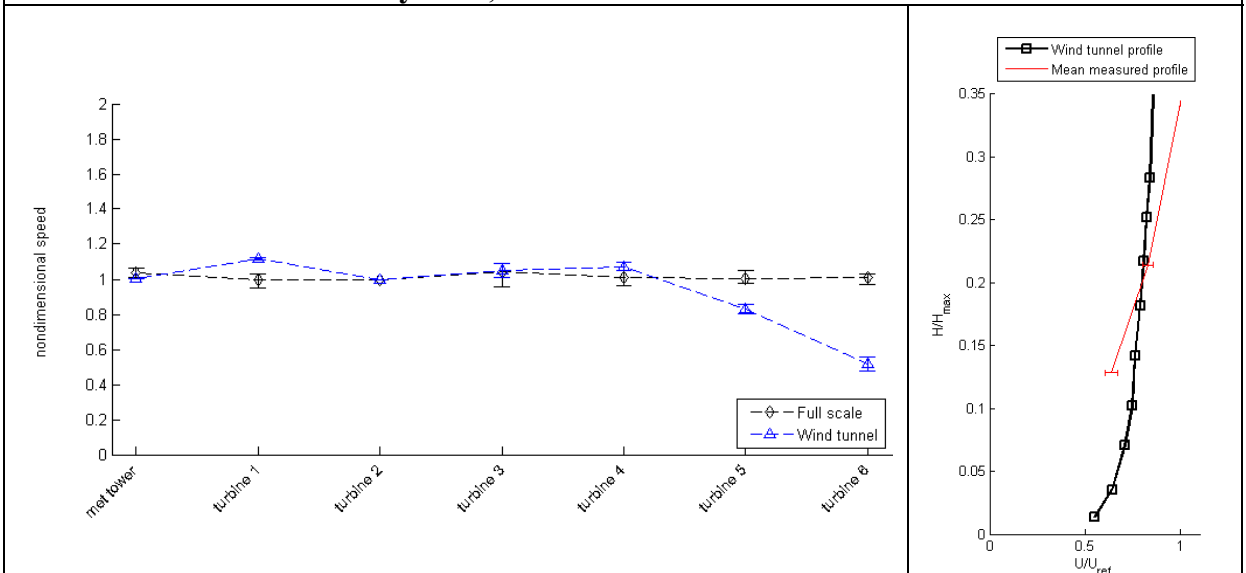
**Centralized** wind tunnel result set description:

- Direction **315°**;
- “No forest” case;
- Full scale data for **the year 2008**;



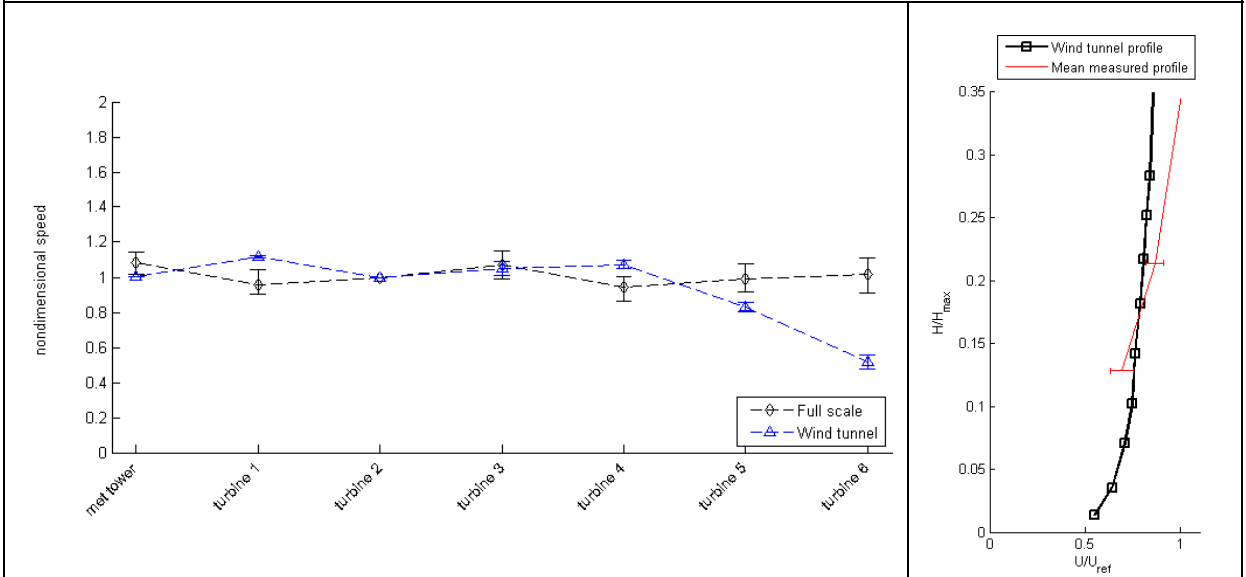
Wind tunnel result set description:

- Direction **202.5°**;
- “No forest” case;
- Full scale data for **January 2008**;



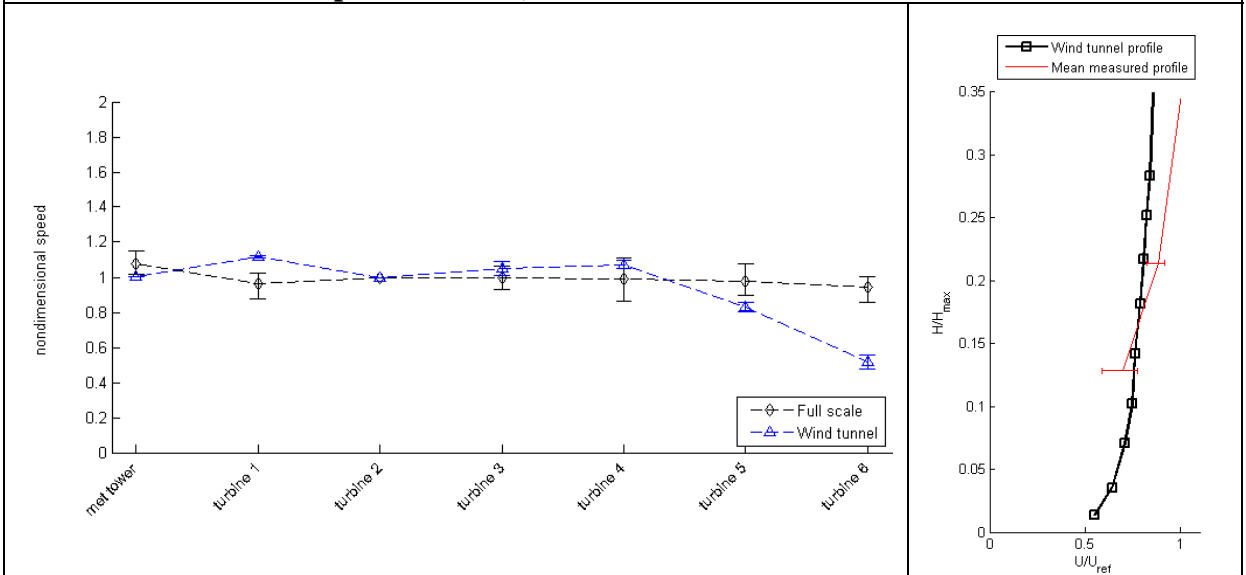
Wind tunnel result set description:

- Direction **202.5°**;
- “No forest” case;
- Full scale data for **March 2008**;



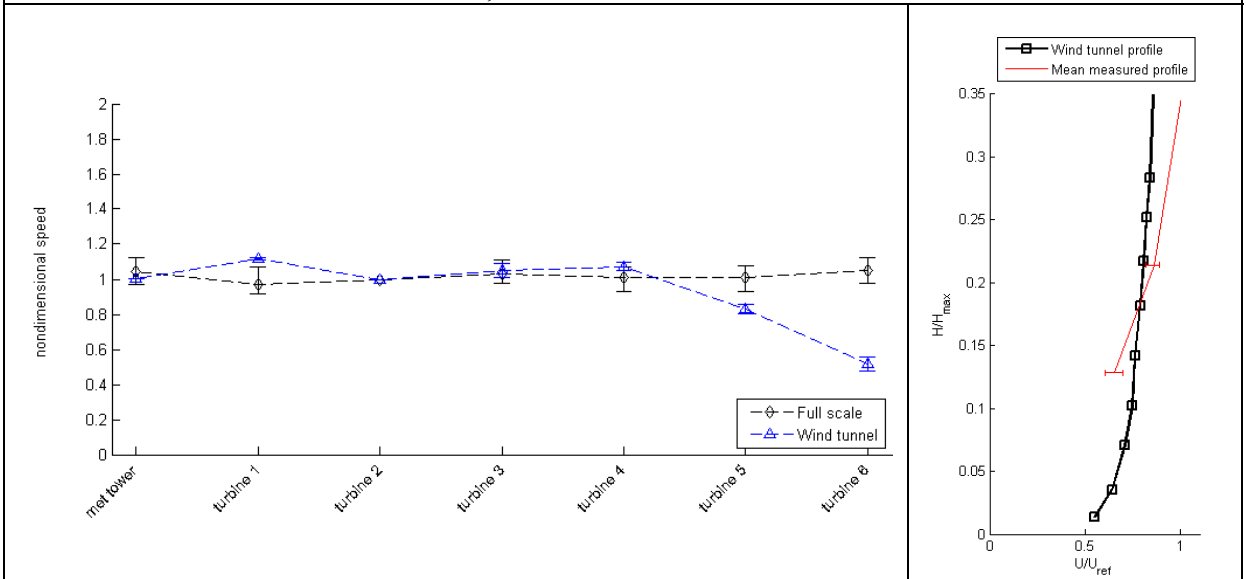
Wind tunnel result set description:

- Direction **202.5°**;
- “No forest” case;
- Full scale data for **September 2008**;



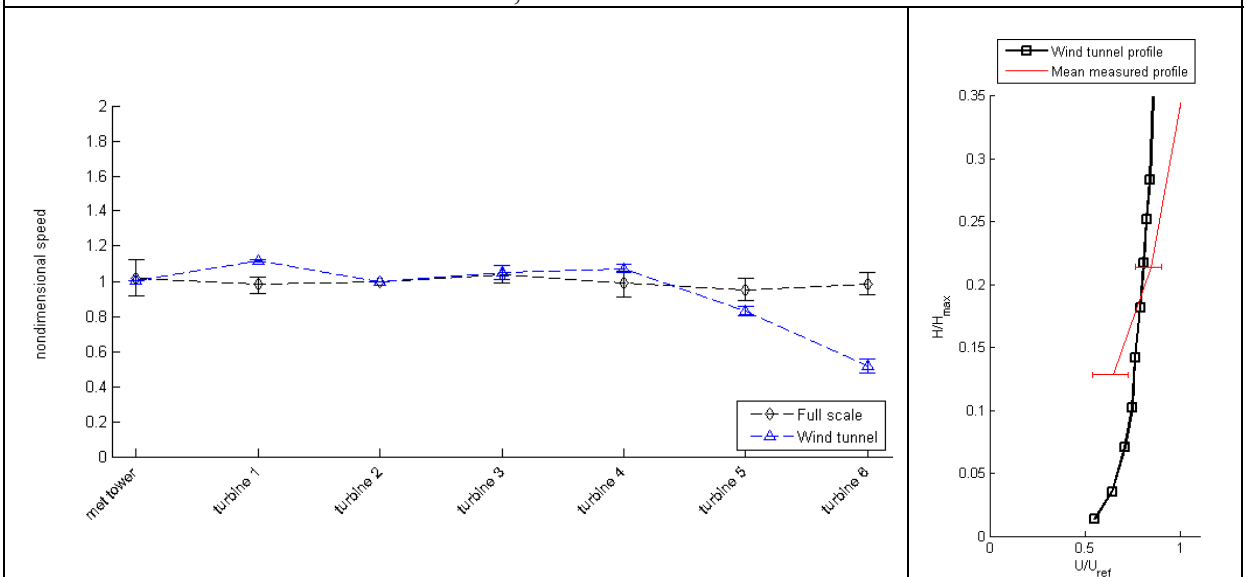
Wind tunnel result set description:

- Direction **202.5°**;
- “No forest” case;
- Full scale data for **October 2008**;



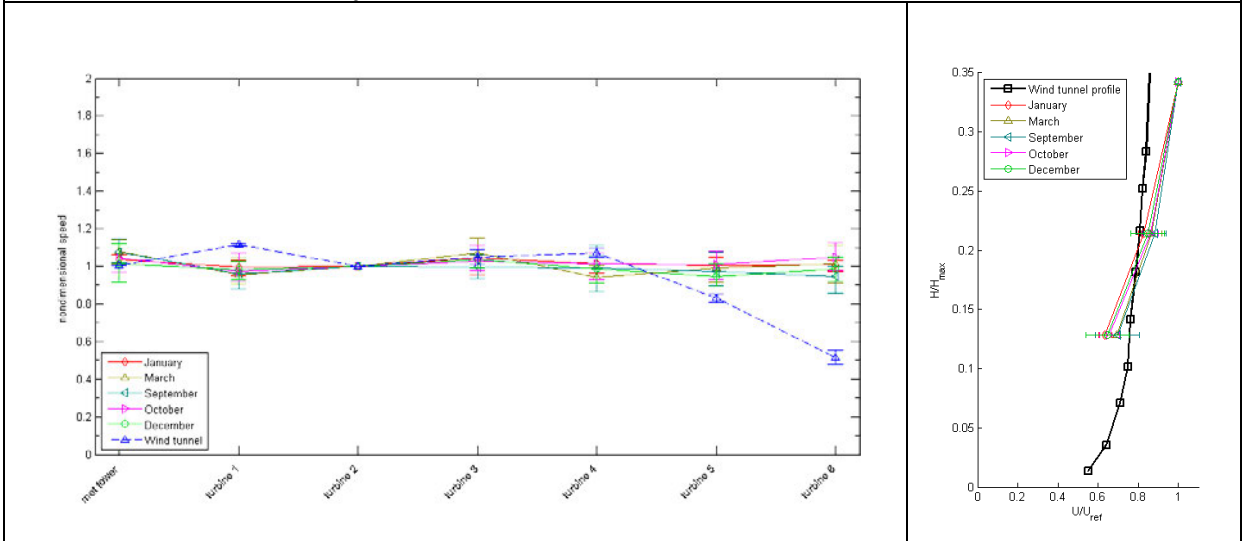
Wind tunnel result set description:

- Direction **202.5°**;
- “No forest” case;
- Full scale data for **December 2008**;



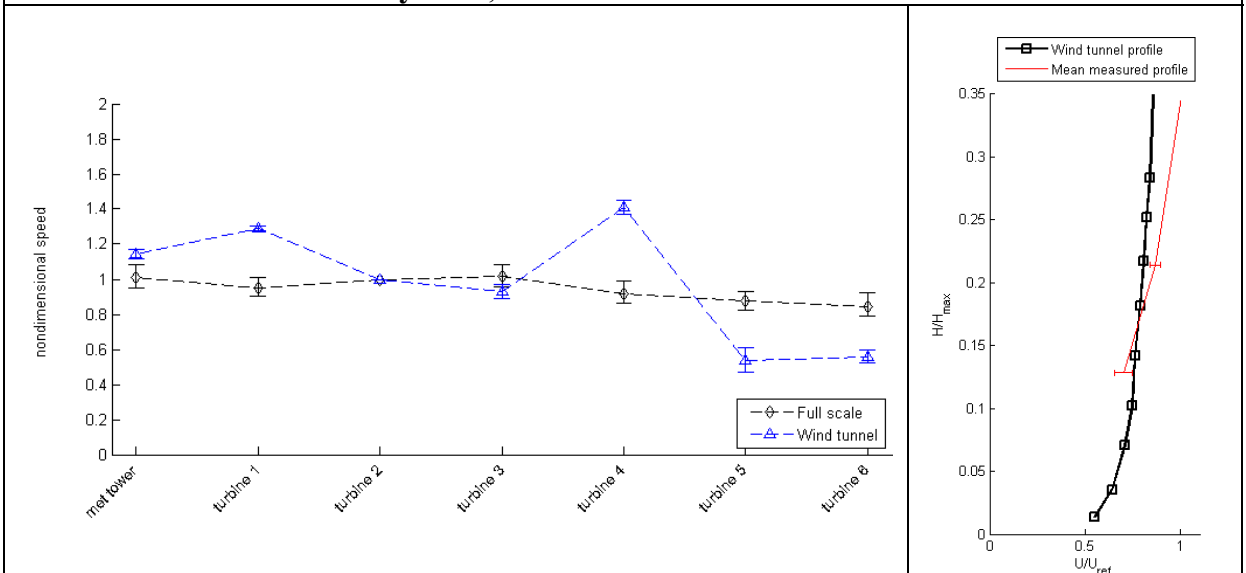
**Centralized** wind tunnel result set description:

- Direction **202.5°**;
- “No forest” case;
- Full scale data for **the year 2008**;



Wind tunnel result set description:

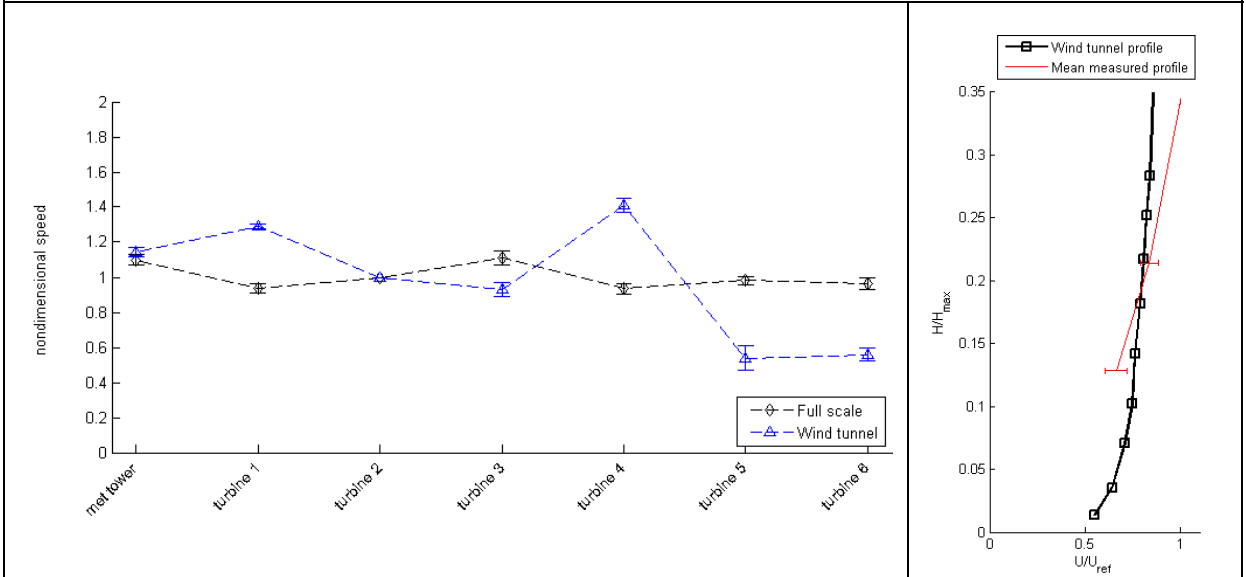
- Direction **157.5°**;
- “No forest” case;
- Full scale data for **January 2008**;





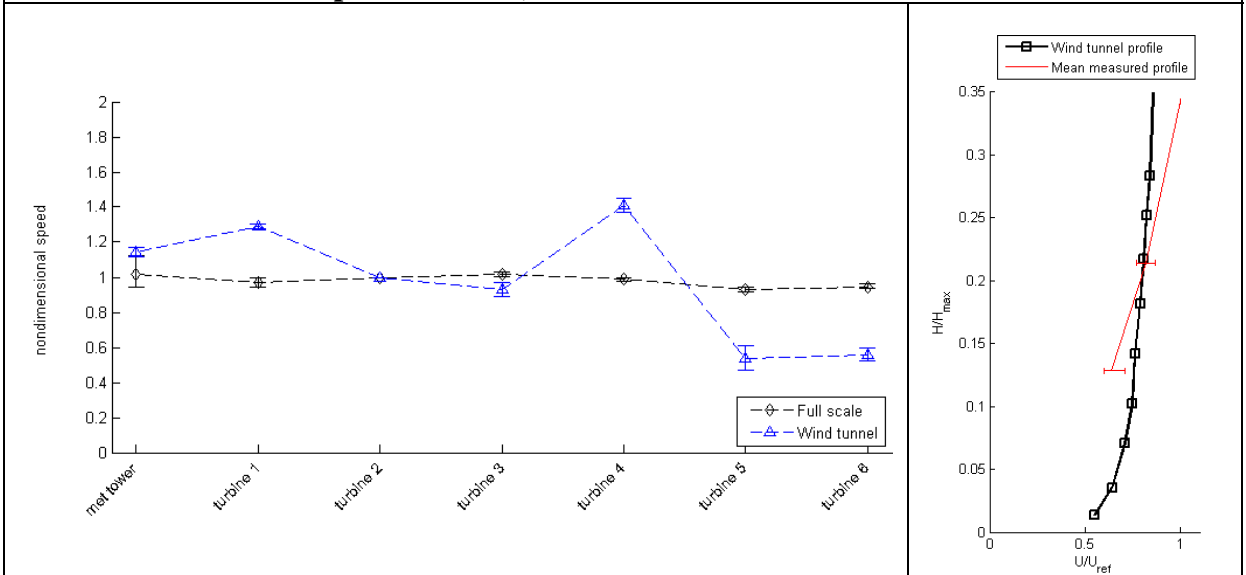
Wind tunnel result set description:

- Direction **157.5°**;
- “No forest” case;
- Full scale data for **March 2008**;



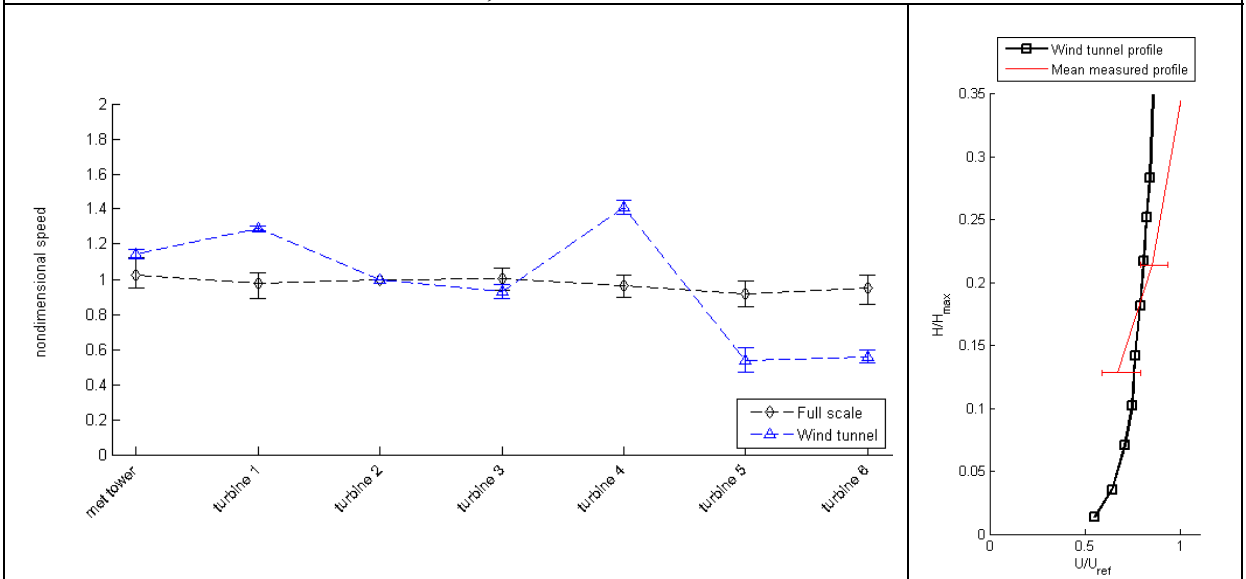
Wind tunnel result set description:

- Direction **157.5°**;
- “No forest” case;
- Full scale data for **September 2008**;



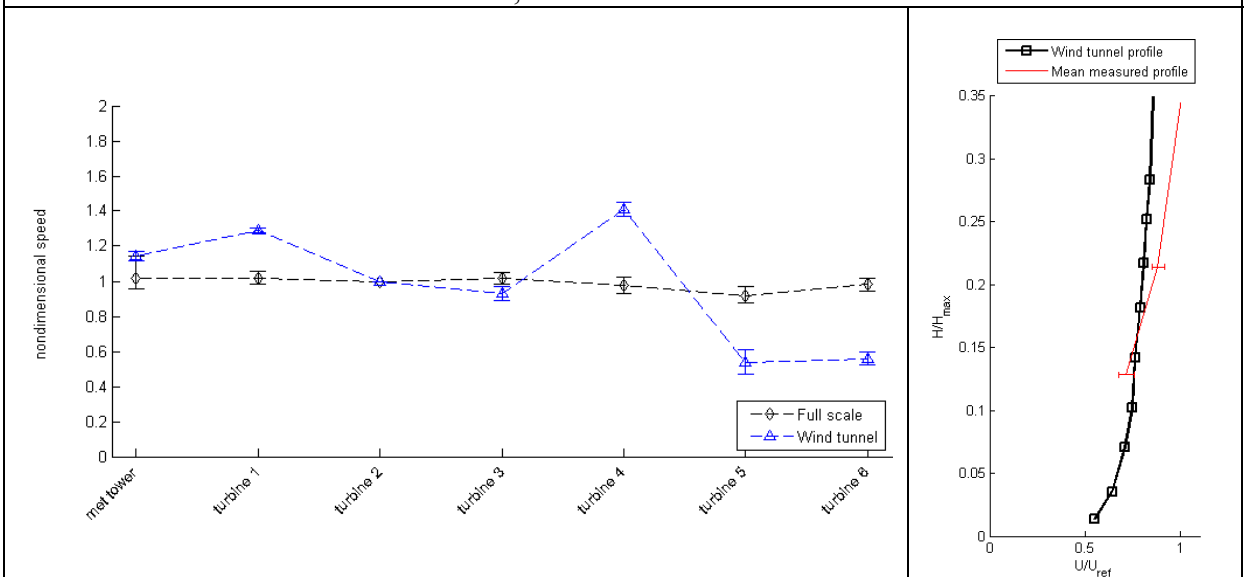
Wind tunnel result set description:

- Direction **157.5°**;
- “No forest” case;
- Full scale data for **October 2008**;



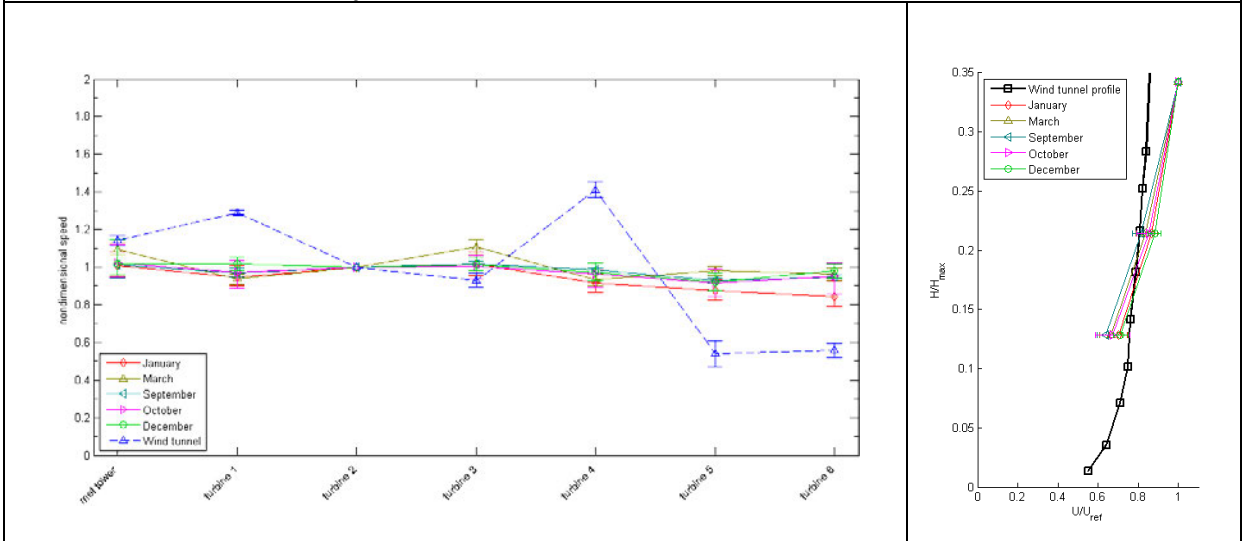
Wind tunnel result set description:

- Direction **157.5°**;
- “No forest” case;
- Full scale data for **December 2008**;



**Centralized** wind tunnel result set description:

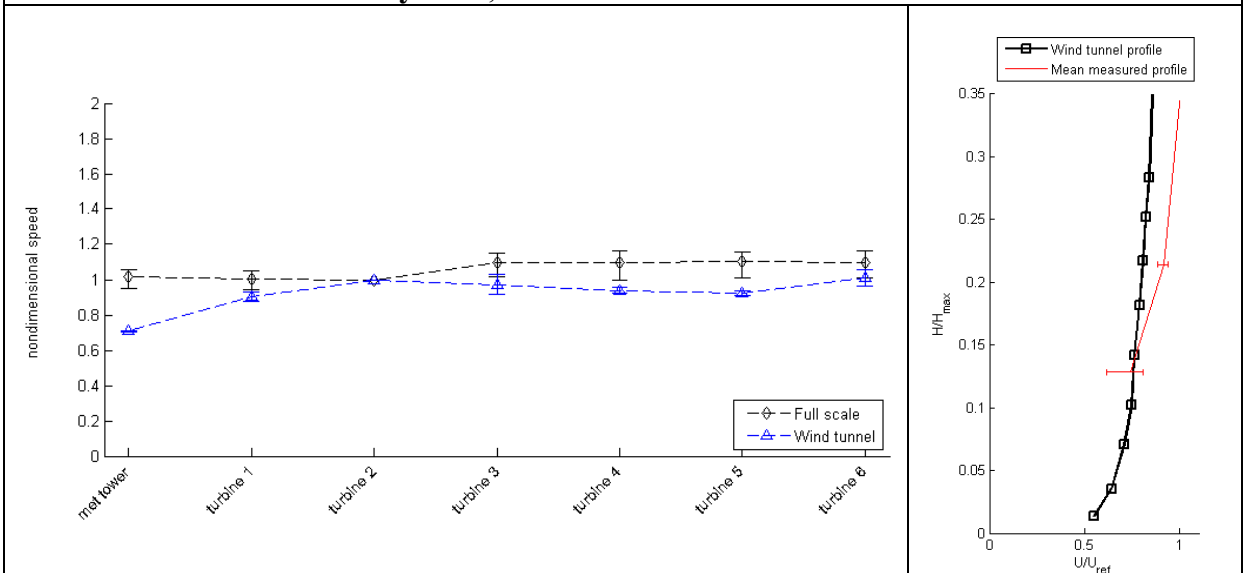
- Direction **157.5°**;
- “No forest” case;
- Full scale data for **the year 2008**;



**2. “90% canopy model” test case**

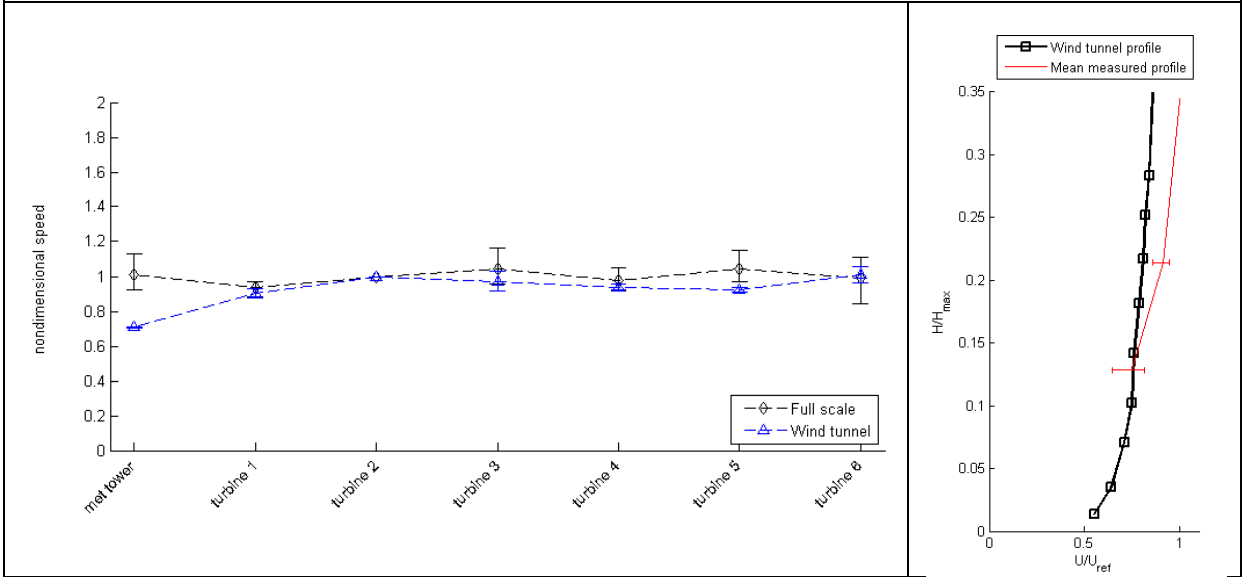
Wind tunnel result set description:

- Direction **315°**;
- “90% canopy model” case;
- Full scale data for **January 2008**;



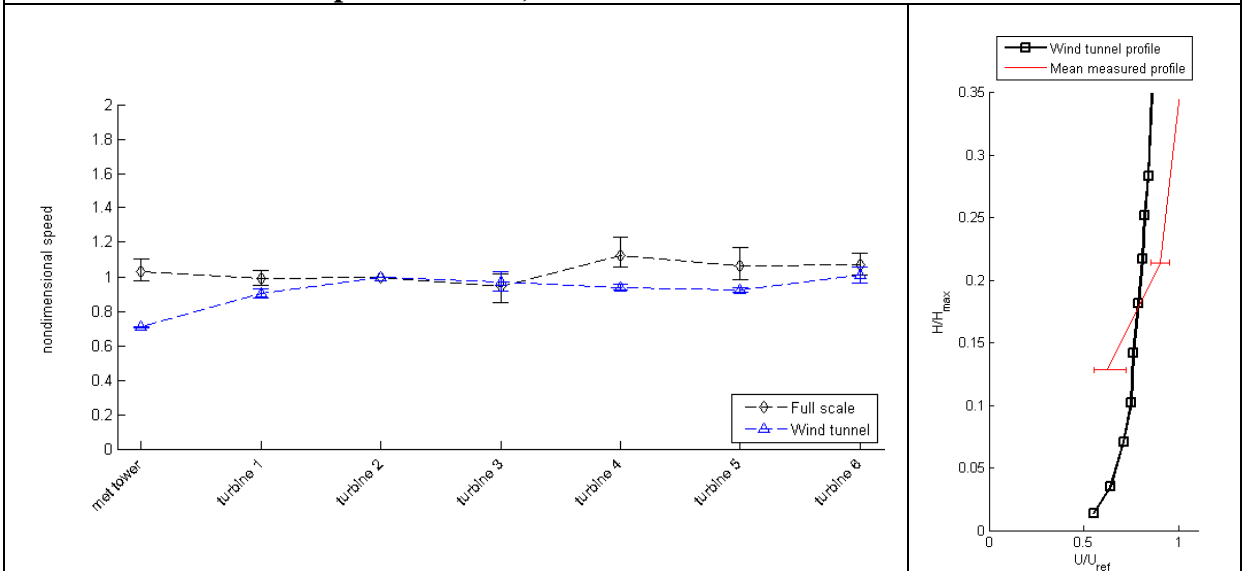
Wind tunnel result set description:

- Direction **315°**;
- “90% canopy model” case;
- Full scale data for **March 2008**;



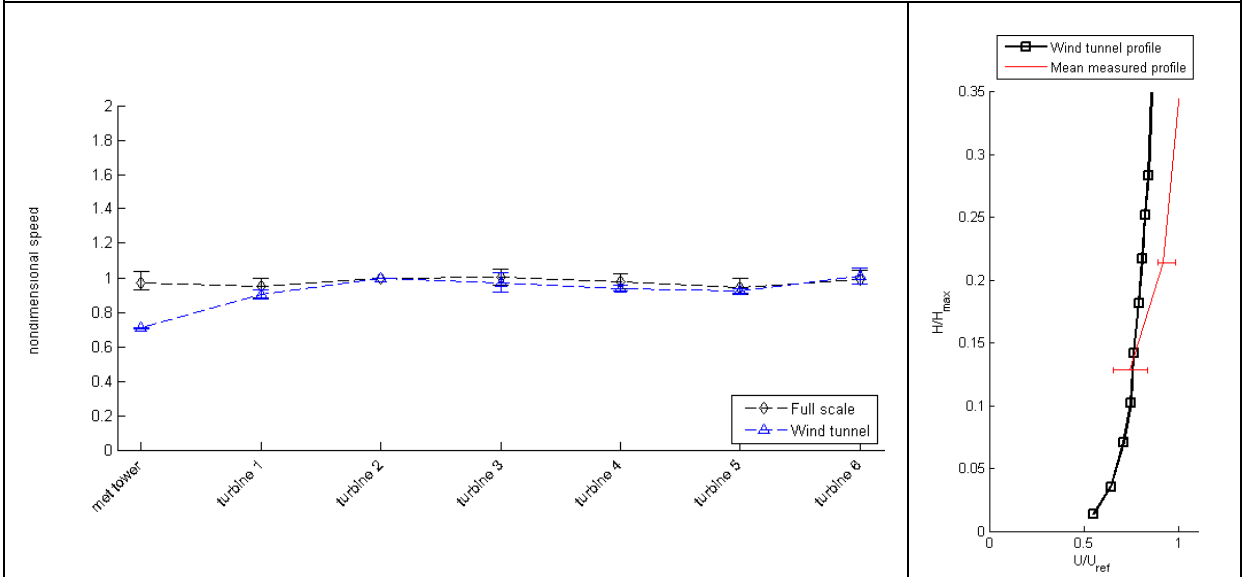
Wind tunnel result set description:

- Direction **315°**;
- “90% canopy model” case;
- Full scale data for **September 2008**;



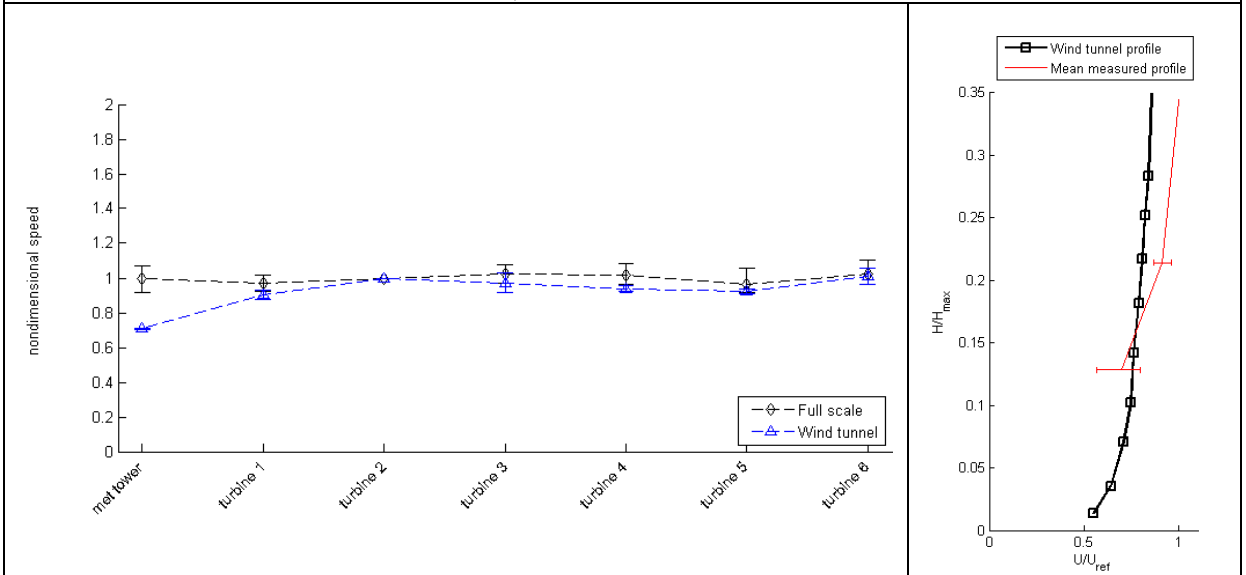
Wind tunnel result set description:

- Direction **315°**;
- “90% canopy model” case;
- Full scale data for **October 2008**;



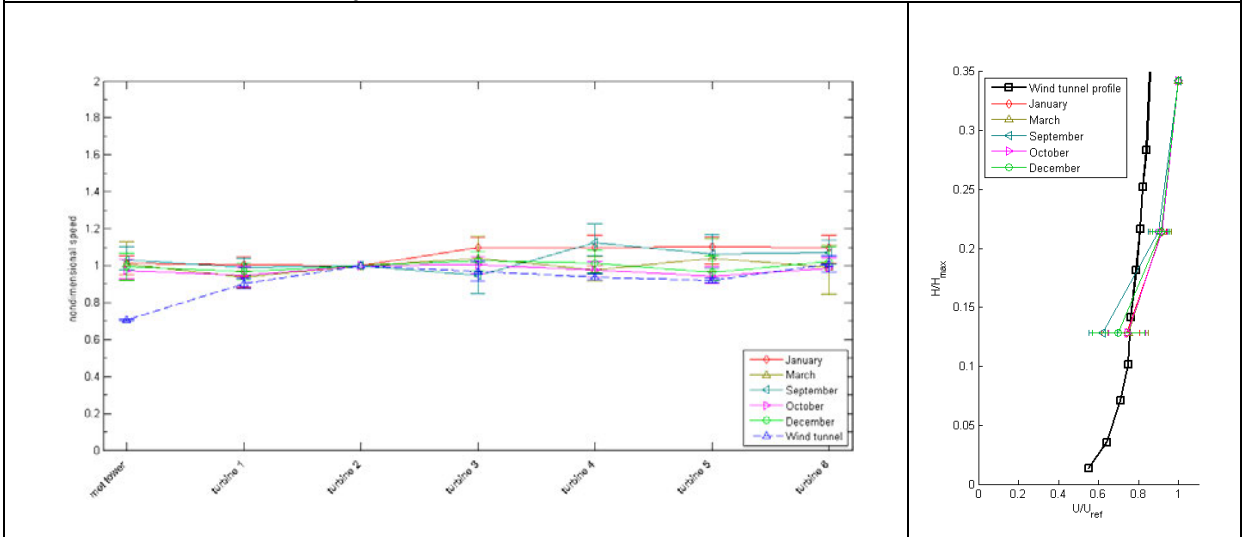
Wind tunnel result set description:

- Direction **315°**;
- “90% canopy model” case;
- Full scale data for **December 2008**;



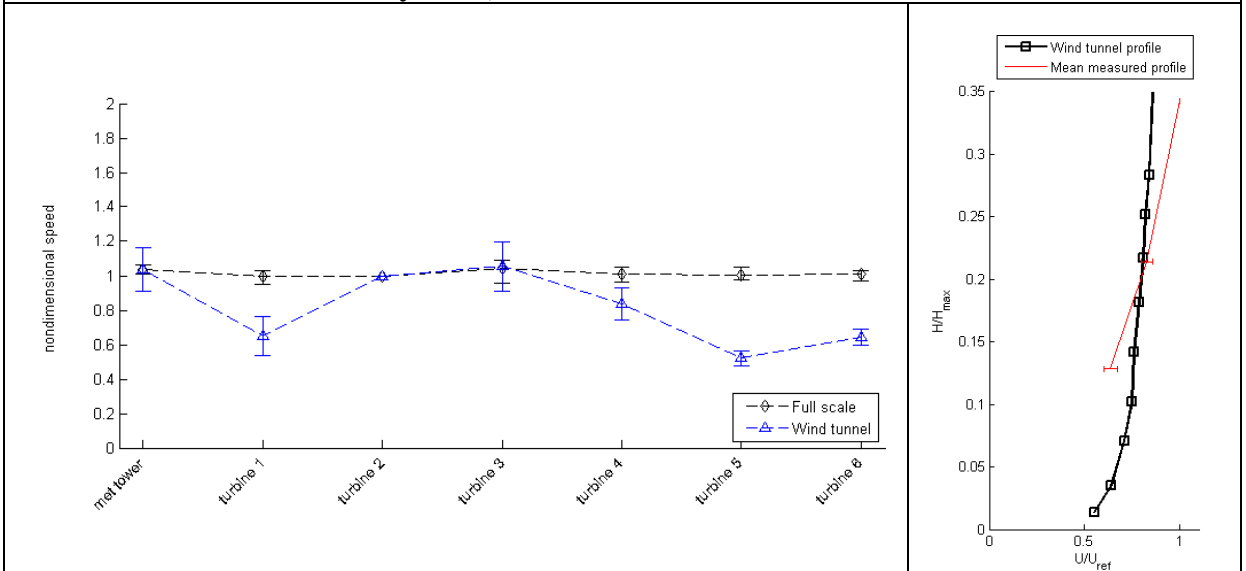
**Centralized** wind tunnel result set description:

- Direction **315°**;
- “90% canopy model” case;
- Full scale data for **the year 2008**;



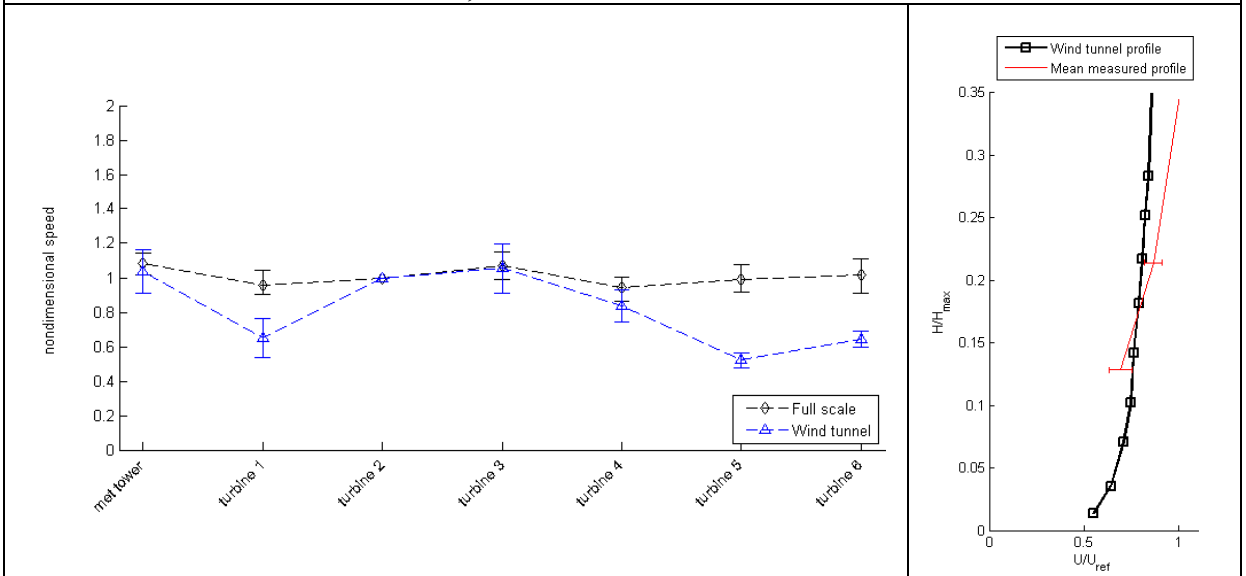
Wind tunnel result set description:

- Direction **202.5°**;
- “90% canopy model” case;
- Full scale data for **January 2008**;



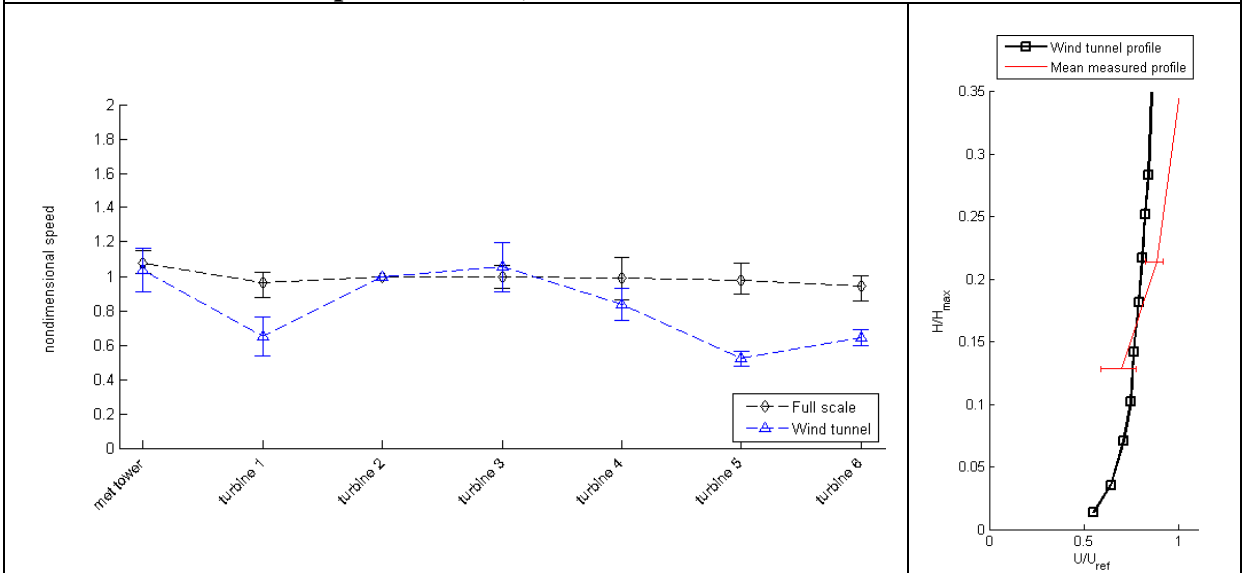
Wind tunnel result set description:

- Direction **202.5°**;
- “90% canopy model” case;
- Full scale data for **March 2008**;



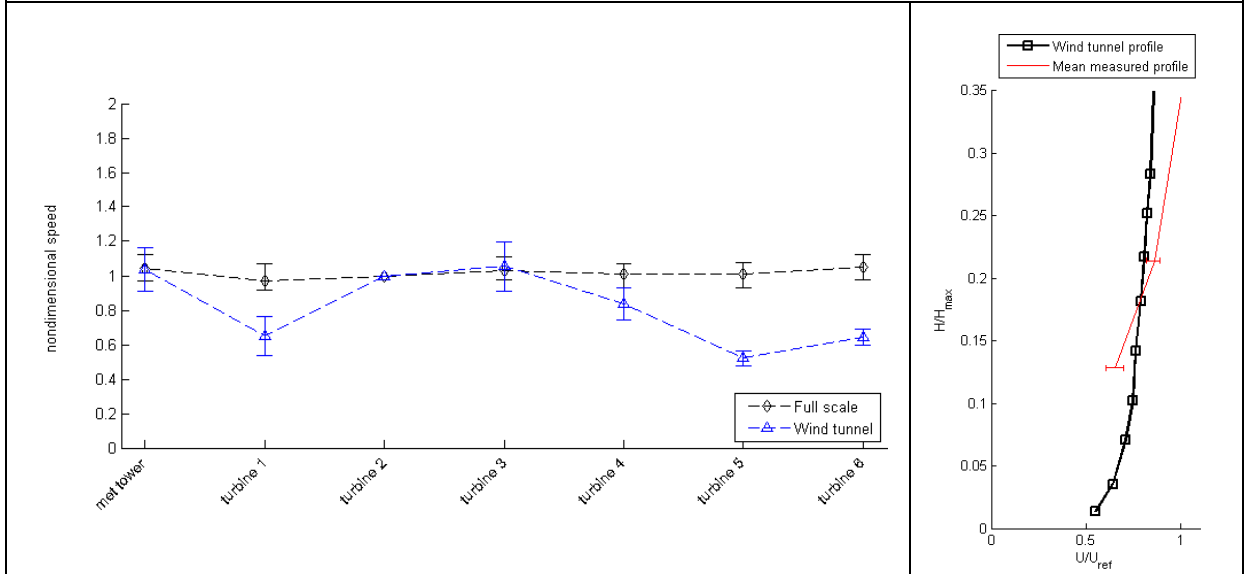
Wind tunnel result set description:

- Direction **202.5°**;
- “90% canopy model” case;
- Full scale data for **September 2008**;



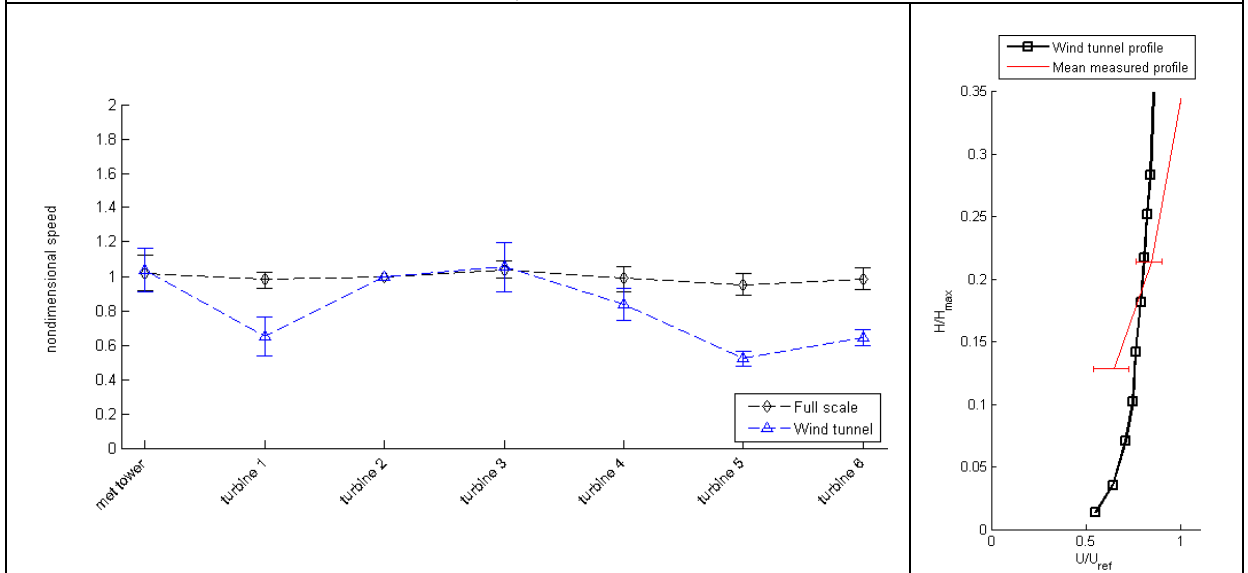
Wind tunnel result set description:

- Direction **202.5°**;
- “90% canopy model” case;
- Full scale data for **October 2008**;



Wind tunnel result set description:

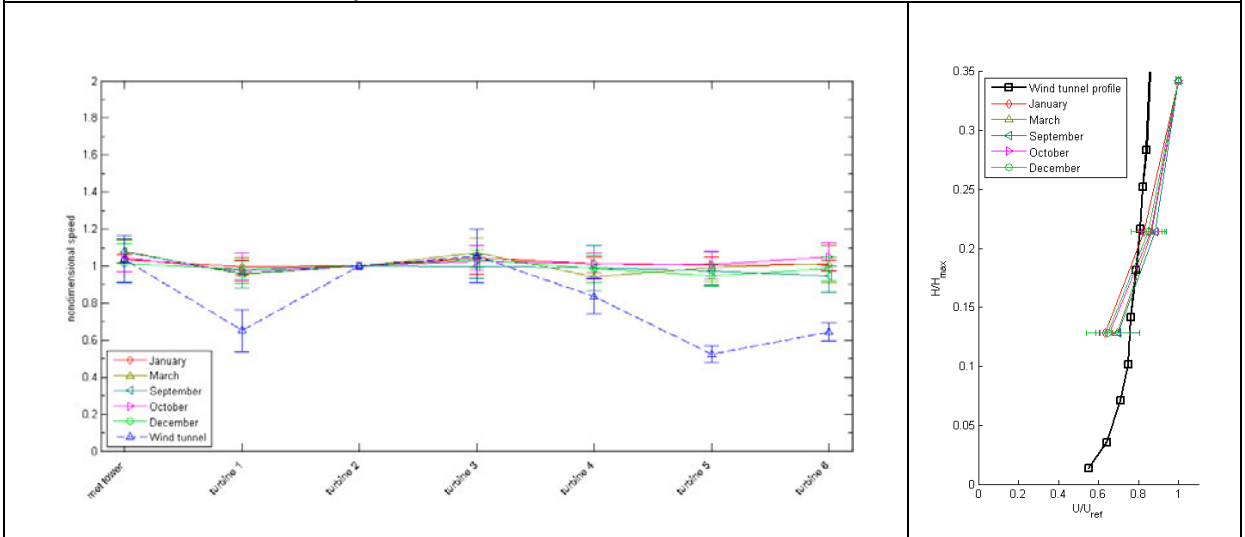
- Direction **202.5°**;
- “90% canopy model” case;
- Full scale data for **December 2008**;





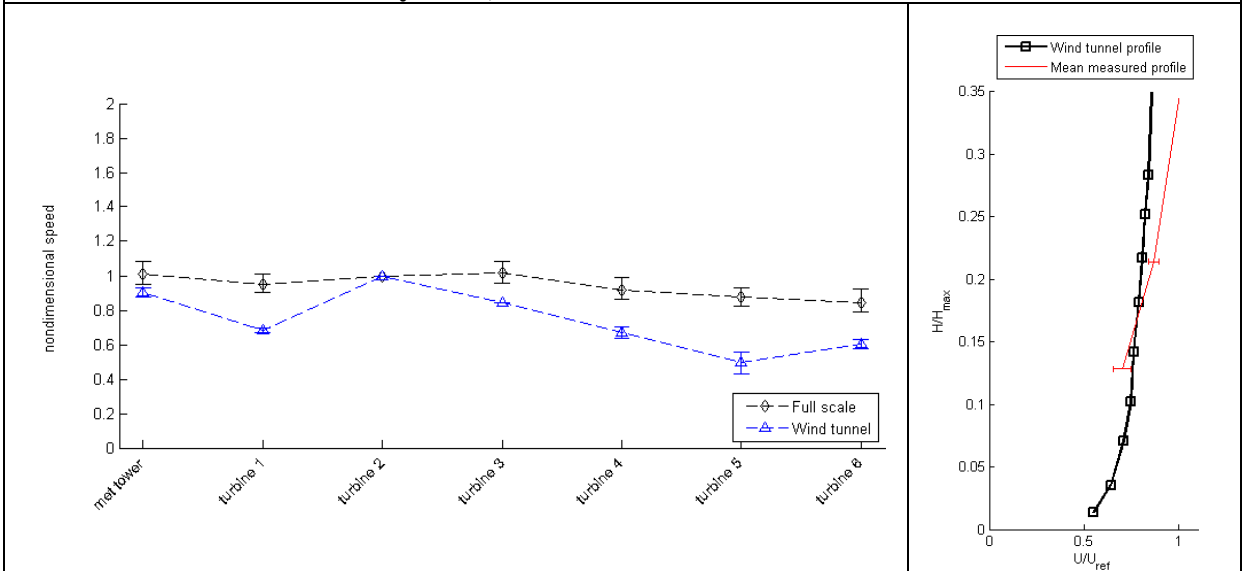
**Centralized** wind tunnel result set description:

- Direction **202.5°**;
- “90% canopy model” case;
- Full scale data for **the year 2008**;



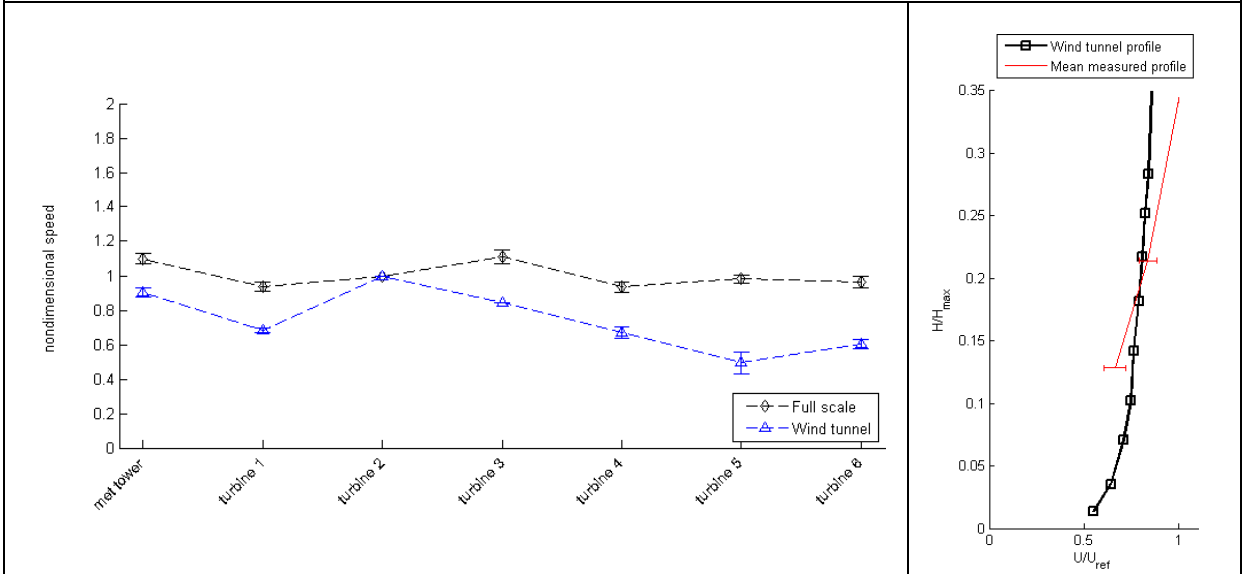
Wind tunnel result set description:

- Direction **157.5°**;
- “90% canopy model” case;
- Full scale data for **January 2008**;



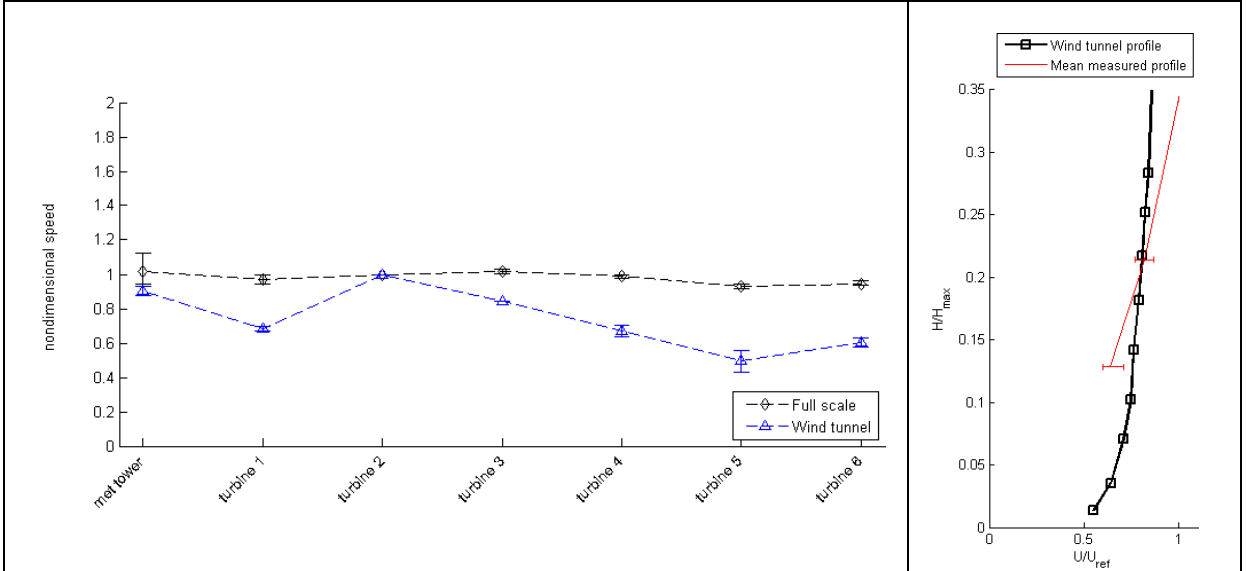
Wind tunnel result set description:

- Direction **157.5°**;
- “90% canopy model” case;
- Full scale data for **March 2008**;



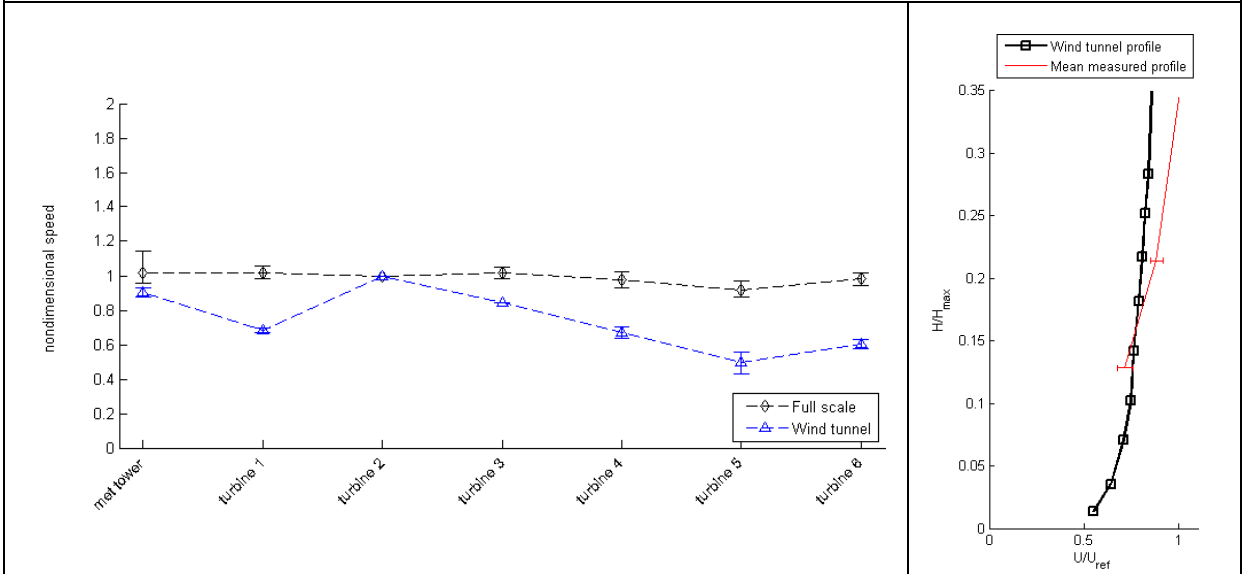
Wind tunnel result set description:

- Direction **157.5°**;
- “90% canopy model” case;
- Full scale data for **September 2008**;



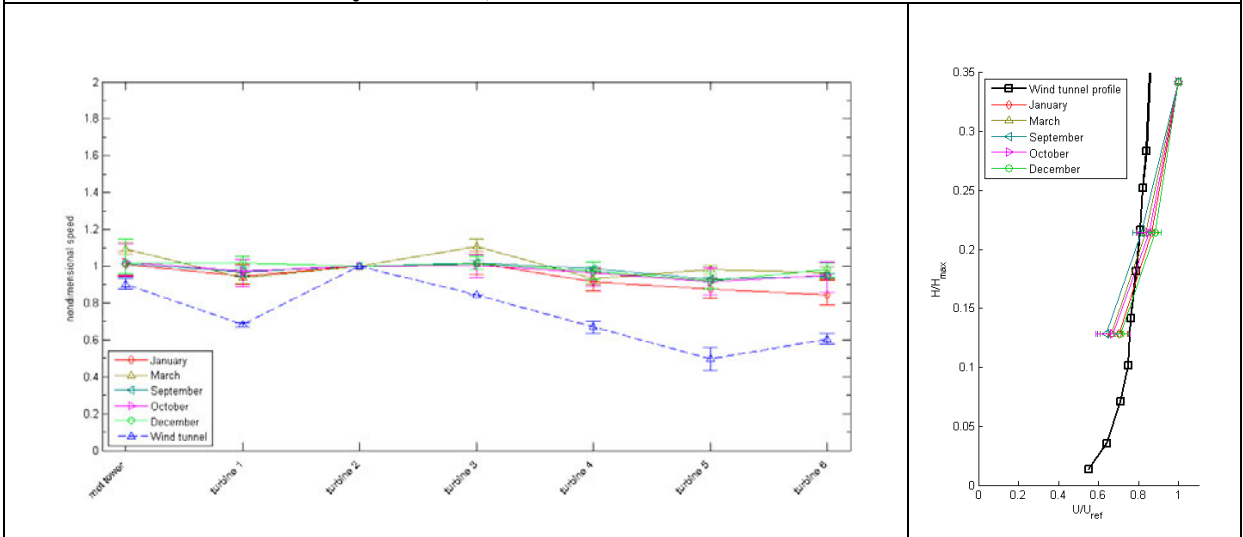
Wind tunnel result set description:

- Direction **157.5°**;
- “90% canopy model” case;
- Full scale data for **December 2008**;



Centralized wind tunnel result set description:

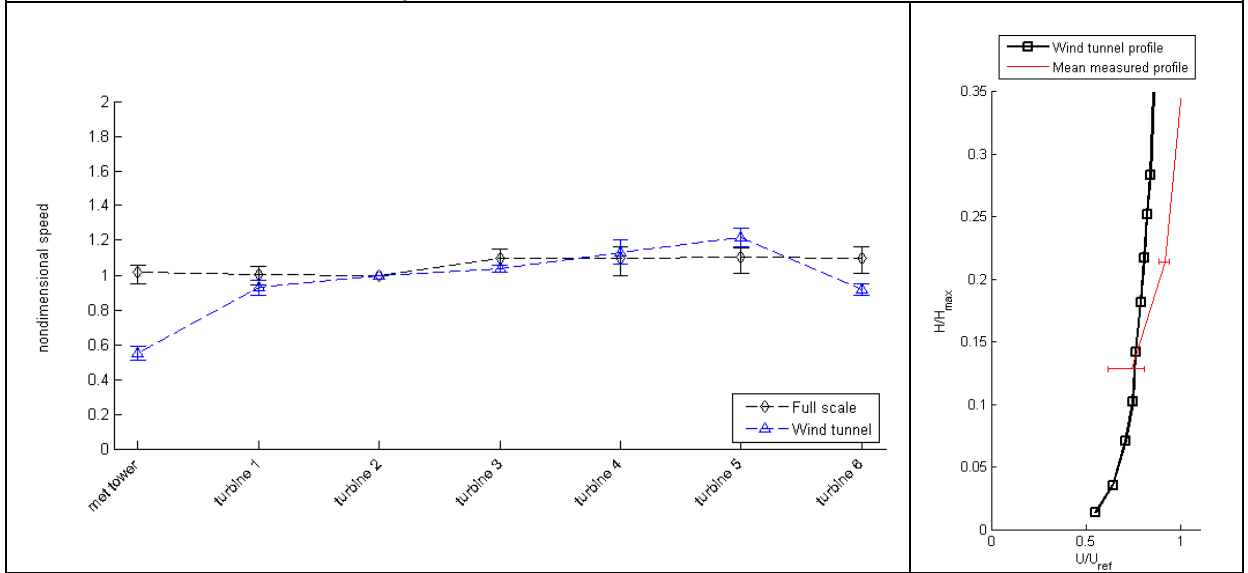
- Direction **157.5°**;
- “90% canopy model” case;
- Full scale data for **the year 2008**;



### 3. “48% canopy model” test case

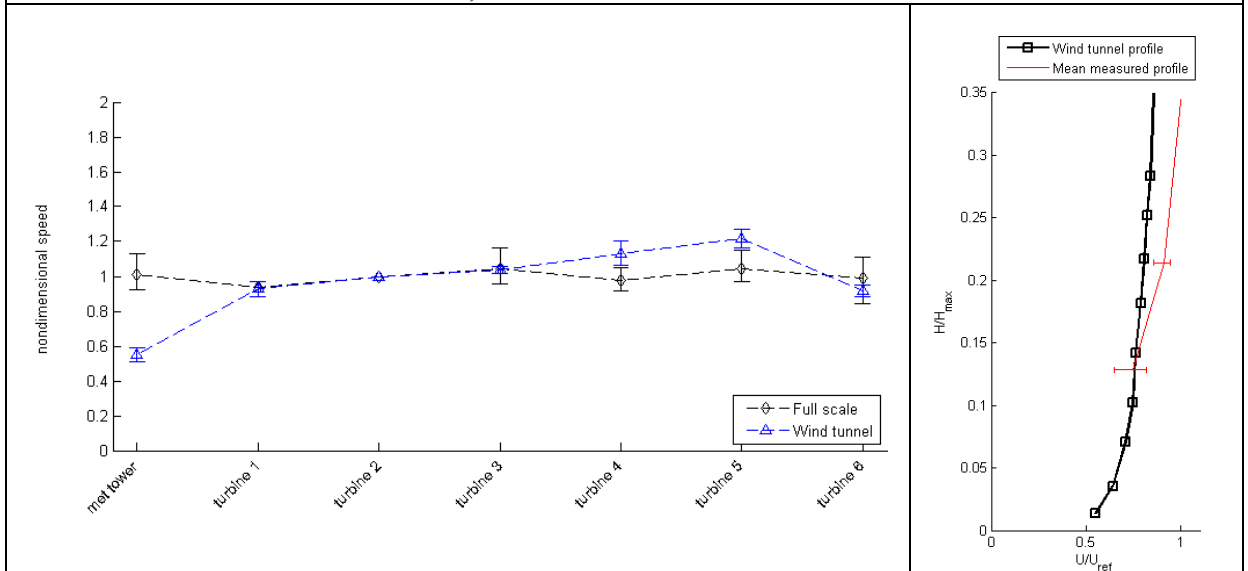
Wind tunnel result set description:

- Direction **315°**;
- “48% canopy model” case;
- Full scale data for **January 2008**;



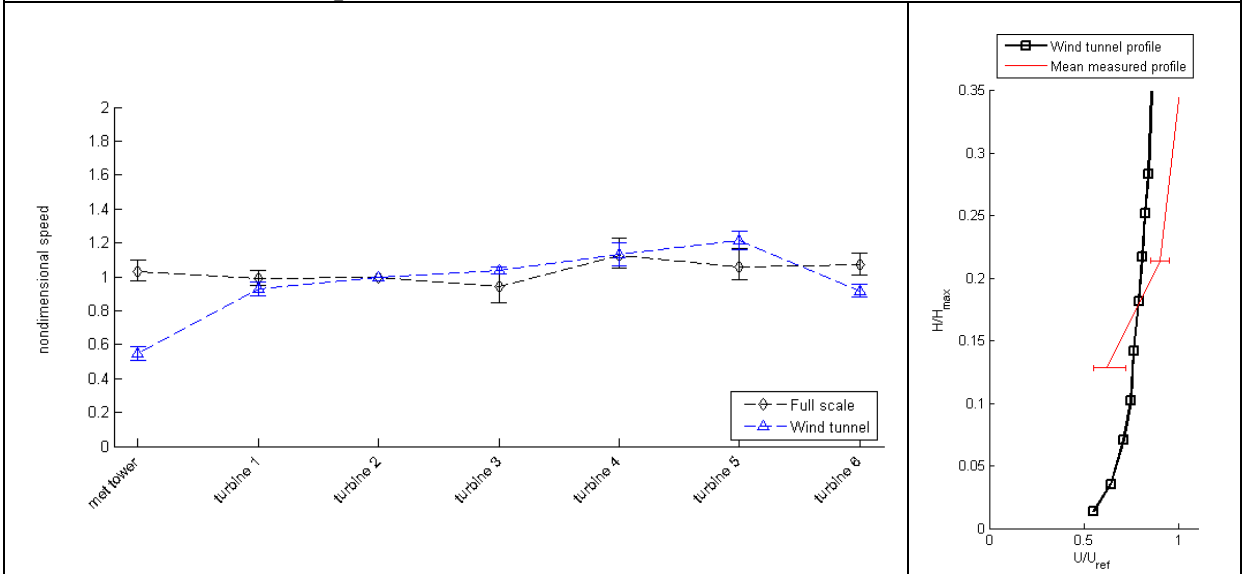
Wind tunnel result set description:

- Direction **315°**;
- “48% canopy model” case;
- Full scale data for **March 2008**;



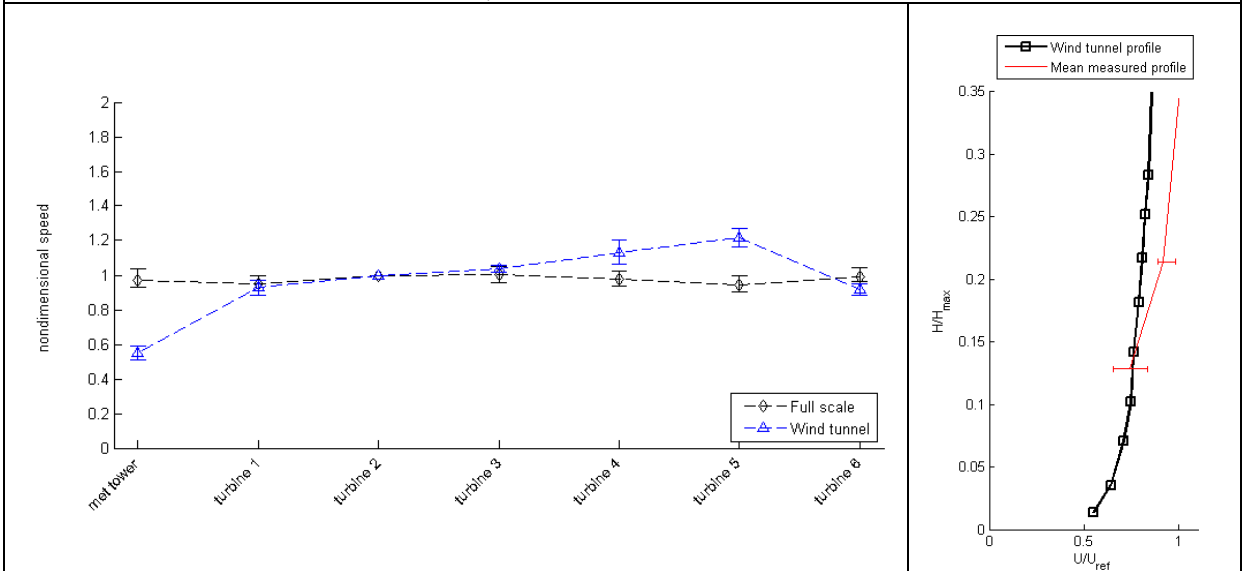
Wind tunnel result set description:

- Direction **315°**;
- “48% canopy model” case;
- Full scale data for **September 2008**;



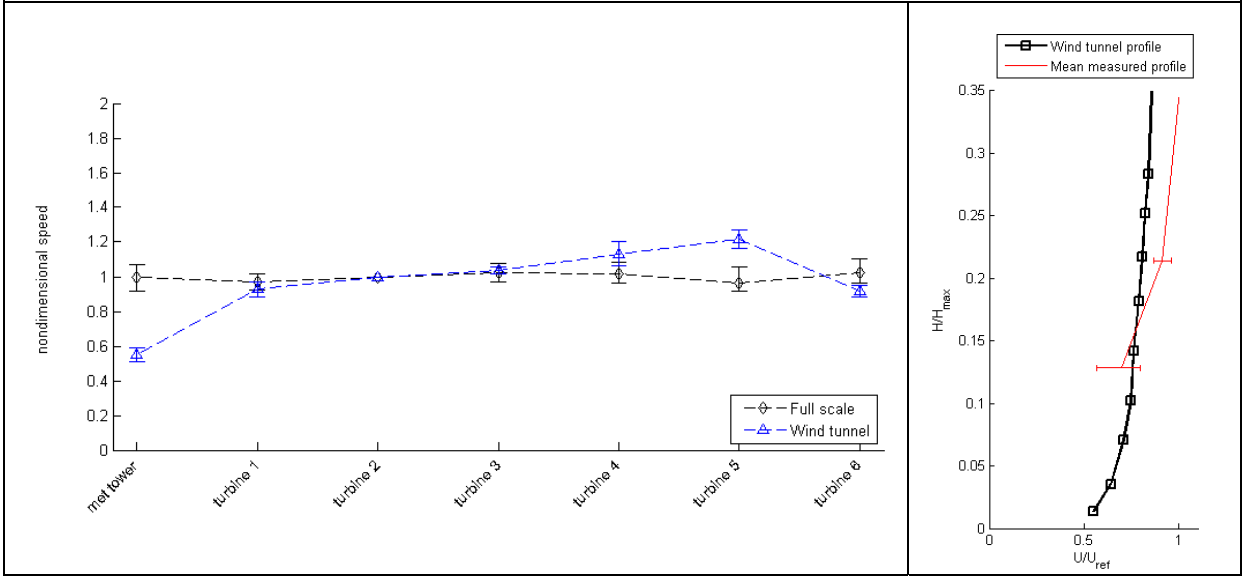
Wind tunnel result set description:

- Direction **315°**;
- “48% canopy model” case;
- Full scale data for **October 2008**;



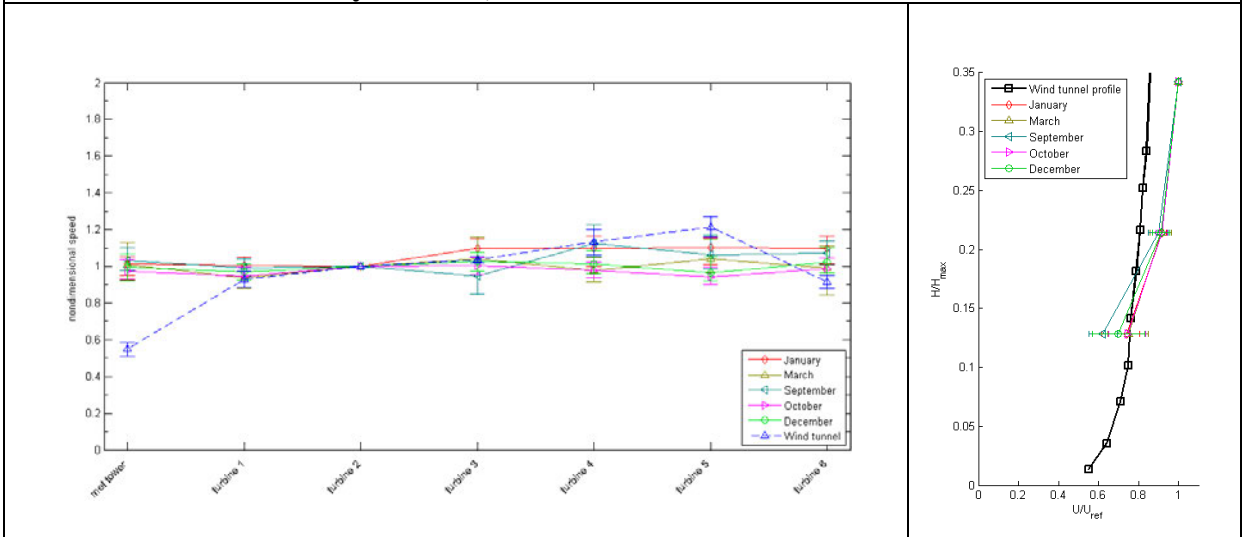
Wind tunnel result set description:

- Direction **315°**;
- “48% canopy model” case;
- Full scale data for **December 2008**;



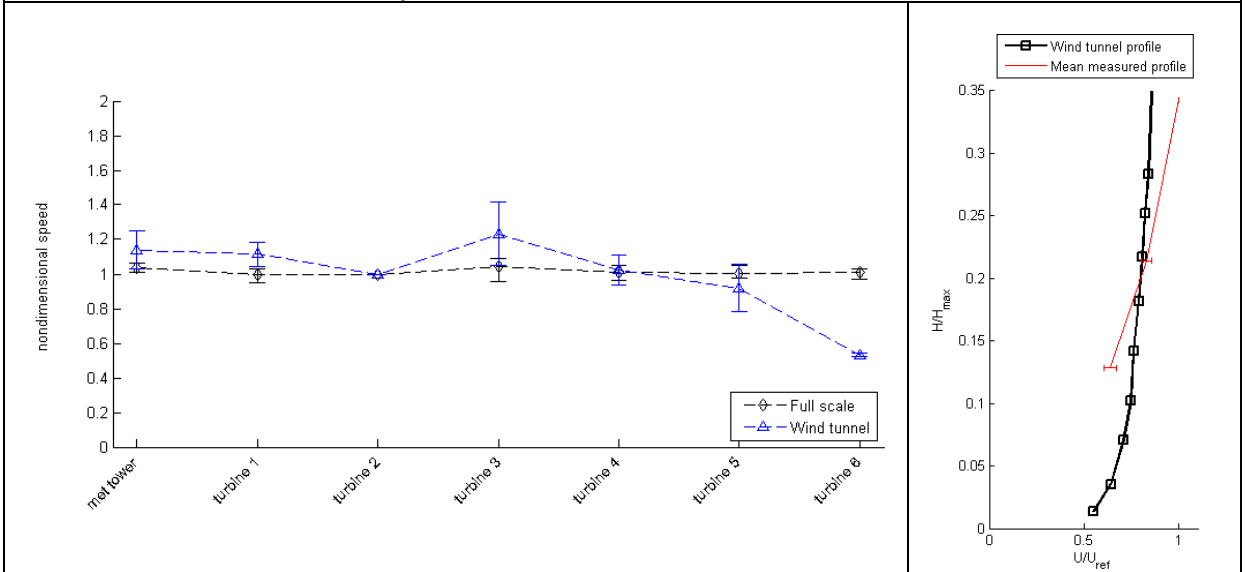
Centralized wind tunnel result set description:

- Direction **315°**;
- “48% canopy model” case;
- Full scale data for **the year 2008**;



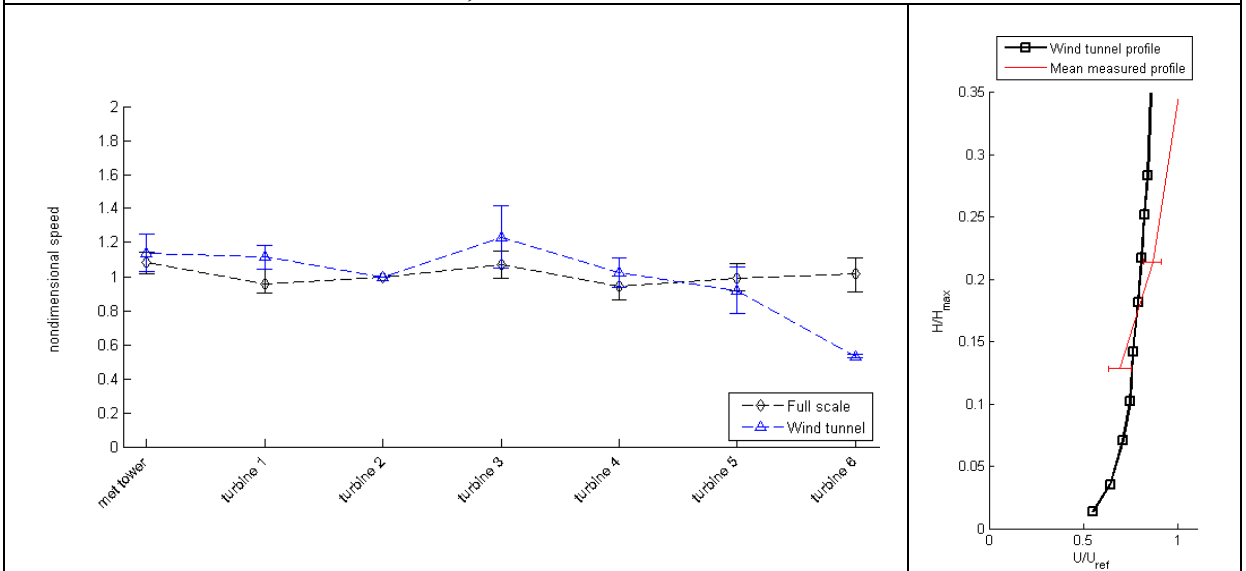
Wind tunnel result set description:

- Direction **202.5°**;
- “48% canopy model” case;
- Full scale data for **January 2008**;



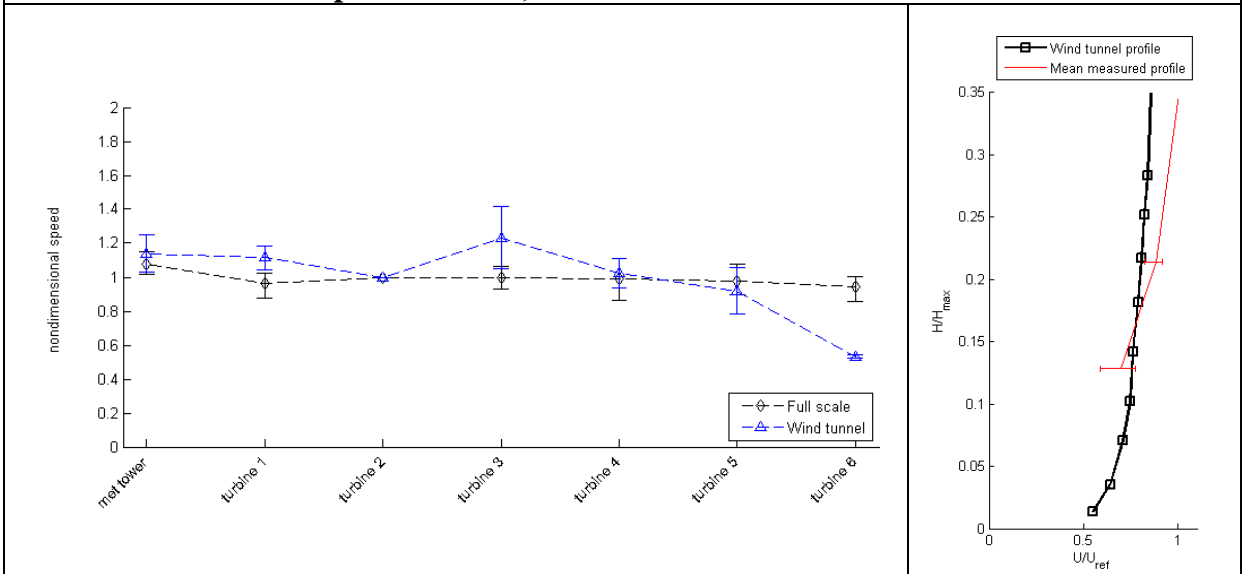
Wind tunnel result set description:

- Direction **202.5°**;
- “48% canopy model” case;
- Full scale data for **March 2008**;



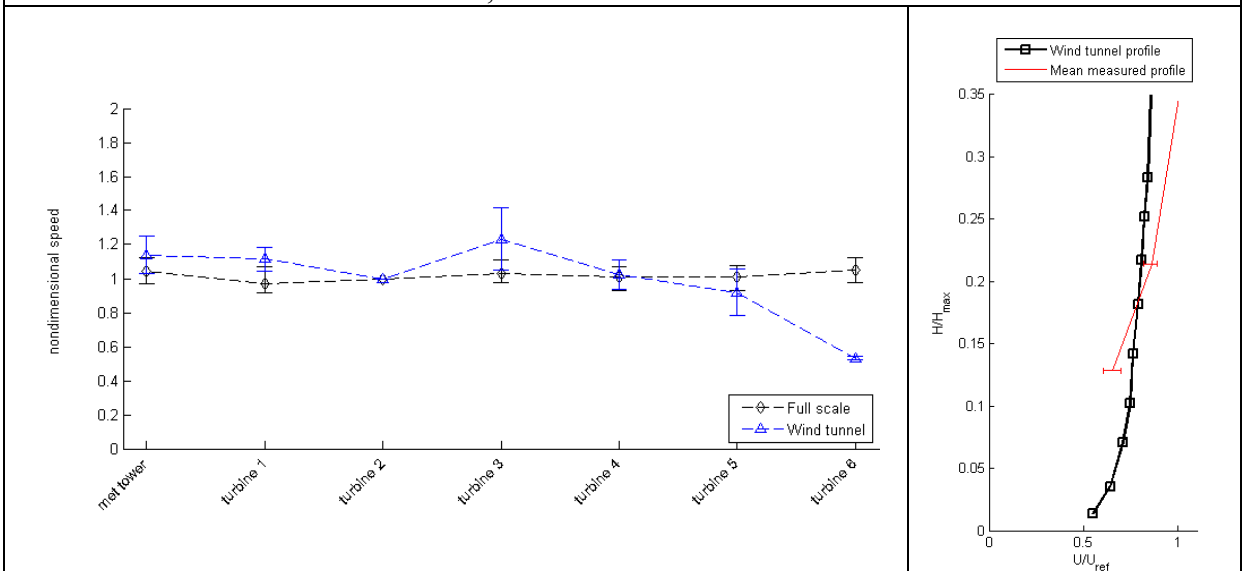
Wind tunnel result set description:

- Direction **202.5°**;
- “48% canopy model” case;
- Full scale data for **September 2008**;



Wind tunnel result set description:

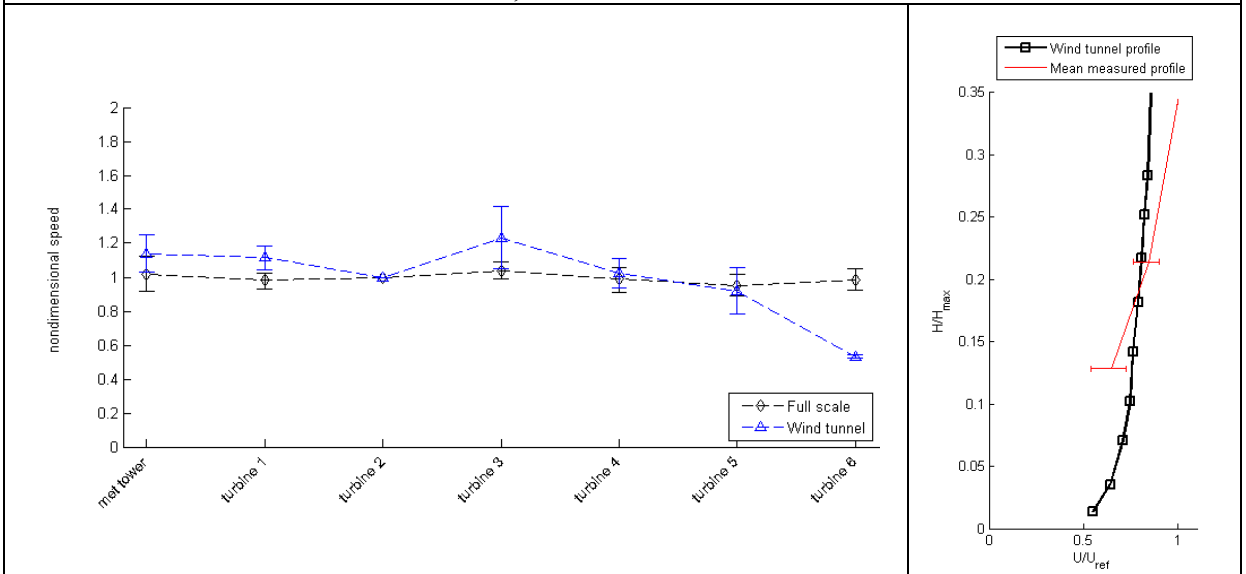
- Direction **202.5°**;
- “48% canopy model” case;
- Full scale data for **October 2008**;





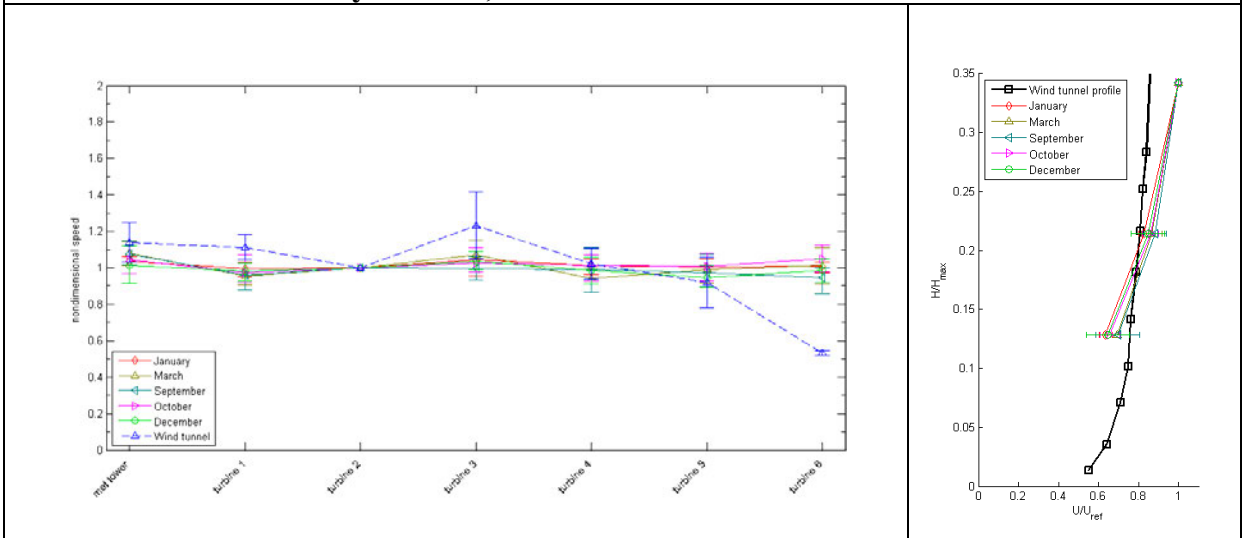
Wind tunnel result set description:

- Direction **202.5°**;
- “48% canopy model” case;
- Full scale data for **December 2008**;



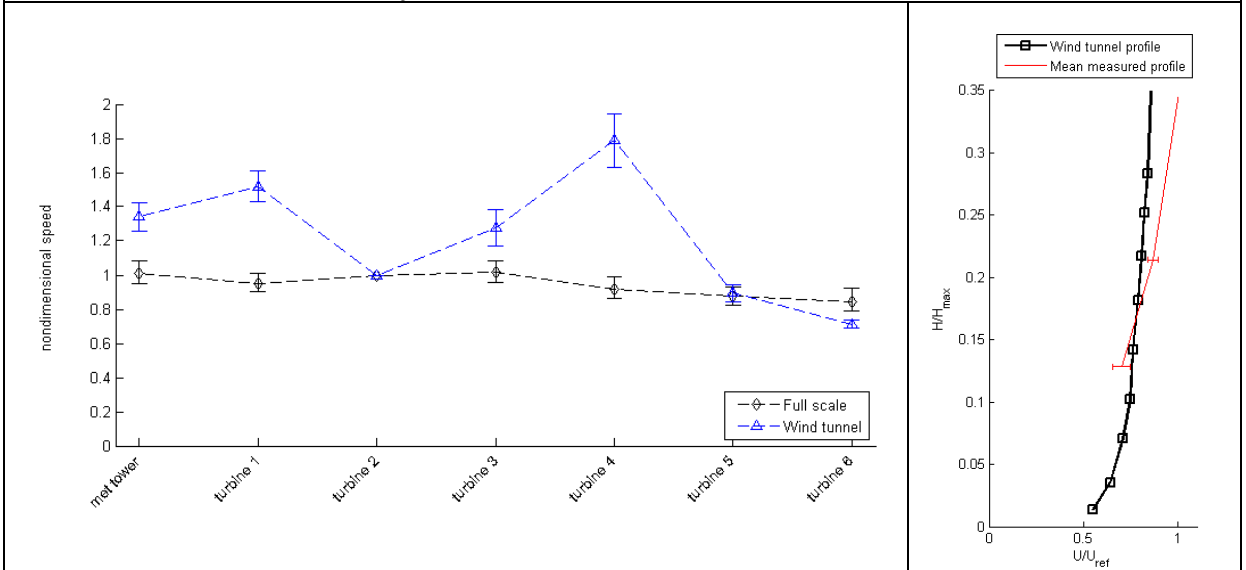
Centralized wind tunnel result set description:

- Direction **202.5°**;
- “48% canopy model” case;
- Full scale data for **the year 2008**;



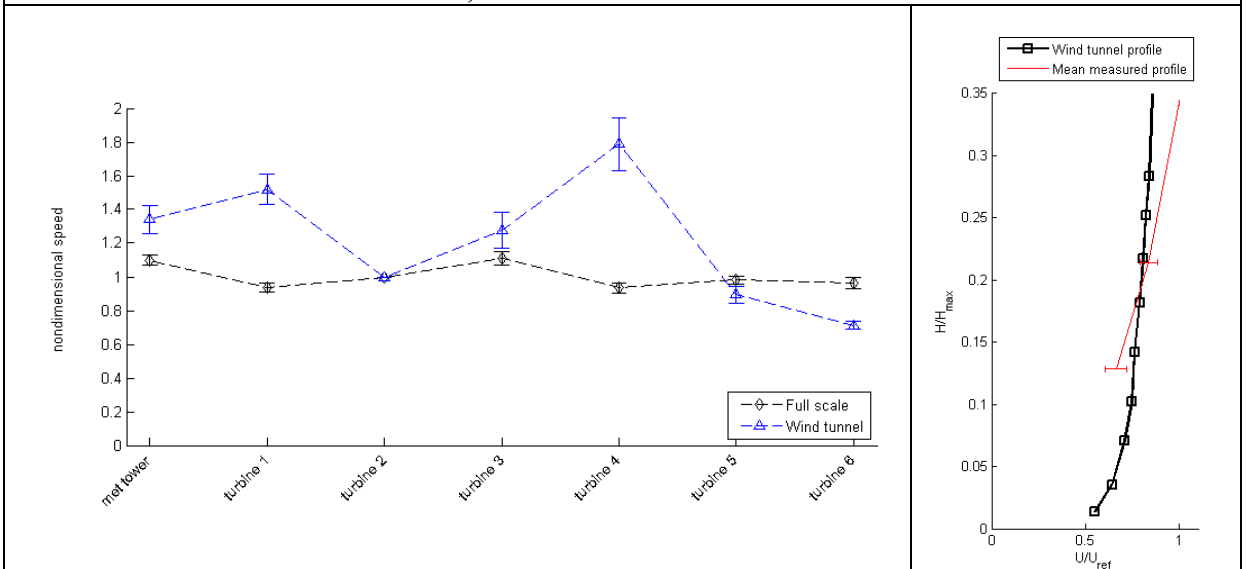
Wind tunnel result set description:

- Direction **157.5°**;
- “48% canopy model” case;
- Full scale data for **January 2008**;



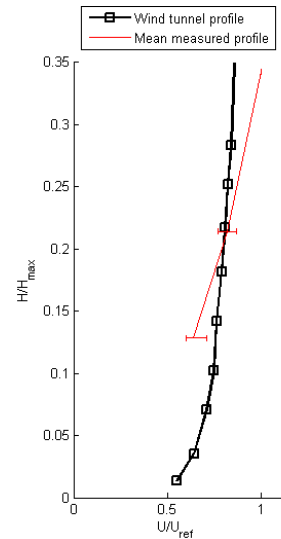
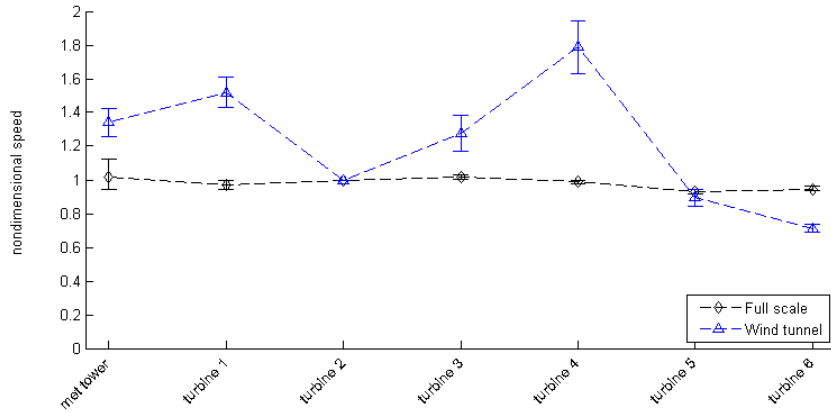
Wind tunnel result set description:

- Direction **157.5°**;
- “48% canopy model” case;
- Full scale data for **March 2008**;



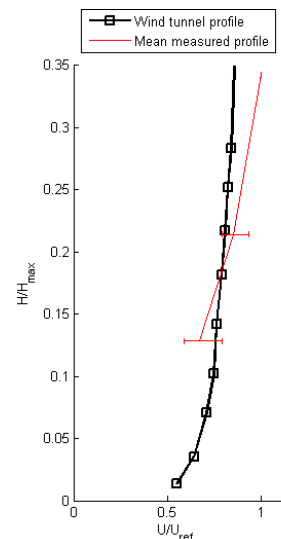
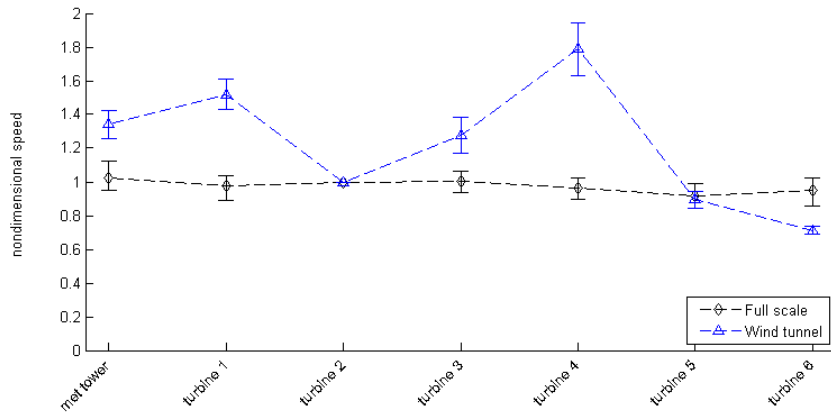
Wind tunnel result set description:

- Direction **157.5°**;
- “48% canopy model” case;
- Full scale data for **September 2008**;



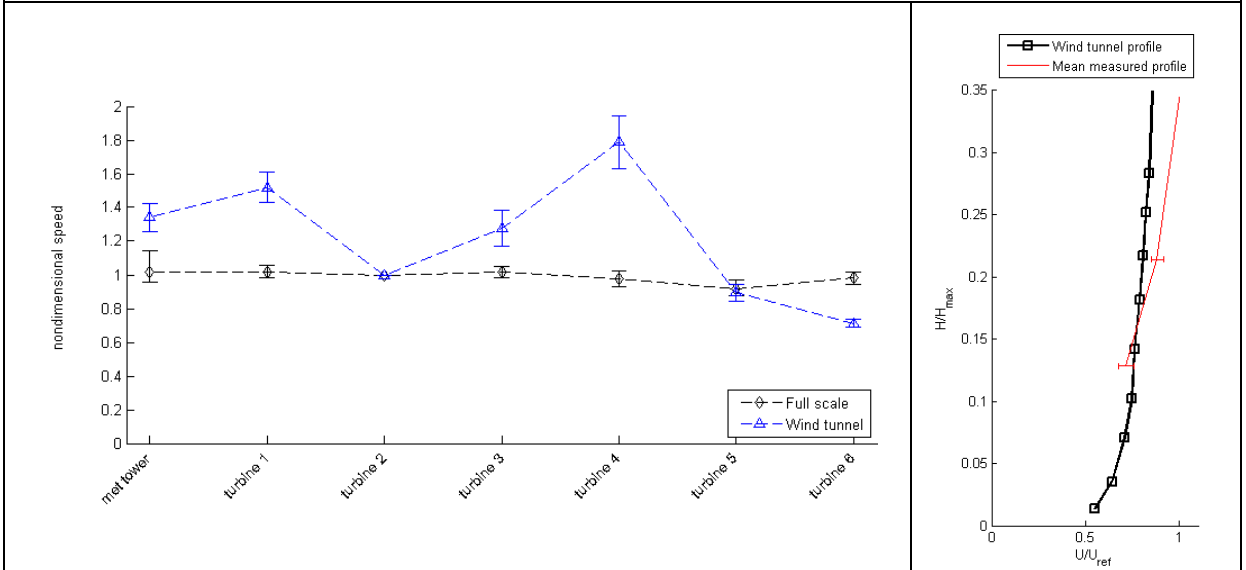
Wind tunnel result set description:

- Direction **157.5°**;
- “48% canopy model” case;
- Full scale data for **October 2008**;



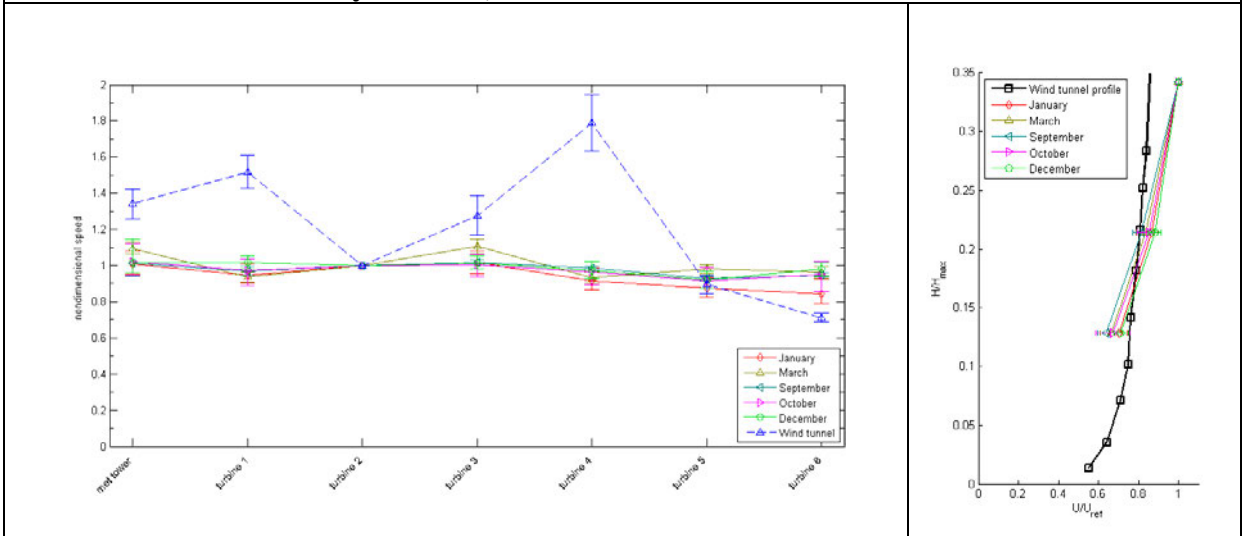
Wind tunnel result set description:

- Direction **157.5°**;
- “48% canopy model” case;
- Full scale data for **December 2008**;



Centralized wind tunnel result set description:

- Direction **157.5°**;
- “48% canopy model” case;
- Full scale data for **the year 2008**;



**Appendix D:** Experimental model and placement in the wind tunnel



Figure D.1: Topographic model placement in the wind tunnel showing installed ramps and Cobra probes.

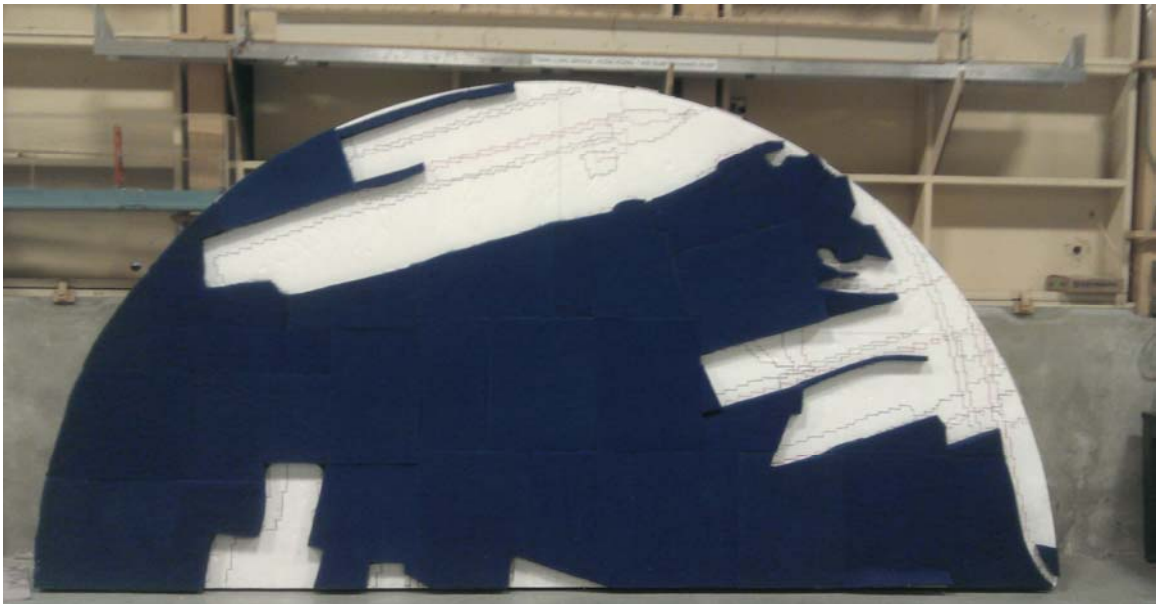


Figure D.2: Experimental model with blue filter material forest canopy installed.

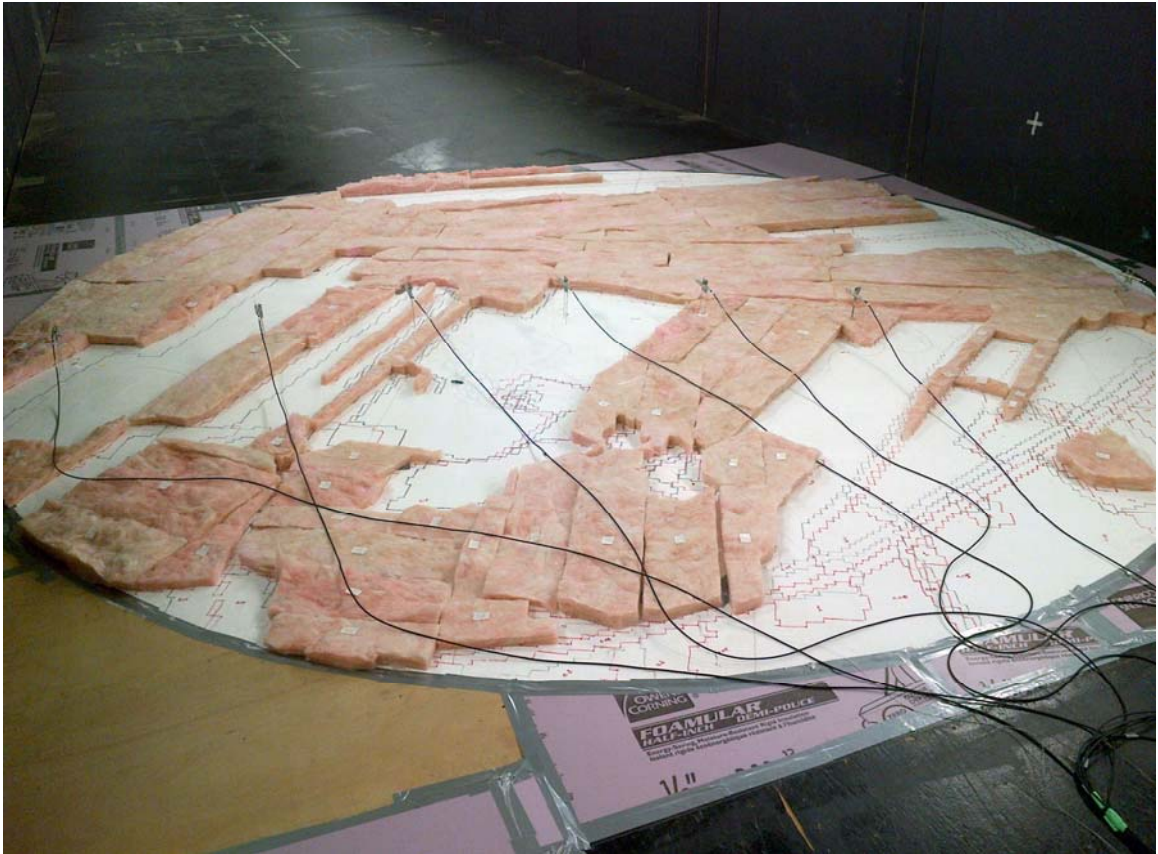


Figure D.3: Experimental model with installed ramps, pink fiber glass forest canopy model and Cobra probes.

## CURRICULUM VITAE

**Name:** Dan-Stefan Parvu

**Post-secondary Education and Degrees:** “Politehnica” University of Bucharest  
Bucharest, Romania  
2006-2010 Bachelor  
(Aerospace Engineering)

**Honors and Awards:** WESNet poster competition  
3<sup>rd</sup> place, Toronto, ON, 2012

**Related Work Experience:** Mechanical Engineer  
AKKA Romserv SRL (Romania)  
2010-2011

Teaching Assistant  
The University of Western Ontario  
2011-2013